A FLUID-FILM BEARING SUPPORTED ELASTIC ROTOR - AN EXPERIMENTAL AND THEORETICAL INVESTIGATION

by

GORDON WILLIAM BEESLEY

A Thesis Submitted for the Degree of

DOCTOR OF PHILOSOPHY

of the University of London
and also for the

DIPLOMA OF IMPERIAL COLLEGE

February 1984

Lubrication Laboratory
Department of Mechanical Engineering
Imperial College of Science and Technology
London SW7 2BX

ABSTRACT

The dynamic behaviour (both synchronous and non-synchronous) of a flexible rotor supported by an oil-film bearing has been investigated theoretically and experimentally.

The analysis was carried out using a numerical method based on the Transfer Matrix Progression Technique. With this approach the bearing fluid-film was represented by a set of eight linear dynamic coefficients obtained from a finite difference solution of the Reynolds equation. The stability of the rotor-bearing system was assessed by combining the Transfer Matrix Method with the Leonhard Locus Technique. Damped first critical speeds were obtained from observation of the systems response to unbalance excitation. The need to calculate the eigen-values of the system was, thus, avoided, and, hence, a considerable amount of computer time was saved.

A test apparatus was developed with a rotor comprising of a heavy flywheel mounted on a light shaft. The rotor was supported at one end by a tight fitting precision rolling contact bearing mounted in a gimbal. The other end of the rotor was supported by the test bearing, a cylindrical journal bearing with axial feed ports, mounted on a variable stiffness undamped pedestal. Changes in bearing clearance and support flexibility on the critical speed of the rotor were investigated.

A reduction in bearing clearance increased the first critical speed of the rotor, and the introduction of support flexibility lowered the critical speed. For the case of a rigid pedestal agreement between theory and experiment to within 3% was obtained.

The effects of journal bearing clearance, oil-supply feed pressure, oil feed groove extent and bearing pedestal flexibility on the stablity threshold were also examined.

Enhanced stability was achieved for a reduction in clearance, increased oil feed pressure, small groove extent and low pedestal flexibility.

When the theoretical and experimental instability thresholds were compared, discrepancies in the range of 6% to 31% were realised. Reasons for these differences were investigated and discussed.

ACKNOWLEDGEMENTS

I would like to acknowledge with gratitude the help of the following people during the course of this research:

The Science and Engineering Research Council for providing the research grant.

Dr. C. Ettles for providing the opportunity to undertake the work and for supervising the first part of it.

Professor A. Cameron for supervising the final stage of the research and for his helpful comments during the preparation of the thesis.

Mr. P. Saunders of the Mechanical Engineering Department for his assistance during the design of the test apparatus, and the interest he has shown throughout the work.

Mr. A. Dowden and the technical staff of the Mechanical Engineering Department Workshop, for applying their expertise to the building of the test machine.

Mr. R. Gunn of the Mechanical Engineering Deparatment for lending items of electrical instruments.

Colleagues in the Lubrication Section, especially Mr. R. Dobson and Mr. T. Whymark for their help.

Dr. R. Wordsworth of the Biomechanics Section for his help in correcting the thesis.

Mr. M Rahmanzadeh-Asl of the Lubrication Section and Mr. R. Gozdawa of CompAir for their helpful discussion of the work.

Miss K. Ottmann for meticulously typing the thesis.

My family for their support, and Alice and Rachel for their patience and encouragement.

CONTENTS

Page

Page

LIST OF FIGURES

Figure | Page

Figure | Page

Figure | Page

Figure | Page

LIST OF TABLES

LIST OF PLATES

NOMENCLATURE

a	: Major Semi-axis of Elliptical Orbit
b	: Minor Semi-axis of Elliptical Orbit
c	: Bearing Radial Clearance
c_{xx}, c_{xy}, ...	: Linear Damping Coefficients
$c_{\theta\theta}$, $c_{\theta\phi}$, ...	: Rotational Damping Coefficients
C_{xx}, C_{xy}, ...	: Non-Dimensional Linear Damping Coefficients
$C_{\theta\theta}$, $C_{\theta\phi}$, ...	: Non-Dimensional Rotational Damping Coefficients
d	: Shaft Diameter
D	: Bearing Diameter, $D=2R$
e	: Eccentricity of Journal w.r.t. Bearing Centre
E	: Youngs Modulus for Shaft Material
F_ε, F_ϕ	: Oil-Film Forces
F_ε^*, F_ϕ^*	: Non-Dimensional Oil-Film Forces
g	: Acceleration Due to Gravity
h	: Film Thickness
h^*	: Non-Dimensional Film Thickness, h/c
i	: $\sqrt{-1}$
I	: Second Moment of Area of Shaft Section About a Diameter
I_p	: Polar Moment of Inertia
I_T	: Transverse Moment of Inertia
k_{xx}, k_{xy}, ...	: Linear Stiffness Coefficients
$k_{\theta\theta}$, $k_{\theta\phi}$, ...	: Rotational Stiffness Coefficients

K_{xx}, K_{xy}, ...	:	Non-Dimensional Linear Stiffness Coefficients
$K_{\theta\theta}$, $K_{\theta\phi}$, ...	:	Non-Dimensional Rotational Stiffness Coefficients
$k_{p,x}$, $k_{p,y}$	:	Pedestal Stiffness
k_R	:	Rotor Stiffness
l	:	Shaft Element Length
L	:	Bearing Length
m	:	Shaft Element Mass
m_u	:	Mass Unbalance
M_B	:	Bearing Support Mass
M_R	:	Total Rotor Mass
M_x, M_y	:	Bending Moment
N	:	Rotational Shaft Speed (RPM)
N_T	:	Threshold Rotational Shaft Speed (RPM)
P	:	Bearing Pressure
P^*	:	Non-Dimensional Bearing Pressure, $\dfrac{P}{6\omega\eta(R/c)^2}$
P_f	:	Oil Feed Pressure
r	:	Unbalance Mass Radial Position
S	:	Sommerfeld Number, $\dfrac{W/LD}{N\eta}\left(\dfrac{c}{R}\right)^2$
t	:	Time
$[\bar{T}_P]$	:	Point Transfer Matrix
$[\bar{T}_F]$	:	Field Transfer Matrix
$[\bar{T}_S]$	:	Standard Transfer Matrix
$[\bar{T}_{TB}]$	:	Overall Transfer Matrix
$\bar{U}$	:	Out of Balance Force

V_x, V_y	: Shear Force
W	: Static Load on Bearing
x,y	: Fixed Co-ordinates
X,Y	: Rotating Co-ordinates
x	: Time Dependent Vertical Displacement
y	: Time Dependent Horizontal Displacement
z	: Axial Co-ordinate
Z_{xx}, Z_{xy}, ...	: Linear Support Impedance
$Z_{\theta\theta}$, $Z_{\theta\phi}$, ...	: Rotational Support Impedance
$Z^f{}_{xx}$, $Z^f{}_{xy}$,...	: Oil-Film Impedance
$Z^p{}_{xx}$, $Z^p{}_{yy}$	: Pedestal Impedance

Greek Symbols

α	: Bearing Axial Groove Angle
γ	: Oil Feed Pressure Ratio, $\frac{P_f}{(W/LD)}$
δ	: Shaft Maximum Static Deflection
δ/c	: Flexibility Parameter
δx, δy	: Permanent Shaft Bend
ε	: Bearing Eccentricity Ratio, e/c
η	: Absolute Viscosity of Lubricating Oil
θ	: Angular Co-ordinate and Shaft Slope in x-Direction
$\delta\theta$, $\delta\phi$	: Disc Skew
λ	: Eigen-Value, $\lambda=\sigma+i\Omega$
ρ	: Angular Co-ordinate of Mass Unbalance
σ	: Real Part of λ
ϕ	: Attitude Angle of Line of Centres and Shaft Slope in y-Direction

ψ	: Phase Angle Between Excitating Force and Displacement
ω	: Angular Speed of Shaft (Rad/s)
ω_T	: Threshold Angular Speed of Shaft (Rad/s)
$\omega_{1,x}$, $\omega_{1,y}$	: First Critical Speed of Shaft (Rad/s)
ω_g	: Reference Frequency, $(g/c)^{1/2}$
Ω	: Excitation Frequency (CPM)
Ω_T	: Threshold Frequency (CPM)

Subscripts

I	: Imaginary Part of Complex Quantity
k	: Rotor Station Number
L	: Left Hand Side of Station
n	: Total Number of Stations
R	: Right Hand Side of Station and Real Part of Complex Quantity
T	: Threshold of Instability
u	: Unbalance
x	: Vertical Component
y	: Horizontal Component
ε	: Along the Line of Centre
ϕ	: Normal to the Line of Centres in the Direction of Rotation
*	: Non-Dimensionalised
.	: Time Derivative
-	: Complex Quantity

CHAPTER 1

INTRODUCTION

1.1 STATEMENT OF THE PROBLEM

Today there is an increasing demand for turbomachinery to run at higher operational speeds. In addition, to limit the mass of rotating machinery, and, hence, to some extent the cost, designers are producing rotors which are both lighter and more flexible. As a result the desired running speeds can be above the critical speed of the rotors. A typical example of this is a turbo-generator running beyond its third or fourth critical speed.

These conditions call for a thorough understanding of the dynamic problems likely to be encountered when operating turbomachinery at high speed. Problems encountered in operational machinery may be costly to overcome. Thus, a detailed knowledge of parameters affecting a rotor-bearing system is essential at an early stage in the design.

Generally, the upper limit of safe operation for rotors supported in oil-film bearings is determined by the onset of self-excited or free vibrations. There are important bearing design features and operating conditions which can markedly affect the dynamic behaviour of a rotor-bearing system. Bearing pedestal flexibility, bearing oil feed pressure, the position and extent of oil feed grooves and the bearing radial clearance are among those parameters which affect the dynamic behaviour of rotor-bearing systems in both a synchronous and non-synchronous manner. Little is known about the influence of variations in each parameter, and how they interact with each other.

1.1.1 Terms of Reference

(1) The objective of this investigation is to determine experimentally and theoretically the influence of certain bearing variables on the synchronous and non-synchronous behaviour of a flexible rotor constrained by an oil-film bearing on an undamped elastic support. The behaviour of the rotor can be characterised by the critical speed, the mode shape, the steady state response and the threshold of instability. Experimentally determined values of these parameters will be compared with theoretical predictions.

(2) A numerical approach to the theoretical work is chosen because of the complexity of the problem.

The bearings are treated in detail using linear theory to represent the oil-film forces. Perturbation of thejournal from its equilibrium position is used to derive the stiffness and damping coefficients of the fluid-film. These coefficients are obtained using a finite difference solution for the bearing.

The dynamic behaviour of the combined rotor-bearing system is studied using the Transfer Matrix Method. In this technique a continuous rotor is discretely represented by a series of stations, which compromise of lumped masses connected by massless elastic beam elements. In this manner it is possible to model a complex rotor-bearing system by employing a sufficient number of stations.

1.2 TYPES OF VIBRATION ASSOCIATED WITH ROTOR-BEARING SYSTEMS

Brief descriptions are now given of the main types of vibration encountered in rotor-bearing systems, and frequently referred to in the relevant literature.

(1) Synchronous Whirl

If an unbalance exists in the system it will cause the rotor to deflect. The deflected rotor will whirl about its rotation axis at the rotational speed. Hence, this type of motion is referred to as synchronous whirl. The whirling of the deflected rotor is not strictly a vibration since it does not result in cyclic flexure of the shaft. It appears as vibration, however, when viewed from fixed axes, with aid of radial proximity probes for example.

(2) Critical Speeds

A critical speed occurs when the system experiences a reasonance. In an undamped system the amplitude of the resonance would become infinite. All practical systems, however, possess some form of damping. When rotors are mounted in fluid-film bearings, damping occurs in the fluid-film and this limits the resonance level.

The critical speeds are related to the natural frequencies of a rotor mounted on simple supports. Critical speeds are usually lower than the corresponding natural frequencies because of bearing flexibility. If a rotor runs above its first critical speed it is referred to as flexible, otherwise it is referred to as rigid.

(3) Multiples of Synchronous Frequency

For a horizontal rotating shaft with asymmetric stiffness, the sag along its length will vary as the bending stiffness in a vertical plane changes. Due to the action of gravity energy is fed into the rotor producing a cyclic force primarily at twice the rotation frequency (2f). Although the forcing is in the vertical direction, the bearings couple the vibrations into the horizontal plane. When this twice running frequency tunes into a system resonance, a peak amplitude occurs.

In the experimental work, when the rotor ran at half the critical speed, the 2f component excited the critical speed resonance. Plate 1.1(a) shows the orbit of the shaft centre obtained using proximity probes. The shape of the orbit is due to the presence of the running frequency f, together with the 2f component. Plate 1.2 (b) shows the waveform of the components, with a once per revolution signal below it for reference.

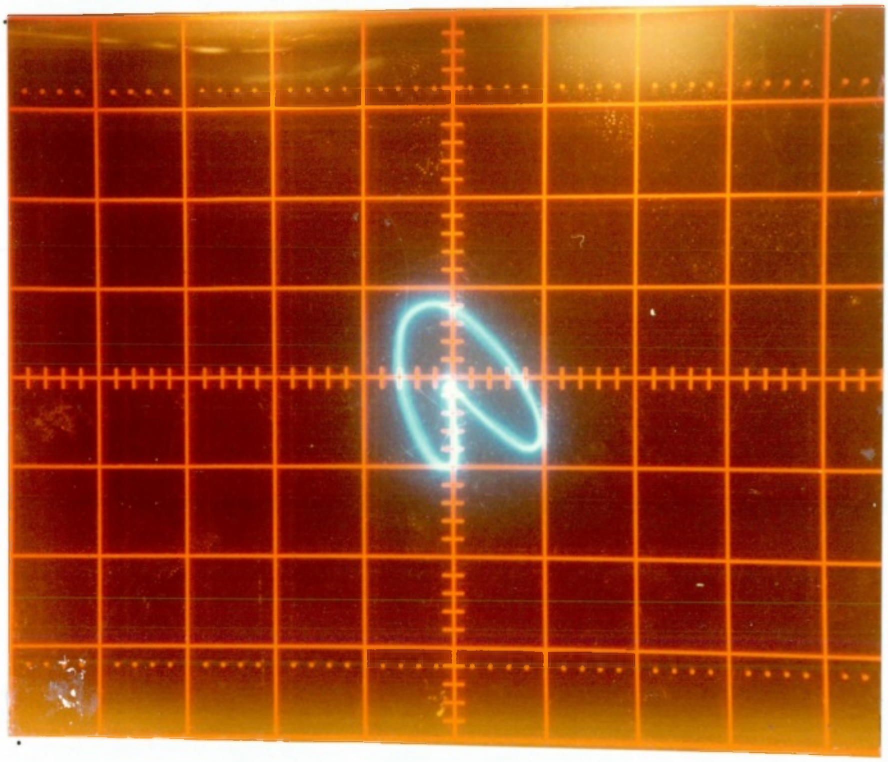

Plate 1.1(a) 2f Orbit at N=1367RPM (5mil/Div) c=3mil, α=90°, P_f=2psi

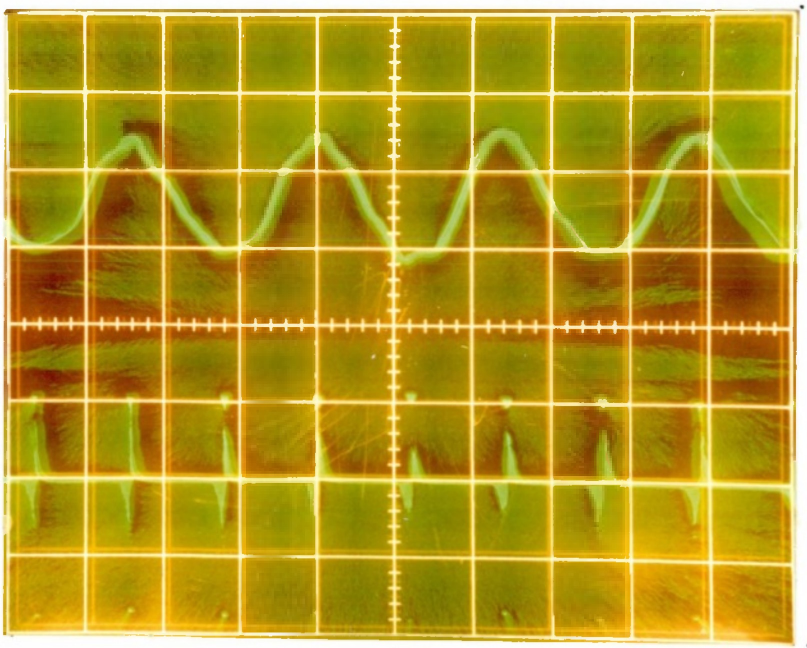

Plate 1.1(b) 1/2f Waveform and 1/Rev Phase Counter Up Trace - 5mil/Div, Time Base - 10msec/Div

(4) Sub-harmonic Vibrations

Sub-harmonic vibrations occur at a fraction of the running speed, usually at 1/2, 1/3, etc. These are forced vibrations arising from the non-linear stiffness characteristics of the oil-film. The amplitude associated with such motion is usually small and does not have any significant effect on the vibration of the system. It can be reduced by improving the balancing of the rotor.

(5) Non-synchronous Vibrations

The four categories of vibration described above referred to stable motion. Non-synchronous vibrations are termed as unstable motion. This phenomenon can occur at a particular speed of rotation, when the rotor precesses about a point in the bearing (initially the equilibrium or steady-state position) at a frequency not synchronous with the speed of rotation. This phenomenon is called oil-whirl, oil-whip or resonant-whip when encountered in rotors mounted on oil-film bearings, and is a concern of this work. Other types of non-synchronous vibration are possible. For example, unstable motion can occur due to internal friction or damping in shrink fits or parts rubbing together, and steam excitation.

Non-synchronous vibration does not require the external force of an unbalance as in synchronous vibration. Instead, the rotation energy of the rotor is fed back into the system via the oil-film, thus, sustaining the unstable motion.

Hence, it is referred to as a "self-excited" vibration. Usually, an increase in speed results in an increase in vibration, with the possibility of damage occurring to the bearings and rotor.

Oil-whirl can occur in rigid and flexible rotors. Generally, whirl commences with a frequency just below half the running speed. An increase in the shaft speed results in a corresponding increase in the whirl frequency and amplitude. Plate 1.2(a) shows a typical whirl orbit of the shaft centre obtained from the test rotor-bearing system. The overlap of the orbits is due to the slow rotation of the whirl orbit during the exposure. Plate 1.1(b) shows the waveform of the 1/2f component together with a once per revolution signal for reference.

Oil-whip generally occurs at shaft speeds in excess of twice the first system critical speed. Rotors with heavily loaded bearings can have instability frequency ratios considerably below half the shaft speed. Internal damping tends to destabilise the system. Its effect is to increase the ratio between instability frequency and running speed. The theoretical limit of the instability ratio is unity.

For oil-whip the frequency of the instability is approximately equal to the first critical speed, and remains constant as the shaft speed is increased. Hence, this type of motion is also referred to as resonant-whip, as the rotor

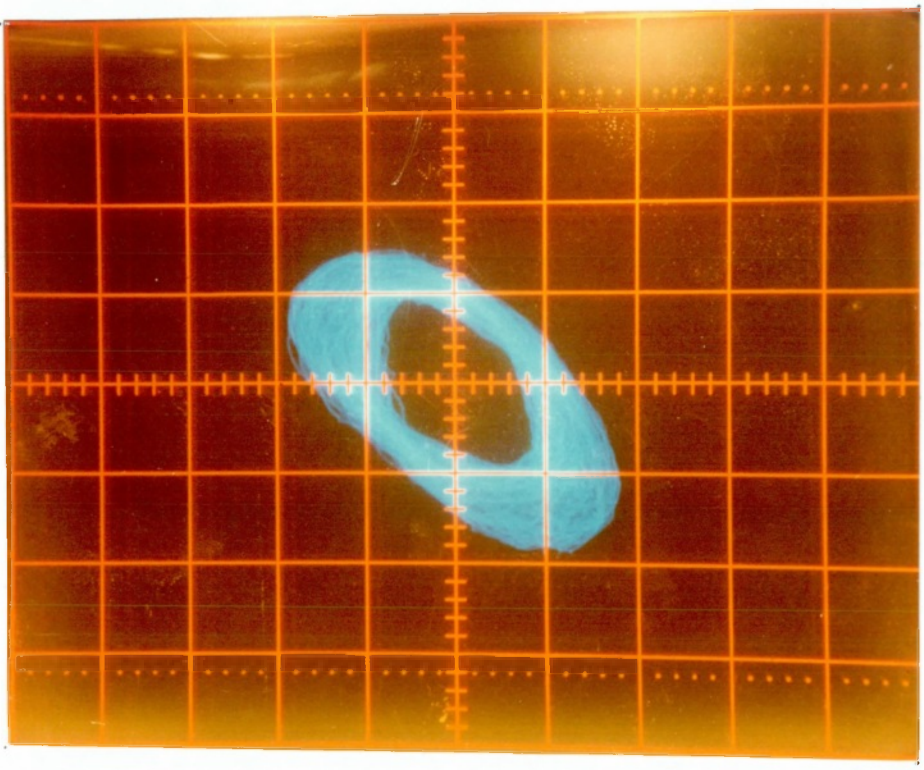

Plate 1.2(a) 1/2f Orbit at N=4905RPM (5mil/Div) c=3mil, α=90°, P_f=2psi

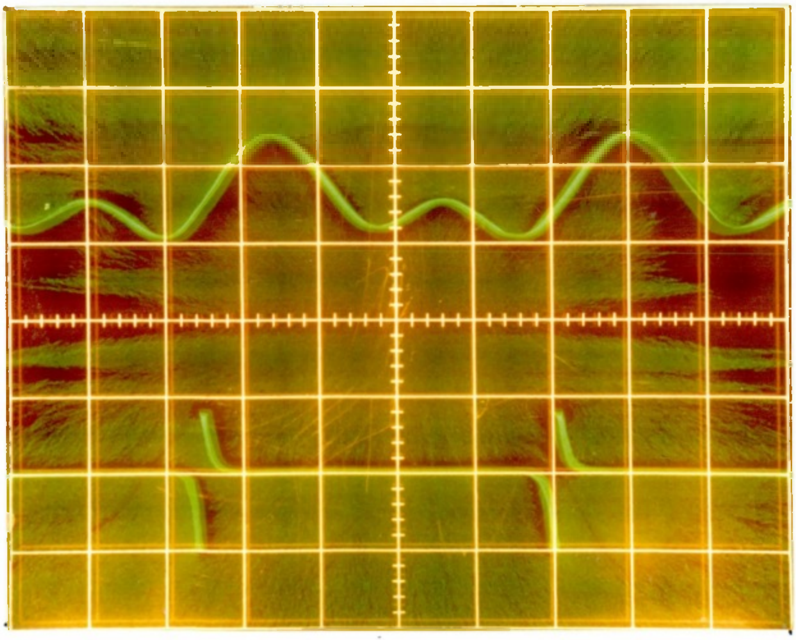

Plate 1.2(b) 2f Waveform and 1/Rev Phase Counter Up Trace - 5mil/Div, Time Base - 10msec/Div

is in a state of resonance corresponding to the first system critical speed. Even for the whip which occurs at two or three times the first critical speed, the instability frequency is still equivalent to the systems first critical speed.

(6) Rotor Response

The steady-state response of a rotor refers to its steady-state amplitudes at any point along the rotor-bearing system. Analytically, it is treated as time independent or linear motion, and the amplitude values are referred to as instantaneous.

The transient response refers to motion that the rotor-bearing system will follow in time, if perturbed sufficiently from its equilibrium position. Analytically, it is treated as time dependent or non-linear motion.

1.3 LITERATURE REVIEW

The first recorded article on the subject of rotor dynamics was presented by Rankine (1) in 1869. Rankine examined the case of a frictionless uniform shaft disturbed from its equilibrium position. Because he neglected the Coriolis force he erroneously concluded that: motion below the critical speed is stable, is neutral or in an "indifferent equilibrium" at the critical speed, and unstable above the critical speed.

During the next fifty years Rankines analysis led engineers to believe that operation above the first critical was impossible. In 1895 De Laval demonstrated experimentally that operation with a steam turbine above its first critical speed was possible. Investigators of the day, however, remained confused about the operation of machinery at high speed.

Dunkerley (2) in 1894 contributed significantly to the understanding of rotor dynamics from his experimental and theoretical investigations. He considered a rotor as a flexible elastic beam and the bearings as simple supports. By neglecting unbalance and damping, a whirling rotor could be considered as an equivalent beam on simple supports. The problem was then reduced to finding the natural lateral frequencies of the beam. With these assumptions the natural lateral frequencies corresponded to the rotor critical speeds. Dunkerley postulated that if the rotor contained an unbalance it would excite these natural frequencies. This would result in large amplitude vibration if the running speed corresponded to any of these frequencies.

It was not until 1919 that Jeffcott (3) produced his celebrated analysis on rotor-dynamics, in which he examined the effects of unbalance on the whirl amplitudes and the forces transmitted to the bearings. Jeffcott neglected the effects of the bearings on the system, but included internal shaft damping.

Jeffcott's model consisted of a uniform massless elastic rotor with an unbalanced concentrated mass at mid-span. Gyroscopic effects were ignored and the rotor supports were assumed to be pinned. Jeffcott considered the shaft deflecting in a plane and then the same deflection precessing at the angular velocity of the rotor.

Jeffcott reached the conclusion that the whirl amplitudes would increase up to the critical speed, and subsequently decrease in amplitude above the critical. Thus, unlike Rankines model Jeffcotts model allowed for safe operation above the critical speed.

In the 1920's rotor design had reached a stage where rotors were operating in regions well above their first critical speed. In some cases severe vibrations were experienced and failures resulted. Investigators of the time were at a loss to explain the cause of these vibrations. At first balancing was suspected, but refinement in balancing did not alleviate the problem.

Newkirk (4) conducted a through investigation of these severe vibrations and failures. He initially restricted his experimental investigations and observations to rotor systems in which the vibrations were attributed to rotor internal friction. He published his findings in his pioneering paper of 1924. In 1925 Newkirk and Taylor (5) subsequently examined the case of severe vibrations arising from rotors supported on oil-film bearings. They called this behaviour oil-whip. Listed below are his main conclusions concerning instability arising from internal friction and oil-film bearings:

(1) The threshold speed and instability amplitude were independent of balancing.

(2) The threshold speed always occurred above the first critical speed and the precession frequency was lower than the running frequency.

(3) In many cases the rate of precession was equivalent to the first critical speed.

(4) The precession frequency was constant and independent of shaft speed.

(5) If rotor speed were increased beyond the threshold, the instability amplitude would increase and could lead to failure of the rotor or bearings.

The critical speed analysis of Jeffcott could not be used to explain the above observations. At this stage in the understanding of rotor dynamics the available theory could only explain synchronous whirling arising for example from rotor unbalance.

Newkirk correctly attributed the instability to the action of the oil-film. However, the method by which the oil-film promoted instability was obscure at the time. Newkirk could not explain why whip did not commence until a speed greater than twice the first critical was reached. He was also perplexed by the influence of support flexibility on stability. He had observed that instability due to internal friction could be eliminated with the introduction of a flexible support, even in the absence of support damping. However, a flexible support allowed violent oil-whip to occur, and support damping was necessary to suppress it.

At the time that Newkirk was conducting his observations on instability, Stodola (6) was examining the influence of oil-film bearings on rotor critical speeds and instability. He introduced the concept of oil-film springs and dampers in order to derive expressions for the oil-film forces. These forces were linearised with respect to the displacement and velocity of the journal from the equilibrium position. Reynold's equation was solved using the Sommerfeld solution, and the four stiffness coefficients were derived. He was unable to derive the velocity dependent damping coefficients and, therefore, ignored them. Stodola arrived at the conclusion that a journal bearing would be stable for eccentricities greater than 0.70. This was in agreement with the experimental work of Hummel (7).

In 1933 Robertson (8) analysed Newkirks experimental findings on oil-whip. He took as a model a 360^{o} infinitely long journal bearing, and applied film forces derived by Harrison (9) in 1913. Robertson came to the remarkable and incorrect conclusion that instability would occur for all speeds. This arose because the steady-state bearing forces derived by Harrison had a 90^{o} attitude angle between applied load and journal displacement, hence, the system possessed no radial stiffness.

Also in 1933 Smith (10) extended Jeffcotts model to include unequal stiffness and damping of the rotor supports. He theoretically confirmed Newkirks observation that unequal support flexibility can improve stability. In addition Smith predicted the existance of backwards whirl occurring between two critical speeds, corresponding to different stiffnesses in two orthogonal planes.

A year later Newkirk and Grobel (11) conducted experiments on the control of instability using bearings with an arrangement of axial grooves in the upper half. They also discussed how oil-whip could develop in a flexible rotor. In the paper of 1925 Newkirk and Taylor (5) had proposed a mechanism to explain oil-whirl. They had postulated that for a shaft speed ω, the mean velocity of the oil drawn into the converging region would be approximately $\omega/2$. Thus, if a disturbance occurred in which the line of centres of the journal and bearing rotated at $\omega/2$, then the wedge into which the oil is pumped would move away from the oil at the same mean velocity. This would result in a loss of hydrodynamic pressure and load carrying capacity. Instability may then occur with energy supplied from rotation feeding the whirling motion. As the shaft speed increased, the mean velocity $\omega/2$ would also increase with a corresponding increase in the whirl frequency.

Although this mechanism satisfactorily explained oil-whirl, it did not explain oil-whip in which increasing the shaft speed beyond the stability threshold had little effect on the instability frequency corresponding to the rotors crtical speed ω_1. Newkirk initially proposed that as shaft speed was increased an increase in side leakage also occurred, which maintained the mean oil velocity constant at $\omega/2$. This explanation was somewhat artificial as it required just the right amount of side leakage and oil flow around the bearing to maintain a constant mean velocity of the oil equal to the rotors first critical speed ω_1.

In the later paper Newkirk and Grobel (11), however, proposed a more sophisticated theory to explain oil-whip. They explained that a periodic disturbance of the oil wedge at a frequency of $\omega/2$ would be in resonance with ω_1 if $\omega=2\omega_1$. As ω_1 was a predominant natural frequency of the system, increasing the shaft speed would still excite the rotor-bearing system at ω_1. The rotational energy of the rotor would be fed back to the whip motion of the rotor via the bearings.

Thus, oil-whip was a rotor dominated phenomenon in which the rotors elasticity controlled the on-set of instability and the whip frequency. In contrast oil-whirl was usually dominated by the elasticity of the oil-film which controlled threshold and frequency of whirl.

Hagg (12) in 1946 showed that the whirl frequency should be less than half the rotational frequency. He considered only small displacements and modelled his system with masses, springs and dampers. Hagg studied the cases of rigid and flexible rotors in fixed bearings and partial bearings under constant loads. Later Hagg and Warner (13) examined oil-whip in flexible rotors with partial arc bearings both theoretically and experimentally. They showed that rotor flexibility diminished the region of stable operation.

The work of Robertson (8) was extended by Poritsky (14) in 1953, who included a radial stiffness term in the oil-film representation. He also excluded from the oil-film forces the contributions arising from the negative pressures. Poritsky argued that the oil wouldnot be able to sustain negative pressures, and would cavitate and foam releasing dissolved air and oil vapour. Considering only small displacements he concluded that a rotor is stable below twice the critical speed. Poritsky also studied the effect of support flexibility and showed that it would reduce system critical speed and hence reduce the threshold of instability.

Earlier in 1949 Cameron and Wood (15) investigated a boundary condition at the cavitation region postulated by Swift and Steber, which today is widely used. They argued that for the correct boundary conditions at cavitation both oil-film pressure and oil-film pressure gradient must be zero. They obtained pressure distributions satisfying these conditions, and determined the axial leakage of oil due to the finite length of bearings.

In 1955 Pinkus (16) conducted an extensive and interesting experimental investigation of oil-film whip in flexible rotors supported by various bearing arrangements. He carried out his tests using two rotors. One of these had a central mass and the total rotor mass was 187lb (85Kg). It had a first critical at approximately 4000 RPM. The second rotor was lighter and had a mass of 67lb (30.45Kg), and had a first critical at 6100RPM. Listed below are Pinkus's major conclusions:

(1) Rotor whip occurred at speeds approximately equal to twice the first natural critical frequency of the shaft.

(2) The frequency of instability beyond the threshold is constant and equal to the first natural critical frequency of the shaft.

(3) With the heavy rotor whip motion stopped at speeds almost equal to three times the first critical.

(4) With the light rotor whip motion could not be stopped.

(5) Rotor unbalance had an insignificant effect on stability.

(6) High loads, high viscosities and a loose bearing housing promoted stability.

(7) Bearing asymmetry was beneficial for stability.

(8) The order of bearing stability, starting with the least stable: plain circular, three groove, elliptical or two-lobe, pressure, tilting pad and three-lobe.

Tondi (17) also confirmed Pinkus's findings that a loose bearing improves stability. He concluded that "bearings with a flexible-element loose bushing are of all the bearings tested undisputably the most resistant to the initiation of self-excited vibrations".

Hori (18) provided a combined theoretical and experimental investigation of oil-whip in 1959. Hori neglected negative pressures and assumed an infinitely long bearing. His analysis was divided into two categories, that is, small and large amplitudes of the journal. A small amplitude vibration is one in which the amplitude of the journal movement is small when compared with the journals eccentricity. Large amplitudes are those for which the shaft bends by a considerable amount.

For small amplitudes the motion of the two journals were considered as identical, and alignment of the shaft and bearings was assumed. Instability was discussed for lightly and heavily loaded bearings as shaft speed was increased from zero. Hori stated that a light rotor could become unstable at speeds below the first critical. However, the amplitude would not build up until the shaft speed exceeded twice the critical speed. He also observed mild whirl before the onset of whip for lightly loaded bearings. Hori concluded that large amplitude vibrations could exist only above twice the critical speed. For both light and heavy bearing loads he predicted that stable operation would be obtained for static eccentricities greater than 0.82. The effects of viscosity on stability were also discussed.

Pinkus (16) also observed mild whirl before the severe vibration associated with whip commenced. Newkirk and Lewis (19) and Newkirk (20) reported from their observations that whirl occasionally occurred simultaneously with whip, but only above twice the critical speed. They found it to be moderately severe, but unlike whip did not build up in amplitude and tended to be erratic.

Newkirk (20) differentiated between the effects of stiff and flexible rotors from observations based on his experimental work. With a stiff rotor he argued that the flexibility of the oil-film would dominate the system, and that for a lightly loaded rotor half frequency whirl could occur. In contrast using a flexible rotor with stiffness less than that of the oil-film would result in a rotor dominated system with the possibility of whip occurring.

A series of papers written in 1959 by Bishop (21), Bishop and Gladwell (22) and Gladwell and Bishop (23), (24) deal with the rotation of flexible shafts. These papers provide a basis for the investigation of rotor-beairng systems. They are mainly concerned with rigid or ideal bearings, but include some discussion on flexible supports. The authors developed expressions for the receptance of uniform and non-uniform beams, and by matching beam and rotor receptance were able to conduct stability analysis.

During the late 1950's several authors published work on the subject of bearing coefficients. Sternlicht (25) derived the coefficients numerically, whereas Hagg and Sankey (26) conducted experimental measurements for different types of oil-film bearings.

Holmes (27) was the first to derive all eight coefficients analytically in 1960. He used the short bearing theory of Ocvirk to solve Reynolds equation and included cavitation of the oil-film. The bearing coefficients were derived by linearising the oil-film forces with respect to small amplitude motion of the journal about its equilibrium position. Holmes then examined the stability of a rigid rotor mounted on identical bearings using the Routh-Hurwitz criteria. He found that for eccentricities $\varepsilon > 0.75$ the system is always stable, and the system is stable for all values of ε if the non-dimensional stability parameter

$$F/mc\omega^2 > 0.17 \quad (1.1)$$

Morrison (28) examined theoretically the role of the oil-film coefficients on the response and stability of the Jeffcott rotor in 1962. He determined the coefficients for a short bearing in terms of the geometry of the static load locus, and used them for dynamic response and critical speed analysis. He pointed out that the velocity coefficients give rise to forces of the same order as those due to the displacement coefficients and, hence, were of equal importance in determining the critical speeds. Morrison used the Leonhard locus to ascertain the stability of the system. This locus can be used to indicate when the real part of the roots of the characteristic equation of motion becomes positive and, thus, when instability will occur.

In the same year as Morrison, Lund and Sternlicht (29) also conducted a theoretical investigation of the Jeffcott rotor mounted on oil-film bearings of L/D=1/2 and 1. They found that the action of the oil-film reduces the critical speed of the rotor by a substantial amount. They derived a non-dimensional force transmitted to the bearing pedestals and concluded that for maximum attenuation it was desirable to operate at low eccentricity. Low eccentricity, however, could adversely affect the stability of the system. They lumped the cross-coupled coefficients with the main coefficients, but the manner in which this is done is rather vague and their results are not general.

In 1965 Morton (30) contributed a paper on the dynamics of large turborotors mounted in journal bearings on flexible supports. The rotor-bearing model is represented by a system of second order differential equations of the form:

$$[M][\ddot{q}] + [C][\dot{q}] + [K][q] = [F(t)] \qquad (1.2)$$

where the column vector [q] represents the generalised co-ordinates of the rotor motion in the x and y directions. The coefficients of the matrices in equation (1.2) are obtained from the first three "pinned-pinned" modes. Solution of [q] is achieved by assuming harmonic motion and inverting the resulting dynamic stiffness matrix.

Morton extended his second order differential equation system to consider a non-isotropic rotor in non-isotropic bearings subject to unbalance and gravity forcing. He discussed the receptance approach to an isotropic rotor in non-isotropic bearings. Morton verified his assumption that three rotor modes are sufficient and provided receptance curves for the oil-film and pedestal combination.

Also in 1965 Gunter (31) made a comprehensive study of the field of synchronous and non-synchronous whirling. He took as his model the Jeffcott rotor mounted on flexible pedestals. He examined the effects of oil-film bearings on the synchronous behaviour of the rotor, but the majority of the work is concerned with rigid bearings on flexible supports. He included internal damping in his model and examined the system stability for damped symmetric and asymmetric support stiffness. He concluded that there was an optimum value of foundation damping to promote stability; excessive damping caused a reduction in stability. Symmetric support stiffness alone promoted instability unless damping was included, whereas, asymmetric support stiffness improved stability even in the absence of support damping. Gunter used his predictions to explain the experimental observations of Newkirk (4) and Newkirk and Taylor (5).

Again in the same year Lund (32) carried out a theoretical analysis on the instability of a flexible rotor constrained by gas bearings mounted on flexible damped supports. His model used plain cylindrical bearings and he derived frequency dependent spring and damping coefficients. He concluded that flexible undamped supports lowered the threshold. However, with support damping included, a significant increase in stability threshold was achieved.

In 1967 Lund and Saibel (33) considered a non-linear representation of fluid-film forces, the resulting non-linear differential equations were solved using an averaging method. They presented non-dimensional stability plots for cylindrical and concial whirl, and presented graphs for obtaining the parameters of limit cycles. Their non-linear analysis confirmed experimental observations that at high eccentricity values the whirl orbit limit cycles were crescent shaped and not elliptical. They also stated that the results of their non-dimensional analysis could be applied to flexible as well as rigid rotors.

In the same year, Lund and Orcutt (34) conducted an experimental and theoretical investigation of three configurations of a flexible rotor mounted in oil-film bearings. They used a recurrence method of analysis based on the technique of Phrol (35) to represent the elastic and inertia properties of the rotor-bearing system. The method incorporated the eight linearised stiffness and damping coefficients. Instead of using an approximated lumped mass method the authors used an exact distributed mass technique which included gyroscopic effects. Elliptical orbits were calculated at selected points along the rotor and compared with the corresponding measured values. In general, good agreement was obtained.

Lund and Orcutt examined the first three critical speeds of the rotor. The first two are associated with rigid body modes, that is, circular and conical synchronous whirl. The third critical speed corresponded to the first bending mode of the rotor. They concluded that for the first three critical speeds the omission of damping could lead to enormous errors. This conclusion was only true for the rigid body modes where bearing damping was effective in controlling the peak amplitudes and the position of the critical speed. The third critical speed was found to be uneffected by damping.

In 1968 Morton (36) discussed massive rotor-bearing systems with asymmetric coupling due to the bearings. He examined the undamped critical speeds and non-synchronous vibration, and related experimental results to the theoretical model formulated in his previous paper (30). Morton determined the undamped resonant frequencies by matching the real part of the oil-film impedance with the rotor impedance.

Using a similar method he predicted the stability threshold by plotting the locus of the real part of the bearing impedance for the ratio of Ω/ω (where Ω = whirl frequency and ω = shaft speed) at which the imaginary part of the bearing impedance becomes zero. He also plotted the undamped rotor impedence, and showed that the threshold occurred when the real part of the bearing impedance was equal and opposite to the rotor impedance. The overall system was then in a state of neutral stability.

Holmes and Parkins (37) investigated the unbalance response of a small turborotor in 1969. The rotor, which was assumed to be rigid was supported by journal bearings on elastic supports. The system equations were used to study the dynamics of the rotor-bearing configuration. Assuming harmonic motion the authors reduced the system equations to the form:

$$[K][q] = [F] \tag{1.3}$$

where [q] defines the horizontal and vertical co-ordinates of the system. Inversion of the dynamic stiffness matrix [K] enables equation (1.3) to be solved for [q].

Holmes and Parkins obtained the undamped natural frequencies of the system by impedance matching, and found them to be close in value with the theoretical critical speeds. Fairly good agreement was obtained between the experimental and theoretical critical speeds. They found that the oil-film damping resulted in a considerable reduction in the amplitudes of both symmetrical and asymmetrical modes of vibration. Theoretical values of amplitude were found to agree to within 50% with measured values.

Kikuchi (38) conducted an interesting theoretical and experimental investigation of unbalance response, which was published in 1970. He examined the steady-state response of three rotor-bearing configurations. Two of the rotors were supported by two journal bearings and each employed three shrink fitted discs. The third was supported by three journal bearings and utilised five shrink fitted discs.

Kikuchi (38) included in his analysis the moments arising from the static inclination of the journal within its bush. The bearing moments and forces within the oil-film were linearised with respect to the equilibrium position of the journal. Using short bearing theory, he derived expressions for the bearing forces in terms of eight linear and eight rotational coefficients, obtained using Taylor's expansion. The Transfer Matrix Method was used to analyse the response of the rotor-bearing system.

Kikuchi (38) obtained good agreement between predicted and measured steady-state amplitudes. For one case only 6% error was reported. When rotational coefficients were ignored, errors for the case of small bearing clearance increased to 70%. He concluded that the method of analysis produced good agreement with observations, particularly when the moments of the oil-film were included in the bearing representation.

In 1972 Kirk and Gunter (39) conducted a theoretical investigation of support flexibility and damping on the synchronous response of the Jeffcott rotor. They included the bearings in their analysis, and examined the conditions under which the support would act as a dynamic absorber at the critical speed. Plots of rotor and support amplitudes, phase angles and forces transmitted were produced.

These researchers concluded that if damping were neglected, support flexibility caused two critical speeds to occur. One critical was higher and the other was lower than the original critical on rigid supports. The critical speed response might be eliminated by having a low mass ratio (support mass/rotor mass) and flexible supports with optimum damping. Support mass ratio should be kept low to achieve minimum amplitude. Excessive support damping with low mass ratio could result in excessive forces transmitted.

Kirk and Gunter (39) examined the transient behaviour of the rotor. They concluded that the optimum damping based on the minimisation of steady-state response produced satisfactory response, that is, a rapid reduction of the initial transient motion and reduced forces transmitted.

Dostal, Roberts and Holmes (40) published an interesting paper in 1974, on the control of stability using an external damper on the shaft. The rotor consisted of a long flexible shaft mounted in two journal bearings. The Transfer Matrix technique was used to analyse the rotor-bearing system, which included internal and external damping. The bearings were represented by the eight dynamic coefficients.

Predictions of stability threshold were obtained using the Leonhard Locus method. They also used two other techniques to assess the system stability, so that a comparison could be made with the Leonhard Locus method.

One method involved matching the impedance of the rotor with that of the bearing and was similar to the method of Morton (36).

In the other technique the model representation of the system was subjected to a sinusoidal force, in which the frequency of the force was assumed to be close to the natural frequency of the system. If the system was assumed to be close to the borderline of instability, then it would have a small value of positive or negative damping and would temporarily act like a single degree of freedom system. By plotting the response to the forcing frequency in polar form (Kennedy and Pancu Plot) it was possible to determine the threshold of instability by observing the slope of the plot. If the slope was positive then the effective damping was negative, and if the slope was negative then the effective damping was positive. The threshold occurred where the slope changed from positive to negative.

Dostal (40) et al concluded that a small amount of external damping increased the stability threshold, and this effect became pronounced at high eccentricity. Thus, an external damper was a useful method of controlling stability, particularly when access to the shaft is possible. Instability onset speeds of two to three times the first critical speed were obtained by varying the operating conditions of the bearings. Good agreement between theory and experiment was obtained for the case of no external damper. Dostal et al found that the inclusion of internal damping in the theory was necessary to improve agreement when the external damper was used.

In the same year Lund (41) carried out an analysis of the stability and the damped critical speeds of a flexible rotor supported on fluid-film bearings. The analytical results were compared with those obtained from an industrial multistage compressor.

Lunds method of analysis was based on the techniques of Myklestad (42) and Phrol (35). But instead of using distributed mass to represent the rotor-bearing system as he had done in his previous paper (34), he adopted the simpler lumped mass method. With the later technique, which is an approximation when compared to the exact representation of distributed mass, sufficient number of stations must be taken to ensure adequate representation of the highest mode in the speed range of interest. The required number of stations is usually achieved by taking four or five stations times the highest mode of interest (i.e. four to five stations per node).

Also included in the analysis were internal hysteretic damping and aerodynamic forces. The bearings were represented by the eight linearised dynamic coefficients. Lund discussed the damped natural frequencies of the system and their usefulness in predicting critical speeds. He also pointed out that the method is useful for investigating the effects of the bearing and shaft parameters on the stability of the system.

Stability and damped critical speeds were also examined by Bansal and Kirk (43) in 1975. They used the Transfer Matrix technique (Myklestad-Phrol). They examined intershaft journal bearing instability in a dual rotor system, and looked at radial misalignment and its effect on stability. They produced a chart showing forwards and backwards whirl frequencies obtained from the eigen-values of the system, and demonstrated that gyroscopic effects caused this mode splitting. Bansal and Kirk showed that dynamic misalignment increased the instability onset speed, as does an increase in shaft stiffness.

Hahn (44) using linearised theory and the short bearing approximation generated design maps for flexible rotors. These maps indicated regions where operation should be avoided, and could be used to determine the effects of changing shaft speed, lubricant viscosity and bearing clearance. He concluded that:

(1) Increased flexibility lowered the stability threshold.
(2) Changing bearing clearance would not, in general, affect the location of critical speed resonance.
(3) Decrease in clearance decreased the damping at resonance.

Pollmann and Schwerdtfeger (45) wrote a paper which was published in 1976. In it they described experiments conducted on a test model which simulated a two pole 60Hz generator with an output of approximately 600MW. They introduced non-dimensional parameters L^*, D^*, η^*, ψ^* and ω_c^*. These represented rotor length, rotor diameter, oil viscosity, relative bearing clearance and eigen frequency ratio, respectively. The diameter and length of the rotor were reduced in the ratio of $D^*=5$, and $L^*=3$, respectively. By selecting η^* and ψ^*, it was possible to ensure that the operating characteristics (Sommerfeld Number and rotor flexibility = δ/c, where δ = static deflection and c = bearing radial clearance) were kept similar.

Pollmann examined the response and stability of four bearings. These were: a cylindrical bearing with two 30° axial feed grooves, a two-wedge bearing with two 30° axial feed grooves, a two-wedge bearing with a groove in the upper wedge, and a tilting pad bearing with five equal segments.

For the tilting pad bearing the resonance peaks for the first and second modes of vibration were found to be 60 and 112 times the unbalance radius, respectively. The two-wedge bearing with groove in the upper half had resonance peaks considerably smaller than the tilting pad bearing, and was approximately the same as the two-wedge bearing with axial grooves. The cylindrical bearing became unstable before the second mode, but had a resonance peak for the first mode similar to the two-wedge bearings.

Pollmann (45) ascertained system damping from the decay of shock induced vibration. After a shock the rotor vibrates in its lowest eigen frequency, and the attenuation (decay) constant can be determined from the amplitude plotted against time in logarithmic scale. This enables the stability of the system to be assessed.

The cylindrical bearing became unstable at approximately $\omega/\omega_{c1}=2.0$, where ω = rotation speed and ω_{c1} = critical speed without bearing influence. The two-wedge bearing with axial grooves became unstable at $\omega/\omega_{c1}=5.0$, and the two-wedge bearing with upper half groove and the tilting pad bearing were stable over the entire region ($0.0 \leqslant \omega/\omega_{c1} \leqslant 6.0$). For the two-wedge bearing with axial grooves, Pollmann observed that an increase in oil pressure increased the instability onset speed. Low frequency vibrations were also influenced by oil pressure.

An interesting experimental and theoretical investigation of rotor-bearing stability by Kikuchi and Kobayashi (46) was published in 1977. This work was an extension of Kikuchi's investigation of rotor-bearing response to unbalance (38). The authors again investigated three basic rotor-bearing systems. Two of the rotors comprised three discs on a shaft supported by two oil-film bearings. The third rotor comprised five discs on a shaft mounted on three bearing supports. The rotor with the three discs could be changed from a symmetric rotor to an unsymmetric rotor with overhung shaft. The effects of different L/D and c/R ratios were also examined.

They again included the eight rotational coefficients (38) as well as the eight linear coefficients, obtained using short bearing theory. The rotational coefficients were included to take into account the moments acting on the journal due to its inclination within the bearing bush. The stability of the system was assessed using the Transfer Matrix Method in conjunction with the Leonhard Locus Plot.

Kikuchi and Kobayashi concluded that for most shaft systems, the oil-film property of the bearing given by short bearing theory gives good agreement with measured values of instability onset speeds. In some shaft systems gyroscopic moments could have a pronounced effect on stability. Even for a high eccentricity of ε=0.8, a large disc gyroscopic moment could greatly reduce system stability. Bearing oil-film moment tended to increase the stability threshold, but the effect in most shaft systems was insignificant.

Akkok and Ettles (47) performed an interesting investigation of the effects of bearing load and oil supply feed pressure on the stability of a rigid test rotor with a grooved journal bearing. This work was presented in 1978. Comparison with linear theory was made using the dynamic coefficients and the Routh-Hurwitz criteria to assess the system stability. They investigated the effects of sub-ambient as well as ambient cavitation boundary conditions, and the effects of increased feed pressure on the instability speed in their theoretical analysis.

From a comparison of measured instability onset speeds with calculated values, Akkok and Ettles found that the Reynolds boundary condition implying cavitation at ambient pressure appeared to apply, regardless of the bearing load. Reduction in bearing load had no significant effect on measured instability speeds. This was confirmed using Reynolds boundary condition. Reduction in feed pressure enhanced stability. Slight unbalance had little effect on the stability threshold, but could effect the way in which whirl appeared.

In contrast to the above work Cole (48) had found from his work on film extent in a rigid rotor with a glass bush, that increased oil pressure supply helped to stabilise the bearing but no attempt was made to pursue the matter any further. He also observed that the position of the oil groove had an effect on stability. If the groove was positioned in the inlet region of the oil-film, then enhanced stability was obtained, whereas, if the groove was positioned in the outlet region decreased stability was observed. Cole did not examine the effect of increased oil supply pressure in conjunction with groove position.

Akkok and Ettles (47) observation that increased oil pressure destabilised their rigid rotor had been noted by other researchers. Pinkus (16) and Pope (49) reported similar findings from their work with flexible rotors. Pollmann (45) and Newkirk and Lewis (19) reported similar conclusions to those of Cole (48), from their investigations with flexible rotors. Apart from Pollmann's reported findings for a two-lobe bearing, no detailed experimental work and correlation with theoretical analysis has been conducted on the oil supply pressure and its effects on the stability of a flexible rotor.

In 1979 Akkok and Ettles (50) examined theoretically the effects of groove size and bore shape on the stability of a rigid rotor. As in their previous paper (47), linear theory was used to predict stability thresholds. The dynamic coefficients representing the various groove sizes and bore shapes were obtained from a finite difference solution of Reynolds equation. The Routh-Hurwitz criteria was used to assess system stability.

Akkok and Ettles concluded that increased groove angle α had a strong destabilising effect, as does an increase in the aspect ratio L/D. A stabilising effect is obtained by increasing the bearing preload Δ, and all bearing types exhibited higher thresholds at large values of eccentricity ε. For fixed values of α, Δ and L/D, the bore shapes in increasing order of stability were found to be: circular, two-lobe, offset halves and three lobe.

Akkok (51) confirmed experimentally the findings of his earlier paper (50), of the effect on stability of groove angle and bearing preload. He also confirmed the increasing order of stability for circular, two-lobe and offset halves bore shapes.

Very little work has been published concerning the effect of feed groove extent on stability. Experimental and theoretical work conducted in (50) and (51), described the effects of feed groove extent on the stability of rigid rotors. Hagg and Warner (13) carried out an investigation of the effects on stability of the extent of the partial arc circular bearings supporting a flexible rotor. Tests were conducted for a full circular bearing and 160^{o} partial bearing, both with an L/D aspect ratio of 1.25. However, they compared their results with calculated stability curves for a 120^{o} partial bearing with L/D=1. Gyroscopic effects were also ignored, and these are known to have a pronounced affect on stability for some rotor-bearing systems (46).

In 1978 Tonnesen and Lund (52) conducted experiments on system stability for two rotors, weighing 88lb (40Kg) and 412.5lb (187.5Kg) respectively. The rotors were supported in cylindrical bearings with two axial grooves. The diameters of the journals were 2.46in (62.7mm), the L/D ratio was 0.3 and the radial clearance was 0.0022in (0.055mm). The lighter rotor was basically a uniform shaft with a bearing span of 34.6in (880mm) and diameter of 3.15in

(80mm). The second rotor contained six heavy discs, shrink fitted to the shaft. It had the same bearing span and shaft diameter as the lighter rotor. The heavier rotor contained an overhung disc, and experiments were conducted with and without this disc in place. The bearing supports of the heavier rotor could be changed to flexible supports, and contained a facility so that they could be operated as squeeze film damper bearings. By means of pressure tappings, Lund and Tonnesen were able to measure static and dynamic pressures at two locations in the bottom half of the bearing, 15° either side of the vertical and in the mid-plane. They stated that the pressure readings obtained, were more sensitive to the different frequencies excited than the capacitance probes used to monitor shaft vibration.

Lund and Tonnesen used the linear method of analysis given in (41) to predict the behaviour of the rotor-bearing system. The eight dynamic coefficients for the axial groove bearing were obtained by numerical solution of Reynolds equation. The coefficients were derived as functions of the Sommerfeld Number, and, hence, vary with speed and viscosity as the oil becomes hotter. They obtained instability thresholds by examining the sign of the logarithmic decrement. This indicated the system damping in terms of decay (stable) or growth (unstable) of the response to self-excitation.

They concluded that the flexible support with damping allowed the rotor to be operated up to its maximum speed of 20,000 RPM without instability occurring. Predictions of damped natural frequencies and instability onset speeds were in good agreement with experimental findings. They found that unbalance could excite the damped natural frequencies of the sytem. Unbalance could also initiate self-excited whirl with the result that the threshold was lowered. This contradicted the observations of (4), (5), (16), (47) and Tondl (53).

Lund and Tonnesen (52) remarked on the problem of modelling the system and obtaining accurate values of the spring and damping coefficients which correspond to the operating conditions of the bearings. They found that as the shaft speed was increased, an increase in the discrepancy between the measured position of the journal and its calculated position occurred.

Although they examined the effect of a flexible support on the damped natural frequencies and the stability of their rotor-bearing systems; they did not conduct a systematic investigation of pedestal flexibility since their support had a fixed stiffness.

In the last 28 years a considerable amount of effort has been devoted to examining the effect of fluid film bearings on critical speeds and instability thresholds e.g. (16), (18), (19), (29), (41), (43), (44), (45), (46) and (53). However, less attention has been given to the effect of support or pedestal flexibility on the critical speeds and the system stability. Generally, the work undertaken has been either experimental in nature e.g. (4), (5), (16) and (17), or theoretical e.g. (10), (14), (31), (32) and (39). Papers (4), (10) and (31) were concerned with flexible rotors mounted on ideal or rigid bearings on flexible pedestals, and therefore neglected the bearings. Tondl (53) conducted experimental and theoretical work, but he restricted his experiments to a rotor mounted in rolling element bearings on flexible pedestals. Holmes and Parkins (37) included pedestal and bearing flexibility, but limited their investigations to a rigid rotor.

Lanes, Flack and Lewis (54) conducted an investigation into the stability and response of a flexible rotor mounted in three types of journal bearings, the results of which were published in 1981. The rotor contained three discs mounted on a shaft of length 21in (533.4mm) and with a maximum diameter of 1in (25.4mm) and a minimum diameter of 0.75in (19.1mm). The combined mass of the shaft and discs was 29.8lb (13.55Kg). The rotor-bearing system had first and second critical speeds (bending modes) at 2550 RPM and 9800 RPM, respectively. The three bearings tested were axial groove, three-lobe and pressure-dam, with different L/D and c/R ratios. The bearings were interchangeable, and were mounted in pedestals on top of oil-filled and temperature-controlled reservoirs. By rotating the bearings within their pedestals, Lanes et al were able to examine the effect of groove position on response and stability.

They observed that all the bearings exhibited instability due to whip, the frequency of which corresponded to the first critical speed. The threshold speed of the pressure-dam bearing was slightly higher than the axial groove bearing. The three-lobe bearing had the highest instability threshold, and allowed the rotor to operate above its second critical speed. They found that groove position had an important effect on the response and stability of the axial groove and three-lobe bearings. A groove angle position of 75° (with respect to the load direction) resulted in minimum response and maximum threshold speed for both bearing types. They remarked that experimental stability threshold values were significantly higher than predicted (16% to 37%) for all bearing types and discussed possible reasons.

1.4 OUTLINE OF THESIS

In Chapter 2, the solution of the Reynolds equation for fluid-film bearings using a finite difference procedure is presented. The eight linear dynamic coefficients representing the stiffness and damping properties of the fluid-film are obtained from perturbation of the journal from its equilibrium position.

Chapter 3 describes the Tranfer Matrix technique by which the dynamics of the rotor-bearing system are studied. The properties of the fluid-film bearings are included in the Transfer Matrix analysis.

Chapter 4 is concerned with a description of the design and commissioning of the experimental apparatus. Details of instrumentation used and the adopted experimental procedure are given.

In Chapter 5, comparisons between measured and predicted critical speeds for rigid and flexible pedestals are presented. Results for the response of the rotor-bearing system are also given. The results are discussed and reasons are given for some of the discrepancies.

Chapter 6 is concerned with an investigation of the rotor-bearing system stability for rigid and flexible pedestals. The method of obtaining the system stability using the Leonhard Locus Plot is described. Results are presented for the effects on the threshold of stability of hysteresis, bearing feed pressure, feed groove extent, and position of feed groove with respect to the inlet and outlet film regions. The results are discussed and comparison is made with predicted values. Reasons for departure from predicted values and some investigations are presented.

Finally, in Chapter 7 overall conclusions are presented and suggestions for further investigations are made.

CHAPTER 2

DYNAMICALLY LOADED JOURNAL BEARINGS

2.1 INTRODUCTION

This chapter describes the form of the Reynolds equation which is solved to obtain the eight linearised dynamic coefficients, which are subsequently used to represent the dynamic properties of oil-film for rotor-bearing system (Chapter 3).

Brief details are given of how Reynolds equation is solved using a finite difference procedure, the boundary conditions applied and the method of obtaining the dynamic coefficients from theoretical incremental perturbation of the journal..

2.2 REYNOLDS EQUATION

2.2.1 Reynolds Equation in Non-Dimensional Form

The full form of the Reynolds equation for a dynamically loaded journal bearing, shown in Figure 2.1 is fully derived in the textbooks of Cameron (55) and Pinkus and Sternlicht (56), and is given for an isoviscous lubricant as (it is assumed that the viscosity can be treated as an effective uniform viscosity at the operating condition):

$$\frac{\partial}{\partial x}\left(h3\frac{\partial P}{\partial x}\right)+\frac{\partial}{\partial z}\left(h3\frac{\partial P}{\partial z}\right)=6\eta\left[(\omega-2\frac{d\phi}{dt})\,R\frac{dh}{dx}+2\frac{de}{dt}\cos\theta\right] \quad (2.1)$$

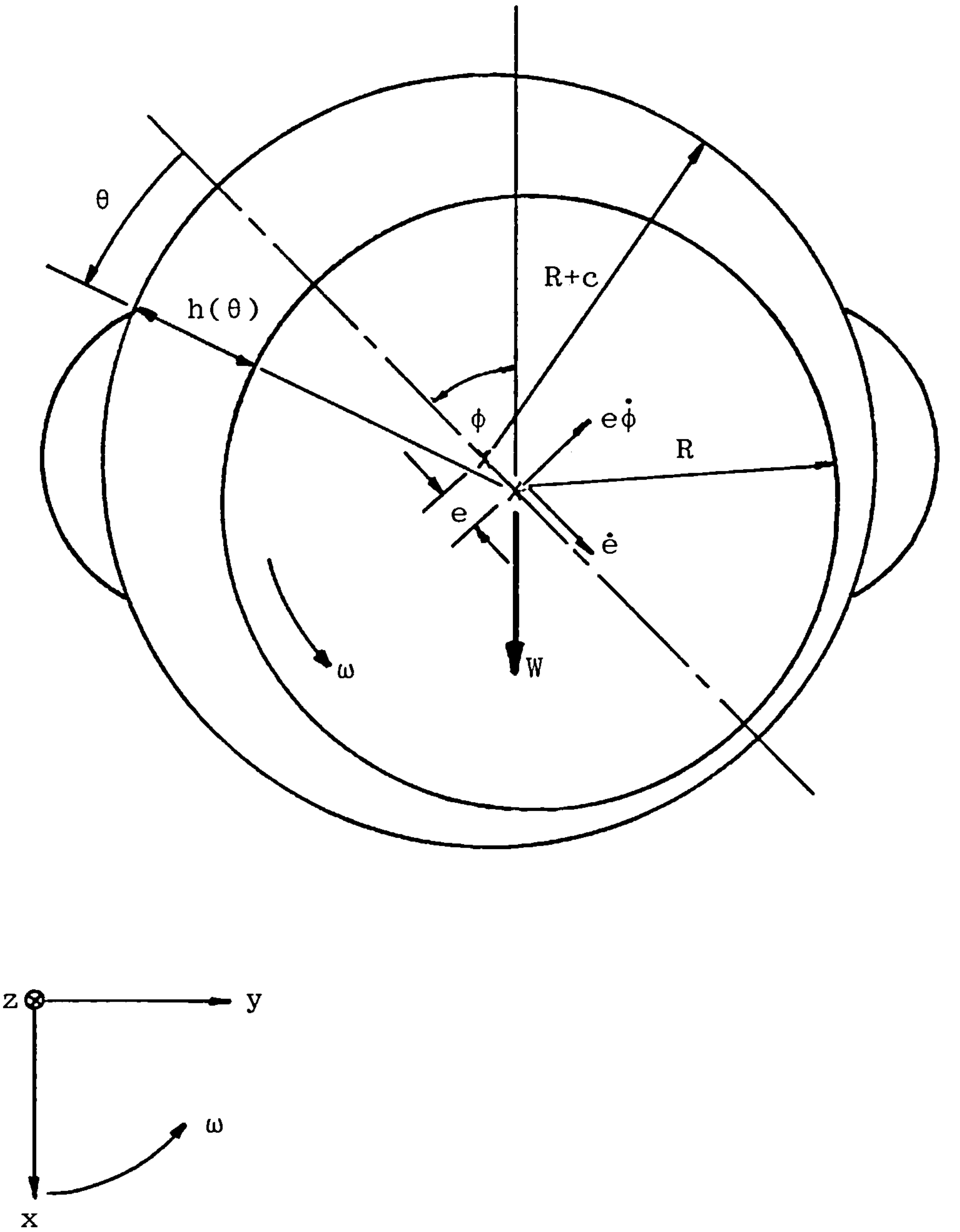

Figure 2.1 Dynamically Loaded Journal Bearing

It is convenient to use the non-dimensional form of the equation in order to maintain the generality of the solution. Introducing the following non-dimensional variables:

$$\theta = \frac{x}{R} \tag{2.2}$$

$$z^* = \frac{z}{L/2} \tag{2.3}$$

$$h^* = \frac{h}{c} \tag{2.4}$$

where film thickness, h, is given by:

$$h = c + e\cos\theta \tag{2.5}$$

and c is the radial clearance

$$\varepsilon = \frac{e}{c} \tag{2.6}$$

$$\dot{\varepsilon} = \frac{1}{\omega}\frac{d\varepsilon}{dt} \tag{2.7}$$

$$\dot{\phi} = \frac{1}{\omega}\frac{d\phi}{dt} \tag{2.8}$$

$$P^* = \frac{P}{6\omega\eta(R/c)^2} \tag{2.9}$$

into equation (2.1) gives the following non-dimensional form of the Reynolds equation

$$\frac{\partial}{\partial\theta}\left(h^{*3}\frac{\partial P^*}{\partial\theta}\right) + \left(\frac{D}{L}\right)^2 h^{*3}\frac{\partial^2 P^*}{\partial z^{*2}} = -\varepsilon\,(0.5-\dot{\phi})\sin\theta + \dot{\varepsilon}\cos\theta \tag{2.10}$$

2.2.2 Boundary Conditions at Feed Grooves

The boundary conditions for a bearing with axial grooves are (dropping the * from equation (2.10)):

$$P(\theta_{in},z) = P(\theta_{out},z) = 0 \qquad (2.11)$$

$$P(\theta,1) = P(\theta,-1) = 0 \qquad (2.12)$$

For the case where the feed pressure is increased significantly above zero gauge pressure (ambient pressure), a non-dimensional feed pressure ratio, γ , is defined such that (see Appendix A for derivation):

$$P_f = 0.5\ \gamma\ F \qquad (2.13)$$

where P_f is the non-dimensional feed pressure and F is the non-dimensional bearing load.

Hence equation (2.11) may be written as:

$$P(\theta_{in},Z) = P(\theta_{out},Z) = P_f \qquad (2.14)$$

2.2.3 Cavitation Boundary Conditions

Cavitation was allowed for by setting all negative pressures to zero as they were generated. This condition is known as the Reynolds boundary condition and is defined mathematically as:

$$\frac{\partial P}{\partial \zeta} = 0 \quad \text{when } P = 0 \qquad (2.15)$$

at the cavitation boundary of the oil-film, where ζ is a co-ordinate in the θ-z surface, normal to the cavitation boundary.

When the pressure distribution, which is a function of the bearing bore geometry, aspect ratio, eccentricity and feed pressure, is obtained, the steady-state and dynamic characteristics of the oil-film can be computed.

2.2.4 Finite Difference Solution of Reynolds Equation

The Reynolds equation (2.10) was solved using a two-dimensional finite difference procedure (see Appendix B).

The mesh size used in the computations was 72 divisions circumferentially and 10 divisions axially for half the bearing.

The Gauss-Seidel iteration method was applied to the finite difference equation and the following convergence limit was imposed which had to be satisfied before the termination of the iterative procedure:

$$\sum\sum\left(\frac{P_{ij}{}^{k} - P_{ij}{}^{k-1}}{P_{ij}{}^{k}}\right) \leqslant 10^{-6} \qquad (2.16)$$

2.3 THE STEADY-STATE CHARACTERISTICS OF AN OIL-FILM

2.3.1 Dimensional Form of the Oil-Film Forces

The principal steady-state characteristics are the bearing load capacity and attitude angle for a given eccentricity.

With the chosen bearing geometry with axial grooves, the eccentricity and attitude angle are preset and a solution of the Reynolds equation (2.10) for steady-state conditions (ie: $\dot{\varepsilon} = \dot{\phi} = 0$) gives the pressure distribution generated in the wedge.

The oil film forces F_ε and F_ϕ along and perpendicular to the line of centres respectively (see Figure 2.1) are obtained by integration as follows:

$$F_\varepsilon = \int_{-L/2}^{L/2} \int_0^{2\pi} P\cos\theta(Rd\theta)dz \qquad (2.17)$$

$$F_\phi = \int_{-L/2}^{L/2} \int_0^{2\pi} P\sin\theta(Rd\theta)dz \qquad (2.18)$$

2.3.2 Non-Dimensional Form of the Oil-Film Forces

By the use of the non-dimensional variables defined in equations (2.2) to (2.9), the following non-dimensional oil-film forces may be written:

$$F_\varepsilon^* = \frac{F_\varepsilon/LR}{6\omega\eta(R/c)^2} = \int_0^1 \int_0^{2\pi} P^*\cos\theta d\theta dz^* \qquad (2.19)$$

$$F_\phi^* = \frac{F_\varepsilon/LR}{6\omega\eta(R/c)^2} = \int_0^1 \int_0^{2\pi} P^*\sin\theta d\theta dz^* \qquad (2.20)$$

and the attitude angle in centrally loaded bearings (as shown in Figure 2.1) is:

$$\phi = \tan^{-1}\left(- \frac{F_{\phi}^{*}}{F_{\varepsilon}^{*}} \right) \qquad (2.21)$$

Having obtained an accurate attitude angle, ϕ^{k}, it is possible to compute a new ϕ^{k+1} from a similar procedure. This iterative process may converge slowly. Hence, a relaxation factor greater than 1.0 can be employed to increase the convergence rate.

In the computer programme for the bearings, Appendix C, a relaxation factor of 0.5 was used. Although under-relaxation of the attitude angle resulted in slower convergence, it was found to be more appropriate for a wider range of eccentricity (ε), feed pressure ratio (γ) and groove angle (α).

An over-relaxation factor of 1.8 was used in the convergence of the pressure distribution around the bearing (Section 2.2.4), and it was found to apply for all the values of ε, γ and α that were considered.

A sufficient condition for convergence of the attitude angle was set as $\left|\phi^{k+1} - \phi^{k}\right| \leqslant 0.001^{\circ}$. This process locates the shaft at the correct equilibrium position (steady-state running position) where all the forces in the horizontal direction are zero. Then, for this position, the load capacity can be expressed in terms of the Sommerfield number as:

$$S = \frac{P_b}{N\eta}\left(\frac{c}{R}\right)^2 = 6\pi\,(F_\varepsilon{*}{*}2 + F_\phi{*}{*}2)0.5 \qquad (2.22)$$

where P_b = projected bearing load = W/LD

The forces in the polar co-ordinate system are related to the forces in the cartesian co-ordinated system as follows:

$$\begin{bmatrix} F_x \\ F_y \end{bmatrix} = \begin{bmatrix} \cos\phi & -\sin\phi \\ \sin\phi & \cos\phi \end{bmatrix} \begin{bmatrix} F_\varepsilon \\ F_\phi \end{bmatrix} \qquad (2.23)$$

2.4 DYNAMIC CHARACTERISTICS OF AN OIL-FILM

2.4.1 Dynamic Coefficient Representation of an Oil-Film

The hydrodynamic oil-film forces, obtained from equations (2.19) and (2.20), computed from the Reynolds equation (2.10) is a non-linear function of the eccentricity, the attitude angle, and the corresponding velocity components.

If the journal is in motion at the co-ordinates (x,y) around the equilibrium position, then the dynamic part of the oil-film can be linearised for small amplitude motion. This can be achieved by the first order Taylor expansion of the film force about the equilibrium (steady-state) position. The dynamic part of the film force can be expressed as:

$$\Delta f_x = - k_{xx} x - k_{xy} y - c_{xx} \dot{x} - c_{xy} \dot{y} \qquad (2.24)$$

$$\Delta f_y = - k_{yx} x - k_{yy} y - c_{yx} \dot{x} - c_{yy} \dot{y} \qquad (2.25)$$

where the oil-film stiffness coefficients are defined as:

$$k_{xx} = - \frac{\partial f_x}{\partial x} \qquad (2.26a)$$

$$k_{xy} = - \frac{\partial f_x}{\partial y} \qquad (2.26b)$$

$$k_{yx} = - \frac{\partial f_y}{\partial x} \qquad (2.26c)$$

$$k_{yy} = - \frac{\partial f_y}{\partial y} \qquad (2.26d)$$

and the damping coefficients are defined as:

$$c_{xx} = - \frac{\partial f_x}{\partial \dot{x}} \qquad (2.27a)$$

$$c_{xy} = - \frac{\partial f_x}{\partial \dot{y}} \qquad (2.27b)$$

$$c_{yx} = - \frac{\partial f_y}{\partial \dot{x}} \qquad (2.27c)$$

$$c_{yy} = - \frac{\partial f_y}{\partial \dot{y}} \qquad (2.27d)$$

where f_x and f_y are the components of the fluid-film force.

The first index of the coefficients indicates the direction of the fluid film force and the second index indicates the direction of the perturbation.

In general, due to the anisotropy of the oil-film, the direction of the perturbation is not colinear with that of the disturbing force. Therefore, the cross-coupling terms are introduced.

2.4.2 Non-dimensional Form of the dynamic coefficients

In rotor bearing dynamic analysis, it is common practice to non-dimensionalise the oil-film force with the steady load (static reaction of the weight of the rotor on the journal).

This is achieved by introducing the following non-dimensional variables:

$$x^* = \frac{x}{c} \tag{2.28a}$$

$$y^* = \frac{y}{c} \tag{2.28b}$$

$$\dot{x}^* = \frac{\dot{x}}{c\omega} \tag{2.28c}$$

$$\dot{y}^* = \frac{\dot{y}}{c\omega} \tag{2.28d}$$

$$\Delta F_x = \frac{\Delta f_x}{W} \tag{2.29a}$$

$$\Delta F_y = \frac{\Delta f_y}{W} \tag{2.29b}$$

$$F_x' = \frac{f_x}{W} \tag{2.30a}$$

$$F_y' = \frac{f_y}{W} \tag{2.30b}$$

and the non-dimensional coefficients are expressed as:

$$K_{xx} = k_{xx}\frac{c}{W} = -\frac{\partial F_x'}{\partial x^*} \tag{2.31a}$$

$$K_{xy} = k_{xy}\frac{c}{W} = -\frac{\partial F_x'}{\partial y^*} \tag{2.31b}$$

$$K_{yx} = k_{yx}\frac{c}{W} = -\frac{\partial F_y'}{\partial x^*} \tag{2.31c}$$

$$K_{yy} = k_{yy}\frac{c}{W} = -\frac{\partial F_y'}{\partial y^*} \tag{2.31d}$$

$$C_{xx} = c_{xx}\frac{\omega c}{W} = -\frac{\partial F_x'}{\partial \dot{x}^*} \tag{2.32a}$$

$$C_{xy} = c_{xy}\frac{\omega c}{W} = -\frac{\partial F_x'}{\partial \dot{y}^*} \tag{2.32b}$$

$$C_{yx} = c_{yx}\frac{\omega c}{W} = -\frac{\partial F_y'}{\partial \dot{x}^*} \tag{2.32c}$$

$$C_{yy} = c_{yy}\frac{\omega c}{W} = -\frac{\partial F_y'}{\partial \dot{y}^*} \tag{2.32d}$$

Equations (2.24) and (2.25) can now be expressed in the form:

$$\begin{bmatrix} \Delta F_x \\ \Delta F_y \end{bmatrix} = -\begin{bmatrix} K_{xx} & K_{xy} \\ K_{yx} & K_{yy} \end{bmatrix}\begin{bmatrix} x^* \\ y^* \end{bmatrix} - \begin{bmatrix} C_{xx} & C_{xy} \\ C_{yx} & C_{yy} \end{bmatrix}\begin{bmatrix} \dot{x}^* \\ \dot{y}^* \end{bmatrix} \tag{2.33}$$

2.5 COMPUTATIONAL METHOD OF DERIVING COEFFICIENTS

The linearised dynamic coefficients of the oil film are obtained from the perturbation solution of the Reynolds equation (2.10). Small perturbations in displacement and velocity about the equilibrium journal position give the incremental fluid-film forces which are used to calculate the coefficients defined in equations (2.31) and (2.32).

2.5.1 Stiffness Coefficients

For the computation of the stiffness coefficients, the journal centre is displaced form its equilibrium locus position, J_o, to a disturbed position, J_1, in the y-direction, as shown in Figure 2.2, where the journal is in equilibrium, i.e. $\dot{x}^* = \dot{y}^* = 0$. Then, the fluid-film force at the disturbed position for the eccentricity ratio of ε is the same as that for the journal at J_2 on the equilibrium locus, where $o_B\ J_2$ represents an eccentricity ratio equal to ε.

The direction of the force is inclined from the vertical load direction by an angle ψ. Then, the additional oil-film forces are:

$$\Delta F_x' = F'\cos\psi - 1 \qquad (2.34a)$$

$$\Delta F_y' = F'\sin\psi \qquad (2.34b)$$

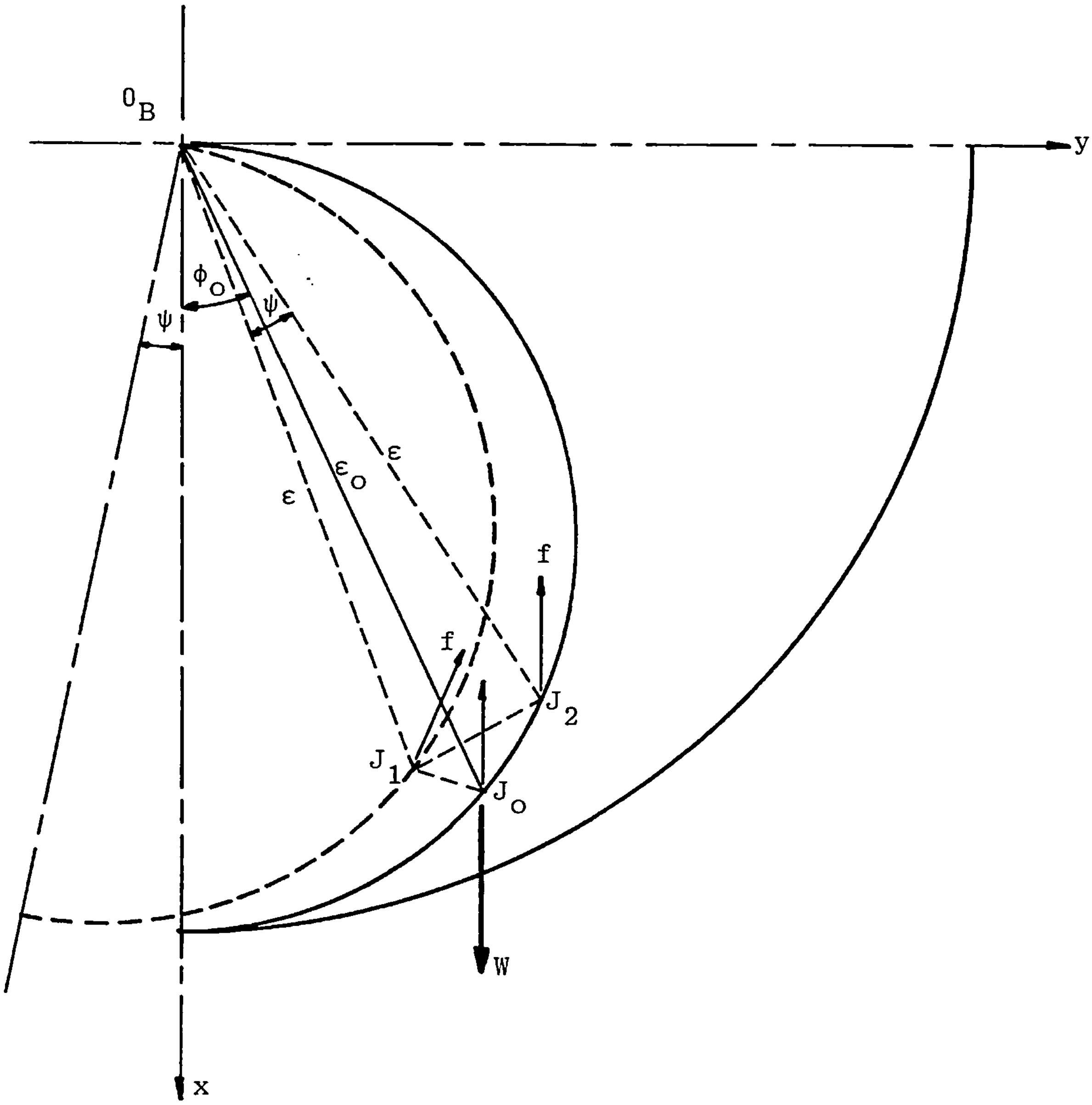

Figure 2.2 Oil-Film Forces at the Displaced Journal Position

The corresponding stiffness coefficients are:

$$K_{xy} = -\frac{\partial F_x'}{\partial y^*} = -\frac{\Delta F_x'}{y^*} \quad x^* = \dot{x}^* = \dot{y}^* = 0 \qquad (2.35a)$$

$$K_{yy} = -\frac{\partial F_y'}{\partial y^*} = -\frac{\Delta F_y'}{y^*} \quad x^* = \dot{x}^* = \dot{y}^* = 0 \qquad (2.35b)$$

Similiarly, by a small displacement in the x-direction and calculation of the additional film force components gives the other two stiffness coefficients K_{xx} and K_{yx}.

2.5.2 Damping Coefficients

For the computation of the damping coefficients, the journal is given small velocities in the x-direction and the y-direction in turn, from the equilibrium position, ie $x^* = y^* = 0$.

The velocity components along the line of centres and normal to it are calculated from the following transformation:

$$\begin{bmatrix} \dot{\varepsilon} \\ \dot{\phi} \end{bmatrix} = \begin{bmatrix} \cos\phi & \sin\phi \\ -\dfrac{\sin\phi}{\varepsilon} & \dfrac{\cos\phi}{\varepsilon} \end{bmatrix} \begin{bmatrix} \dot{x}^* \\ \dot{y}^* \end{bmatrix} \qquad (2.36)$$

The Reynolds equation (2.10) is solved with these velocity components and the resulting additional film force components are used to calculate the damping coefficients given in equations (2.32).

In the computation of the linearised dynamic coefficients by direct perturbations of the journal position and velocity, the magnitude of perturbations were found to be immaterial provided these were small.

In the present research, the non-dimensional displacement and velocity perturbations were set at 0.001.

CHAPTER 3

TRANSFER MATRIX REPRESENTATION OF ROTOR-BEARING SYSTEMS

3.1 INTRODUCTION

The principle of the Transfer Matrix Method (TMM) is derived from the numerical method originally developed by Holzer for solving torsional problems and later developed by Myklestad (42) and Prohl (35). Myklestad applied the technique to obtaining the modes of vibration of aeroplane wings and Prohl applied it to finding the natural frequencies of beams and shafts. The more familiar form of the TMM was introduced by Thomson (57) for the study of the vibration of beams. The method is now fully documentated in the excellent book by Pestel and Leckie (58).

In 1970 the method was extensively developed by Ruhl (59) for rotor-bearing systems. Ruhl presented a thorough study of the TMM and also the finite element technique, and compared the accuracy of the two methods for calculating the stability and response of uniform elastic massive rotors and elastic rotors with descrete mass at mid-span.

Lund (41) and Lund and Orcutt (34) also used the TMM. In (34) a distributed mass technique was used to study the response to unbalance of a flexible rotor and comparison of results with experiment was made. A lumped mass method was used in (41) to compare the theory with experiment for the analysis of critical speed and stability of a flexible rotor.

Bansal and Kirk (43) in 1975 derived the damped critical speeds and stability of rotor-bearing systems using the TMM. They compared the results of (41) for a uniform rotor mounted on fluid-film bearings with an L/D of 1/4, and obtained agreement of predicted instability to within 0.5%. They also examined the effects of misalignment on stability of multi-spool turbo engines.

Dostal (60) and Dostal et al (40) used the method in the study of the control of the unbalance response and stability of a long flexible shaft, by the use of an external damper mounted on the shaft.

Kikuchi (38) used the TMM for the analysis of the unbalance response of rotor-bearing systems containing several discs and bearings and compared results with those obtained from different types of experimental rotors. Kikuchi and Kobayashi (46) extended their previous work (38), to examine the stability of rotors with several discs and bearings.

More recently Ruddy (61) used the TMM and compared it with the finite element method, to examine the accuracy of both techniques for computing the three lowest natural frequencies of a simply supported beam.

The general approach to this method is to divide a system consisting of a shaft supported on bearings and carrying flywheels, impellers etc; into a number of elements with simple elastic and dynamic properties which can be expressed in matrix form. Thus, the variables (referred to as state variables and expressed in the form of generalised deflections and forces) fully describing a state at one end of the element are expressed as a linear combination of the state variables at the other end. The matrix so obtained is called the Transfer Matrix (TM).

Since the size of the TM depends on the number of variables in the state vector and not on the number of elements, the TMM is ideally suited for systems with a predominantly chain character.

To assemble the elements of the system it is only necessary to multiply all the element matrices together. This generates the overall TM of the system, which expresses the generalised forces and deflections at one end of the system as a linear combination of the generalised forces and deflections at the other end.

By applying boundary conditions to these equations the frequency determinant can be formulated. In the case of synchronous vibration ($\omega = \Omega$) the frequency determinant is zero at every natural frequency of the system. For non-synchronous vibration ($\omega \neq \Omega$) the locus of the frequency determinant in the complex plane (Leonhard Locus) enables the stability of the system to be assessed.

3.2 MATHEMATICAL MODEL OF ROTOR-BEARING SYSTEM

3.2.1 Lumped Parameter Approximation

A rotor-bearing system is basically one with distributed parameters, but for the purposes of computation it is convenient to replace it with an approximately equivalent system having a finite number of degrees of freedom.

Thus, a continuous rotor can be modelled as a system with n-degrees of freedom by dividing the rotor into n-lumped rigid masses located at n-stations and connected by massless elastic beam or shaft elements of uniform stiffness.

A more complex and accurate form of mass distribution can be used, but this is seldom done because of the greater complexity involved.

3.2.2 Co-ordinate System Representation

In Figure 3.1 is shown an analytical model representing a uniform rotor supported on oil-film bearings which in turn are supported on flexible pedestals. A more detailed representation of the bearing and pedestal model is shown in Figure 3.8 and is explained in more detail in Section 3.3.4, where the TM representation of the bearing-pedestal is developed.

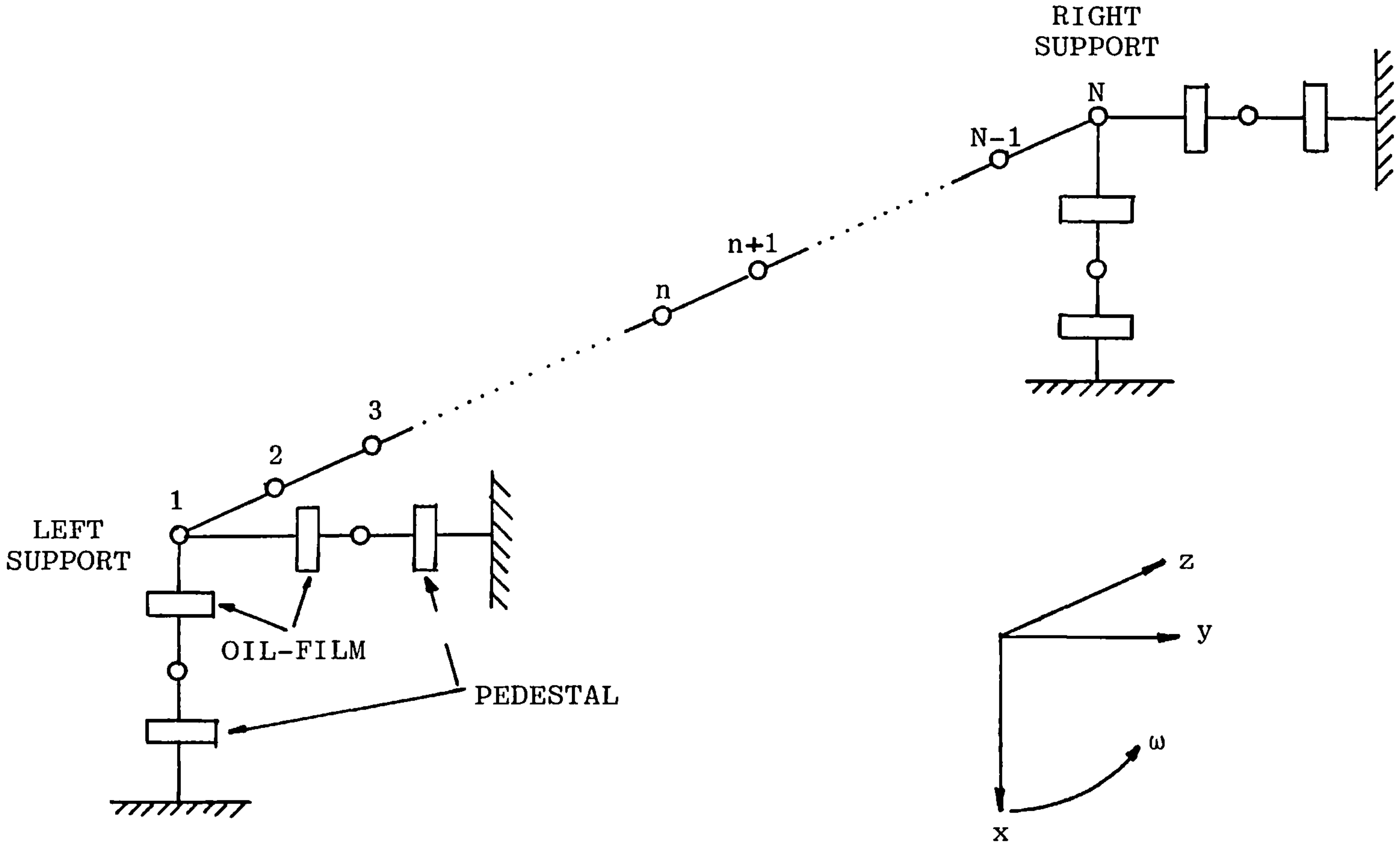

Figure 3.1 Lumped Mass Model Representing Rotor with Journal Bearings and Flexible Supports

The co-ordinate system selected to define the rotor motion in space and time is an (x-y) Cartesian co-ordinate system, where the x-axis coincides with the direction of the gravitational forces, and is the same as the system adopted for the bearing (Chapter2). The (x-y) origin is fixed at the statically deflected equilibrium position of the initially straight shaft, at each station along the shaft.

The (x-y) origin of the TM bearing element at any rotational speed coincides with the steady-state equilibrium position of the journal (ε, ϕ) within the bearing bush. Figure 3.2 depicts the complete co-ordinate system used.

3.2.3 State Variables

As the vibration of a rotating shaft supported in asymetrical bearings is a combination of lateral vibration in the horizontal and vertical planes, the state vector may be defined by the following eight time-dependent variables: deflections (x, y), slope (θ, ϕ), bending moment (M_y, M_x) and shear force (V_x, V_y), and are expressed in column matrix form.

The sign convention adopted is shown in Figure 3.3 and is the same as that used by Pestel and Leckie (58), with the exception that the coordinate axis directions have been changed. Displacement and force are represented by straight arrows, and slope and moment are represented by curved arrows.

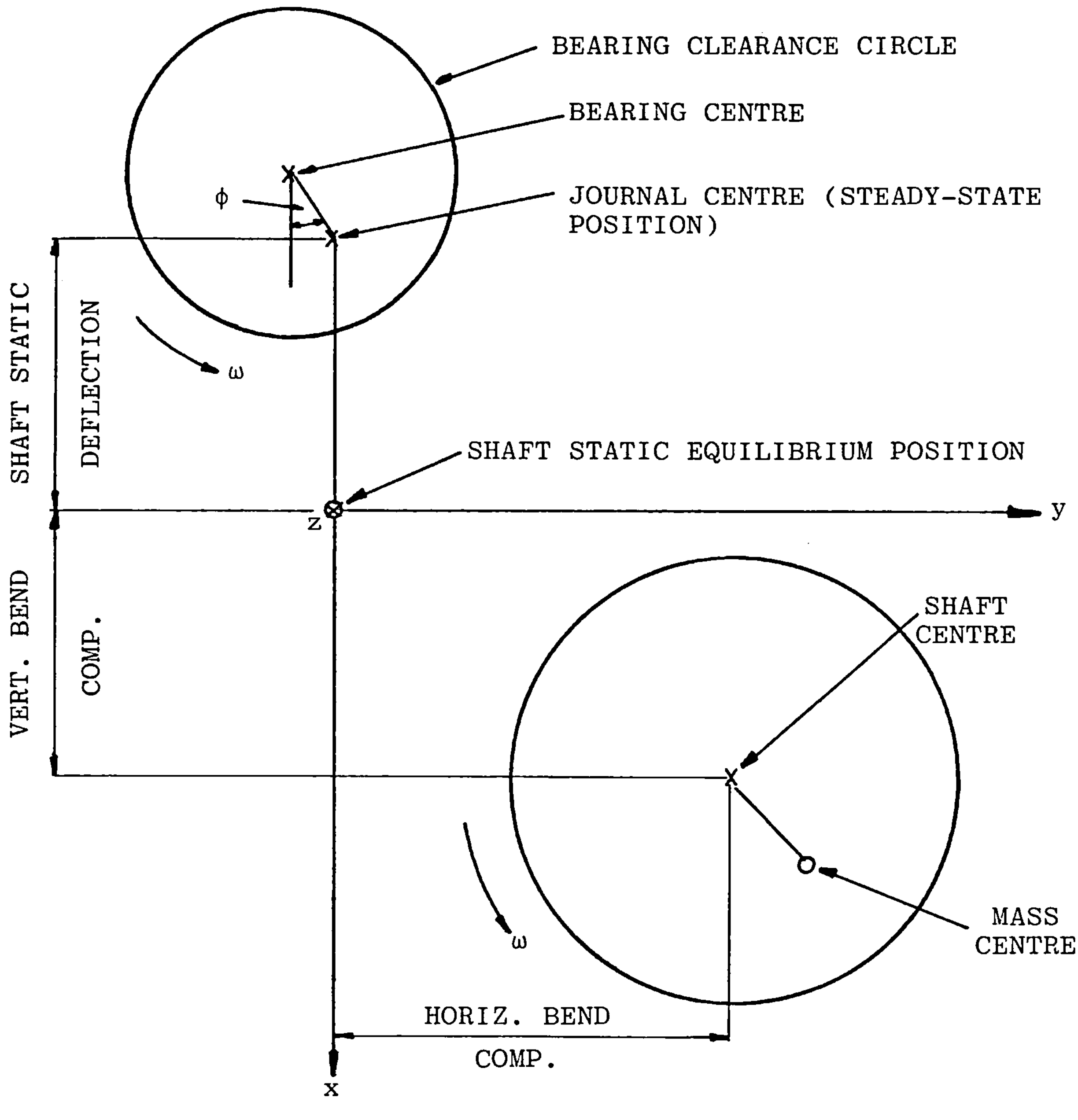

Figure 3.2 Journal and Shaft Equilibrium Positions

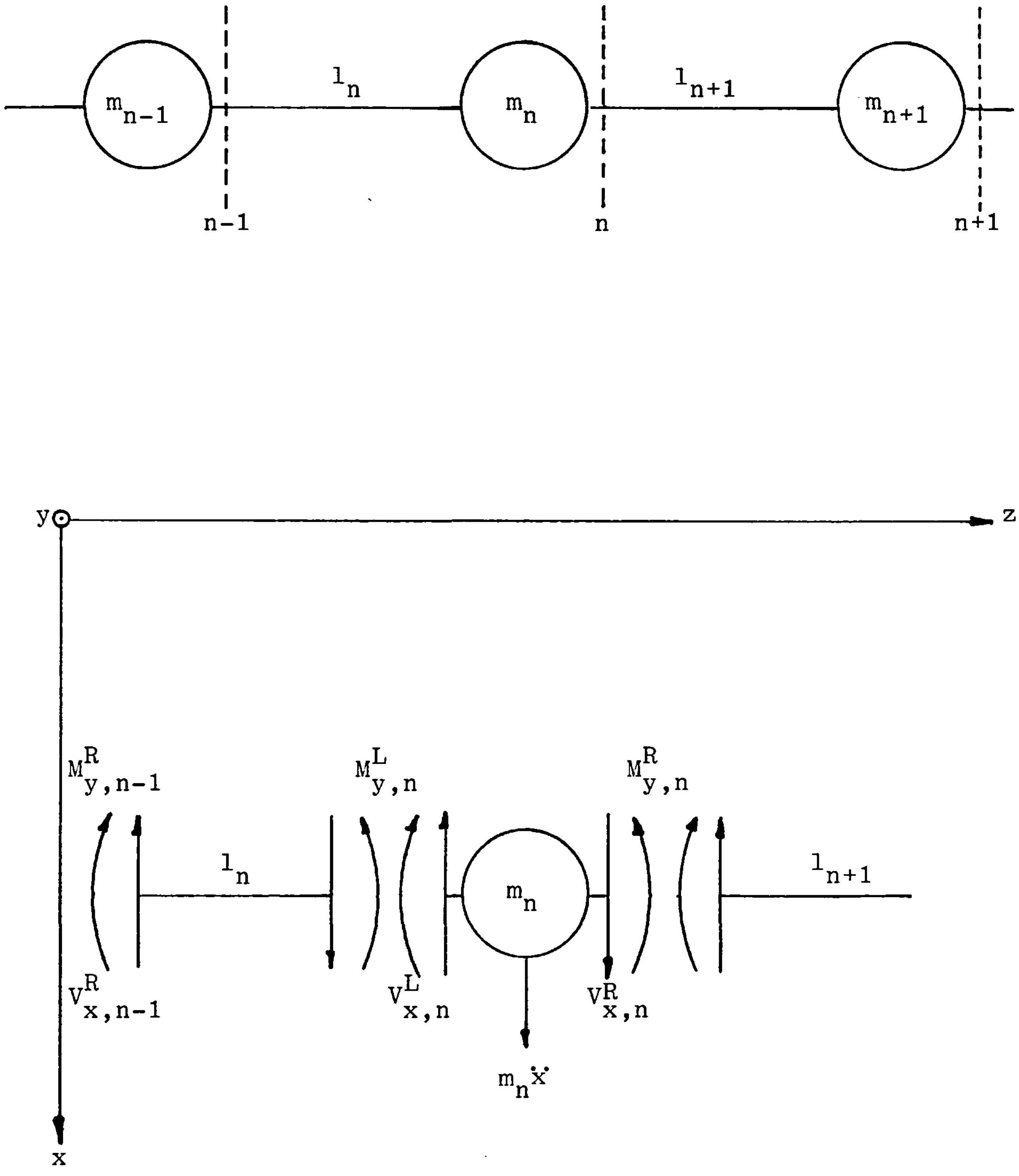

Figure 3.3 Idealised Beam with Lumped Masses Indicating Sign Convention

Because of the damping present in the system (only damping in the bearing and support will be considered), all the state variables are complex quantities.

If steady-state harmonic motion of the shaft is assumed, the state variables can be represented by:

$$x = R_e(\bar{x}e^{i\Omega t}) \tag{3.1a}$$

$$\theta = R_e(\bar{\theta}\, e^{i\Omega t}) \tag{3.1b}$$

$$M_y = R_e(\bar{M}_y e^{i\Omega t}) \tag{3.1c}$$

$$V_x = R_e(\bar{V}_x e^{i\Omega t}) \tag{3.1d}$$

$$y = R_e(\bar{y}e^{i\Omega t}) \tag{3.2a}$$

$$\phi = R_e(\bar{\phi}\, e^{i\Omega t}) \tag{3.2b}$$

$$M_x = R_e(\bar{M}_x e^{i\Omega t}) \tag{3.2c}$$

$$V_y = R_e(\bar{V}_y e^{i\Omega t}) \tag{3.2d}$$

where $\bar{x}$, $\bar{\theta}$, $\bar{M}_y$, $\bar{V}_x$, $\bar{y}$, $\bar{\phi}$, $\bar{M}_x$ and $\bar{V}_y$ are complex quantities and may be expressed in the form:

$$\bar{x} = x_R + ix_I \tag{3.3a}$$

$$\overline{y} = y_R + iy_I \qquad (3.3b)$$

etc

and equations (3.1) and (3.2) can be written as:

$$x = (x_R^2 + x_I^2)^{1/2} \cos(\Omega t + \psi_x) \qquad (3.4a)$$

$$y = (y_R^2 + y_I^2)^{1/2} \cos(\Omega t + \psi_y) \qquad (3.4a)$$

etc

where:

$$\psi_x = \tan^{-1}(x_I/x_R) \qquad (3.5a)$$

$$\psi_y = \tan^{-1}(y_I/y_R) \qquad (3.5b)$$

etc

3.3 DERIVATION OF THE ELEMENT TRANSFER MATRICES

3.3.1 Assumptions

The general representation of the rotor bearing system shown in Figure 3.1, consists of three basic elements:

(i) massless elastic beam element with permanent distortion;

(ii) mass element with mass unbalance, rotary polar and transverse moment of inertia;

(iii) oil-film bearing supported on an elastic pedestal.

To facilitate the derivation of the TM of the above (i) to (iii) elements, several assumptions will be made:

(i) linear elasticity;

(ii) torsional stiffness is assumed to be infinite;

(iii) no axial stress (two-dimensional problem);

(iv) EI is constant for each beam element;

(v) all rotating parts are axially symmetrical;

(vi) shear force is constant for each element and has a discontinuity at each end.

3.3.2 Transfer Matrix of Massless Elastic Beam Element

The elastic properties of an initially straight beam can be represented by a uniform massless elastic beam element, and since the beam is assumed to be massless, static properties suffice to describe the element.

By applying simple beam theory as found in reference (62) and the notation shown in Figure 3.4, state variables at station n can be expressed in terms of the state variables at the adjacent station n-1. A full derivation can be found in reference (58).

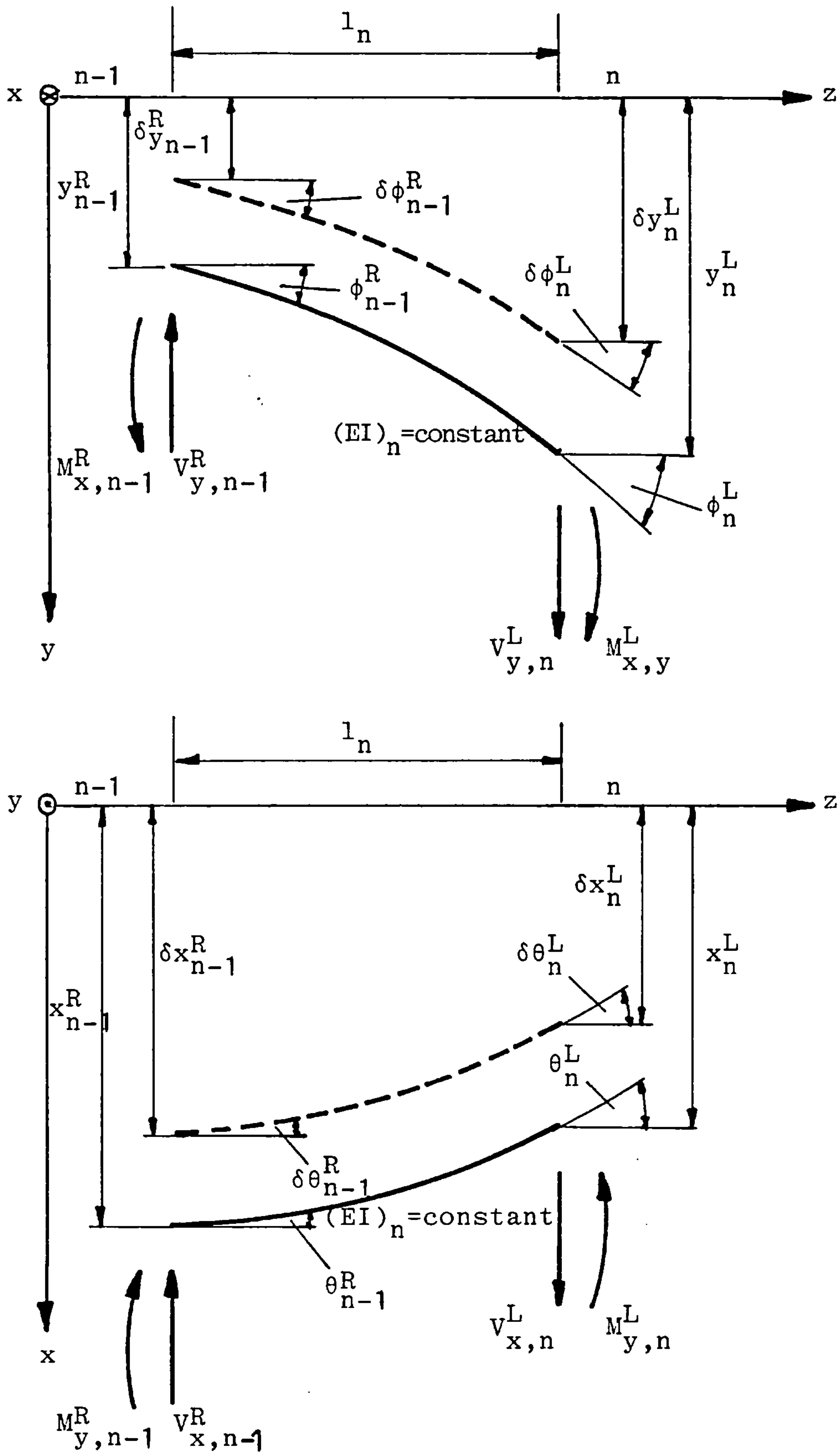

Figure 3.4 Massless Elastic Beam Element

For the x-z plane:

$$-x^L{}_n = -x^R{}_{n-1} + \theta^R{}_{n-1} l_n + M^R{}_{y,n-1} \frac{l_n{}^2}{2(EI)_n} + V^R{}_{x,n-1} \frac{l_n{}^3}{6(EI)_n} \quad (3.6a)$$

$$\theta^L{}_n = \theta^R{}_{n-1} + M^R{}_{y,n-1} \frac{l_n}{(EI)_n} + V^R{}_{x,n-1} \frac{l_n{}^2}{2(EI)_n} \quad (3.6b)$$

$$M^L{}_{y,n} = M^R{}_{y,n-1} + V^R{}_{x,n-1}\, l_n \quad (3.6c)$$

$$V^L{}_{x,n} = + V^R{}_{x,n-1} \quad (3.6d)$$

and similiarly for the y-z plane:

$$y^L{}_n = y^R{}_{n-1} + \phi^R{}_{n-1} l_n + M^R{}_{x,n-1} \frac{l_n{}^2}{2(EI)_n} + V^R{}_{y,n-1} \frac{l_n{}^3}{6(EI)_n} \quad (3.7a)$$

$$\phi^L{}_n = \phi^R{}_{n-1} + M^R{}_{x,n-1} \frac{l_n}{(EI)_n} + V^R{}_{y,n-1} \frac{l_n{}^2}{2(EI)_n} \quad (3.7b)$$

$$M^L{}_{x,n} = M^R{}_{x,n-1} + V^R{}_{y,n-1}\, l_n \quad (3.7c)$$

$$-V^L{}_{y,n} = - V^R{}_{y,n-1} \quad (3.7d)$$

Equations (3.6) and (3.7) can now be written in matrix form, Figure 3.5. This TM is refered to as a field transfer matrix, $[\overline{T}_F]_n$, as it relates the state variables, Z, at the left of station n to those at the right of station n-1. The TM of Figure 3.5 can be expressed in the form:

$$\{\overline{Z}\}^L{}_n = [\overline{T}_F]_n \{\overline{Z}\}^R{}_{n-1} \quad (3.8)$$

$$
\begin{bmatrix} -\bar{x} \\ \bar{\theta} \\ \bar{M}_y \\ \bar{V}_x \\ \hline \bar{y} \\ \bar{\phi} \\ \bar{M}_x \\ -\bar{V}_y \\ \hline 1 \end{bmatrix}_n^L
=
\left[\begin{array}{cccc:cccc:c}
1 & l & \dfrac{l^2}{2EI} & \dfrac{l^3}{6EI} & 0 & 0 & 0 & 0 & \Delta x \\
0 & 1 & \dfrac{l}{EI} & \dfrac{l^2}{2EI} & 0 & 0 & 0 & 0 & \Delta\theta \\
0 & 0 & 1 & l & 0 & 0 & 0 & 0 & 0 \\
0 & 0 & 0 & 1 & 0 & 0 & 0 & 0 & 0 \\
\hdashline
0 & 0 & 0 & 0 & 1 & l & \dfrac{l^2}{2EI} & \dfrac{l^3}{6EI} & \Delta y \\
0 & 0 & 0 & 0 & 0 & 1 & \dfrac{l}{EI} & \dfrac{l^2}{2EI} & \Delta\phi \\
0 & 0 & 0 & 0 & 0 & 0 & 1 & l & 0 \\
0 & 0 & 0 & 0 & 0 & 0 & 0 & 1 & 0 \\
\hdashline
0 & 0 & 0 & 0 & 0 & 0 & 0 & 0 & 1
\end{array}\right]_n
\cdot
\begin{bmatrix} -\bar{x} \\ \bar{\theta} \\ \bar{M}_y \\ \bar{V}_x \\ \hline \bar{y} \\ \bar{\phi} \\ \bar{M}_x \\ -\bar{V}_y \\ \hline 1 \end{bmatrix}_{n-1}^R
$$

Figure 3.5 Transfer Matrix for Massless Elastic Beam Element

If the shaft is permanently warped or bent in the unloaded condition, the displacement and slope equations (3.6a), (3.6b), (3.7a) and (3.7b) must be corrected by an amount equal to the bend:

$$\Delta x = -\delta x_n + \delta x_{n-1} + \delta\theta_{n-1}\, l_n \qquad (3.9a)$$

$$\Delta y = \delta y_n - \delta y_{n-1} - \delta\phi_{n-1}\, l_n \qquad (3.9a)$$

$$\Delta\theta = \delta\theta_n - \delta\theta_{n-1} \qquad (3.10a)$$

$$\Delta\phi = \delta\phi_n - \delta\phi_{n-1} \qquad (3.10b)$$

The extra terms, equations (3.9) and (3.10) can be accommodated in the standard (8x8) matrix by extending the state variable columns of both sides by 1, Figure 3.5, and by introducing an extra row (for symmetry) and column in the TM, thus making the matrix (9x9). The extra right hand column generated in the TM is called the "forcing column" and equations (3.9) and (3.10) are inserted here.

It is important to include the extra terms of warping in the TM of the beam elements Figure 3.5, as the extra forces and moments can greatly modify the response of a rotor. Such forces and moments could arise from a bent shaft which carries a massive disc, or if the bending results in misalignment of the journal bearings. Additional gyroscopic moments can also be introduced from a disc which is skewed relative to the shaft.

The extra forces and moments of warping and or skewing are obtained by multiplying the TM's of mass point (Figure 3.7, Section 3.3.3), bearing point (Figure 3.9, Section 3.3.4) and elastic beam element (Figure 3.5) together. Thus, these forces do not have to be derived separately.

3.3.3 Transfer Matrix of Rigid Mass with Rotary, Polar-Transverse Moments of Inertia

Mass and inertia properties of a shaft element can be analytically represented by an element of mass m, polar inertia I_P and transverse inertia I_T. To eliminate any consideration of beam properties the mass element is taken to be a thin rigid disc, Figure 3.6.

The rotor unbalance is defined by a mass unbalance m_u and its position by polar co-ordinates (r,ρ), Figure 3.6. To represent the components of the unbalance force $\bar{U}$, a set of orthogonal axes (X-Y) rotating with the shaft with an angular velocity ω are introduced. At any instant of time the instantaneous position of the rotating axes with respect to the fixed axes (x-y) is given by ωt.

The components of the unbalance force are given by:

$$U_X = |\bar{U}| \cos\rho = m_u r\omega^2 \cos\rho \qquad (3.11a)$$

$$U_Y = |\bar{U}| \sin\rho = m_u r\omega^2 \sin\rho \qquad (3.11b)$$

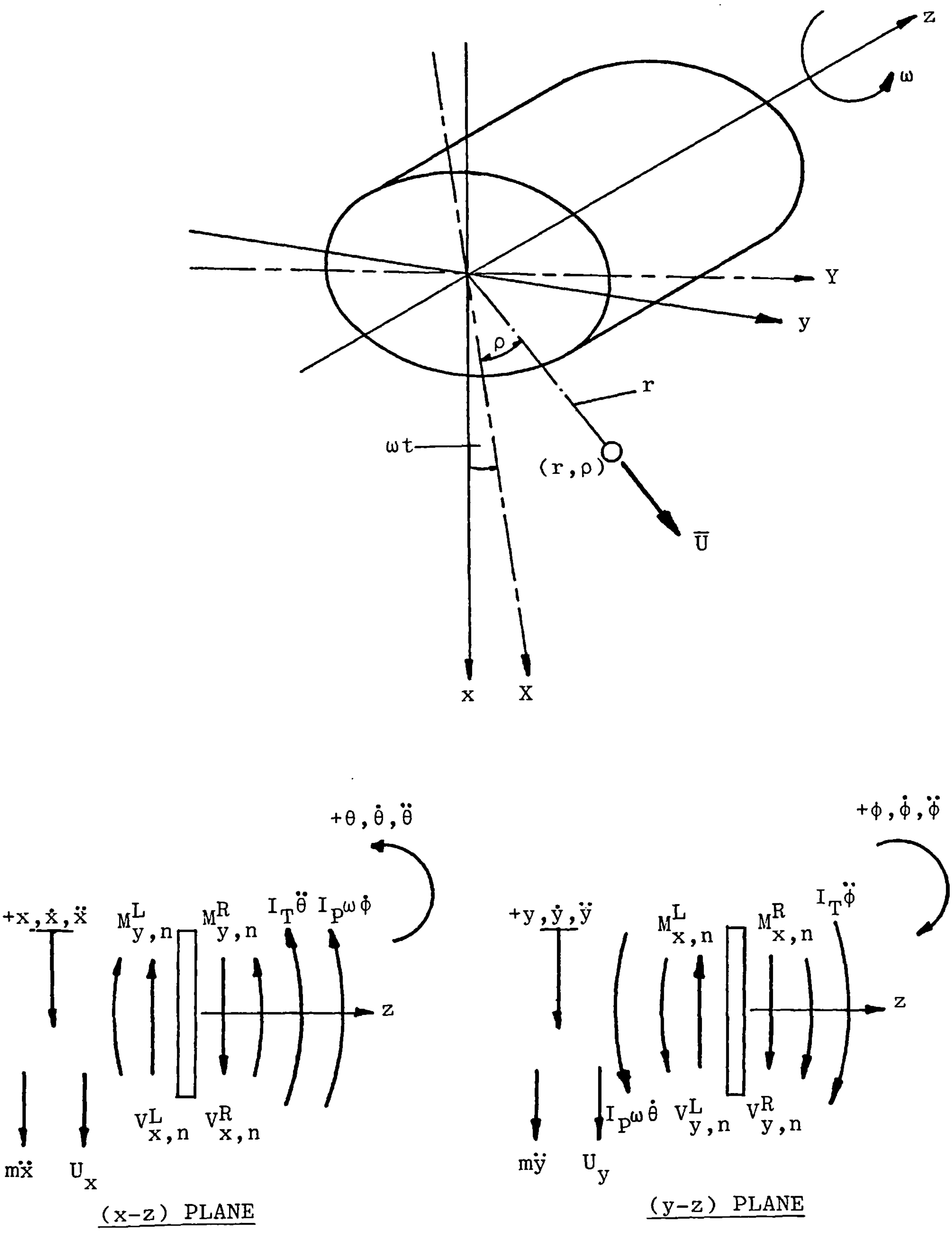

Figure 3.6 Mass Element

Transforming the unbalance forces from rotating to fixed co-ordinates gives:

$$U_x = U_X \cos \omega t - U_Y \sin \omega t \qquad (3.12a)$$

$$U_y = U_X \sin \omega t + U_Y \cos \omega t \qquad (3.12b)$$

and expressed in complex form

$$U_x = (U_X + i\ U_Y)e^{i\omega t} \qquad (3.13a)$$

$$U_y = -i(U_X + i\ U_Y)e^{i\omega t} \qquad (3.13b)$$

where only the real part of the right hand side of equation (3.13) applies. Using equation (3.11) enables equation (3.13) to be written as:

$$U_x = m_u r\omega^2(\cos\rho + i\sin\rho) \qquad (3.14a)$$

$$U_y = m_u r\omega^2(\sin\rho - i\cos\rho) \qquad (3.14b)$$

Applying Newton's 2nd law of motion of a rigid body to the forces in the free-body diagram of Figure 3.6, and considering equilibrium of forces it is possible to write:

$$m\ddot{x} = V^R{}_{x,n} - V^L{}_{x,n} + U_x \qquad (3.15a)$$

$$m\ddot{y} = V^R{}_{y,n} - V^L{}_{y,n} + U_y \qquad (3.15b)$$

Substituting for $\ddot{x}$ and $\ddot{y}$ from the differentiation of equations (3.1a) and (3.2a) gives:

$$V^R{}_{x,n} = V^L{}_{x,n} - m\Omega^2 x - U_x \tag{3.16a}$$

$$V^R{}_{y,n} = V^L{}_{y,n} - m\Omega^2 y - U_y \tag{3.16b}$$

As shown in (34) for very small orbits the effect of gyroscopic moment coupling may be represented as the moments induced by rotations of the mass in the separate x-z and y-z planes.

Thus, a moment summation including the gyroscopic forces in the latter way provides:

$$I_T\ddot{\theta} = M^R{}_{y,n} - M^L{}_{y,n} + I_p\omega\dot{\phi} \tag{3.17a}$$

$$I_T\ddot{\phi} = M^R{}_{x,n} - M^L{}_{x,n} - I_p\omega\dot{\theta} \tag{3.17b}$$

Substituting for $\dot{\theta}$, $\dot{\phi}$, $\ddot{\theta}$ and $\ddot{\phi}$ from the differentiation of equations (3.1b) and 3.2b) yields:

$$M^R{}_{y,n} = M^L{}_{y,n} - I_T\Omega^2\theta - i\Omega I_p\omega \tag{3.18a}$$

$$M^R{}_{x,n} = M^L{}_{x,n} - I_T\Omega^2\phi + i\Omega I_p\omega \tag{3.18b}$$

and since the mass element is assumed to be infinitely short geometric compatability must apply:

$$x^{R}_{n} = x^{L}_{n} \quad , \quad y^{R}_{n} = y^{L}_{n} \tag{3.19a}$$

$$\theta^{R}_{n} = \theta^{L}_{n} \quad , \quad \phi^{R}_{n} = \phi^{L}_{n} \tag{3.19b}$$

Equations (3.16), (3.18) and (3.19) yield the TM of the mass element, Figure 3.7, and is referred to as a point matrix as it relates the state variables to the left and right of the same station n. Thus, Figure 3.7 can be expressed in matrix notation as:

$$\{\overline{Z}\}^{R}_{n} = [\overline{T}_{p}]_{n}\{\overline{Z}\}^{L}_{n} \tag{3.20}$$

For the mass elements of a round shaft I_p and I_T are given by:

$$I_p = 1/8 \ m \ d_n^2 \tag{3.21a}$$

$$I_T = m(1/16 \ d_n^2 + 1/12 \, l_n^2) \tag{3.21b}$$

From Figure 3.7 it can be seen that the TM of a mass element is also extended (compare with Figure 3.5) to include a "forcing column" in which the unbalance forces U_x and U_y are inserted. Also, the sign U_x in equation (3.14a) has been made negative in order that both U_x and U_y are positive in the TM element Figure 3.7.

$$
\begin{bmatrix} -\bar{x} \\ \bar{\theta} \\ \bar{M}_y \\ \bar{V}_x \\ \hline \bar{y} \\ \bar{\phi} \\ \bar{M}_x \\ -\bar{V}_y \\ \hline 1 \end{bmatrix}_n^R
=
\left[\begin{array}{cccc|cccc|c}
1 & 0 & 0 & 0 & 0 & 0 & 0 & 0 & 0 \\
0 & 1 & 0 & 0 & 0 & 0 & 0 & 0 & 0 \\
0 & -I_T\Omega^2 & 1 & 0 & 0 & -i\Omega I_p\omega & 0 & 0 & 0 \\
m\Omega^2 & 0 & 0 & 1 & 0 & 0 & 0 & 0 & U_x \\
\hline
0 & 0 & 0 & 0 & 1 & 0 & 0 & 0 & 0 \\
0 & 0 & 0 & 0 & 0 & 1 & 0 & 0 & 0 \\
0 & i\Omega I_p\omega & 0 & 0 & 0 & -I_T\Omega^2 & 1 & 0 & 0 \\
0 & 0 & 0 & 0 & m\Omega^2 & 0 & 0 & 1 & U_y \\
\hline
0 & 0 & 0 & 0 & 0 & 0 & 0 & 0 & 1
\end{array}\right]_n
\cdot
\begin{bmatrix} -\bar{x} \\ \bar{\theta} \\ \bar{M}_y \\ \bar{V}_x \\ \hline \bar{y} \\ \bar{\phi} \\ \bar{M}_x \\ -\bar{V}_y \\ \hline 1 \end{bmatrix}_n^L
$$

Figure 3.7 Transfer Matrix for Mass Element

3.3.4 Transfer Matrix of Bearing and Pedestal Support

The element used to represent a journal bearing mounted on a flexible pedestal is shown in Figure 3.8, where it is assumed that the dynamic properties of the bearing can be represented by four linear spring coefficients k_{xx}, k_{xy}, k_{yx} and k_{yy}, plus four linear damping coefficients c_{xx}, c_{xy}, c_{yx} and c_{yy} (as derived in Chapter 2, equations (2,26) and (2.27)).

It is also possible to include in the analysis an analogous set of rotational spring and damping coefficients representing the moment forces acting on the journal bearing due to its inclination.

Thus, the dynamic oil-film force and moments in the (x-y) plane can be expressed as follows:

$$\Delta f_x = - k_{xx}\, x - k_{xy}\, y - c_{xx}\, \dot{x} - c_{xy}\, \dot{y} \qquad (3.22a)$$

$$\Delta f_y = - k_{yx}\, x - k_{yy}\, y - c_{yx}\, \dot{x} - c_{yy}\, \dot{y} \qquad (3.22b)$$

$$\Delta t_y = - k_{\theta\theta}\, \theta - k_{\theta\phi}\, \phi - c_{\theta\theta}\, \dot{\theta} - c_{\theta\phi}\, \dot{\phi} \qquad (3.23a)$$

$$\Delta t_x = - k_{\phi\theta}\, \theta - k_{\phi\phi}\, \phi - c_{\phi\theta}\, \dot{\theta} - c_{\phi\phi}\, \dot{\phi} \qquad (3.23b)$$

On substituting for x, $\dot{x}$, y, $\dot{y}$, etc from equations (3.1) and (3.2) and expressing the bearing coefficient in complex impedance form, equations (3.22) and (3.23) become:

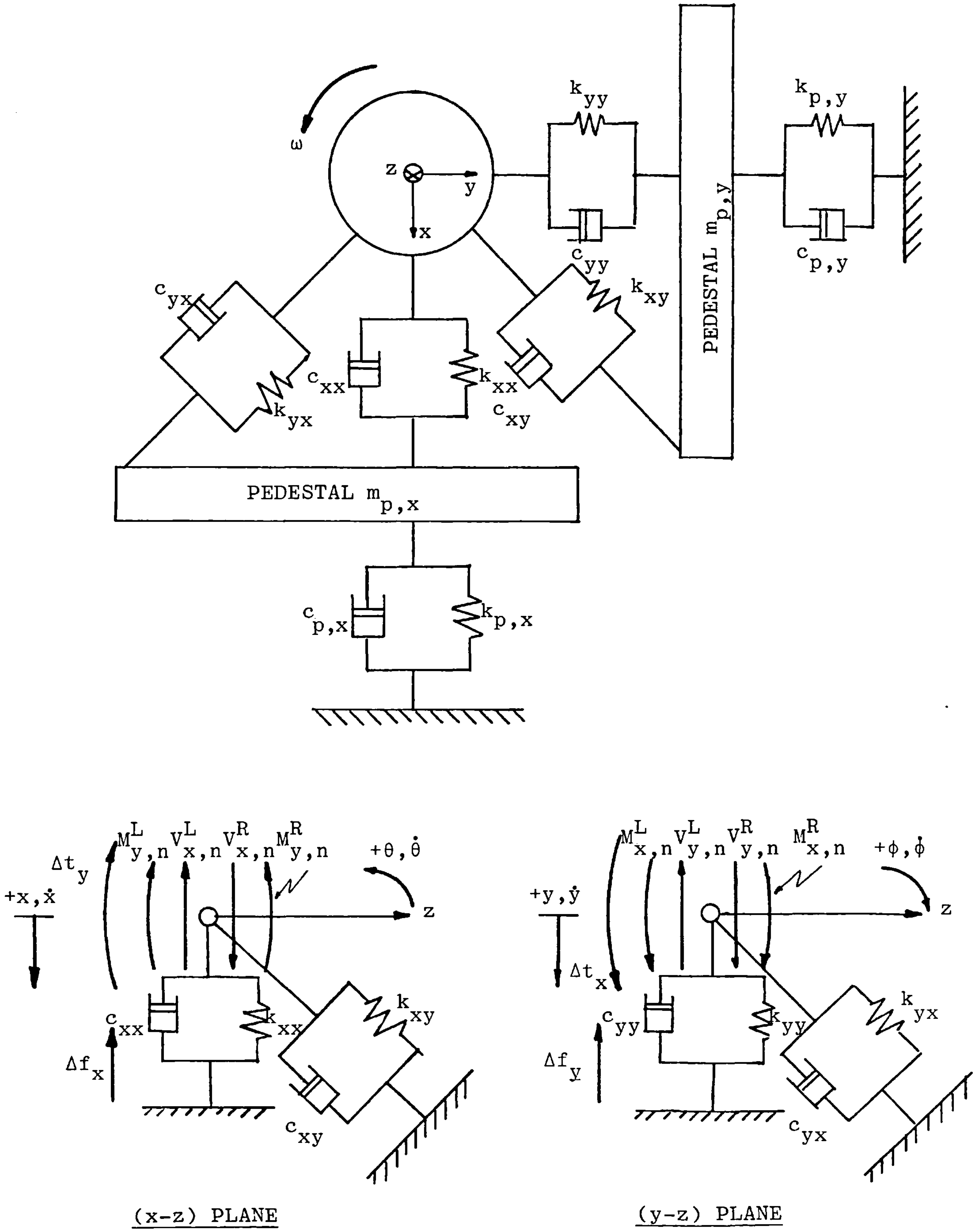

Figure 3.8 Journal Bearing Element

$$\Delta f_x = Z_{xx}\, x + Z_{xy}\, y \tag{3.24a}$$

$$\Delta f_y = Z_{yx}\, x + Z_{yy}\, y \tag{3.24b}$$

$$\Delta t_y = Z_{\theta\theta}\, \theta + Z_{\theta\phi}\, \phi \tag{3.25a}$$

$$\Delta t_x = Z_{\phi\theta}\, \theta + Z_{\phi\phi}\, \phi \tag{3.25b}$$

where the first subscript in the impedance refers to the direction of the force and the second denotes the direction of the movement.

From reference to Figure 3.8, the discontinuity of the bearing forces and moments introduced by the restoring forces expressed in equations (3.24) and (3.25) respectively, can be derived from a consideration of the equilibrium of the bearing element:

$$V^R{}_{x,n} = V^L{}_{x,n} + Z_{xx}\, x + Z_{xy}\, y \tag{3.26a}$$

$$V^R{}_{y,n} = V^L{}_{y,n} + Z_{yx}\, x + Z_{yy}\, y \tag{3.26b}$$

$$M^R{}_{y,n} = M^L{}_{y,n} + Z_{\theta\theta}\, \theta + Z_{\theta\phi}\, \phi \tag{3.27a}$$

$$M^R{}_{x,n} = M^L{}_{x,n} + Z_{\phi\theta}\, \theta + Z_{\phi\phi}\, \phi \tag{3.27b}$$

and since the bearing element is considered to be infinitely short, geometric compatability must apply (equation (3.19)).

Combining equations (3.26), (3.27) and (3.19) gives the TM of the bearing element Figure 3.9, where the oil-film impedances of equations (3.24) and (3.25) are given by:

$$Z_{xx} = \frac{W}{c}\left(K_{xx} + i\,\frac{\Omega}{\omega}\,C_{xx}\right) \qquad (3.28a)$$

$$Z_{xy} = \frac{W}{c}\left(K_{xy} + i\,\frac{\Omega}{\omega}\,C_{xy}\right) \qquad (3.28b)$$

$$Z_{yx} = \frac{W}{c}\left(K_{yx} + i\,\frac{\Omega}{\omega}\,C_{yx}\right) \qquad (3.28c)$$

$$Z_{yy} = \frac{W}{c}\left(K_{yy} + i\,\frac{\Omega}{\omega}\,C_{yy}\right) \qquad (3.28d)$$

$$Z_{\theta\theta} = \frac{WL^2}{c}\left(K_{\theta\theta} + i\,\frac{\Omega}{\omega}\,C_{\theta\theta}\right) \qquad (3.29a)$$

$$Z_{\theta\phi} = \frac{WL^2}{c}\left(K_{\theta\phi} + i\,\frac{\Omega}{\omega}\,C_{\theta\phi}\right) \qquad (3.29b)$$

$$Z_{\phi\theta} = \frac{WL^2}{c}\left(K_{\phi\theta} + i\,\frac{\Omega}{\omega}\,C_{\phi\theta}\right) \qquad (3.29c)$$

$$Z_{\phi\phi} = \frac{WL^2}{c}\left(K_{\phi\phi} + i\,\frac{\Omega}{\omega}\,C_{\phi\phi}\right) \qquad (3.29d)$$

where K_{xx}, C_{xx}, ..., $K_{\theta\theta}$, $C_{\theta\theta}$, ..., are the non-dimensional linear and rotational bearing coefficients respectively.

The TM of the bearing element is also represented by a point matrix and thus, can again be represented by equation (3.20):

$$
\begin{bmatrix} -\overline{x} \\ \overline{\theta} \\ \overline{M}_y \\ \overline{V}_x \\ \hline \overline{y} \\ \overline{\phi} \\ \overline{M}_x \\ -\overline{V}_y \\ \hline 1 \end{bmatrix}_n^R
=
\left[\begin{array}{cccc|cccc|c}
1 & 0 & 0 & 0 & 0 & 0 & 0 & 0 & 0 \\
0 & 1 & 0 & 0 & 0 & 0 & 0 & 0 & 0 \\
0 & Z_{\theta\theta} & 1 & 0 & 0 & Z_{\theta\phi} & 0 & 0 & 0 \\
-Z_{xx} & 0 & 0 & 1 & Z_{xy} & 0 & 0 & 0 & 0 \\
\hline
0 & 0 & 0 & 0 & 1 & 0 & 0 & 0 & 0 \\
0 & 0 & 0 & 0 & 0 & 1 & 0 & 0 & 0 \\
0 & Z_{\phi\theta} & 0 & 0 & 0 & Z_{\phi\phi} & 1 & 0 & 0 \\
Z_{yx} & 0 & 0 & 0 & -Z_{yy} & 0 & 0 & 1 & 0 \\
\hline
0 & 0 & 0 & 0 & 0 & 0 & 0 & 0 & 1
\end{array}\right]_n
\cdot
\begin{bmatrix} -\overline{x} \\ \overline{\theta} \\ \overline{M}_y \\ \overline{V}_x \\ \hline \overline{y} \\ \overline{\phi} \\ \overline{M}_x \\ -\overline{V}_y \\ \hline 1 \end{bmatrix}_n^L
$$

Figure 3.9 Transfer Matrix for Bearing Element

$$\{\overline{Z}\}^R{}_n = [\overline{T}_p]_n\{\overline{Z}\}^L{}_n$$

An advantage of expressing the bearing forces and moments in impedance form is that more complicated models of the bearing may easily be included in the TM of the bearing.

Thus, if the bearing oil film has an impedance Z^f, and is supported on a flexible pedestal with impedance Z^p, the total impedance of the oil film and pedestal can be obtained by adding together the receptances (inverse of impedance) of the oil film R^f and pedestal R^p, and inverting to obtain the overall impedance of the oil film and pedestal.

That is:

$$R^f{}_{xx} = \frac{1}{Z^f{}_{xx}} \quad , \qquad R^p{}_{xx} = \frac{1}{Z^p{}_{xx}} \tag{3.30}$$

and therefore the total receptance is given by:

$$R_{xx} = R^f{}_{xx} + R^p{}_{xx} = \frac{1}{Z^f{}_{xx}} + \frac{1}{Z^p{}_{xx}} \tag{3.31}$$

$$R_{xx} = \frac{Z^f{}_{xx} + Z^p{}_{xx}}{Z^f{}_{xx} \quad Z^p{}_{xx}} \tag{3.32}$$

and the total impedance is:

$$Z_{xx} = \frac{1}{R_{xx}} = \frac{Z^f{}_{xx} \quad Z^p{}_{xx}}{Z^f{}_{xx} + Z^p{}_{xx}} \tag{3.33a}$$

and similarly for the y-direction:

$$Z_{yy} = \frac{1}{R_{yy}} = \frac{Zf_{yy} \quad ZP_{yy}}{Zf_{yy} + ZP_{yy}} \qquad (3.33b)$$

where the impedance of the pedestal is given by:

$$ZP_{xx} = -m_{p,x}\Omega^2 + k_{p,x} + i\Omega c_{p,x} \qquad (3.34a)$$

$$ZP_{yy} = -m_{p,y}\Omega^2 + k_{p,y} + i\Omega c_{p,y} \qquad (3.34b)$$

3.4 ASSEMBLY OF TRANSFER MATRICES

3.4.1 Elimination of Intermediate State Variables

In general the state variables to the left and right of an element are related by the T.M. of that element in such a way that:

$$\{\overline{Z}\}^R_n = [\overline{T}]_n \quad \{\overline{Z}\}^L_n \qquad (3.35)$$

$$\{\overline{Z}\}^R_{n+1} = [\overline{T}]_{n+1} \{\overline{Z}\}^L_{n+1} \qquad (3.36)$$

for $1 \leqslant n \leqslant N$.

With the additional condition of geometric compatability, no external forces or moments acting and with the sign of convention adopted, it is possible to write:

$$\{\overline{Z}\}^R_n = \{\overline{Z}\}^L_{n+1} \qquad (3.37)$$

Thus, substitution of equation (3.37) into equation (3.35) yields:

$$\{\bar{Z}\}^{L}_{n+1} = [\bar{T}]_n \{\bar{Z}\}^{L}_{n} \tag{3.38}$$

and insertion of equation (3.38) into equation (3.36) gives:

$$\{\bar{Z}\}^{R}_{n+1} = [\bar{T}]_{n+1} [\bar{T}]_n \{\bar{Z}\}^{L}_{n} \tag{3.39}$$

Thus, repeated substitution N-times permits the development of an overall expression relating the state variables at the left and right boundaries of the model: i.e.

$$\{\bar{Z}\}^{R}_{N} = [\bar{T}]_N [\bar{T}]_{N-1} \ldots\ldots [\bar{T}]_1 \{\bar{Z}\}^{L}_{1} \tag{3.40}$$

where

$$[\bar{T}_T] = [\bar{T}]_N [\bar{T}]_{N-1} \ldots\ldots [\bar{T}]_1 \tag{3.41}$$

is referred to as the overall system transfer matrix $[\bar{T}_T]$.

or $$[\bar{T}_T] = \prod_{n=1}^{N} [\bar{T}_n] \tag{3.42}$$

and $$\{\bar{Z}\}^{R}_{N} = [\bar{T}_T] \{\bar{Z}\}^{L}_{1} \tag{3.43}$$

3.4.2 Standard Transfer Matrix Element

To simplify the data required for the evaluation of the T.M. elements at each station, multiplying all three T.M. elements together, Figures 3.7, 3.9 and 3.5 respectively, in the order indicated below, generates a standard T.M. element, $[T_s]$, Figure 3.10, incorporating the properties of mass element, bearing element and massless elastic beam element in one T.M. element.

$$[\bar{T}_s] = [\bar{T}]_{mass} \ [\bar{T}]_{bearing} \ [\bar{T}]_{beam} \qquad (3.44)$$

3.4.3 Boundary Conditions

In general four of the eight state variables at each end of the rotor system will be zero. For example in the different supports given below, the following boundary conditions will apply:

Pinned-pinned rotor

$$x_1 = x_N = y_1 = y_N = 0 \qquad (3.46a)$$

$$M_{y,x} = M_{y,N} = M_{x,1} = M_{x,N} = 0 \qquad (3.46b)$$

free-free rotor

$$M_{y,1} = M_{y,N} = M_{x,1} = M_{x,N} = 0 \qquad (3.47a)$$

$$V_{x,1} = V_{x,N} = V_{y,1} = V_{y,N} = 0 \qquad (3.47b)$$

Clamped-clamped rotor

$$x_1 = x_N = y_1 = y_N = 0 \qquad (3.48a)$$

$$\theta_1 = \theta_N = \phi_1 = \phi_N = 0 \qquad (3.48b)$$

and of course a combination of pinned, free or clamped for a particular rotor (the experimental rotor is modelled as

$$
\begin{bmatrix} -\bar{x} \\ \bar{\theta} \\ \bar{M}_y \\ \bar{V}_x \\ \hline \bar{y} \\ \bar{\phi} \\ \bar{M}_x \\ -\bar{V}_y \\ \hline 1 \end{bmatrix}
=
\left[\begin{array}{cccc:cccc:c}
1 & l & \frac{l^2}{2EI} & \frac{l^3}{6EI} & 0 & 0 & 0 & 0 & \Delta x \\
0 & 1 & \frac{l}{EI} & \frac{l^2}{2EI} & 0 & 0 & 0 & 0 & \Delta\theta \\
0 & T_{\theta\theta} & 1+T_{\theta\theta}\frac{l}{EI} & 1+T_{\theta\theta}\frac{l^2}{2EI} & 0 & T_{\theta\phi} & T_{\theta\phi}\frac{l}{EI} & T_{\theta\phi}\frac{l^2}{2EI} & \Delta\theta T_{\theta\theta}+\Delta\phi T_{\theta\phi} \\
T_{xx} & T_{xx}l & T_{xx}\frac{l^2}{2EI} & 1+T_{xx}\frac{l^3}{6EI} & T_{xy} & T_{xy}l & T_{xy}\frac{l^2}{2EI} & T_{xy}\frac{l^3}{6EI} & \Delta x T_{xx}+\Delta y T_{xy}+U_x \\
\hdashline
0 & 0 & 0 & 0 & 1 & l & \frac{l^2}{2EI} & \frac{l^3}{6EI} & \Delta y \\
0 & 0 & 0 & 0 & 0 & 1 & \frac{l}{EI} & \frac{l^2}{2EI} & \Delta\phi \\
0 & T_{\phi\theta} & T_{\phi\theta}\frac{l}{EI} & T_{\phi\theta}\frac{l^2}{2EI} & 0 & T_{\phi\phi} & 1+T_{\phi\phi}\frac{l}{2EI} & 1+T_{\phi\phi}\frac{l^2}{2EI} & \Delta\theta T_{\phi\theta}+\Delta\phi T_{\phi\phi} \\
T_{yx} & T_{yx}l & T_{yx}\frac{l^2}{2EI} & T_{yx}\frac{l^3}{6EI} & T_{yy} & T_{yy}l & T_{yy}\frac{l^2}{2EI} & 1+T_{yy}\frac{l^3}{6EI} & \Delta x T_{yx}+\Delta y T_{yy}+U_y \\
\hdashline
0 & 0 & 0 & 0 & 0 & 0 & 0 & 0 & 1
\end{array}\right]
\begin{bmatrix} -\bar{x} \\ \bar{\theta} \\ \bar{M}_y \\ \bar{V}_x \\ \hline \bar{y} \\ \bar{\phi} \\ \bar{M}_x \\ -\bar{V}_y \\ \hline 1 \end{bmatrix}
$$

Figure 3.10 Standard Transfer Matrix Element where:

$$
\begin{aligned}
T_{\theta\theta} &= -I_T\Omega^2 + Z_{\theta\theta} \\
T_{\theta\phi} &= -i\Omega I_p\omega + Z_{\theta\phi} \\
T_{\phi\phi} &= -I_T\Omega^2 + Z_{\phi\phi} \\
T_{\phi\theta} &= i\Omega I_p\omega + Z_{\phi\theta} \\
T_{xx} &= m\Omega^2 - Z_{xx} \\
T_{xy} &= + Z_{xy} \\
T_{yy} &= m\Omega^2 - Z_{yy} \\
T_{yx} &= + Z_{yx} \\
U_x &= -m_u r\omega^2(\cos\rho + i\sin\rho) \\
U_y &= m_u r\omega^2(\sin\rho - i\cos\rho) \\
\Delta x &= -\delta x_n + \delta x_{n-1} + \delta\theta_{n-1} l_n \\
\Delta y &= \delta y_n - \delta y_{n-1} - \delta\phi_{n-1} l_n \\
\Delta\theta &= \delta\theta_n - \delta\theta_{n-1} \\
\Delta\phi &= \delta\phi_n - \delta\phi_{n-1}
\end{aligned}
\qquad (3.45)
$$

free-pinned). A rotor support can be considered pinned if rolling element bearings of short L/D are used, and clamped if the L/D is long. Whereas, a rotor supported on a journal bearing (flexible support) can be considered as free.

3.4.4 Solution for Free Vibration

For the case of free vibration the extra forcing column in the T.M. can be ignored, thus reducing the T.M. to (8x8). As stated in Section 3.4.3, in general, four of the eight state variables at each end of the rotor will be zero. Solving the T.M. for the model of the experimental rotor will serve to illustrate how the method is applied. For the model used, the lefthand support is taken as free and the righthand support is taken as pinned.

Using equation (3.43) relating the overal T.M. in terms of the state variable vectors at the left and right hand boundaries, and applying the boundary conditions of equation (3.47) for the state variable $\{\overline{Z}\}_1^L$ and equation (3.46) for the state variable $\{\overline{Z}\}_N^R$ gives:

$$\begin{bmatrix} 0 \\ 0 \\ 0 \\ 0 \end{bmatrix}_N^R = \begin{bmatrix} t_{11} & t_{12} & t_{15} & t_{16} \\ t_{31} & t_{32} & t_{35} & t_{36} \\ t_{51} & t_{52} & t_{55} & t_{56} \\ t_{71} & t_{72} & t_{75} & t_{76} \end{bmatrix} \begin{bmatrix} -\overline{x} \\ \overline{\theta} \\ \overline{y} \\ \overline{\phi} \end{bmatrix}_1^L \qquad (3.49)$$

where t_{11}, t_{12}, t_{15}, ... etc are the complex elements of the overall T.M. element. It can be seen that due to the boundary conditions at the left hand support, it is not necessary to calculate all the columns at each station of the T.M. element. In this particular case columns 3, 4, 7 and 8 can be omitted, this technique is referred to as the abridged method of matrix multiplication (58).

Expressing equation (3.49) in the form gives:

$$\{\bar{Z}_B\}_N^R = [\bar{T}_{TB}]\ \{\bar{Z}_B\}_1^L \qquad (3.50)$$

Equation (3.49) or (3.50) is equivalent to a set of homogeneous equations and for a nontrivial solution it is necessary that the determinant of the matix $[\bar{T}_{TB}]$ (where $[\bar{T}_{TB}]$ is the overall T.M. for the boundary conditions that apply) is zero.

$$\text{ie} \quad \text{Det}\left|\ \bar{T}_{TB}\ \right| = 0 \qquad (3.51)$$

As $\left|\bar{T}_{TB}\right|$ is a function of rotor whirl frequency, Ω , all frequencies for which equation (3.51) is satisfied are natural frequencies, Ω_n, of the rotor-bearing system.

Natural mode shapes of vibration are obtained by assigning an arbitrary value to one of the state variables of $\{\bar{Z}_B\}_1^L$ and solving for the remaining variables from equations (3.50).

For example, letting y=1 in equation (3.49) yields:

$$\begin{bmatrix} -t_{15} \\ -t_{35} \\ -t_{75} \end{bmatrix} = \begin{bmatrix} t_{11} & t_{12} & t_{16} \\ t_{31} & t_{32} & t_{36} \\ t_{71} & t_{72} & t_{76} \end{bmatrix} \begin{bmatrix} -\overline{x} \\ \overline{\theta} \\ \overline{\phi} \end{bmatrix}_1^L \qquad (3.52)$$

Inversion of the (3x3) matrix will give the solution vector for the state variables at the left hand boundary station. i.e.

$$\begin{bmatrix} -\overline{x} \\ \overline{\theta} \\ \overline{\phi} \end{bmatrix}_1^L = \begin{bmatrix} t_{11} & t_{12} & t_{16} \\ t_{31} & t_{32} & t_{36} \\ t_{71} & t_{72} & t_{76} \end{bmatrix}^{-1} \begin{bmatrix} -t_{15} \\ -t_{35} \\ -t_{75} \end{bmatrix} \qquad (3.53)$$

Calculating the intermediate state vectors is then achieved by matrix multiplication.

eg at station 1 $\{\overline{Z}\}_1^R = [\overline{T}]_1\{\overline{Z}\}_1^L$ (3.54a)

eg at station 2 $\{\overline{Z}\}_2^R = [\overline{T}]_2[\overline{T}_1]\{\overline{Z}\}_1^L$ (3.54b)

eg at station n $\{\overline{Z}\}_n^R = [\overline{T}]_n[\overline{T}]_{n-1}\ldots[\overline{T}]_2[\overline{T}]_1\{\overline{Z}\}_1^L$ (3.54c)

or in general $\{\overline{Z}\}_n^R = \prod_{k=1}^{n}[\overline{T}]_k\{\overline{Z}\}_1^L$ (3.54d)

3.4.5 Solution for Forced Response

A dynamic response due to harmonic forcing, which may have constant amplitude or be a function of rotational speed, and response due to static forces can be cal-culated by the T.M.M.

The forcing function is included in the T.M. by insertion into the nineth column (the "forcing column") of the extended (8x8) T.M. Thus, a discontinuity of the shear force due to an arbitrary external force $\overline{F}$ gives:

$$V^R{}_{x,n} = V^L{}_{x,n-1} + F_x \tag{3.55a}$$

$$V^R{}_{y,n} = V^L{}_{y,n-1} + F_y \tag{3.55b}$$

and can be represented by a (9x9) matrix, ie:

$$\begin{bmatrix} -\overline{x} \\ \overline{\theta} \\ \overline{M}_y \\ \overline{V}_x \\ \hline \overline{y} \\ \overline{\phi} \\ \overline{M}_x \\ -\overline{V}_y \\ \hline 1 \end{bmatrix}_n^R = \left[\begin{array}{cccc|cccc|c} 1 & & & & & & & & \\ & 1 & & & & & & & \\ & & 1 & & & & & & \\ & & & 1 & & & & & F_x \\ \hline & & & & 1 & & & & \\ & & & & & 1 & & & \\ & & & & & & 1 & & \\ & & & & & & & 1 & -F_y \\ \hline & & & & & & & & 1 \end{array}\right] \begin{bmatrix} -\overline{x} \\ \overline{\theta} \\ \overline{M}_y \\ \overline{V}_x \\ \hline \overline{y} \\ \overline{\phi} \\ \overline{M}_x \\ -\overline{V}_y \\ \hline 1 \end{bmatrix}_{n-1}^L \tag{3.56}$$

The method for obtaining the response is analogous to that obtaining the overall T.M. for the free vibration case (Section 3.4.4, equation (3.49). Thus:

$$\begin{bmatrix} 0 \\ 0 \\ 0 \\ 0 \\ \hline 1 \end{bmatrix}_N^R = \left[\begin{array}{cccc|c} t_{11} & t_{12} & t_{15} & t_{16} & t_{19} \\ t_{31} & t_{32} & t_{35} & t_{36} & t_{39} \\ t_{51} & t_{52} & t_{55} & t_{56} & t_{59} \\ t_{71} & t_{72} & t_{75} & t_{76} & t_{79} \\ \hline 0 & 0 & 0 & 0 & 1 \end{array}\right] \begin{bmatrix} -\overline{x} \\ \overline{\theta} \\ \overline{y} \\ \overline{\phi} \\ \hline 1 \end{bmatrix}_1^L \qquad (3.57)$$

where the same boundary conditions apply as for the case of free vibration. Complex elements t_{19}, t_{39}, t_{59} and t_{79} are the extra elements arising from the forcing column.

Equation (3.57) is equivalent to a set of non-homogeneous equations which are directly solvable. Thus, by transposing elements t_{19}, ... , t_{79} and inverting the remaining matrix (as was done in Section 3.4.4.) gives the state vectors at the left hand boundary:

$$\begin{bmatrix} -\overline{x} \\ \overline{\theta} \\ \overline{y} \\ \overline{\phi} \end{bmatrix}_1^L = \begin{bmatrix} t_{11} & t_{12} & t_{15} & t_{16} \\ t_{31} & t_{32} & t_{35} & t_{36} \\ t_{51} & t_{52} & t_{55} & t_{56} \\ t_{71} & t_{72} & t_{75} & t_{76} \end{bmatrix}^{-1} \begin{bmatrix} -t_{19} \\ -t_{39} \\ -t_{59} \\ -t_{79} \end{bmatrix} \qquad (3.58)$$

For any value of the forcing function F, equation (3.58) can be solved and the response of the rotor at any station k along the shaft can be obtained by applying equation (3.54d)

$$\text{ie} \quad \{\bar{Z}\}_n^R = \prod_{k=1}^{n} [\bar{T}]_k \{\bar{Z}\}_1^L$$

The elliptical whirl orbits can be calculated from the amplitudes along the real and immaginary (x-y) axes as shown in reference (34). The equations of the elliptical motion are given in Appendix D.

The computer programmes based on the T.M.M. are given in Appendix E.

CHAPTER 4

DESIGN AND COMMISSIONING OF THE EXPERIMENTAL APPARATUS

4.1 INTRODUCTION

As the validity of all theories depends on how closely they match physical measurements from a qualitative as well as quantitative point of view, so in this project experimental work was envisaged from the start.

Thus, an experimental rig was designed and commissioned to investigate the effects of important bearing parameters and the flexibility of the bearing pedestal on the critical speed and instability of a damped elastic rotor-bearing system.

The test apparatus and instrumentation were designed to study the above requirements. This chapter describes the design, testing and operation of the experimental equipment used in the critical speed and stability experiments.

4.2 MECHANICAL DESIGN REQUIREMENTS

With the general trend for rotors becoming lighter, more flexible and running above their first critical speed, it was decided to design a rotor of this type to do this.

An obvious configuration was to mount the rotor on two identical test bearings but this would lead to difficulty in obtaining exact similarity between the bearings, particularly since it was intended to investigate a wide range of bearing parameters and flexibility of pedestal support. The basic system chosen is, therefore, similar to the small rigid rotor-bearing system used by Akkok and Ettles (47) in which one bearing is a tight clearance rolling contact bearing acting as a hinge and the other bearing is the one under test. The mass of the rotor was concentrated towards the test bearing by means of a heavy disc or flywheel mounted on the shaft, and, thus introduced gyroscopic effects.

In rotor-bearing investigations it is desirable to have control of several important independent parameters which ideally should be easily set and varied. This was an important consideration to be borne in mind during the rig design. The main parameters of interest are listed below, but not in any particular order of importance.

4.2.1 Bearing Parameters

(a) clearance

(b) load

(c) bore shape

(d) feed groove extent

(e) supply feed pressure

(f) pedestal flexibility

(g) viscosity of lubricant

4.2.2 Shaft Parameters

(a) flexibility

(b) flywheel position

(c) rotational speed

(d) alignment between bearing supports

4.3 DESIGN OF EXPERIMENTAL APPARATUS

Figure 4.1 shows a detailed assembly of the test rotor and Table 4.1 lists the numbered parts referred to in Figure 4.1. Plate 4.1 shows the layout of the experimental rig without instrumentation. The main parts of the rig can be conveniently labelled and described as follows:

4.3.1 Shaft

The main test shaft was 0.984in (25mm) diameter, 27.5in (698.5mm) in length between supports, weighed 8.07lb (3.67kg) and was made of steel EN24. This shaft was split into three parts and had a link section 3in (76.2mm) long and located 9.8in (248.9mm) away from the journal bearing support. The link section was assembled with the main shaft parts to form the test shaft. Several of the link sections were made with different diameters, thus, allowing the flexibility of the main test shaft to be widely varied by interchanging link sections. During the machining of the shaft special attention was paid to its straightness and to the concentricity of shaft, flywheel and journal. The

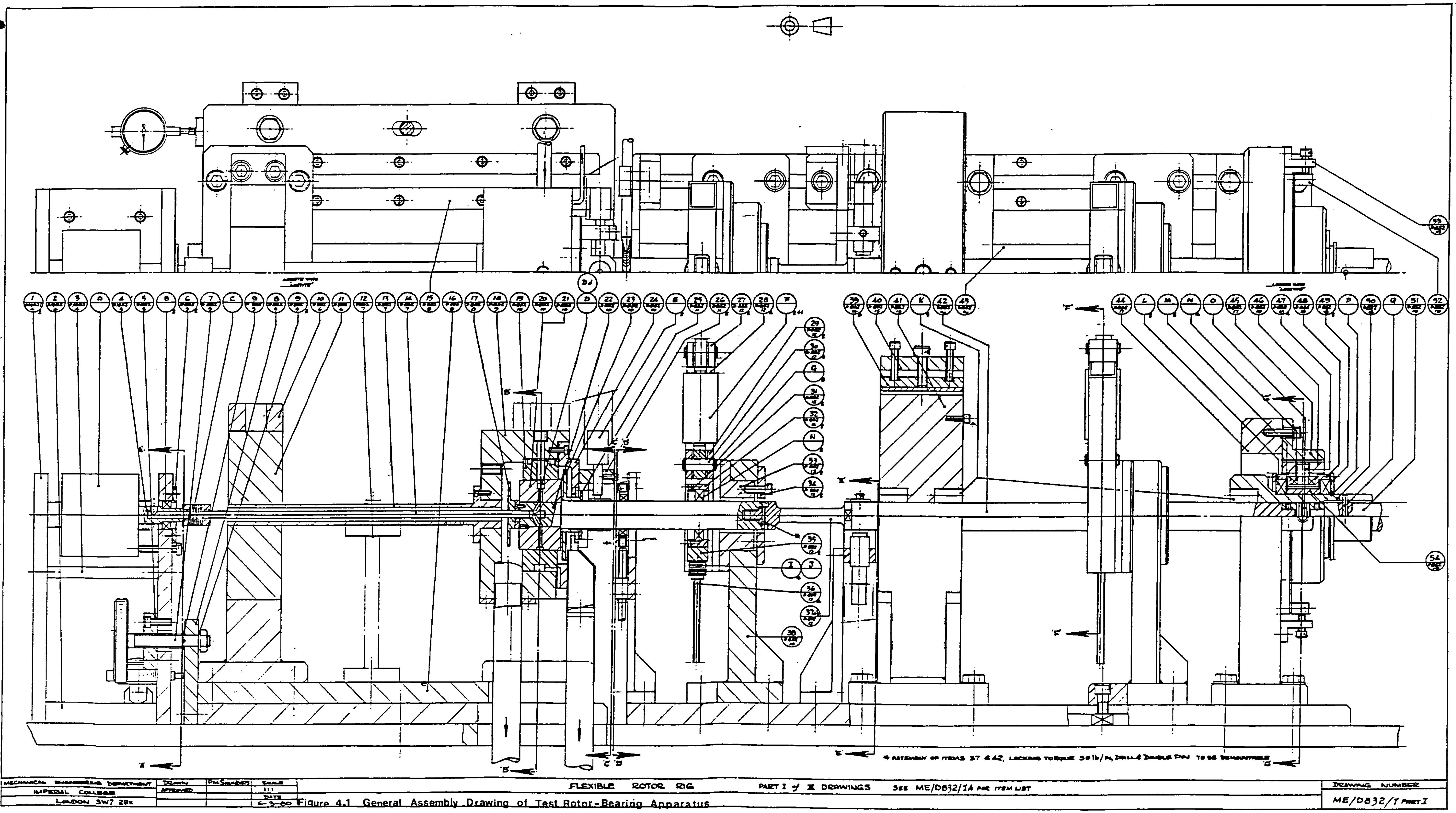

Figure 4.1 General Assembly Drawing of Test Rotor-Bearing Apparatus

ME/D832/1a

DRAWING NUMBER

ITEM No	No OFF	DESCRIPTION	REMARKS	FINISH
1	2	END PLATE	STEEL	OIL BLUE
2	1	BASE PLATE	STEEL	OIL BLUE
3	1	SUPPORT	STEEL	OIL BLUE
4	1	SPINDLE	SILVER STEEL	
5	1	PLATE	STEEL	OIL BLUE
6	2	END PLATE	STEEL	OIL BLUE
7	1	SCREW	STEEL	OIL BLUE
8	1	PLATE	STEEL	OIL BLUE
9	2	WASHER	STEEL HARDEN & GRIND	
10	1	SUPPORT BLOCK	STEEL	OIL BLUE
11	1	INSERT	STEEL	OIL BLUE
12	1	STEADY	STEEL	OIL BLUE
13	1	CANTILEVER BEAM	STEEL	OIL BLUE
14	1	QUILL SHAFT	STEEL, HYPERDERMIC	
15	8	CLAMP STRIP	STEEL	OIL BLUE
16	1	SLIDING BASE PLATE	STEEL	OIL BLUE
17	1	OIL FLINGER	BRASS	
18	1	JOURNAL BEARING HOUSING	STEEL	OIL BLUE
19	1	JOURNAL BEARING	HARD BRONZE	
20	1	INNER BEARING	STEEL EN24	
21	1	" " DUMMY	"	
22	1	MAIN SHAFT (PART I)	STEEL EN24	
23	1	OIL FLINGER	BRASS	
24	1	END CAP & OIL DRAIN	BRASS	
25	1	OIL FLINGER SMALL	STEEL	OIL BLUE
26	2	TRANSDUCER BRACKET	STEEL	OIL BLUE
27	2	BEAM	STEEL	OIL BLUE
28	4	ARM	STEEL TUBE 1"x1"x1/8"	[illegible]
29	2	LINK ARM	STEEL	OIL BLUE
30	4	PIN	STEEL SILVER	
31	2	CLAMP RING	STEEL	OIL BLUE
32	2	BEARING RING	STEEL	OIL BLUE
33	2	SUPPORT BOSS	STEEL	OIL BLUE
34	2	CLAMP DISC	STEEL	OIL BLUE
35	2	LOADING ARM	STEEL	OIL BLUE
36	2	LOADING ROD	STEEL HIGH TENSILE	[illegible]
37	1	LINK SHAFT (PART I)	STEEL EN24	
37a	1	" "	" "	
37b	1	"	" "	
38	1	DE-LOADING BRACKET	STEEL	OIL BLUE
39	6	SHOE	STEEL & P.T.F.E. STRIP 1/8"	
40	1	GUARD	STEEL	OIL BLUE
41	1	MASS SOLID	STEEL	OIL BLUE
42	1	MAIN SHAFT (PART II)	STEEL EN24	
43	1	GUIDE STRIPS	STEEL	OIL BLUE
44	1	REAR MOUNTING	STEEL	OIL BLUE
45	1	MOUNTING PLATE	STEEL	OIL BLUE
46	1	RING	STEEL	OIL BLUE
47	2	SCRD PIN	STEEL 1/4" BSF GRUB SCR	
48	1	BEARING RING	STEEL	OIL BLUE
49	2	CLAMP RING	STEEL	OIL BLUE
50	1	DRIVE COLLAR	STEEL	OIL BLUE
51	1	DRIVE SHAFT	STEEL EN24	
52	3	BLOCK	STEEL	OIL BLUE
53	3	BRACKET	STEEL	OIL BLUE
54	1	SPACER	STEEL	OIL BLUE
55	1	BRACKET	STEEL	OIL BLUE
56	1	BRACKET	STEEL	OIL BLUE
57	2	CAP	STEEL	OIL BLUE
58	2	END PLATE	STEEL	OIL BLUE
59	1	BASE	STEEL	OIL BLUE
60	1	BRAKE DISC	STEEL	
61	1	BRAKE BOSS	STEEL	OIL BLUE
62	1	BASE PLATE (GROUND FINISH)	STEEL 60"x18"x1"	

ITEM No	No OFF	DESCRIPTION	REMARKS	FINISH
63	1	PLATE	STEEL	OIL BLUE
64	1	BRACKET	STEEL	OIL BLUE
65	2	NOZZEL	BRASS	
66	2	CLAMP	BRASS	
67	1	TURBINE	ALUM ALLOY	
68	20	T NUT	STEEL	OIL BLUE
69	1	RING	STEEL EN24	
70	1	MOUNTING	STEEL	PAINT
71	2	HOLDER	STEEL	OIL BLUE
72	1	SUPPORT	STEEL	PAINT
73	1	FRONT DRAIN PIPE	BRASS	
74	1	REAR DRAIN PIPE	BRASS	
75	4	GUIDE STRIP	STEEL	OIL BLUE
76	4	GUIDE BLOCK	STEEL	OIL BLUE
77				
78				
79				
80	1	SUB-FRAME	R.H.S. & PLATE	PRIME
81	2	SIDE FRAME	R.H.S. & PLATE	PRIME
82	4	END BARS	R.H.S. & PLATE	PRIME
83	2	HANGER	STEEL	PRIME
84	12	PAD	RUBBER	
85	1	MASS	CONCRETE	
86	1	HINGED GUARD	STEEL	PAINT
87	2	BLOCK	STEEL	OIL BLUE
88	1	SHAFT	SILVER STEEL	
89	2	PULLEY	STEEL	OIL BLUE
90	1	MOTOR DRIVE FRAME	R.H.S. & PLATE	PRIME

LIMITS ON DIMENSIONS
DEC. ±
FRACT. ±
DEC. MM ± 0·25 MM
UNIT MM ± 1 MM
UNLESS SPECIFIED

ITEM No	No OFF	DESCRIPTION	REMARKS
A	1	SLIPRINGS	R.J. MOULDINGS PS4 [illegible]
B	2	BEARING	'SKF' 6000 P5
C	1	FLEXIBLE COUPLING	'PANMAC' ⌀ 1" BORE
D	1	TRANSDUCER PRESSURE	'KULITE' XCQM-147
Dd	1	THERMOCOUPLE	
E	2	CAPACITANCE PROBE	'WAYNE KERR' MC1
F	2	TRANSDUCER LOAD 0-100lbf 0-1000N	'NOVATECH' F201
G	8	SPRING FASTENER TO SUIT ⌀ 5/8 SHAFT	
H	2	BEARING	'SKF' 6005 P5
I	4	SPRING EXTENSION	'TERRY' T32970
J	4	SPRING COMPRESSION	'TERRY' D12280
K	3	RINGFEEDER LOCKING ELEMENT	25x50
L	2	BEARING	SKF 16008 P6
M	2	BELLEVILLE SPRING	IRC 6008
N	4	BEARING	'BARDEN' SFR6
O	1	FLEXIBLE COUPLING	'PANMAC' 6 1/2 BORE
P	1	SPRING FASTENING TO SUIT 40mm SHAFT	
Q	1	ROLL PIN ⌀ 3/16 x 1 1/2 LONG	
R	1	TOOTHED WHEEL STEEL	'MUFFET' 16-60
S	1	PROBE MAGNETIC	'AIRPAX' 1-0054
T	1	PROBE MAGNETIC	
U	2	BEARING FAG	FAG 6005
V	2	SPRING FASTENER FOR ⌀ 25mm SHAFT	
W	1	DISC BRAKE 'TWIFLEX' M.S.E.	
X	2	CARDAN SHAFT COUPLING FLANGE	1401-065
Y	1	DIAL INDICATOR	'BATY' D3
Z	1	PHOTO ELECTRIC COUNTER	'SCANOMATIC' S322-3
AA	1	BEARING FAG	61806
BB	2	PROBE CAPACITANCE	WAYNE KERR MD1
CC	3	'O' RING	
DD	12	THERMOCOUPLE	
EE			
FF			
GG			
HH	4	AIR MOUNT 'FIRESTONE' No 25 NBD-7042	
II	1	CARDAN SHAFT 'HARDY SPICER' HA001X300-006	
JJ	2	PLUMMER BLOCK	ASAH/UKP206+H2306
KK	1	BELT 'MIRACLO' CONSTRUCTION 86 L1860 TYPE 6 26mm	
*** LL	1	CONTROLLER 'MAWDSLEY'S'	DSS 700
MM	2	COUPLINGS 'DOKO'	100/82 26mm Bore
NN	1	MOTOR 'MAWDSLEY'S'	1120 143
OO			
PP			
QQ			

* MODIFY TO SUIT SHAFT, FIT INDEX MARKER

* * BORE TO SUIT SHAFTS, DRILL & TAP 5/16 B.S.F. FOR GRUB SCR'S

* * * EXTEND CABINET FIXING HOLE TO SUIT ITEM 90

FINISH:- GENERALLY A NEAT MACHINE FINISH, REMOVE ALL SHARP EDGES PROTECT ALL UNSPECIFIED ITEMS FROM CORROSION

TOTAL No OF DRAWINGS. ME/E832/1I, 1II, & 1III TO ME/D832/31

ITEM No	No OFF	DESCRIPTION	MATERIAL	REMARKS

Mechanical Engineering Dept.	DRAWN	P.M. [illegible]	SCALE	TITLE	F.R.R. ITEM LIST FOR SHEETS ME/D832/1 I, II, III
	APPROVED		1:1		
Imperial College,	TRACED		DATE		
London SW7 2BX	CHECKED		27-5-80	AMMDTS	TABLE 4.1 List of Items Referred to in General Assembly Drawing

CLASS

DRAWING NUMBER

GROUP ME/D832/1a

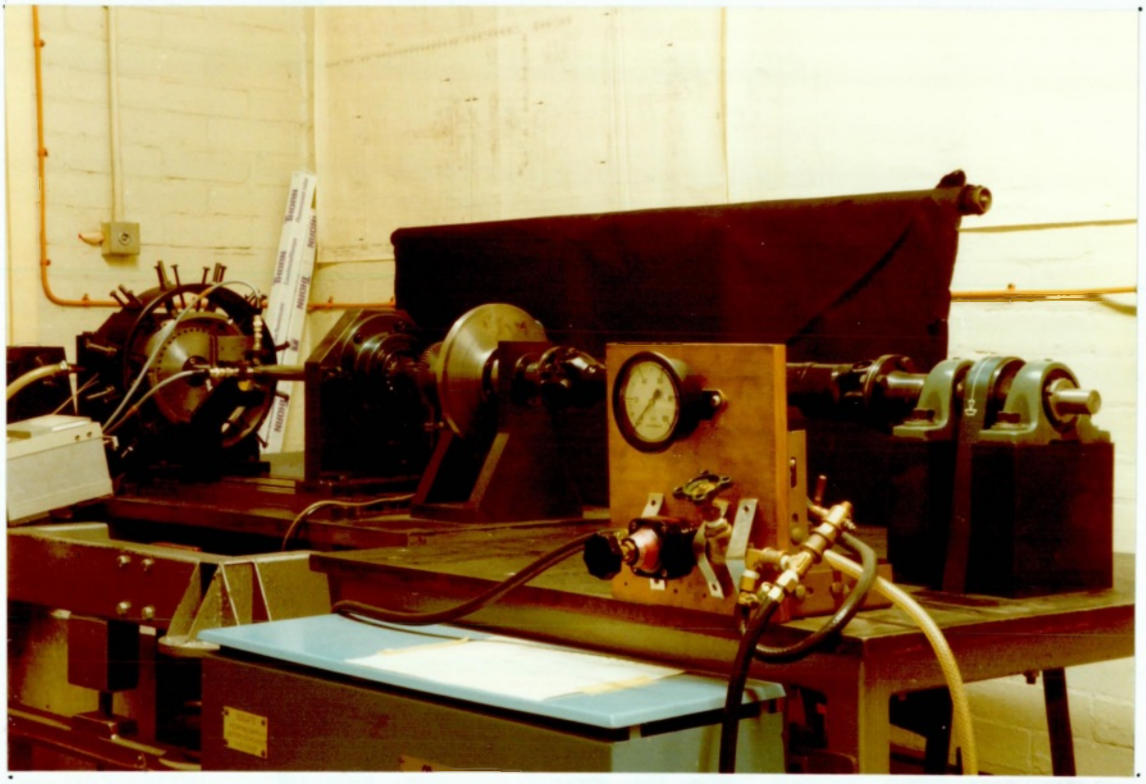

Plate 4.1 Test Rotor and Drive Assembly

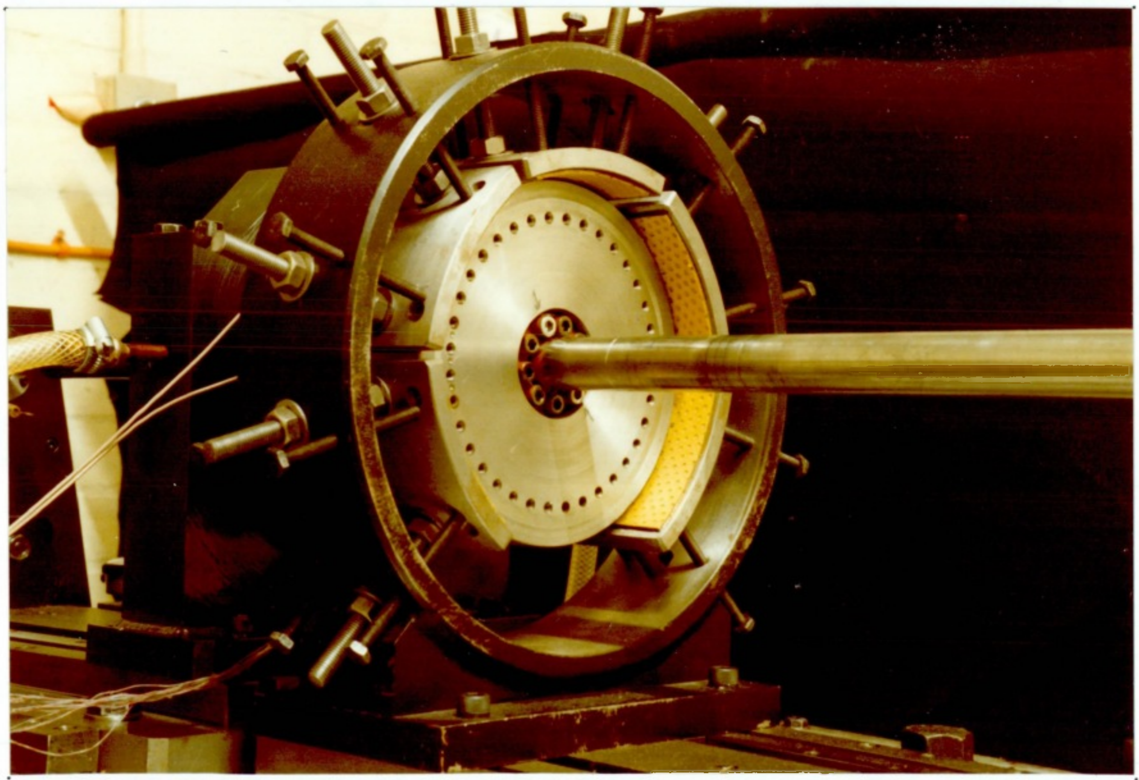

Plate 4.2 Flywheel and Guardring

degree of straightness of the shaft achieved on assembly was within 0.0005in (0.013mm).

4.3.2 Flywheel

The flywheel had a diameter of 6.672in (171.8mm) and length of 3.0in(74.9mm) and a mass of 28.59lb (12.99kg), producing a total rotor mass of 36.66lb (16.66kg). Each side of the flywheel possessed a boss into which was inserted a tapered ring locking device (Ringfeder). This allowed the flywheel to be stationed at any point along the shaft and subsequently locked in that position Plate 4.2. This method of attachment was preferred to the more usual method of shrink fits because the problems associated with this form of fixing, Kimball and Lovell (63), of impellers, flywheels etc, onto a shaft. In the experimental work the distance between the centres of the flywheel and journal support was fixed at 5.0in (127mm). This gave a static deflection of 0.0032in (0.081mm) at the flywheel and 0.0050in (0.127mm) at the shaft centre, with a static load or reaction at the test bearing of 28.68lbf (127.57N) and a measured first critical speed of 2890RPM.

Each face of the flywheel had a concentric series of 36 balancing holes each 10 degrees apart, drilled to a depth of 0.50in (12.7mm) and tapped to 2BA, on a 5.2in (132mm) diameter. This was to facilitate in the balancing of the rotor, Plate 4.2. The assembled rotor was balanced in an Avery-Shenk balancing machine at 1200RPM. The balancing achieved was 0.009oz (0.25g) at plane I (left face of flywheel adjacent to the journal bearing) and 0.018oz (0.50g) at plane II. It was found to be unnecessary to carryout in-situ balancing of the rotor as it was not intended to run the rotor at or near its critical speed, and sufficiently smooth running was obtained below and above the critical speed. Typically, peak to peak synchronous amplitudes at the shaft centre of less than 0.0005in (0.013mm) were measured when the running speed was in the region where instability occured.

To limit the amplitude of the rotor to safe levels a guard-ring was employed for the flywheel, Plate 4.2. This consisted of 6 curved pads or shoes attached by adjusting bolts to a heavy guard-ring, the pad surfaces were lined with a low friction material Glacier DX. The pads were adjusted to restrict the level of vibration of the flywheel and, hence, the shaft to a preset amount.

The guard-ring was attached to a base which could be moved axially and clamped in any position in the same manner as described for the test bearing and gimbal pedestals, Sections 4.3.4 and 4.3.5 respectively.

4.3.3 Test Bearing

The journal and bore of the cylindrical test bearing were tapered with an included angle of 4 degrees, to allow the radial clearance to be varied over a range of 0.0010in

(0.254mm) by moving the bearing relative to the journal. The journal was made from EN24 steel and contained a chromel-alumel thermocouple at its centreplane, about 1mm below the surface. The wires from the thermocouple were fed through a light hollow "quill shaft" made of stainless steel and attached at the outboard end of the journal, to a slip ring assembly. The assembly was driven by the "quill shaft" via a flexible aluminium coupling (Panamec). The journal had a nominal diameter of 2.5in (63.5mm) and was an interference fit with the test shaft.

The bush was made from hard bronze and had a 2.5in (63.5mm) nominal diameter with a length of 1.25in (31.75mm), and hence a length to diameter ratio of 0.5, Figure 4.2. The bush contained two axial feed ports or grooves, arranged at 90 degrees to the load vector. For the initial experiments, the groove angle, α , was 30 degrees giving a groove width of 0.65in (16.51mm). The axial length of the groove was 1in (25.4mm) and its maximum depth was 0.156in (3.97mm), with holes 0.25in (6.35mm) in diameter for feeding oil into the grooves, Figure 4.2.

Bearing temperatures were measured by 12 chromel-alumel therocouples arranged around the mid-plane of the bush, about 1mm below the bush surface Figure 4.3.

To ensure identical tapers on the journal and bush, the bush was lapped to fit a dummy journal which was of the same taper as that of the test journal.

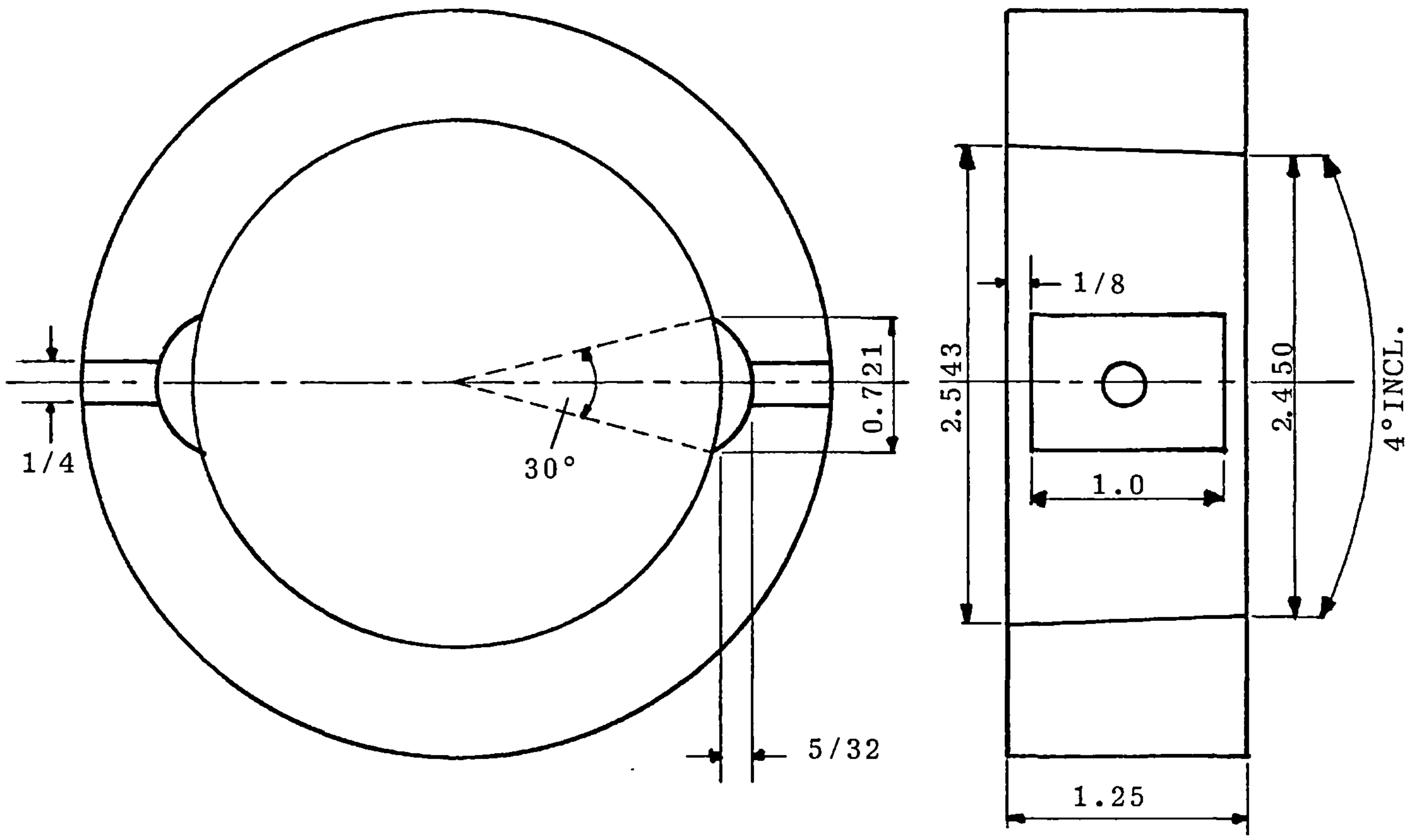

DIMENSIONS IN INCHES SCALE - FULL SIZE MATERIAL - BRONZE

Figure 4.2 View of Bearing Bush Showing Oil Feed Ports

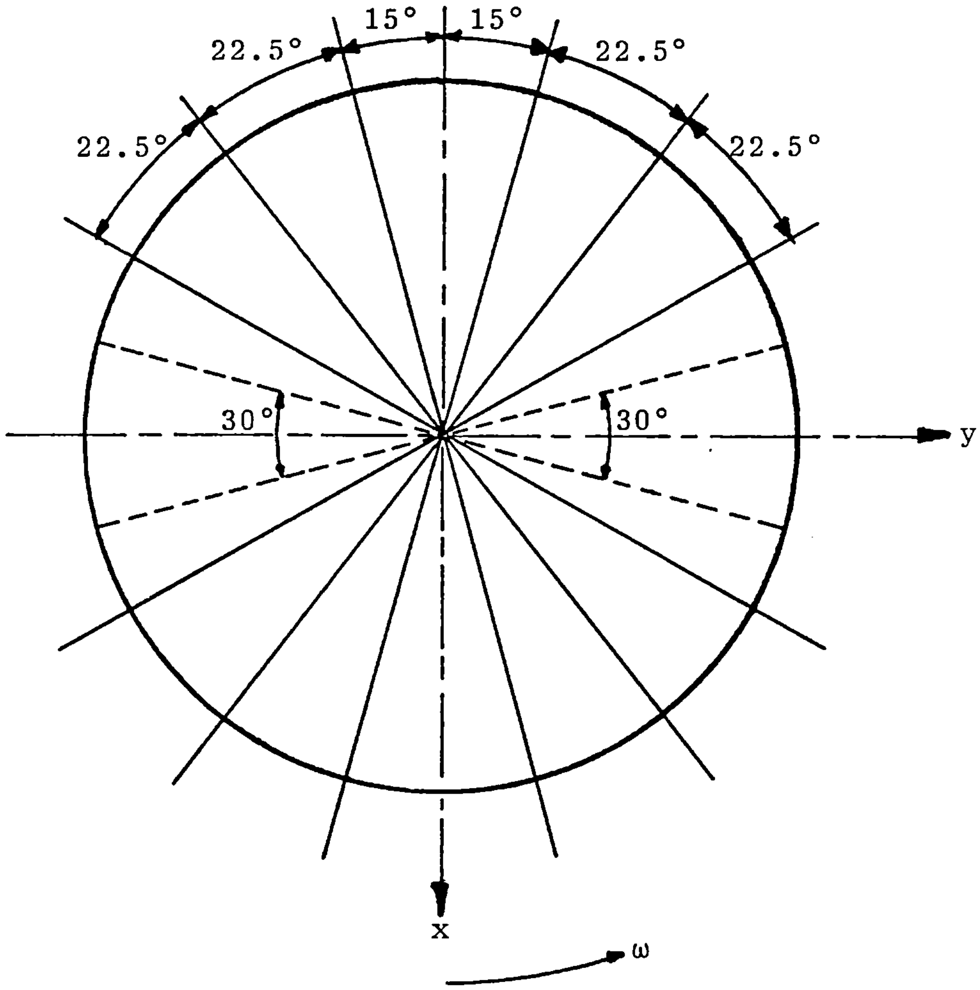

Figure 4.3 Spacing of Thermocouples Around the Bearing Bush

Brass oil-flingers were positioned each side of the journal so that scavenged oil could be returned under gravity to the main supply tank. A free axial gap on each side of the bearing was allowed to ensure that the discharge oil pressure did not exceed ambient pressure.

The bush was an interference fit within a steel bearing housing. To facilitate in the removal of the bush from the housing there were three tapped holes at the back of the housing through which bolts could be inserted to push the bush out. The bearing housing was rigidly clamped by a support pedestal.

4.3.4 Test Bearing Pedestal

As stated in Section 4.2.1, two of the design requirements for the bearing were the ability to change the running clearance and support flexibility. Pedestal flexibility was achieved using a cantilever design in which a hollow circular steel beam (0.70in O.D. and 0.54in I.D.) attached to the rear of the bearing housing could be clamped in any position by axial movement of the pedestal, using a dummy mass to simulate the bearing housing for the flexible support positions. A photograph of the test bearing housing and pedestal is shown in Plate 4.3. Thus, the flexibility of the bearing pedestal could be varied over a wide range, with the bearing rigidly supported when the pedestal was bolted directly under the bearing housing as shown in Plate 4.3.

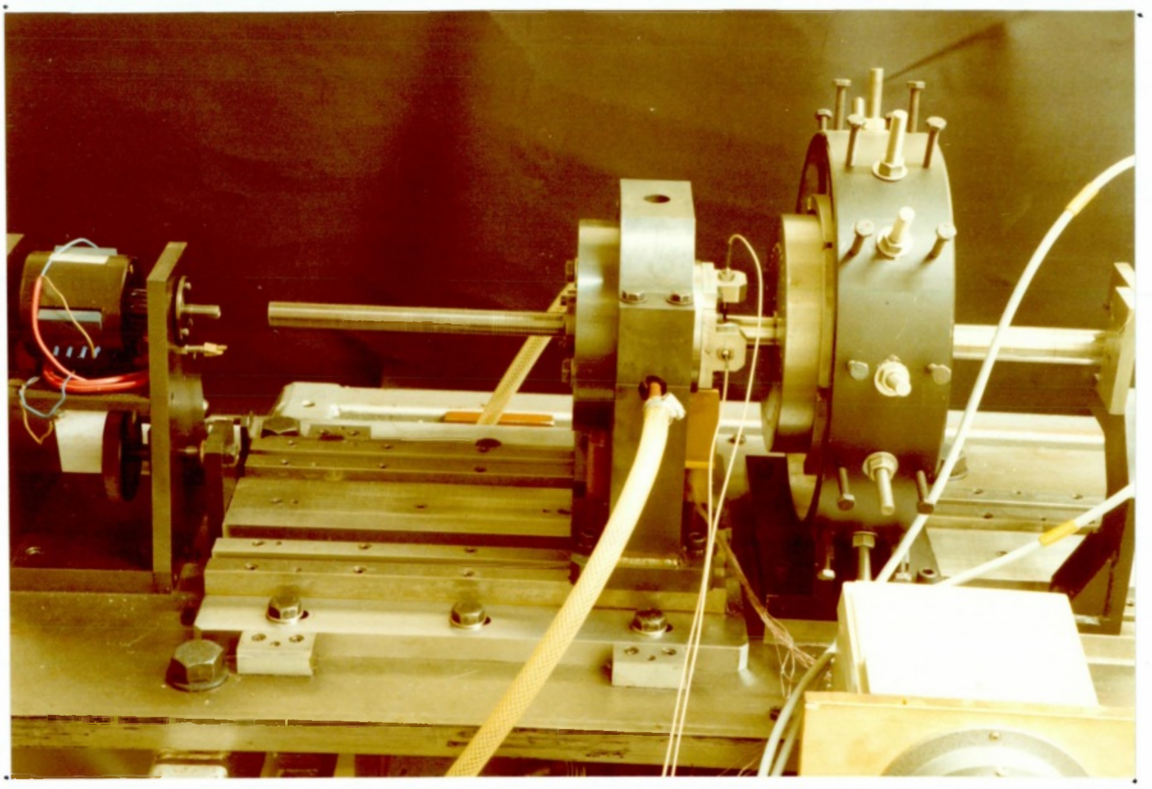

Plate 4.3 Test Bearing Housing and Pedestal

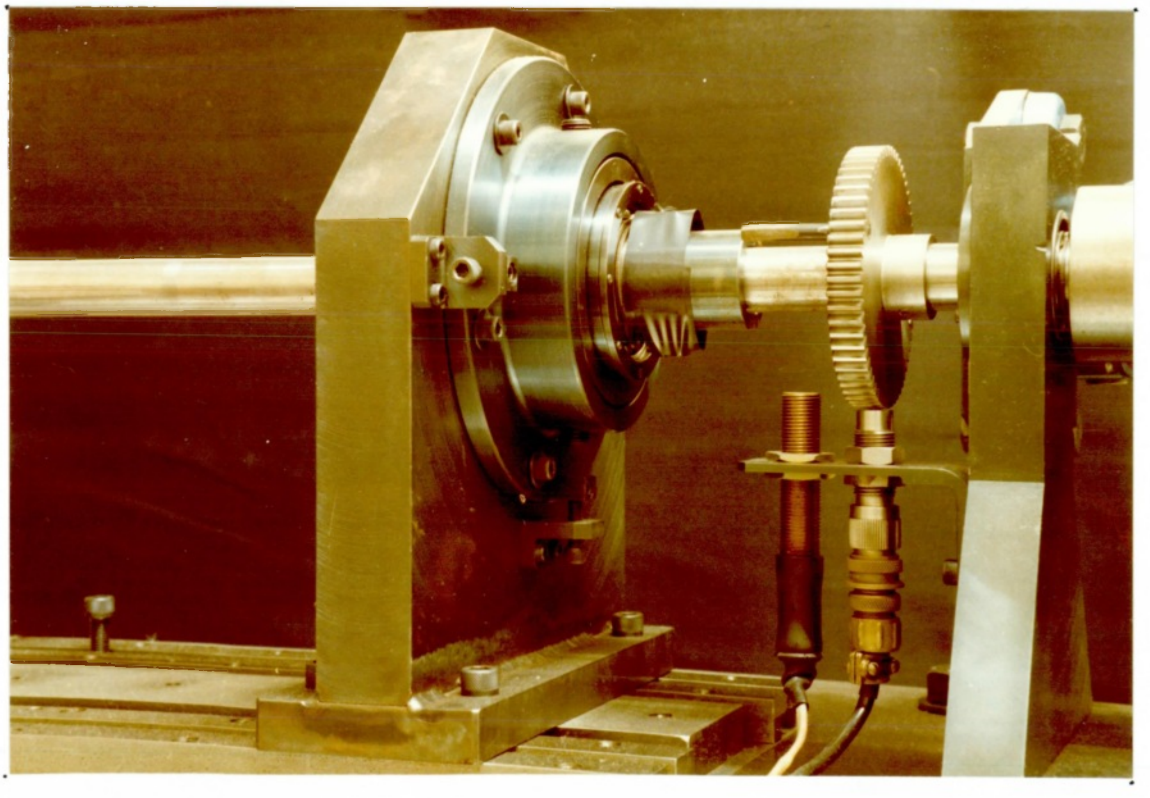

Plate 4.4 Gimbal Pedestal

During the design and machining special care was taken to obtain concentricity of bush, bearing housing and cantilever support beam. To maintain axial alignment of the bearing with that of the shaft for rigid and flexible support conditions, a guide block or "tongue" was attached to the underside of the pedestal using dowels.

A pedestal base plate was constructed in which a channel or guide strip was made from sections of steel bolted to a plate using dowels, Plate 4.3. Hence, by keeping the "tongue" located in its channel as the pedestal was moved to obtain different flexibilities, ensured that axial alignment was maintained. With the aid of T-slots also attached to the pedestal plate it was possible to bolt the pedestal to its plate at any position within its range of movement, Plate 4.3.

Radial clearance could be infinitely varied from zero to 0.010in (0.254mm) by axial movement of the pedestal base plate. This was done using guides located with dowels on each side of the pedestal base plate, Plate 4.3. The guides were bolted to a large main base plate measuring (60x18x1)in or (1524x457.2x25.4)mm and weighing 306lb (139kg). The guides ensured that the pedestal plate was constrained to move in an axial direction only relative to the shaft-bearing axis, thus, maintaining alignment of the bearing and shaft. The pedestal plate could be bolted to the main base plate in any position within its range of movement.

Movement of the pedestal plate was achieved by rotation of the threaded bolt attached to the pedestal plate and slipring assembly support, which in turn was fixed to the main base plate, Plate 4.3.

Clearance was measured by moving the pedestal plate forwards until zero clearance was obtained in the journal (this was tested for by attempting to rotate the main test shaft, which in the zero clearance position was locked) and then zeroing a clock gauge. The pedestal plate was then moved back a known distance (measured on the clock gauge) so that, knowing the taper angle, the running clearance could be found, nominally to within three significant figures.

4.3.5 Gimbal Pedestal

As described in Section 4.2 it was decided to have one test bearing and a rolling contact bearing for the other support, because of the desire to investigate a wide range of bearing parameters. In the work of (47), a self-aligning double row spherical track ball bearing secured by means of a collet to the shaft was employed. Unfortunately, vibrational problems were found to be associated with this method of fixing. Thus, it was decided to mount the rolling element bearing employed in this project in a gimbal support. This would allow the bearing to pivot about two orthogonal planes, acting as a hinged support.

A drive collar was attached to the end of the test shaft opposite to the test bearing, by a Ringfeder locking device (as employed for the flywheel), Figure 4.1. The drive collar was supported within the gimbal mounting by two SKF precision deep groove ball bearings, type 16008 P6, separated by a spacer and two Belleville springs, IEC 6008. It was arranged so that the mid-plane of the two bearings coincided with the gimbal centre line.

A bearing ring was attached to the two bearings by means of clamprings located on the outside of each bearing. The bearing ring contained two diametrically positioned Barden bearings SFR6, which allowed the bearing ring to pivot about a horizontal axis by means of two grub screws, which were screwed through an outer-ring into the Barden bearings, Plate 4.4.

The outer-ring also contained two Barden bearings, which allowed it to pivot about a vertical axis by means of a further two grub screws, which were screwed through the mounting plate into the Barden bearings. The mounting plate was bolted to a rear mounting or pedestal, Figure 4.1 and Plate 4.4.

The driven shaft (test shaft) was connected to the driving shaft via a Panamec flexible coupling BSZ 5, with the gimbal and pedestal so positioned that the centreplane of the coupling coincided with the gimbal plane of action.

As listed in Section 4.2.2, alignment of the shaft with the test bearing was a parameter it was thought desirable to have control of. This was achieved by having clearance holes in the mounting plate. By slackening the bolts securing the mounting plate to the pedestal it was possible to move the test shaft horizontally or vertically. This was achieved by adjustment of screws located against blocks on the mounting plate, Plate 4.4. Movement of the shaft was measured by two clock gauges.

As with the test bearing pedestal the gimbal pedestal also had a guide block or "tongue" located on its underside with dowels. By constraining the guide block to move in its guide channel, axial alignment of the gimbal pedestal was ensured for any position of clamping. Also, with this method shorter test shafts could be employed as the gimbal pedestal would remain aligned as it was moved towards the test bearing. The driving shaft in this case would have to be extended to ensure that the mid-plane of the flexible coupling between driven and driving shaft still coincided with the centreline of the gimbal.

The drive shaft contained a roll pin which located in a channel of the drive collar. This was installed as a safety precaution against breakage of the flexible coupling, leaving the test shaft coasting to a stop. If this were to happen the roll pin would drive the test rotor and it would still be possible to stop the rotor using the disc brake.

4.3.6 Loading Mechanism

To alter the bearing load a mechanism was designed which could apply a maximum load of 31lbf (138N) in any direction in a vertical plane. A front and rear view of the loading device is shown in Plate 4.5. It consisted of a beam connected to two arms which in turn were attached to a support boss which could rotate within the main support bracket. The support boss could be locked in any position by means of a clamp disc.

A Novatech load cell was attached to the beam by means of a self-aligning housing, the lower end of the cell was connected to a link arm via another self-aligning housing. The link arm was connected to a load arm by means of two loading rods. The load arm contained a bearing in its housing which was a sliding fit on the main test shaft, Plate 4.5.

Terry compression springs D 12280, were inserted over each rod and fastened with washers and nuts in such a manner that they located against the underside of the loading arm. Thus, load could be applied to the shaft by compressing the springs equally, the resultant load registered by the load cell.

Changing the direction of the applied load was achieved by slackening the bolts on the clamping disc and rotating the loading mechanism to the desired angle and retightening

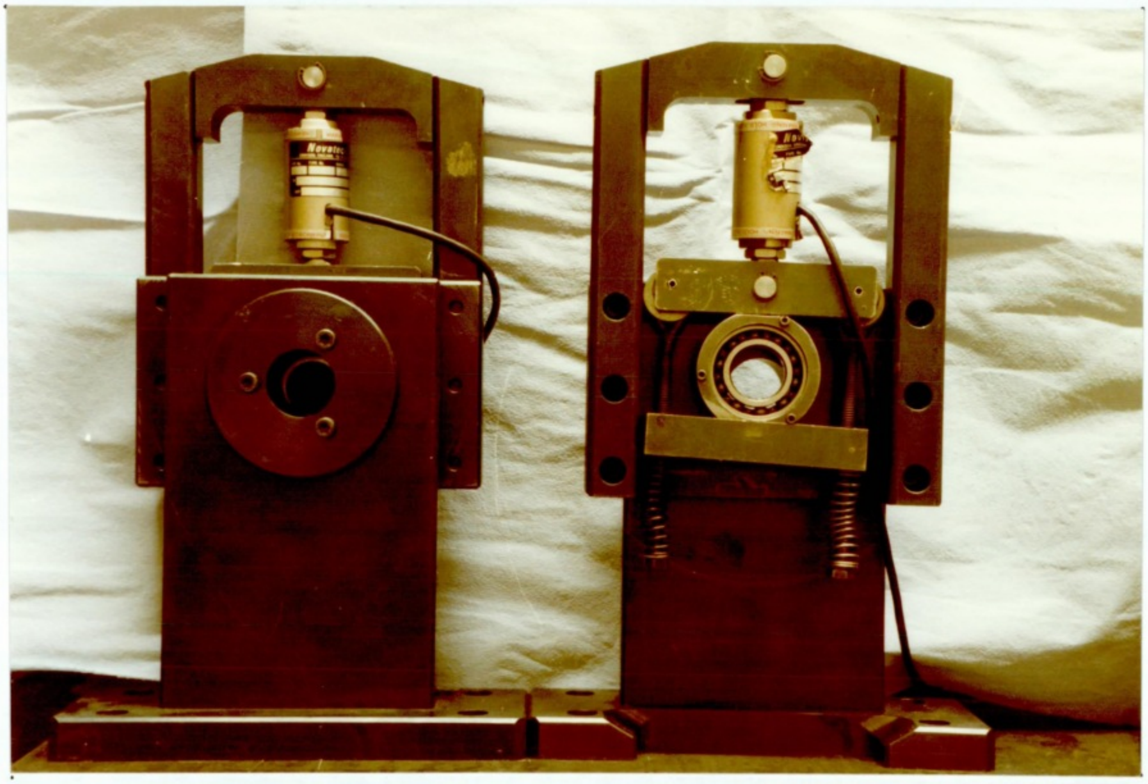

Plate 4.5 Front and Rear Views of Loading Mechanism

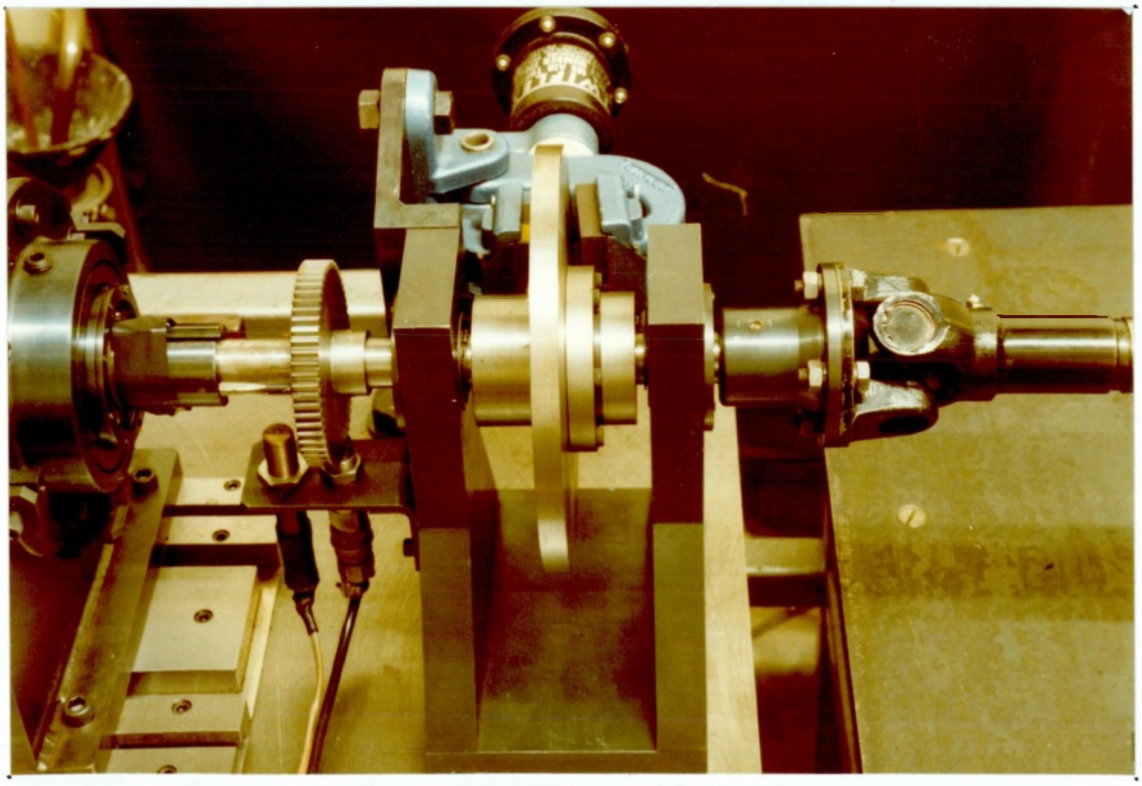

Plate 4.6 Disc Brake Assembly

the bolts. The main support bracket and loading mechanism could be moved axially and bolted in any postion relative to the shaft in the same manner as for the test bearing and gimbal pedestals. Two of the loading devices were constructed.

4.3.7 Oil Supply System

A separate framework was used for the oil supply unit. Oil was supplied from a tank to the test bearing by means of a Varley double helical gear pump. A Fairley filter containing a 1 micron filter element was used to protect the test bearing. A water cooled heat exchanger was incorporated in the by-pass circuit to control the oil temperature in the tank. The oil supply pressure to the bearing was set at the desired value by adjustment of the by-pass valve and a needle valve in the supply line. Oil supply pressure to the bearing was measured using a calibrated Budenburg diaphram gauge.

Flexible pipes were used in the connections between the oil supply framework and immediately prior to the test bearing housing, so that the supply pipe did not affect the housing motion for the flexible pedestal experiments and to prevent the transmission of vibration coming from the gear pump. Drained oil from the bearing was collected under gravity by two flexible pipes and returned to the tank.

The lubricant used in all the test was Shell SAE 30, its viscosity was measured using a Ferranti-Shirley viscometer with a rotating cone contacting a plate. A calibration graph of viscosity against temperature is shown in Figure 4.4.

4.3.8 Drive Unit

A Mawdsley 5.5 HP (4.1KW) DC motor incorporating a thyristor controller was used to vary the speed of the rotor. This provided a speed control from zero to 3000 RPM. The higher speed range necessary for the test rotor was obtained using two crown pulleys and a flat belt. The large pulley was attached to the shaft of the electric motor and the smaller driven pulley was attached to a lay-shaft supported by two self-aligning plummer-blocks, Plate 4.1. This arrangement gave a theoretical top speed of 10,000 RPM.

To prevent vibration from the drive unit reaching the test rotor through the drive conections, the test rotor was coupled to the drive via a Panamec flexible coupling (Section 4.3.5) and a Hardy Spicer cardan shaft with a double universal joint, Plate 4.1. A pneumatically operated Twiflex disc brake was incorporated between the gimbal pedestal and the cardan shaft, Plate 4.6. The cardan shaft was bolted to a flange on the disc brake assembly and also to another flange attached to the driven pulley lay-shaft, Plate 4.1. The disc brake assembly was installed as a safety precaution, allowing the rotor to be slowed down

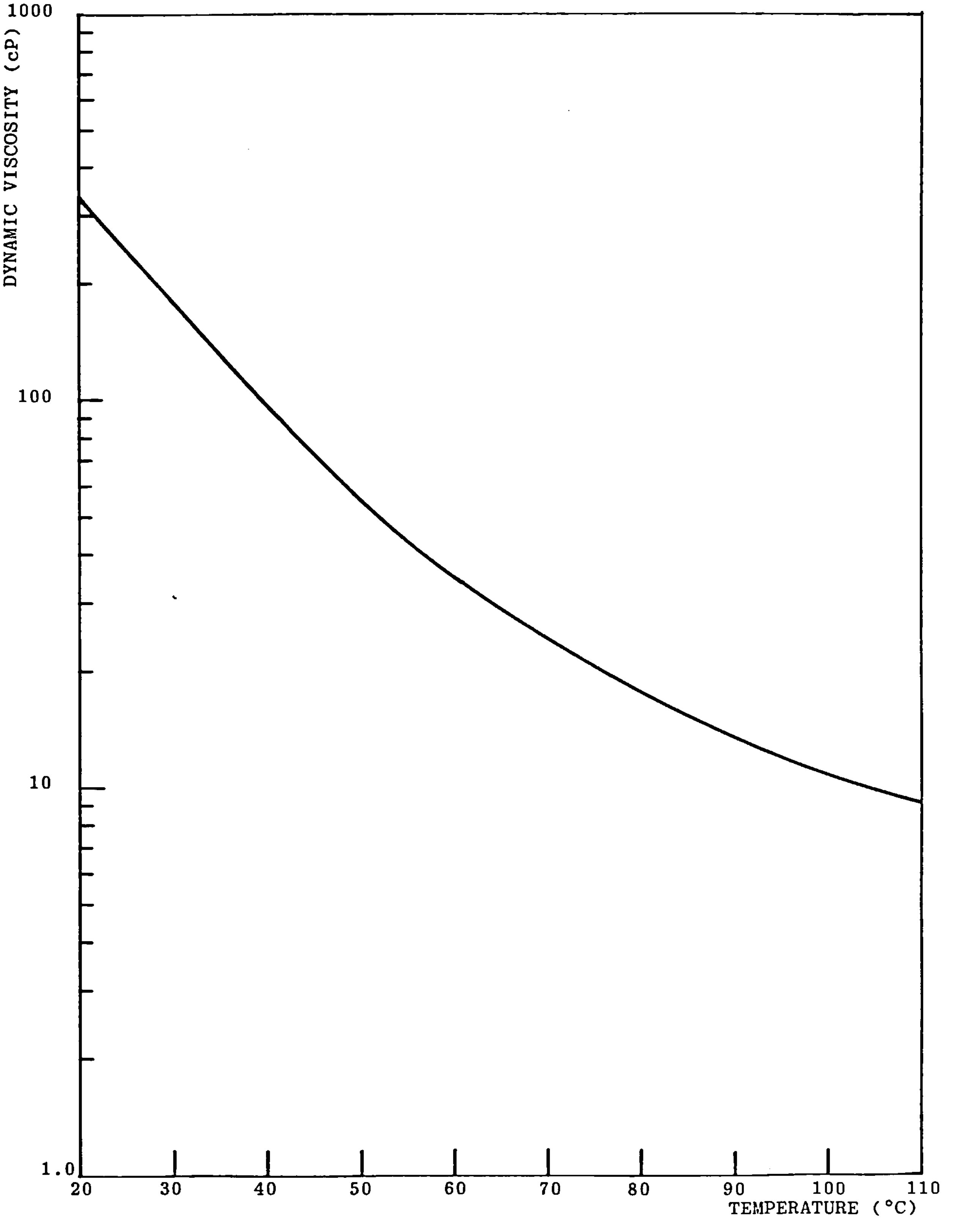

Figure 4.4 Viscosity Calibration for Shell SAE 30

through resonances and stopped rapidly in the event of an emergency. The braking torque could be varied by adjustment of the air supply pressure.

4.3.9 Support Frame

The main base plate together with the test rotor were bolted to a framework made from mild steel box section tubing. The support frame consisted of an upper frame from which was suspended a 1 ton concrete block supported by two steel straps which were bolted to the upper frame. The purpose of the concrete block was to provide a stable platform to which the support pedestals and vibration measuring transducers could be attached.

The upper frame was supported by a lower frame with the aid of eight bolts, two on each side of the frame. When experiments were being conducted the upper frame with the test rotor on its base plate and the suspended concrete block were uncoupled from vibration originating from the drive unit and the foundations by inflation of four Firestone pneumatic tyres or airmounts, one located at each corner of the frame, between the upper and lower frames Plate 4.7. The cardan shaft with its universal joints and splined shaft allowed for the movement between the drive shaft and the test shaft when the airmounts were inflated.

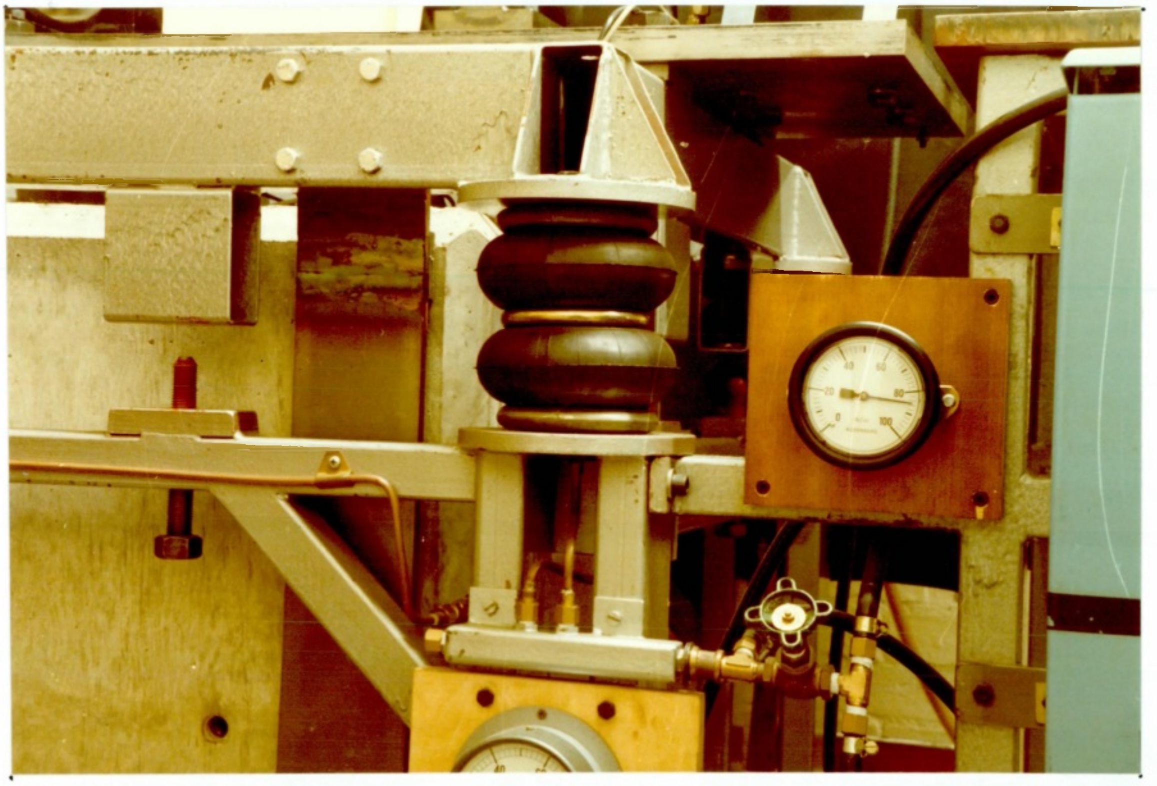

Plate 4.7 Airmounts and Support Framework

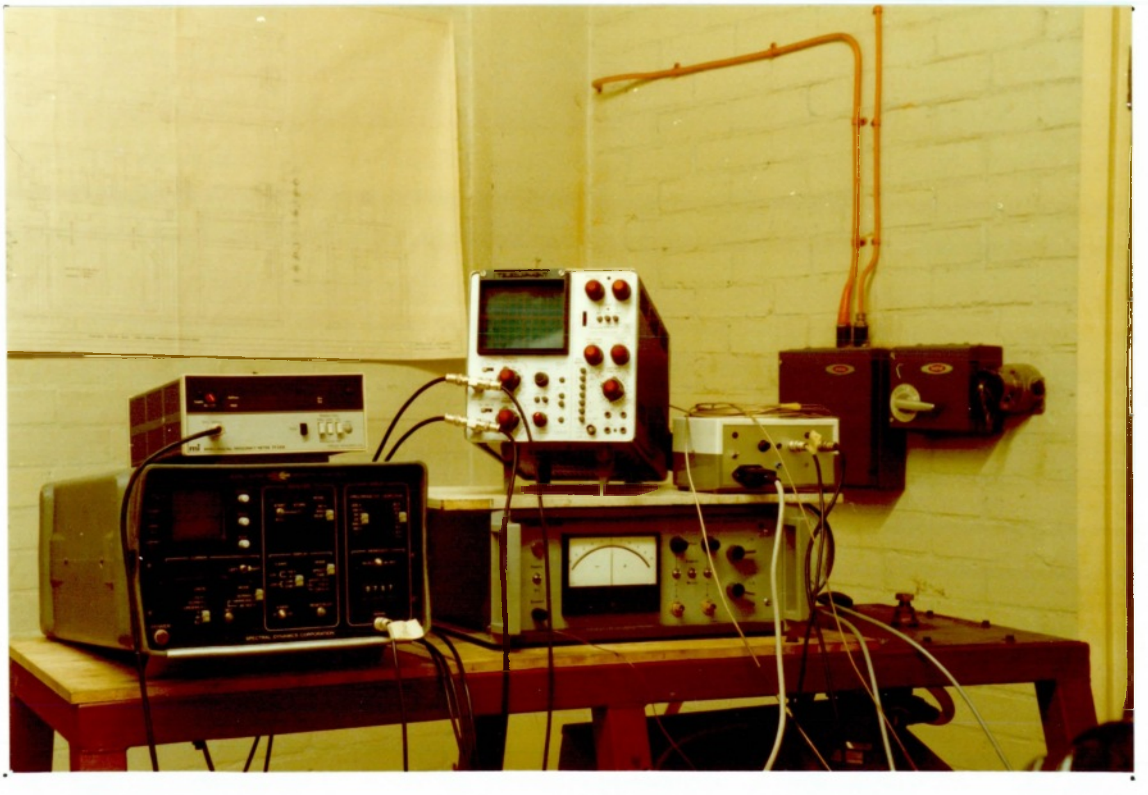

Plate 4.8 Instrumentation

4.4 INSTRUMENTATION

The horizontal and vertical movement of the shaft at the same location was measured by two orthogonally fixed non-contacting capacitive transducers (Wayne Kerr MD1), mounted on a bracket which could be moved along the shaft, thus, allowing the vibration to be monitored at any point, Plate 4.1.

The probes were connected by co-axial cables to a two channel Wayne-Kerr frequency modulated amplifier, Plate 4.8, which gave a voltage analogue of the transducer signals. Each probe was calibrated as a unit, together with its co-axial cable and amplifier, Figures 4.5 and 4.6. The sensitivity of the probes were nominally 1 volt per 0.050in (1.27mm) or 20mV/0.001in (20mV/0.00254mm).

Motion of the test shaft at a distance of 2.0in (52mm) from the mid-plane of the journal was measured by two non-contacting eddy current probes (Dymac M61), fixed at right angles in brackets which were bolted to the bearing housing, Plate 4.3.

The probes were connected by cables to two Dymac eddy probe drivers (type M606) energised by a 24 volts DC power supply, Plate 4.8. The probes and drivers operated by providing a DC voltage proportional to the distance between probe tip and the surface of the shaft being monitored. All

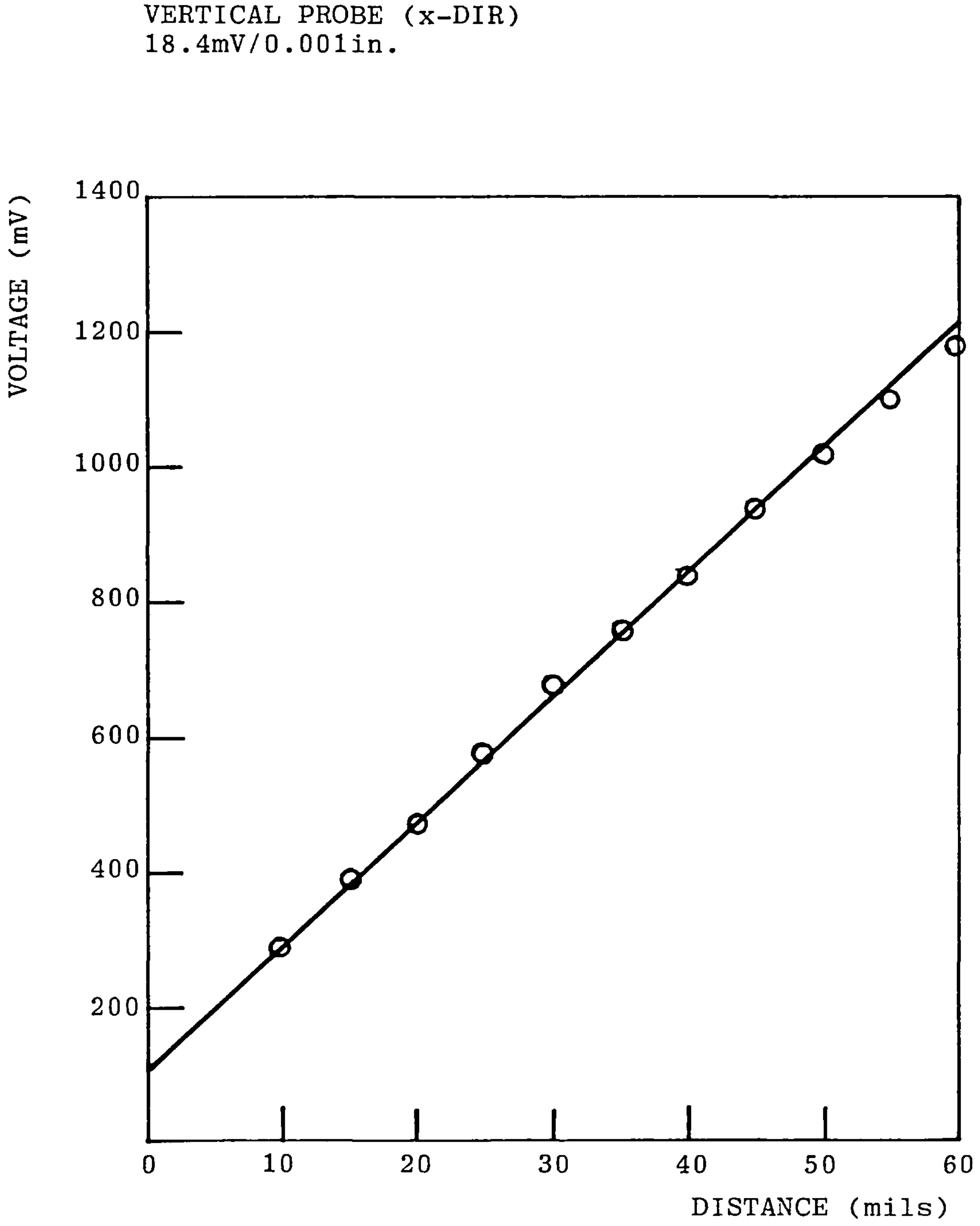

Figure 4.5 Calibration for Vertical MD1 Transducer Probe

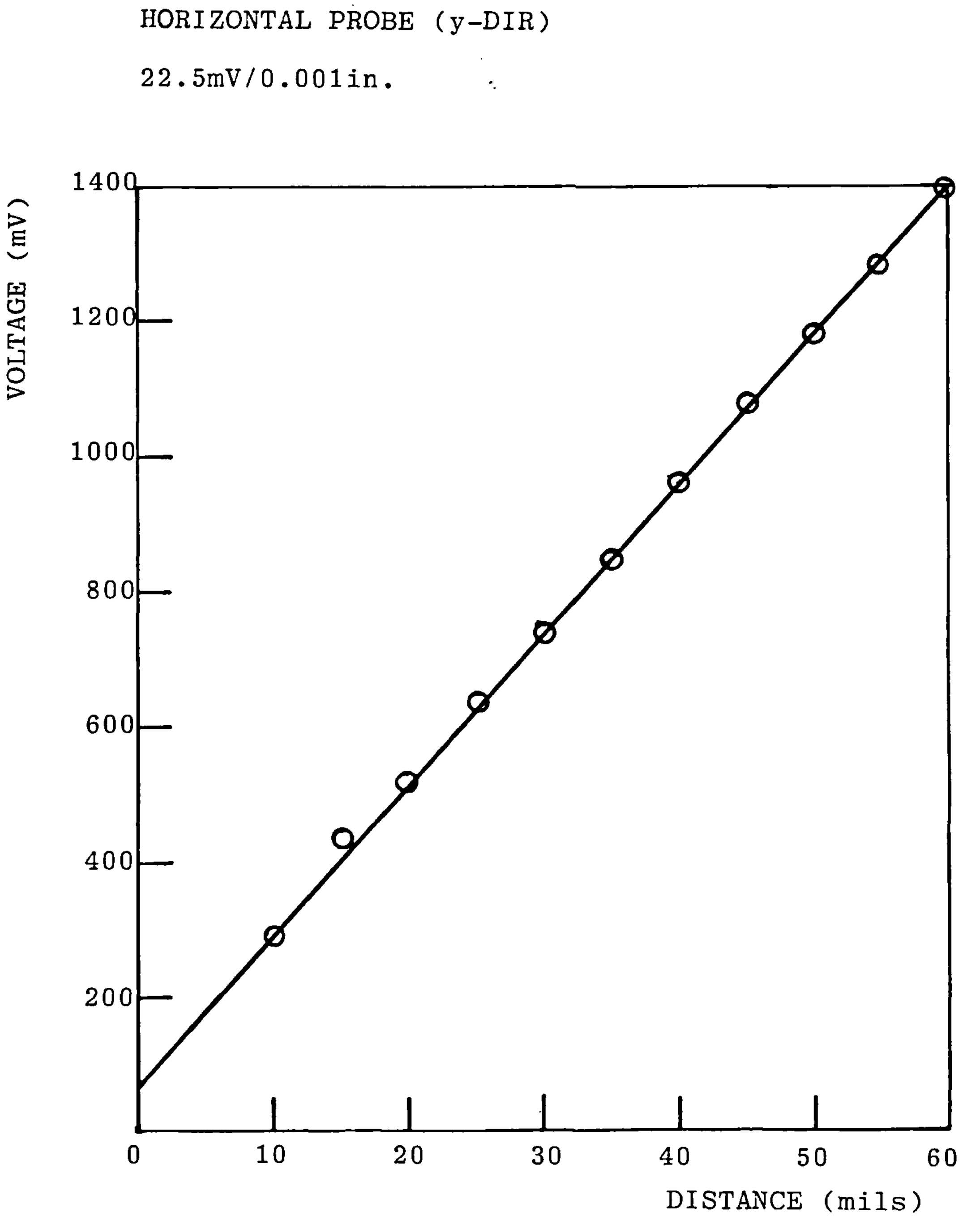

Figure 4.6 Calibration for Horizontal MD1 Transducer Probe

Dymac units were factory calibrated and drivers and eddy probes were interchangeable with less than 5% performance change without recalibration. Hence, it was not necessary to calibrate these units in-situ. The usable range of the probe, at 200mV/0.001in (200mV/0.0254mm) sensitivity, is typically 0 to 0.085in (2.16mm).

The accuracy of both the capacitive probes and the eddy current probes were $\pm$0.0005in ($\pm$0.013mm).

The whirl orbits were observed by connecting either the eddy current probes or the capacitive probes to a dual beam Telequipment oscilloscope set for the x-y mode, Plate 4.8.

Frequencies and amplitudes were measured by connecting anyone of the probes to a single channel Spectral Dynamics micro FFT (Fast Fourier Transform) analyser Plate 4.8, which at any set speed of shaft rotation would display the frequency spectrum. It was possible to set sensitivity controls on the analyser depending on which type of probe was in use, so that amplitudes were obtained in thous or millimeters at half peak or peak to peak values.

The shaft speed was measured by an inductive probe placed close to a 60 teeth disc located on the driving shaft between the disc brake assembly and the gimbal pedestal, Plate 4.4. The probe was connected to a Marconi digital frequency meter which displayed the speed in RPM with an accuracy of $\pm$5 RPM, Plate 4.8.

The chromel-alumel thermocouples located round the bearing bush were connected to a calibrated 10 channel Comark electronic thermometer. This instrument had an accuracy of $\pm 0.5^{o}C$.

The load cells attached to the loading mechanisms were connected to a Novatech digital electronic load indicator (power supply plus amplifier) calibrated in pounds force (lbf) with an accuracy of ± 0.2lbf.

4.5 COMMISSIONING OF EXPERIMENTAL APPARATUS

4.5.1 Shaft and Bearing Alignment Setting

Considerable care was taken in the design and manufacture of the experimental apparatus to assure close alignment between the test bearing and the shaft axis.

It was decided to set the alignment of the test rotor (shaft and bearing) without the flywheel mounted on the shaft, as the shaft would then be approximately straight apart from a small static deflection due to the weight of the shaft (0.001in or 0.025mm at the centre) and lack of straightness due to machining (0.0005in or 0.013mm).

The bearing and gimbal pedestals were bolted in their respective locations with the bearing at zero clearance, using clock gauges (graduated in 0.0001in divisions) to ensure that the pedestals did not move as the clamping bolts were tightened. This was done to ensure that the guide blocks remained located against the sides of their respective guide channels, Sections 4.3.4 and 4.3.5.

The bolts securing the mounting plate to the gimbal pedestal were then loosened and the shaft moved sideways. At the same time the shaft was rotated by hand until it locked in position (that is, the shaft could not be rotated), at which point the horizontal movement was noted using a clock gauge. The shaft was then moved in the opposite direction until the shaft again locked and the reading taken. The shaft was then set at the mean of the two readings and the same procedure was repeated for the vertical direction and again for the horizontal. This ensured that the shaft and bearing were approximately aligned.

The bearing clearance was then set at a nominal value using the method described in Section 4.3.4, again using clock gauges to ensure that the bearing housing did not move as the clamping bolts were tightened. A clearance circle was then established by physically moving the journal around the bush, sufficient to cause contact between the journal and bush with no shaft rotation. At each of the corresponding journal positions, a photo-record obtained from the probes bolted to the bearing housing, in the x-y trace of the oscilloscope enabled one point of the clearance circle to be determined.

The shaft end at the gimbal support was then moved by small amounts horizontally and vertically (the movement noted on the two clock gauges) until the best clearance circle was obtained. The bearing clearance was then set at several values in-turn to check that the clearance circle remained unaltered.

4.5.2 Flywheel Alignment Setting

With the flywheel fixed in position on the test shaft, trial runs were then conducted. Large amplitude vibration of the test rotor was observed at low speed (the speed did not exceed 1000 RPM for safety reasons). It was deduced that the vibration was due to a bend in the test shaft, and the test rotor was subsequently removed from the rig and mounted between centres on a lathe for examination. The bend at the centre of the shaft was found to be 0.003in (0.076mm) and it was at first thought that this had occured during balancing or assembly of the rig. However, when the bolts of the Ringfeders clamping the flywheel to the shaft (Section 4.3.2) were loosened the bend resumed its orginal value of 0.0005in (0.013mm).

The bolts of the Ringfeder had originally being tightened to the recommended torque of 10ft-lbf (13.5N-m), and by repeating the procedure it was found that above a nominal torque value the shaft was again bent, with the flywheel tending to skew.

As the Ringfeder exerts very large locking pressures on the shaft and boss it was thought that tightening the bolts until the shaft was just about to bend would be sufficient to clamp the flywheel. It is important that the bolts should be tightened diametrically, working round the clamping ring and at the same time repeating the procedure for the Ringfeder in the adjacent boss. Paint was then applied to the bolts to help prevent their becoming loose.

With the flywheel mounted on the shaft, both faces and the OD were skimmed in a lathe to reduce the skew of the flywheel to a minimum. The test rotor was again balanced in an Avery-Shenk balancing machine to the levels given in Section 4.3.2. Upon reassembly of the rotor within the rig, the level of vibration was found to have been reduced to an acceptable level, see Section 4.3.2.

4.5.3 Setting Loading Mechanism

Because ot the position of the flywheel it was not possible to position the loading device any closer than 8in (203mm) from the bearing centre. Thus, to obtain a given load at the bearing it was necessary to apply more load to the loading device than if it had been positioned closer to the bearing. This resulted in the shaft bending by a considerable amount and introduced new forces to the system. It was found that with the bearing deloaded the stability of the rotor was increased, and this was attributed to the forces originating from the loading mechanism.

The loading device had been designed so that it would allow the shaft to whirl without impeding its movement, by incorporating freedom of movement in design. Unfortunately, this introduced random vibration which tended to obscure the whirl orbits observed on the oscilloscope. Due to the above mentioned effects on the dynamics of the rotor the use of the loading devices were dispensed with.

4.6 EXPERIMENTAL PROCEDURE

4.6.1 Instability Measurement

To study instability phenomena experimentally, the shaft speed was increased gradually until instability occurred, that is, the threshold was reached. This was observed on the oscilloscope or FFT in the real-time mode, in the form of a non-synchronous vibration of the shaft. The speed was then reduced by 2% to 3% and the rotor was then allowed to run at the reduced speed so that thermal equilibrium of the supply oil, bearing and its housing was obtained. This usually required about 10 to 15 minutes of running time. Bearing temperatures were then recorded and the oil pressure noted. The oil cooler was used to help stabilise the temperature of the oil in the supply tank.

The running speed was then incresed in small increments until non-synchronous vibration set-in. The rotational speed at which this occurred was taken as the instability onset speed (stability threshold). At this threshold speed, the shaft vibration was recorded using the storage facilities of the FFT, the speed was then reduced until the non-synchronous vibration ceased. This avoided subjecting the rotor to excessive vibration for any length of time. The amplitude and frequency of the instability plus the shaft speed were then recorded from the stored frequency spectrum of the FFT.

To correlate the theoretical predictions of threshold speed with the experimentally measured results, the journal running position (equilibrium position) was found from hydrodynamic theory using the measured values of journal speed, bearing clearance and oil viscosity in the Sommerfeld number of equation (2.22). An effective viscosity of the lubricating oil was used in equation (2.22). This was calculated from the mean temperature obtained in the hydrodynamically loaded region of the bearing, and the effective viscosity obtained from Figure 4.4. The corresponding dynamic coefficients, equations (2.31) and (2.32) were then obtained by interpolation from the eccentricity corresponding to the calculated Sommerfeld number.

4.6.2 Critical Speed Measurement

Critical speeds of the test rotor were obtained by accelerating the rotor through its resonance, and at the same time using the peak hold facility of the FFT to store the peak amplitude spectrum of the acceleration run. The critical speed was then obtained by locating the peak amplitude and the corresponding synchronous frequency (critical speed) from the spectrum.

Normally, all amplitudes and frequencies (synchronous and non-synchronous) were measured at steady rotational speeds of the shaft using the real time capability of the FFT.

It was not possible to calculate the running position of the journal at the critical speed, as the rotor was accelerated through its critical speed to avoid damaging vibrations building up. Hence, in the correlation of the predicted critical speeds with those obtained from experimental measurement, an estimated running position of the journal was used. This was obtained by running the rotor at a steady speed at which the vibration level was acceptable (that is, as near the critical as possible), and then calculating the running position of the journal as described in Section 4.6.1. It will be shown in Chapter 5 that for the small range of eccentricity over which the rotor operated, the critical speed could be taken as constant for a given bearing clearance and pedestal flexibility. Hence, measurement of the bearing temperatures at a critical speed was unnecessary.

CHAPTER 5

CRITICAL SPEEDS OF A ROTOR SUPPORTED BY AN OIL-FILM BEARING ON A RIGID AND FLEXIBLE PEDESTAL

5.1 INTRODUCTION

This chapter deals with the measurement of the first damped critical speed of the experimental test rotor. This was mounted in a circular journal bearing of L/D=1/2, and contained two axial feed ports, Section 4.3.3. The bearing was supported by both rigid and flexible pedestals (see Section 4.3.4). The critical speeds were clearly defined by peak amplitude measurement (see Section 4.6.2) and phase angle measurement was not regarded as essential.

Correlation with theory was made using the Transfer Matrix Method detailed in Chapter 3, the four stiffness and damping coefficients given in Chapter 2 were used to represent the dynamic properties of the test bearing. Damped critical speeds of the rotor were predicted from the steady-state peak response to synchronous unbalance (Section 3.4.5).

The computer programmes for the bearing coefficients and rotor bearing system dynamics are detailed in Appendices C and E respectively. A check on the accuracy of the programmes is made by comparison with published data.

For the bearing coefficients the data given by Lund and Thomsen (64) was used in the programmes of Appendix C. Figures 5.1 and 5.2 are plots of the non-dimensional stiffness (K) and damping (C) coefficients against

CIRCULAR BEARING WITH TWO AXIAL GROOVES

L/D=1/2, α=20°, γ=0

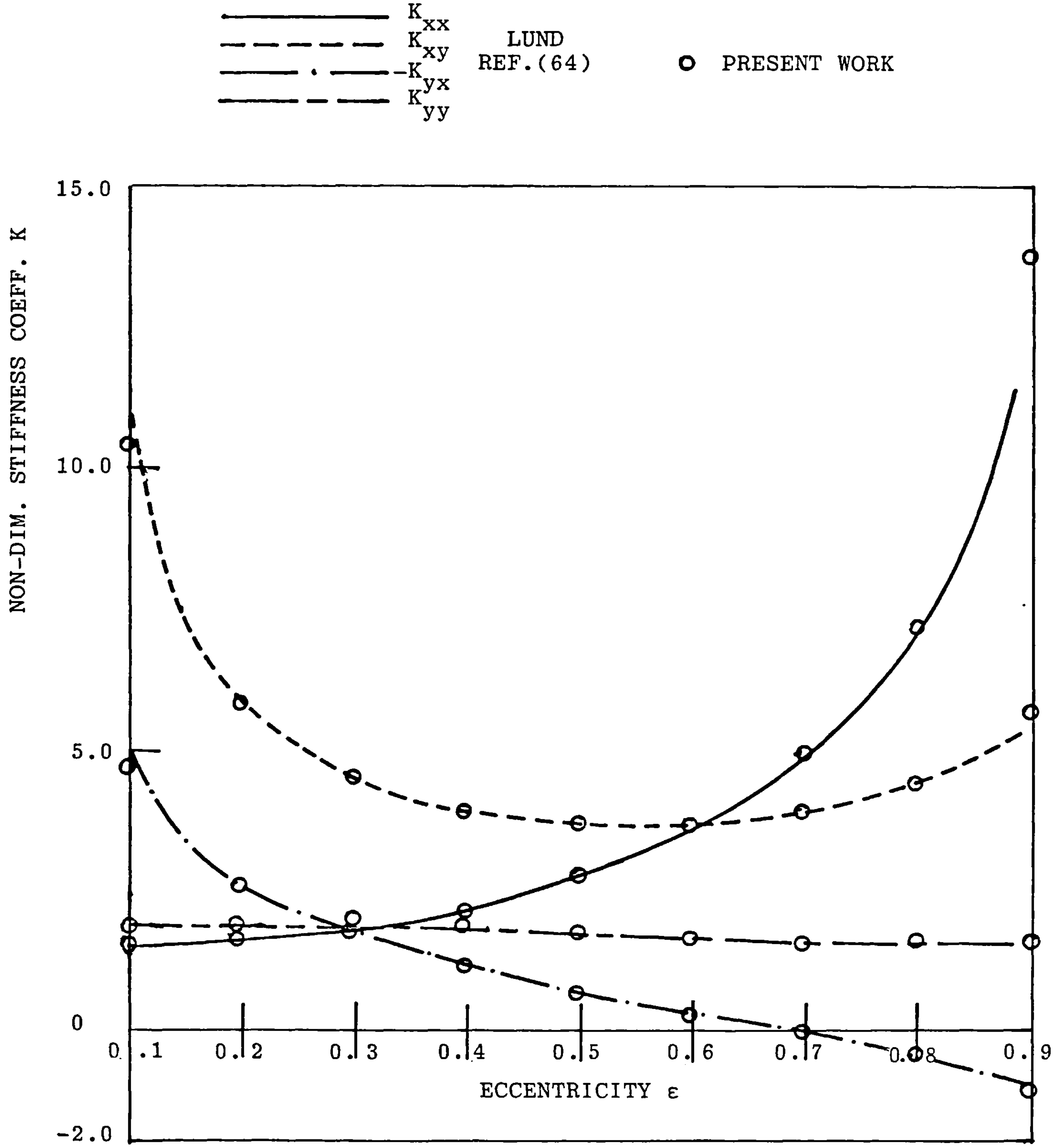

Figure 5.1 Stiffness Coefficients of Lund and Present Work

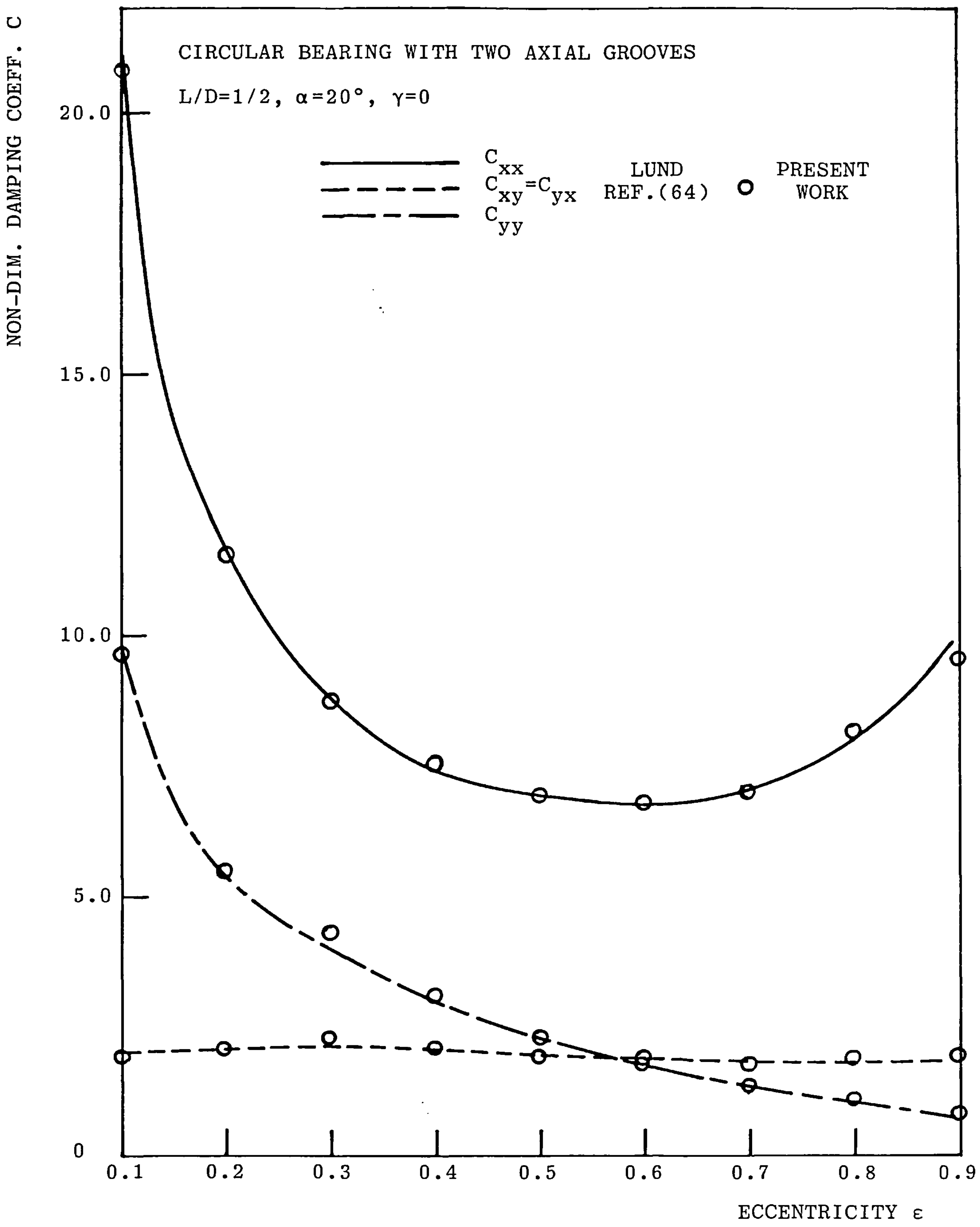

Figure 5.2 Damping Coefficients of Lund and Present Work

eccentricity (ε) given in (64) with those of the present work, for a bearing length to diameter ratio (L/D) of 1/2, angular feed groove width (α) of 20 degrees and non-dimensional feed pressure ratio (γ) of 0. It can be seen from the graphs good agreement is afforded. Figures 5.3 and 5.4 are plots of the coefficients used for the test bearing analysis, with $L/D=1/2$, $\alpha=30^{o}$ and $\gamma=0$.

Testing the computer programmes of Appendix E for the rotor dynamics is detailed in the stability measurement of Chapter 6.

Figure 5.5 is a graph of Sommerfeld Number, Equation 2.22, against eccentricity for $\alpha=30^{o}$, 60^{o}, 90^{o}. Figure 5.6 is a plot of the attitude angle (ϕ) versus eccentricity showing the so called "equilibrium semi-circles".

As detailed in Sections 4.6.1 and 4.6.2, the mean temperature of the lubricant in the bearing was used to estimate an effective viscosity from Figure 4.4. This value was then inserted into Equation 2.22, along with the other bearing parameters to find the Sommerfeld Number and the corresponding eccentricity was interpolated from Figure 5.5. This value of ε was then used to interpolate the corresponding stiffness and damping coefficients of Figures 5.3 and 5.4 respectively, and, hence, to find the dynamic coefficients for the operating conditions of the

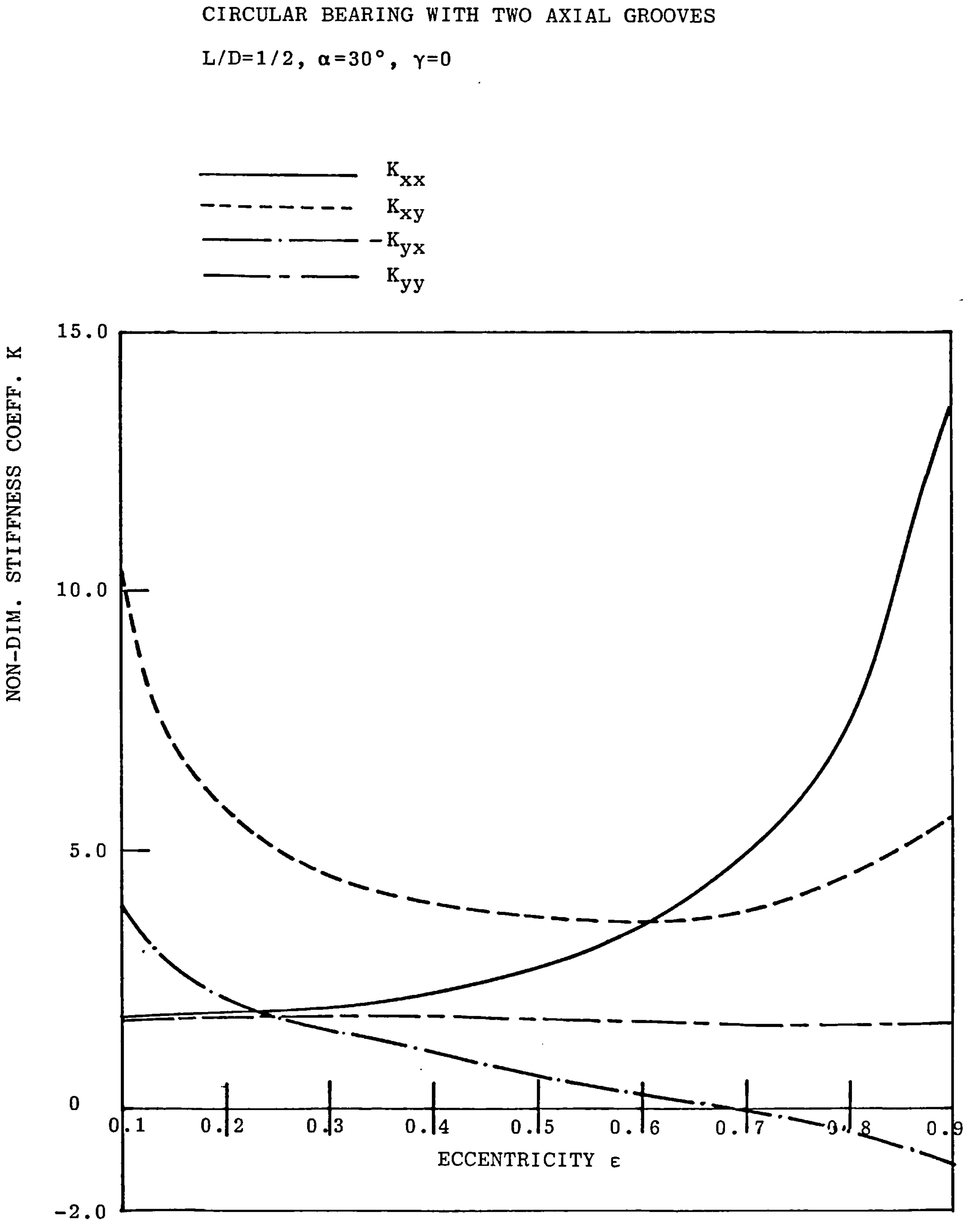

Figure 5.3 Stiffness Coefficients for Test Bearing

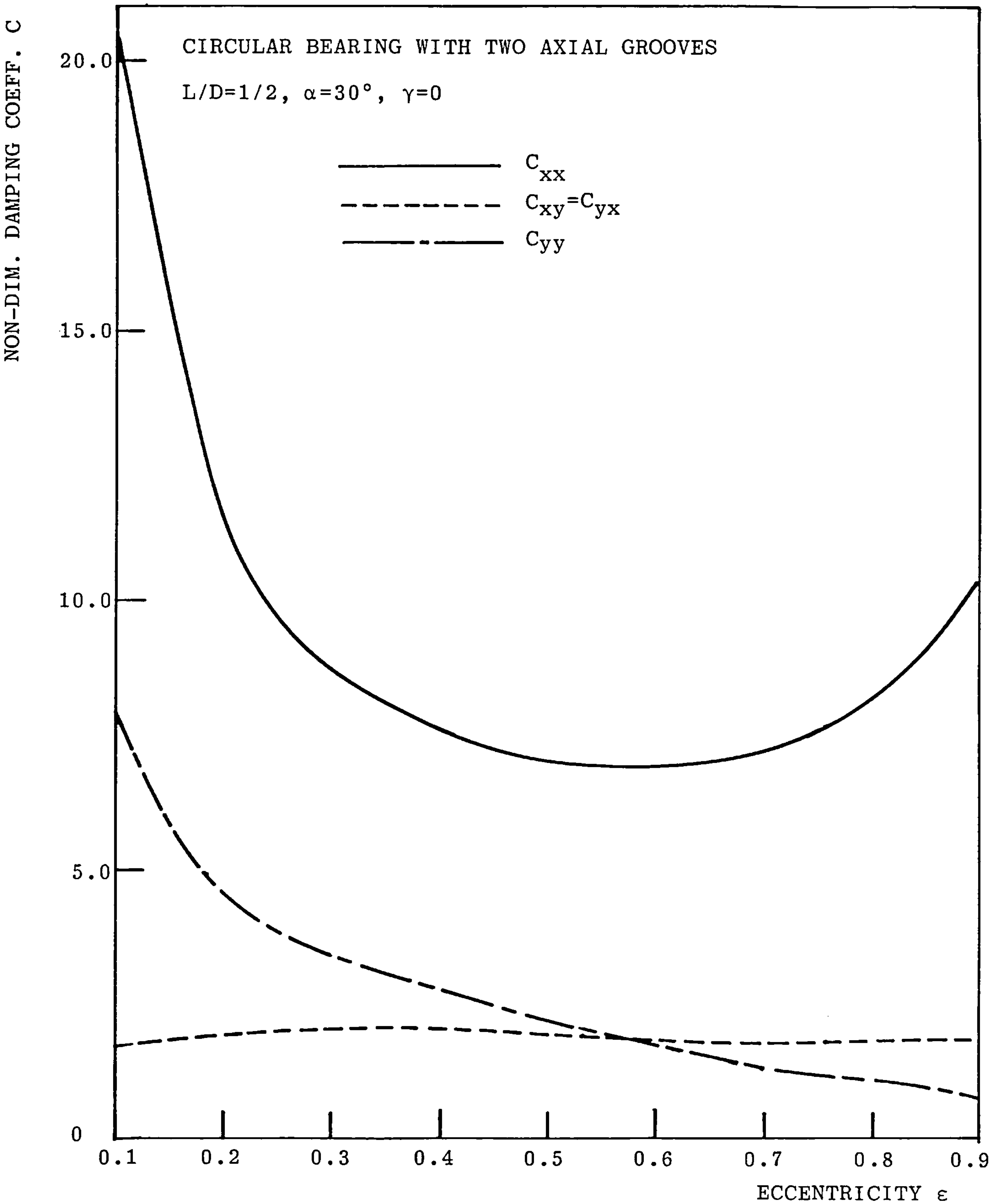

Figure 5.4 Damping Coefficients for Test Bearing

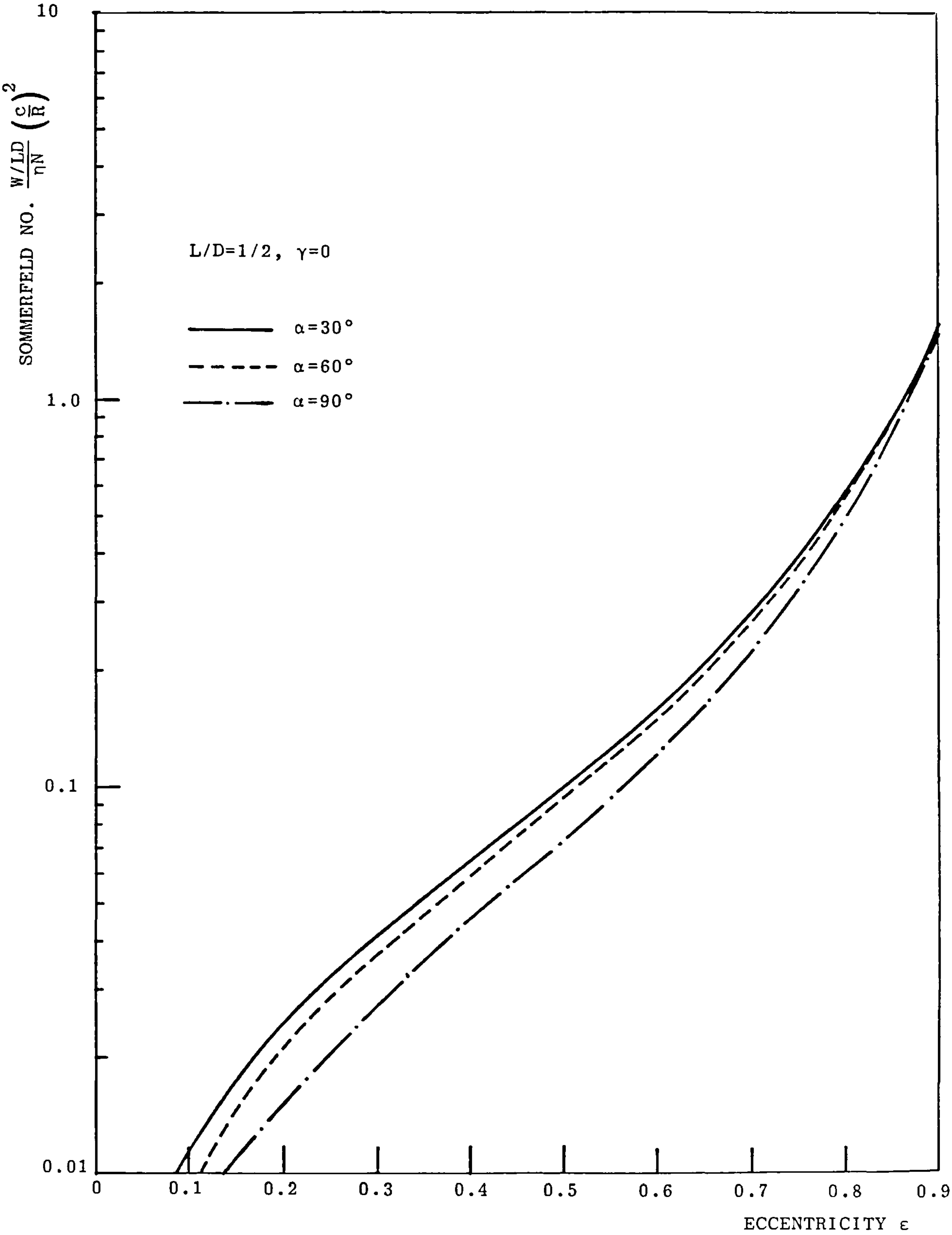

Figure 5.5 Bearing Load Curves for Three Groove Angles

L/D = 1/2, γ = 0

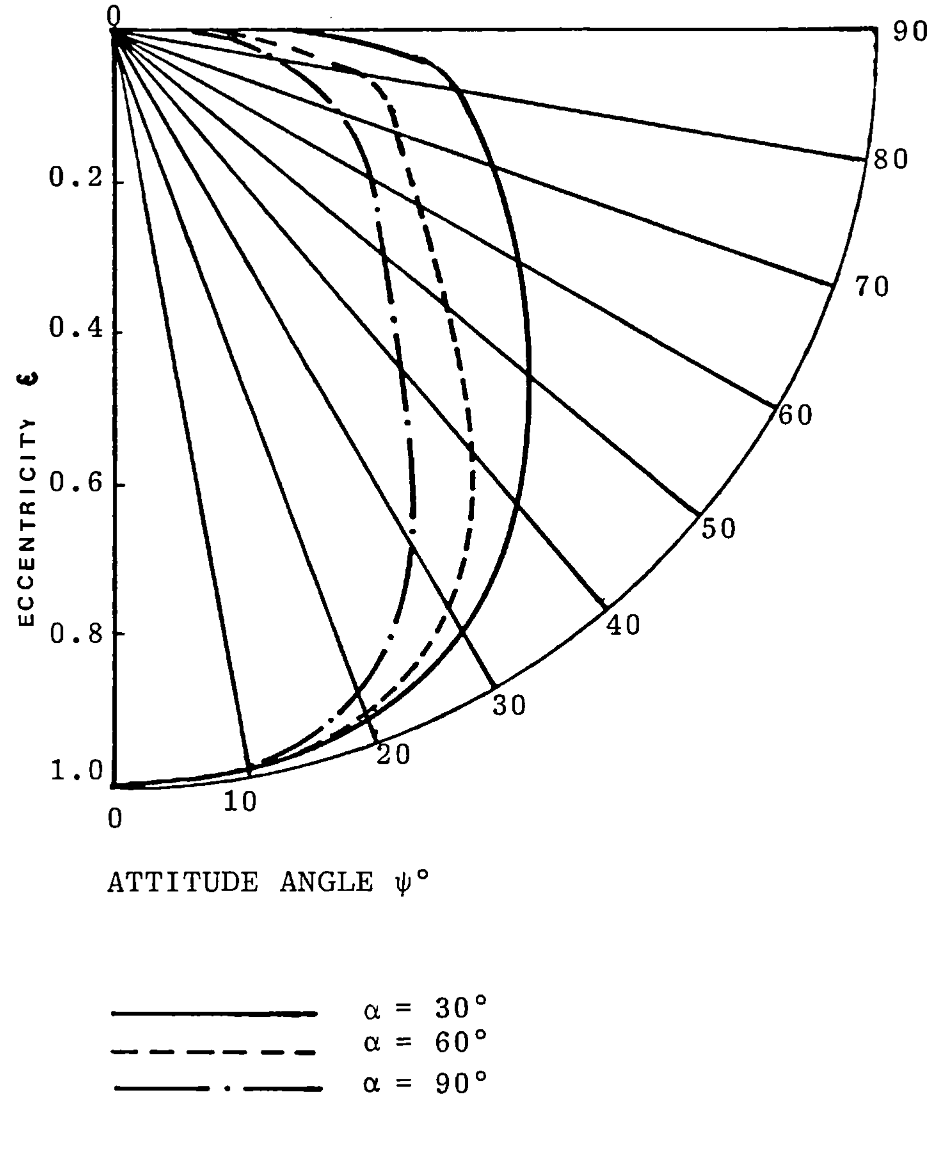

Figure 5.6 Bearing Equilibrium 'Semi-Circles' for Three Groove Angles

test bearing. The dynamic coefficients were also computed for α values of 60° and 90° with $\gamma = 0$.

An important variable is the flexibility parameter of the bearing-rotor system and is defined as δ/c, where δ is the maximum static deflection of the rotor and c is the bearing radial clearance. This quantity indicates the change in flexibility of the rotor as δ varies, for fixed c. In the experimental work δ was fixed at 0.005in (0.127mm) and for comparison with theory c was set at 0.003in (0.076mm) in the calculations, giving a δ/c value of 1.7.

5.2 TEMPERATURE PROFILES AROUND THE BEARING

Figures 5.7, 5.8 and 5.9 show the measured temperature distribution at the mid-plane of the bearing bush, for α values of 30°, 60° and 90° respectively. These were recorded by thermocouples located radially, approximately 1mm from the bore, Section 4.3.3. The bearing clearance was set at 0.003in (0.076mm), giving a c/R value of 0.0024. At each shaft speed the oil feed pressure (P_f) was set at 2psi (13.8KPa), and the oil supply and bearing housing were allowed to reach thermal equilibrium. Assistance in stabilising the oil temperature was provided by the oil cooler, Section 4.3.7.

P_f=2psi, c=0.003in

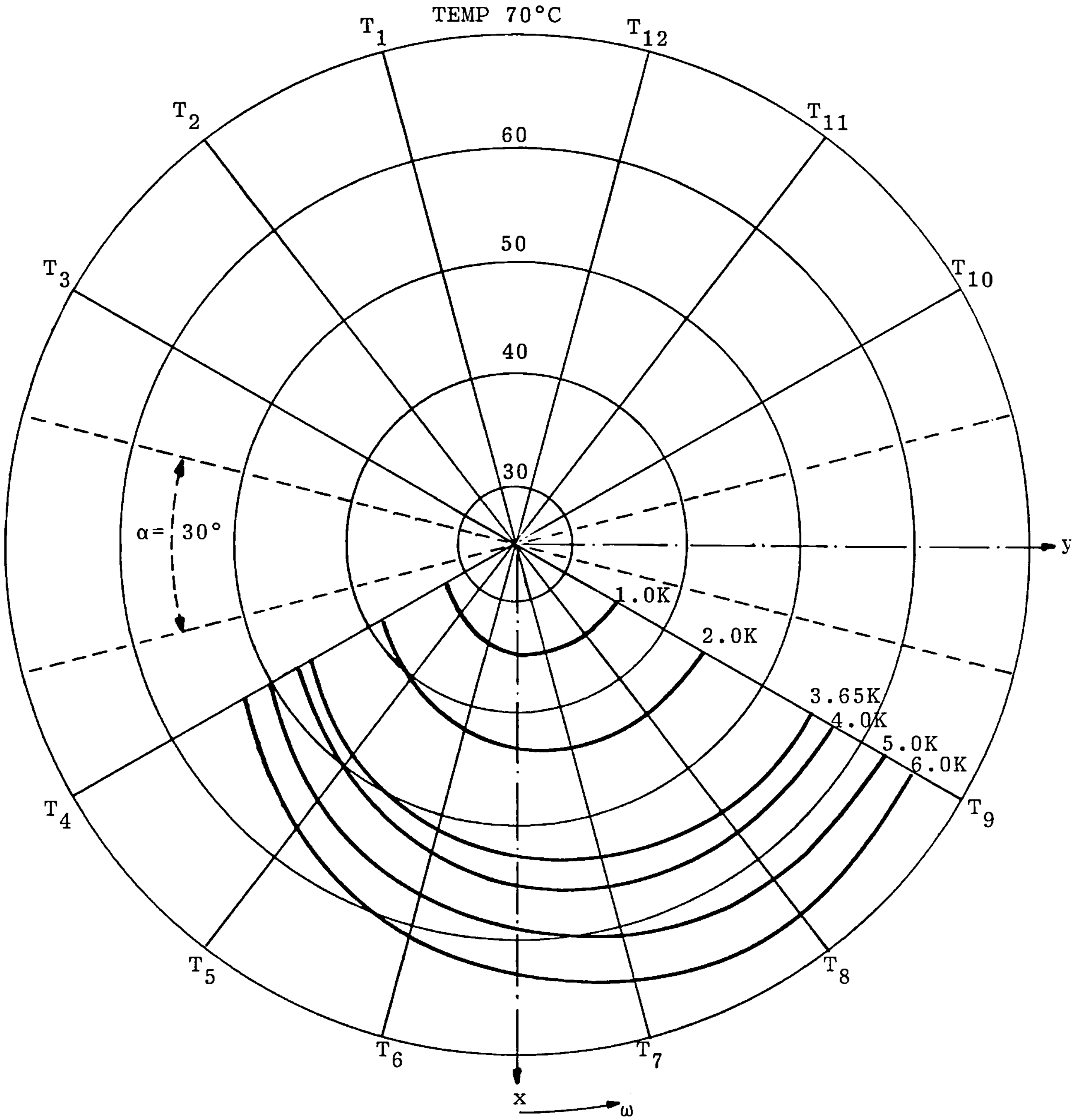

Figure 5.7 Temperature Profile Around Bush as Function of Shaft Speed (RPM) for α = 30°

P_f=2psi, c=0.003in

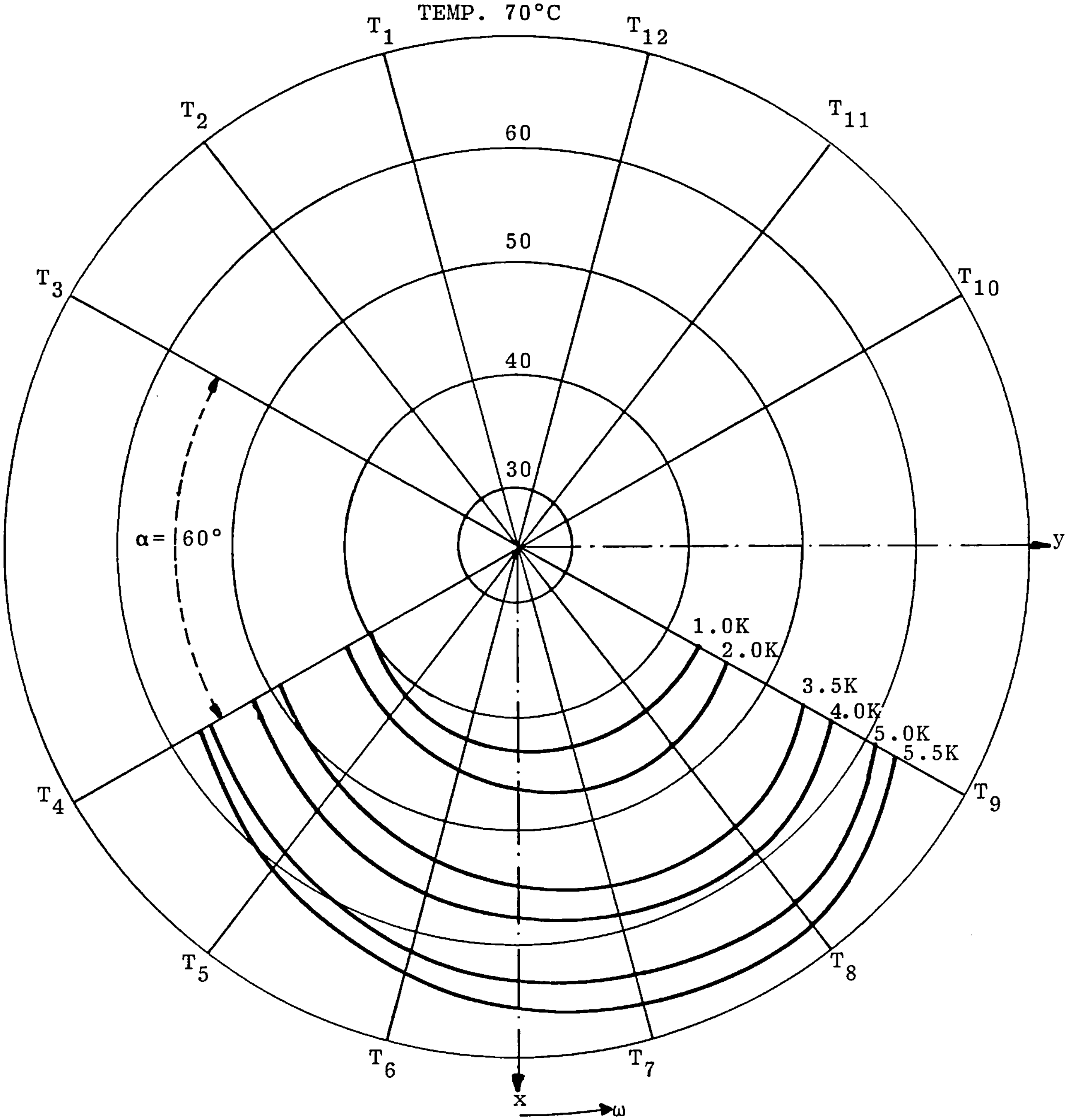

Figure 5.8 Temperature Profile Around Bush as Function of Shaft Speed (RPM) for α = 60°

P_f=2psi, c=0.003in

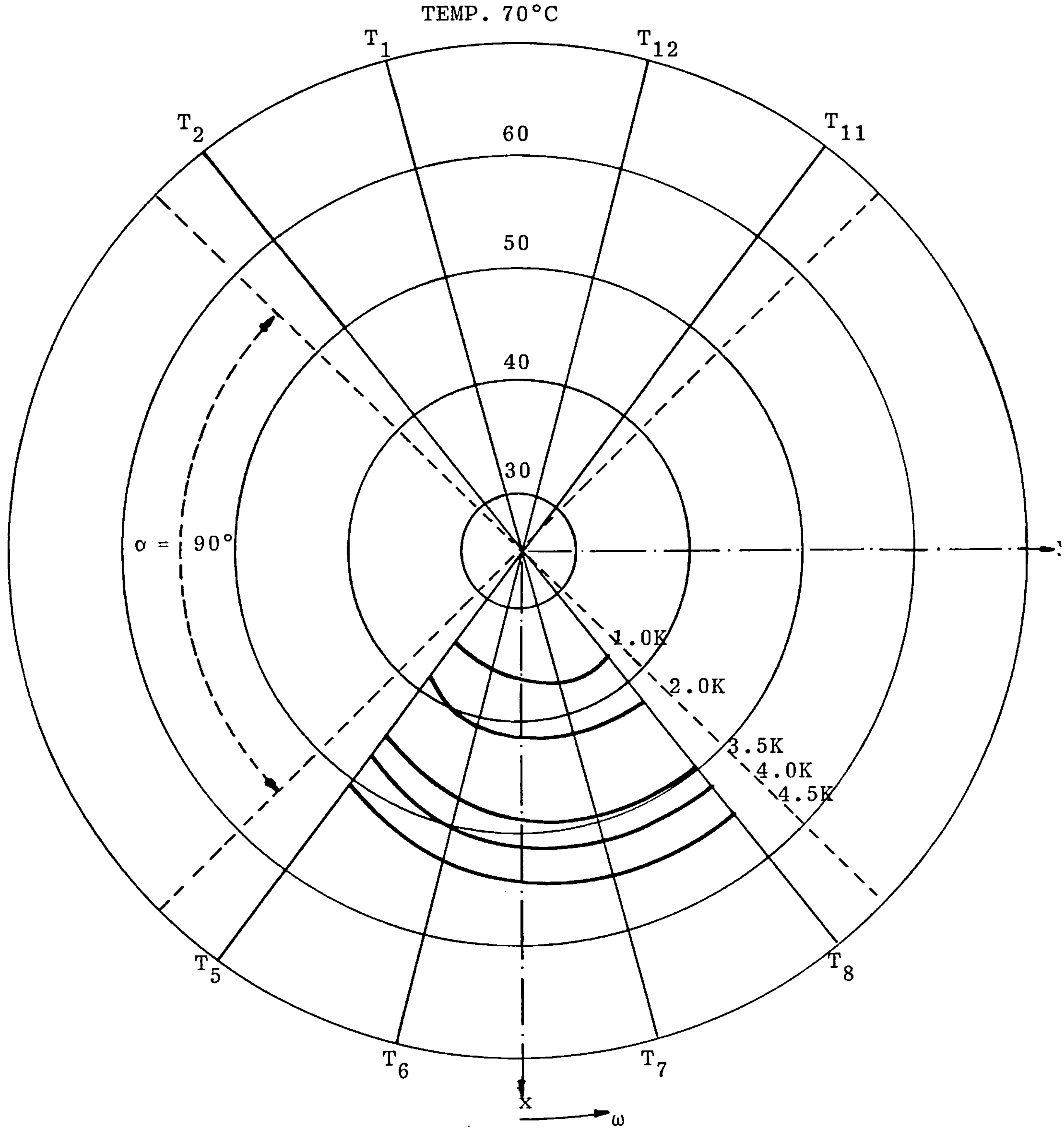

Figure 5.9 Temperature Profile Around Bush as Function of Shaft Speed (RPM) for $\alpha = 90°$

The projected bearing load is defined as (W/LD) where W is the gravitational or steady load on the bearing. This was set at 9.2psi (63.4KPa) for the test bearing and gave a γ value of 0.2 for P_f=2psi. In the theoretical computation of response and critical speed, γ was set at 0 as it was determined that a theoretical γ value of 0.2 had no noticeable effect on the results.

As was expected a temperature rise in the loaded region of the bush was measured in the direction of rotation, with no noticeable rise in the unloaded region. It is observed from Figures 5.7, 5.8 and 5.9 that an increase in speed causes a steady increase in temperature. This was found to occur even though the oil supply temperature was stabilised, and it was observed that changing the oil supply pressure, and hence the flow, had no apparent effect. It would appear that the grooves had little influence in disrupting the circumferential re-circulation of the oil in the bearing film. The operating temperature level, is therefore, governed by an overall heat exchange mechanism for the bearing assembly.

Operating the rotor at between 6000RPM and 7000RPM then decreasing the speed rapidly to a lower level resulted in an immediate drop in the measured temperatures, approaching the temperature of the oil supply. Hence, the thermocouples appear to measure temperatures close to those of the actual oil-film. The mean value of the thermocouple readings in the inlet to outlet film region was used to estimate the effective viscosity.

5.3 DAMPED CRITICAL SPEED ON A RIGID PEDESTAL

Analysis and experiment were carried out to determine the effect of certain bearing parameters upon the first damped critical speed of the test rotor with the residual unbalance present after balancing, Section 4.3.2. Computations were carried out using a mathematical model of the test rotor-bearing system. This model is illustrated in Appendix G, and the physical properties of the test bearing and rotor are listed in Appendix F.

Figure 5.10 shows the calculated effect of the eccentricity upon the critical speed of the rotor in the x and y directions. The occurrence of two critical speeds is due to the asymmetric stiffness of the bearing. The input data for the computer programme is shown in the figure. For reference, the presence of zero as well as non-zero gyroscopic effects are shown. It is immediately obvious that gyroscopic effects have a strong influence on the critical speeds. This effect is more apparent at high eccentricity. In general, gyroscopic effects tend to raise the critical speed because of their stiffening effect upon the shaft.

c=0.003in, α=30°, ω_g=359R/s

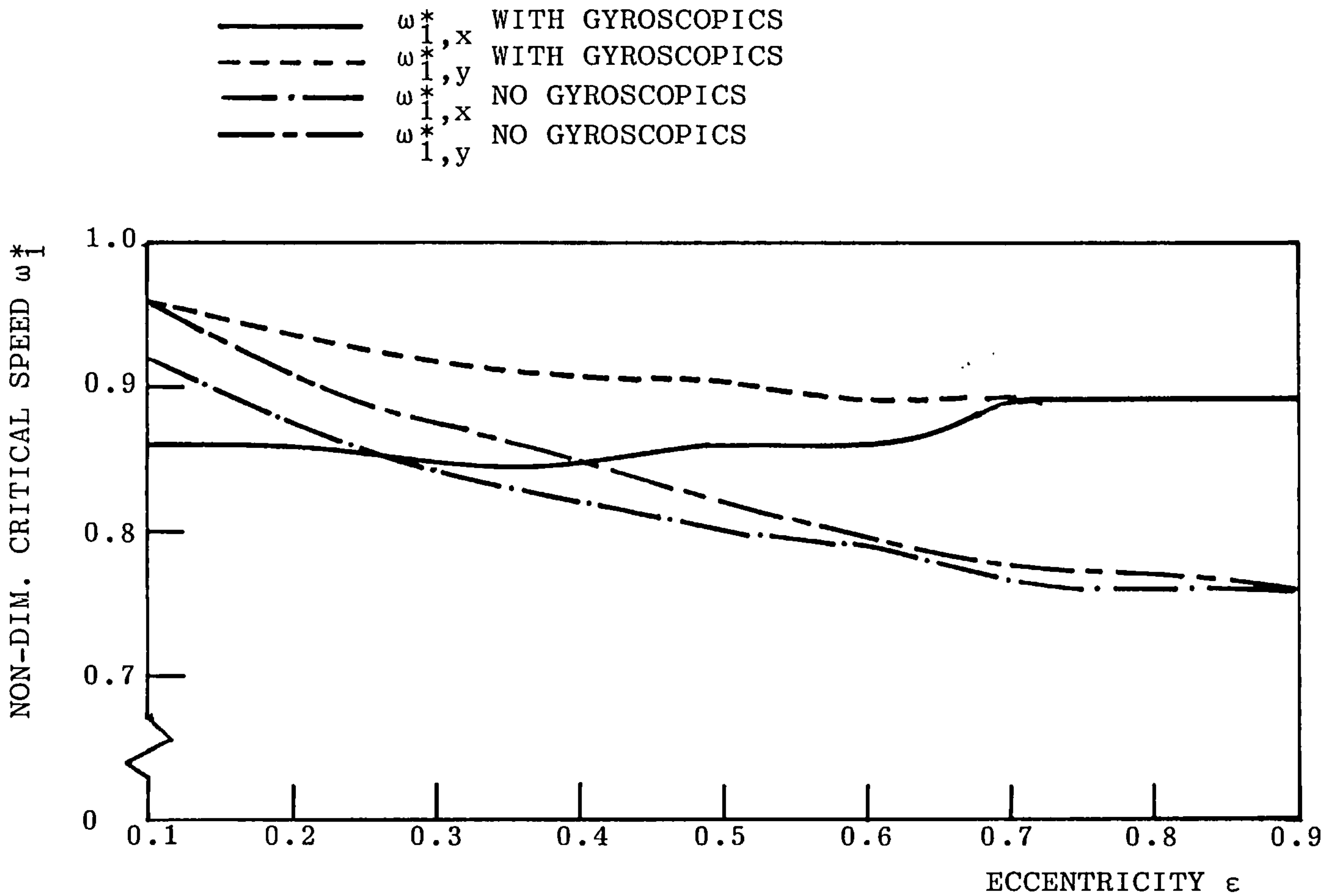

Figure 5.10 Critical Speed Versus Eccentricity for a Rigid Pedestal

It can be seen from Figure 5.10 that for the range of eccentricity ratio $\varepsilon=0.4$ to 0.6, the change in critical speed is very small. This is fortuitous as it was not feasible to calculate the running eccentricity from the Sommerfeld Equation at the critical speed due to large amplitude vibrations occurring at the critical speed, which require a finite time to build up. Thus, the value of ε was estimated at a safe running speed near to the critical speed,and at which the level of amplitude was considered to be acceptable.

Hahn (44) predicted from theoretical work that changing the bearing clearance will not, in general, affect the location of the critical speed resonance. To examine this, the radial clearance (c) of the test bearing was varied from 0.003in (0.076mm) to 0.007in (0.178mm) in steps of 0.001in (0.025mm) and the first damped critical speed was measured at each value. Figure 5.11 shows the variation of critical speed in the x and y directions for both the experimentally measured and the computed values. The calculated values of critical speed were obtained assuming a fixed value of eccentricity. Table 5.1(a) gives the percentage difference between theoretical and experimental values as compared with the theoretical values for the x-direction, and Table 5.1(b) gives the same percentage difference in the y-direction.

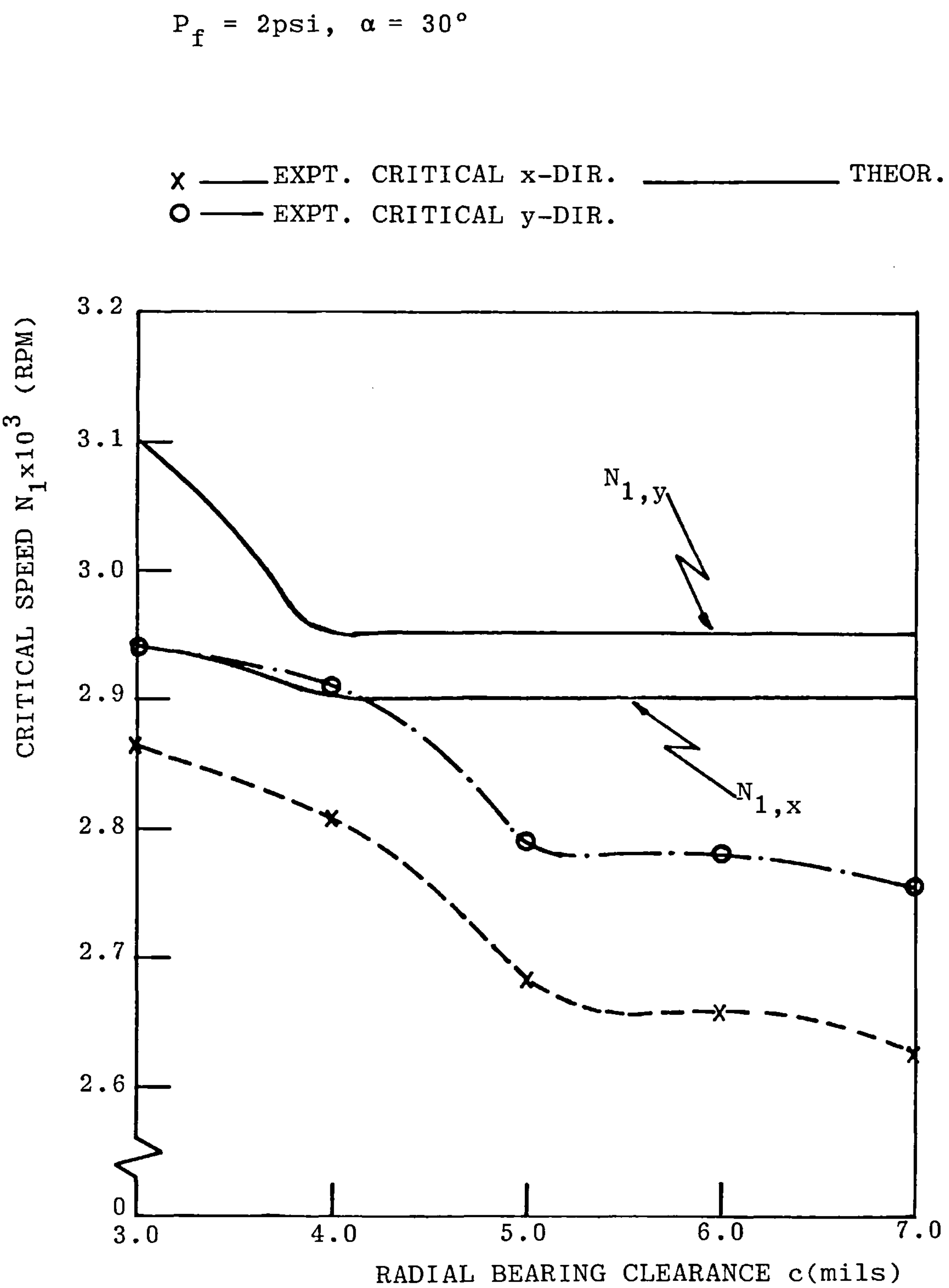

Figure 5.11 Variation of Critical Speed with Clearance for a Rigid Pedestal

RADIAL CLEARANCE c (0.001in)	EXPT. N_1 x-DIR (KRPM)	THEOR. N_1 x-DIR (KRPM)	% DIFFERENCE (THEOR.-EXPT.)/ THEOR.
3	2.865	2.950	2.9
4	2.805	2.900	3.3
5	2.685	2.900	7.4
6	2.655	2.900	8.4
7	2.625	2.900	9.5

TABLE 5.1(a) Effect of Bearing Clearance on Critical Speed in the x-Direction

RADIAL CLEARANCE c (0.001in)	EXPT. N_1 y-DIR (KRPM)	THEOR. N_1 y-DIR (KRPM)	% DIFFERENCE (THEOR.-EXPT.)/ THEOR.
3	2.940	3.100	5.2
4	2.910	2.950	1.3
5	2.790	2.950	5.4
6	2.780	2.950	5.8
7	2.775	2.950	5.9

TABLE 5.1(b) Effect of Bearing Clearance on Critical Speed in the y-Direction

Figure 5.11 and Tables 5.1(a) and 5.1(b) indicate that as the bearing clearance is increased the measured values of critical speed of the rotor in the x and y directions are reduced. The reduction is more pronounced for the clearance range of 0.003in to 0.005in. Subsequent increase in the clearance produced a less obvious drop. Theoretically, a decrease in critical speed for the x and y directions was also obtained as the clearance was increased from 0.003in to 0.004in, thereafter, the criticals remained constant. The agreement between theory and experiment is good, especially at smaller clearances, Tables 5.1(a) and 5.1(b).

The constant value of computed critical speed, Figure 5.11, is probably due to the assumption of constant eccentricity. It is more likely that as the clearance was changed experimentally, small changes in the eccentricity occured. Hence, it is thought that the most probable explanation for the reduction in critical speed with increase in bearing clearance is a change in the bearing oil-film stiffness or damping due to the variation in eccentricity.

Generally, fluid-film damping tends to increase the critical speed. De Choudhury et al (65) and Ruddy and Summers-Smith (66) produced undamped critical speed maps by plotting the critical speeds of the first three lateral modes of vibration against bearing support stiffness. In (65) the change in support stiffness in the horizontal and vertical directions, with speed are also plotted on the same maps. The point of intersection of these curves defines the undamped critical speeds in the horizontal and vertical directions for the different modes of vibration.

De Choudhury determined the damped critical speed from the rotors response to unbalance and found that fluid-film damping has the effect of raising the undamped critical speed. To verify this the oil-film damping coefficients were set to zero in the computer programmes to ascertain the effect on the critical speed. For c=0.003in it was found that the first critical was reduced to 2.7KRPM.

Thus, damping appears to be an unlikely cause of the drop in critical speed, as it raises the critical rather than lowering it. Although, an increase in damping would be expected as the clearance was increased, no significant decrease in the measured amplitudes at steady speeds were found that would indicate this.

The effectiveness of the damping would depend upon where the nodes of vibration were located with respect to the bearings. That is, if the nodes were located at the bearing there would be no relative movement between journal and bush and damping would not be expected to have an effect. If the nodes were located away from the bearings, relative movement between journal and bush would occur. This relative movement would produce a velocity dependent force. The larger the displacement, the larger the velocity, and, thus, the larger the force. In this case the fluid-film damping would raise the undamped critical speed and control vibration amplitudes.

It was found for the test rotor that the computed mode shape had a node located at the journal bearing for the first lateral bending mode of vibration and, hence, damping was not an important factor in controlling critical speed or amplitude levels. It, therefore, appears that the reduction in critical speed resulted from a small reduction in the oil-film stiffness as the clearance was increased.

5.4 RESPONSE TO UNBALANCE

Using the measured value of residual unbalance the computed values of the peak to peak amplitude A_X, occurring at the critical speed at the shaft centre are shown in Figure 5.12. The curves predict the change in amplitude with eccentricity for three values of the groove angle, that is, $\alpha=30^o$, 60^o and 90^o. It can be observed that an increase in groove angle results in an increase in amplitude levels, and that in order to limit amplitudes it is desirable to restrict bearing operation to eccentricities not greater than approximately 0.6. Minimum amplitude for all three α values occurs over the interval of $\varepsilon=0.30$ to 0.35.

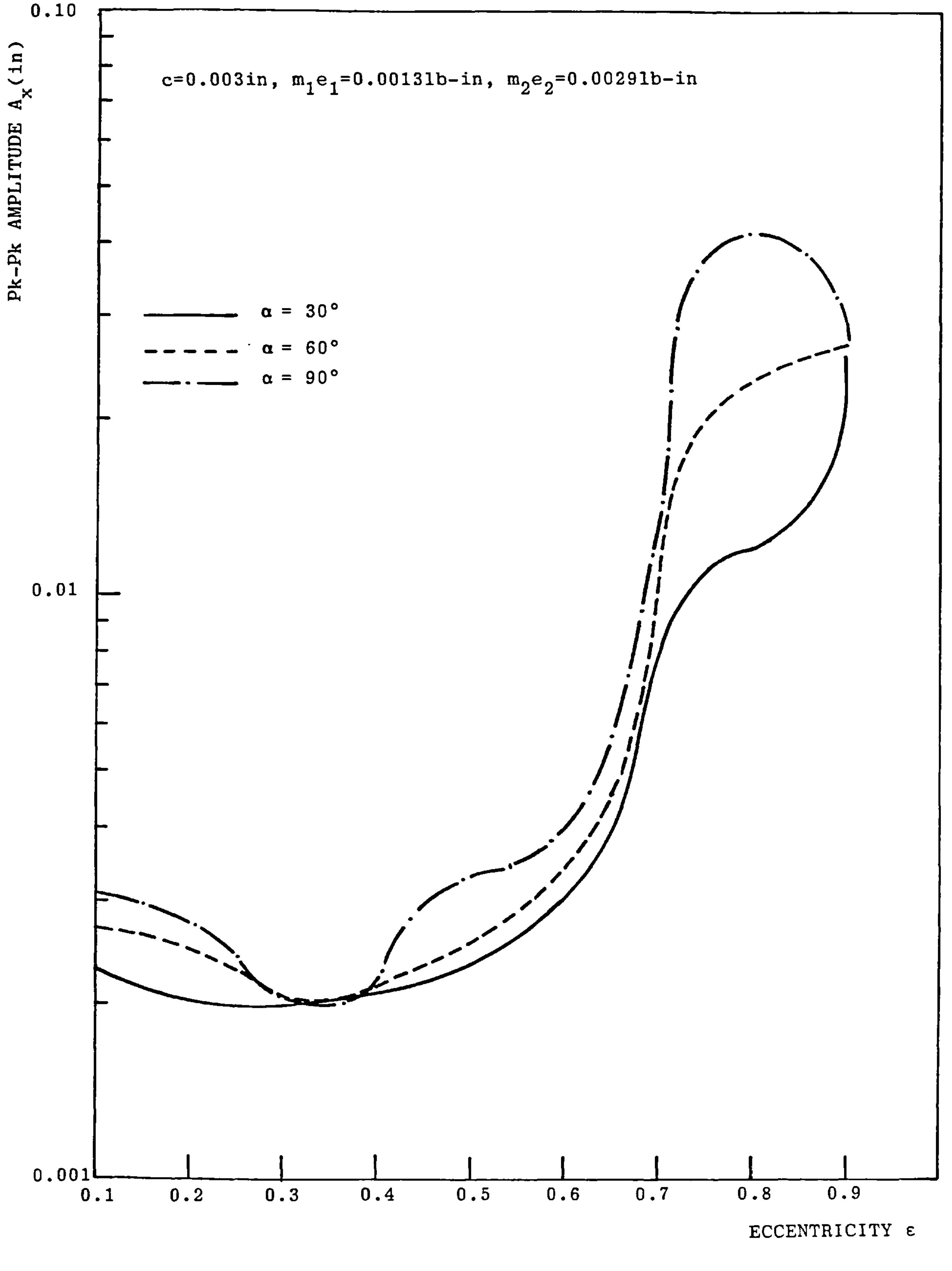

Figure 5.12 Amplitude at Shaft Centre Versus Eccentricity at Critical Speed

Measured levels of amplitude over the entire speed range were found to be much larger than the computed values using the calculated running position of the bearing. For example, the measured value of A_x at the shaft centre for c=0.003in (0.076mm), $\alpha=30^o$ and N=3500RPM was 0.0041in (0.104mm) and the computed value was 0.0012in (0.030mm). Similarly, the values of A_y were of the same order of magnitude as A_x. It was, thus, apparent that other forces were present, apart from residual unbalance.

Careful examination of the rotor revealed that the flywheel was skewed relative to the shaft by a small amount. This was measured using a clock-gauge and was found to be of the order of 0.0005in (0.013mm) and corresponded to a skew angle of 0.00015 radians.

When the skew angle was inserted in the "forcing column", Section 3.3.2, of the computer programme the additional gyroscopic moments arising from the skew of the flywheel gave better agreement with the measured values. Figure 5.13 is a Bode diagram (amplitude against speed) for measured and computed values of the amplitude, A_x, for c=0.003in and $\alpha=30^o$. Theoretically predicted values are still considerably lower when compared with experimental values.

There are several possible causes why experimental values are larger than the computed ones. They are listed

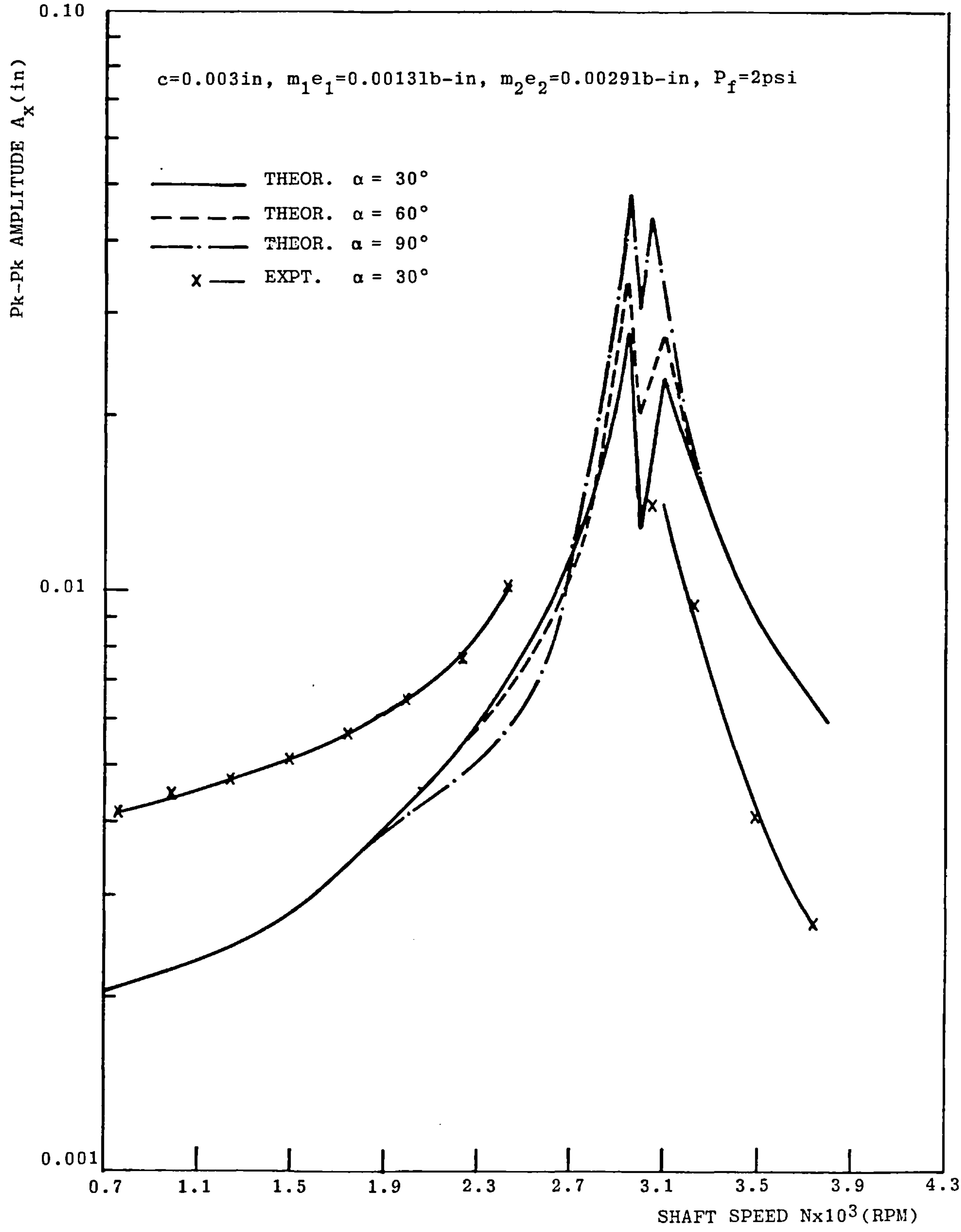

Figure 5.13 Resonance Curve at Shaft Centre

and discussed below:

(i) error in the value of eccentricity;

(ii) flywheel skew;

(iii) shaft warp;

(iv) misalignment of the journal;

(i) From Figure 5.12 for $\alpha=30^{o}$, it can be seen that as the eccentricity increases beyond the range of $\varepsilon=0.30$ to0.35, there is an increase in amplitude. As the shaft speed was increased, frequent checking of the eccentricity was therefore necessary. Bearing temperatures were recorded below and above the critical, and it was observed that the change in mean temperature had no significant effect on the calculated value of eccentricity.

(ii) Although the flywheel skew was measured with the rotor stationary, it is possible that while the shaft was rotating the flywheel could skew relative to the shaft, resulting in additional excitation forces.

(iii) The initial warp or bend of the test shaft was measured, Section 4.3.1, and found to be very small (0.0005in). But running the rotor could have caused the initial bend to change its magnitude and direction. Bishop and Mahalingam (67) have observed such behaviour and suggested that residual strain was responsible. They reached the conclusion that as a shaft passes through a critical it undergoes distortions of varying magnitude and direction, and a small residual strain is retained when the shaft is brought to rest. This residual strain is large enough to effectively alter the magnitude and direction of the initial bend. Both (ii) and (iii) are proportional to ω^2.

(iv) Misalignment of the journal would be present in the test rotor due to static deflection of the journal within the bush. This would introduce moments in the oil-film, thus, setting up addtional forces within the bearing. Kikuchi (38) states that to obtain good agreement between theoretical and measured response, the rotational spring and damping coefficients due to the inclination of the journal within the bearing cannot be neglected when a flexible shaft is used.

The computed response for α values of 60^o and 90^o are also shown in Figure 5.13. It can be seen that an increase in groove angle results in an increase in the steady state peak response of the Bode diagram, but has little effect at other speeds.

It was stated that an increase in bearing clearance was found to have no noticeable effect upon amplitude response at fixed speeds below and above the critical. To check if large clearances reduced the peak response predicted by Barrett et al (68) and Hahn (44), the rotor was accelerated through its critical and the peak amplitude response recorded as described in Section 4.6.2. Unfortunately, it was found that as the clearance was increased the acceleration of the rotor through its critical was also increased, presumably because less friction was developed in the bearing with a corresponding reduction in power consumption. Attempts were made to adjust the acceleration of the rotor to the same value for each clearance setting, but this proved to be unsuccessful. Thus, no meaningful conclusions could be drawn from the results, as it was important to ensure constant acceleration for each clearance in order to compare peak amplitude values. Computed values of peak response at the critical were found to decrease as the clearance was increased. Increasing the clearance by 133% from c=0.003in to 0.007in resulted in a decrease in amplitude of 53% from A_x=0.0283in to 0.0133in.

For the same reason it was not possible to verify the findings shown in Figure 5.13, that is, an increase in peak response with increase in groove angle. This probably was due to a reduction in power consumption in the bearing as the fluid-film extent decreased with increase in groove angle, and a consequent increase in the rotor acceleration.

Figures 5.14, 5.15 and 5.16 are plots at the critical speed, of the computed instantaneous values of peak to peak amplitude A_x, A_y, bending moment M_x, M_y and shear force V_x, V_y, along the shaft for c=0.003in and $\alpha=30^{\circ}$, taking into c=0.003in, m_1e_1=0.0013lb-in, m_2e_2=o.0029lb-in, α=30°

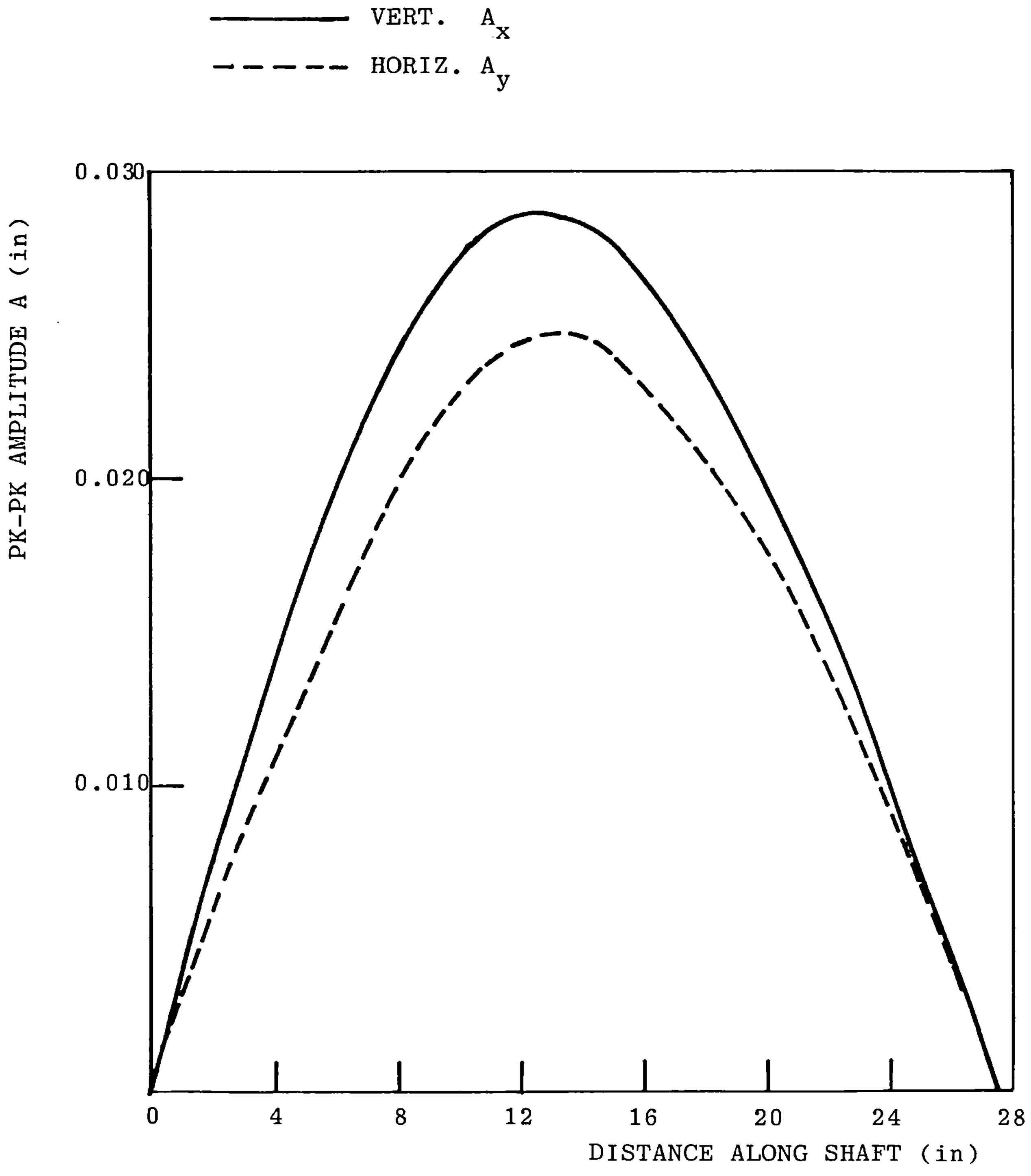

Figure 5.14 Mode Shape at Critical Speed

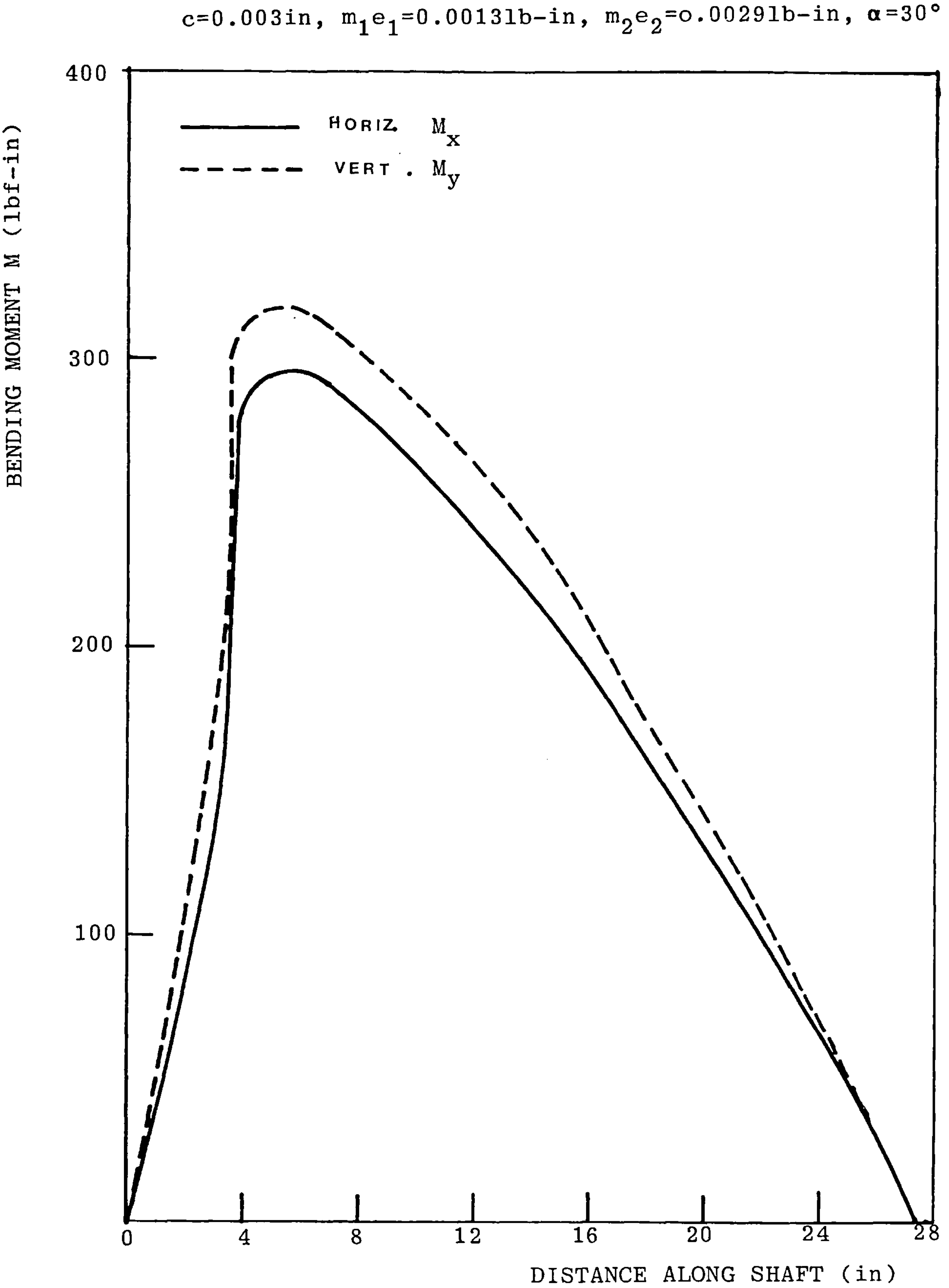

Figure 5.15 Bending Moment at Critical Speed

c=0.003in, m_1e_1=0.0013lb-in, m_2e_2=o.oo29lb-in, α=30°

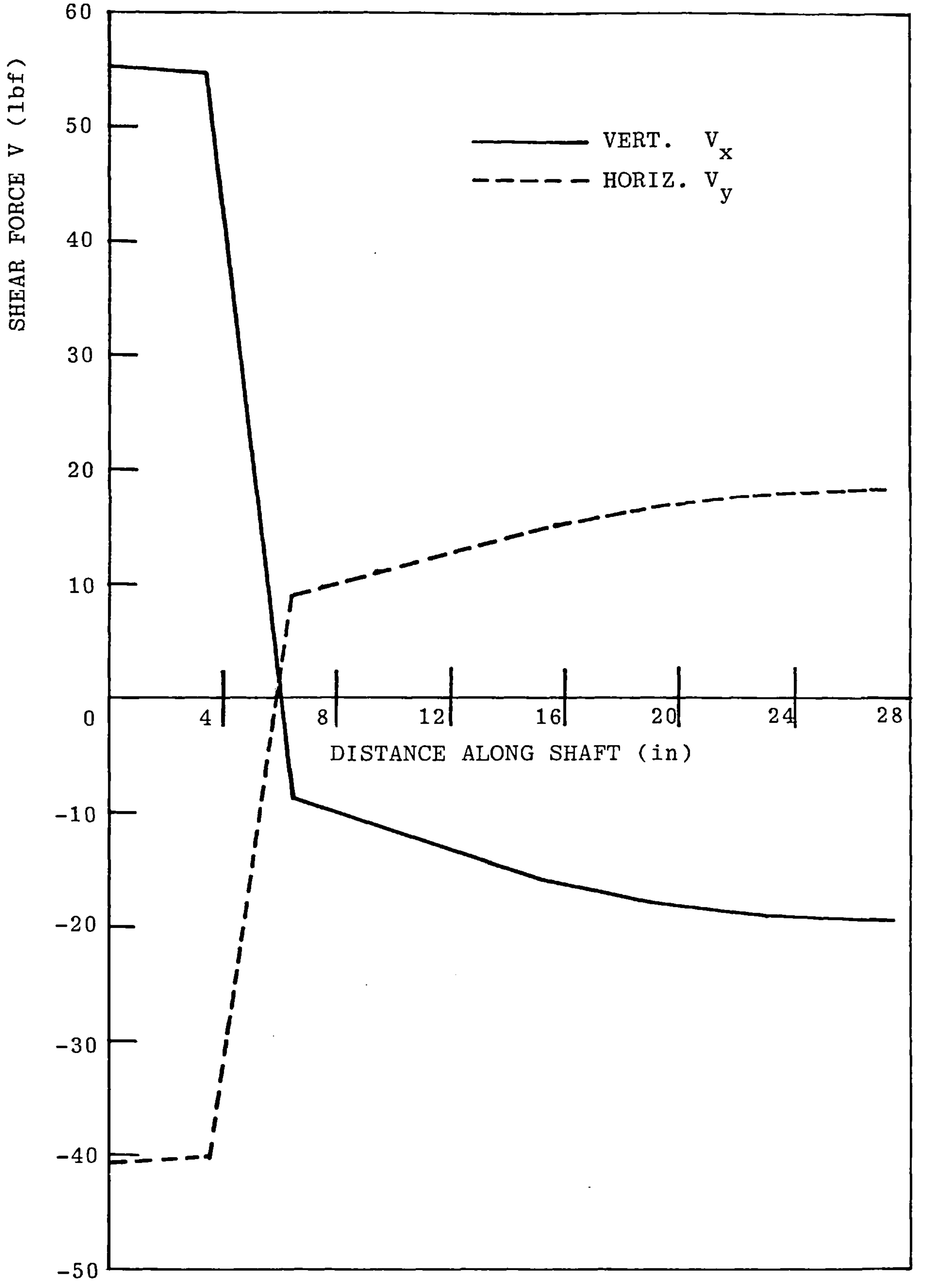

Figure 5.16 Shear Force at Critical Speed

consideration the skew effect. Figures 5.15 and 5.16 can be useful in the design stage as they can be used to predict stresses likely to be encountered in the shaft.

Inspection of Figure 5.14 shows a first lateral bending mode of vibration occurring at the damped critical speed, with nodes located at each support. As the right hand support is effectively pinned a node would be expected to occur at this point.

In general, the effect of oil-film bearings on the mode shape will depend upon their stiffness as compared with that of the rotor. The less stiff bearings are (relative to the shaft), the more likely it is that the nodes will be displaced away from the bearings, and the vibration modes of the rotor-bearing system will be determined by rotor flexibility. Also, reduced bearing stiffness will lower the natural frequencies when compared to the case of rigid supports, with low support stiffness producing free modes of vibration. Conversely, as bearing stiffness is increased relative to the rotor, the bearing will tend to dominate the behaviour of the system producing at high bearing stiffness pinned modes.

5.5 DAMPED CRITICAL SPEED ON A FLEXIBLE PEDESTAL

Figure 5.17 illustrates the computed change in damped critical speed against eccentricity for the case of the test rotor mounted in a journal bearing on an undamped flexible pedestal of specified stiffness. M_B and M_R represent bearing and rotor mass respectively, $k_{p,x}$ and $k_{p,y}$ are stiffnesses of the pedestal in the x and y directions respectively, and k_R represents the stiffness of the rotor. The methods of calculating the rotor and pedestal stiffnesses and non-dimensionalising the pedestal mass and stiffness are given in Appendix H.

For the simple Jeffcott rotor mounted in elastic bearings, supported by flexible pedestals, neglecting bearing and support damping and gyroscopic effects, Gunter (31) found that the attitude angle, ϕ , has a pronounced effect on the critical speed, particularly at high values of ϕ. Figure 5.17 can be interpreted in terms of ϕ. It is seen that high and particularly low values of ϕ have an effect on the critical in the vertical plane. Kirk and Gunter (39) applied an analytical solution to more general equations than those developed in (31) for the Jeffcott model. They found that in the absence of bearing and pedestal damping and gyroscopic terms, two critical speeds were generated, one above and one below the original critical speed of the rotor on rigid supports.

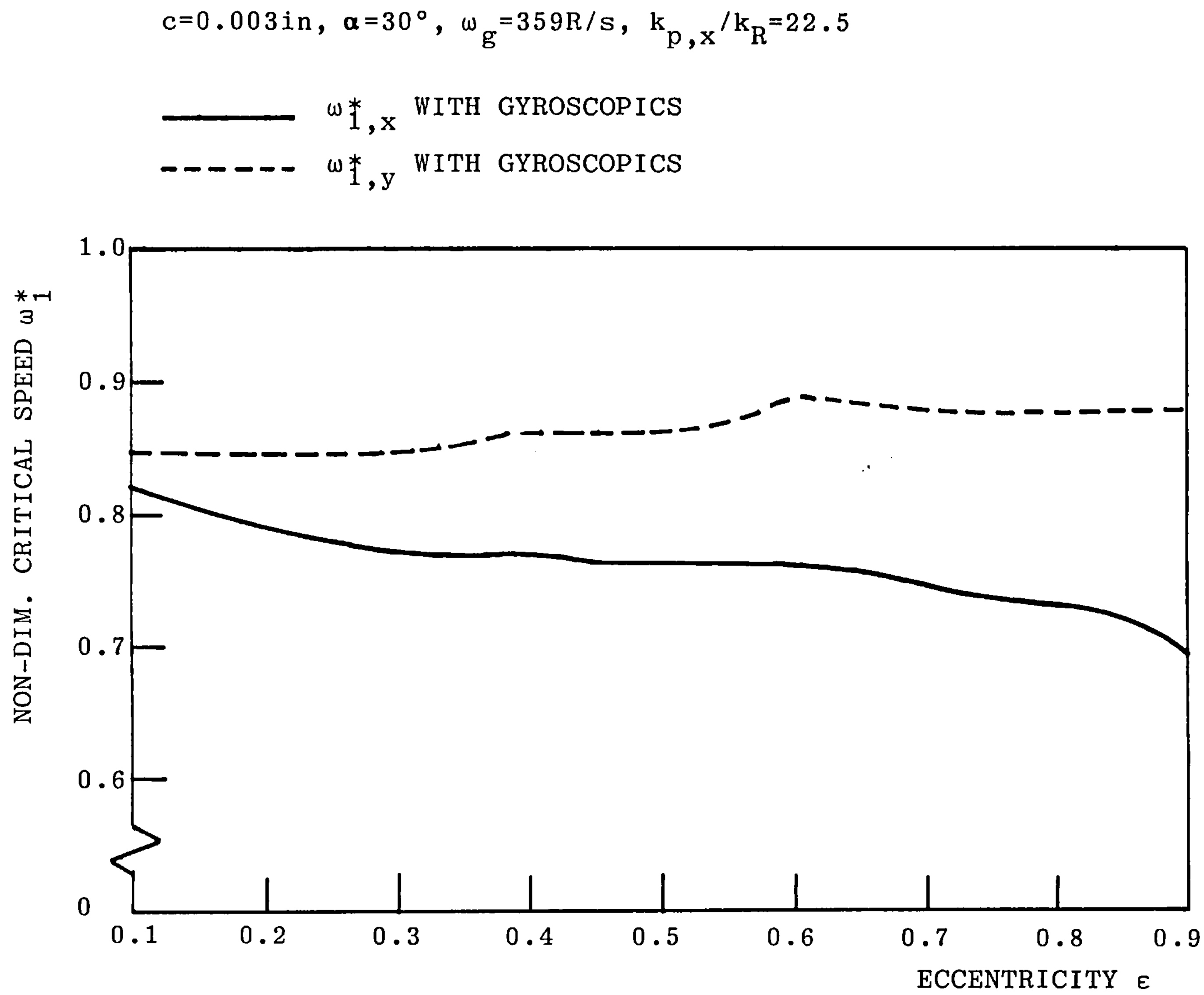

Figure 5.17 Critical Speed Versus Eccentricity for a Flexible Pedestal

Figure 5.18 compares the computed and measured effect of vertical pedestal flexibility ratio, $k_{p,x}/k_R$, where k_R is constant, on the critical speed of the test rotor. The rigid pedestal critical speeds are included for reference. The agreement between theory and experiment is reasonable over the range in which measurements were taken, with experimental values on the conservative side.

It can be observed that decreasing pedestal stiffness reduces rotor critical speed over a particular range, with the critical speed remaining constant above and below this range. It was considered unsafe to attempt to verify experimentally whether further reduction in pedestal stiffness below $k_{p,x}/k_R$=22 had any significant effect on critical speed, because large bearing housing vibration was experienced as the rotor was accelerated through its critical speed.

The reduction in critical speed in the y-direction is less than in the x-direction because the stiffness in the y-direction is greater than in the x-direction. Hence, for a given increase in pedestal flexibility ratio, $k_{p,x}/k_R$, and corresponding decrease in the stiffness ratio $k_{p,x}/k_{p,y}$, the decrease in stiffness in the y-direction is less than in the x-direction.

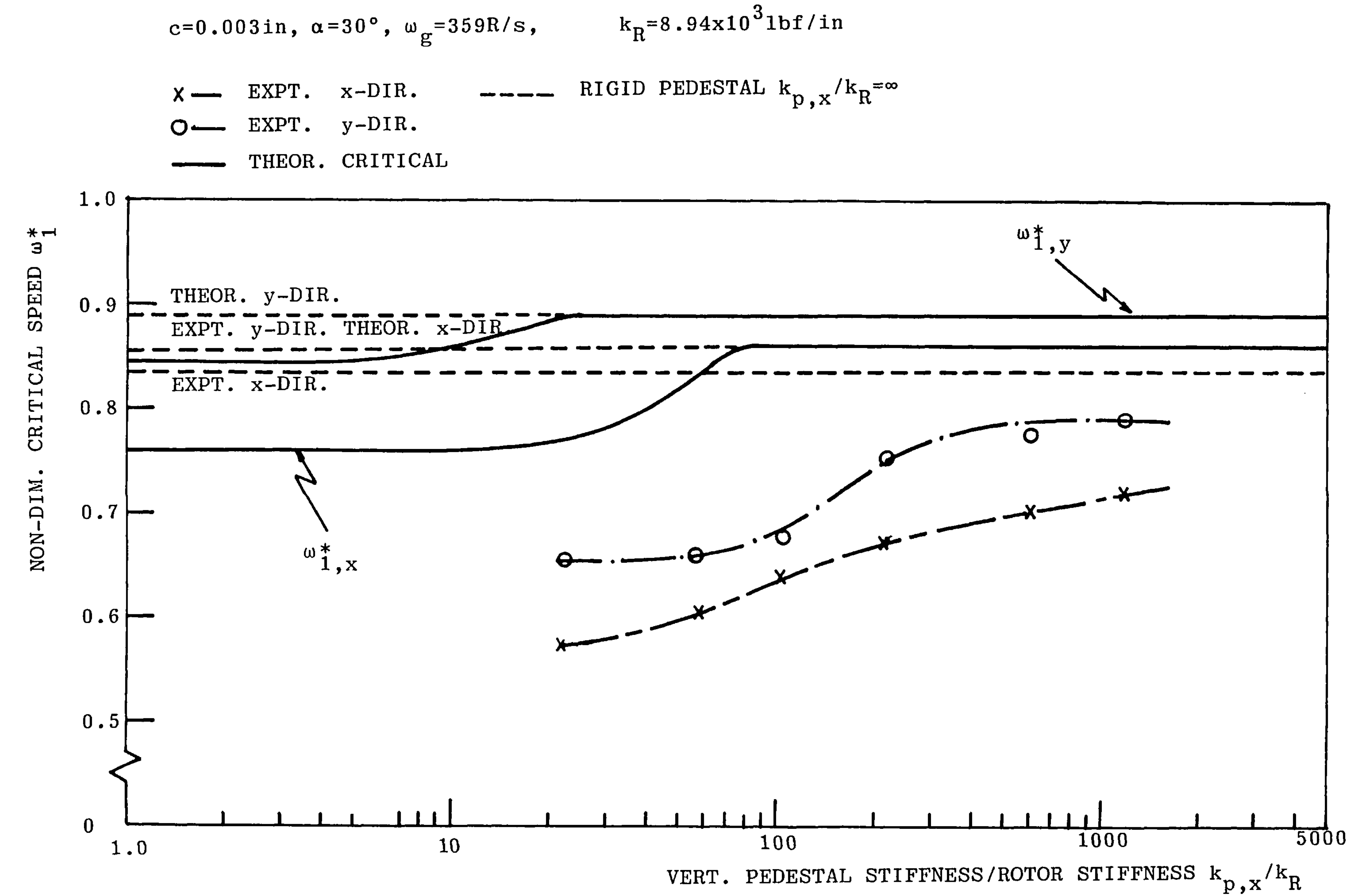

Figure 5.18 Critical Speed Versus Vertical Pedestal Stiffness Ratio

CHAPTER 6

INVESTIGATION OF SYSTEM STABILITY

6.1 INTRODUCTION

This chapter deals with both the experimental and the theoretical investigations of stability of the test rotor-bearing system. The fluid-film bearing is analysed by considering small perturbations of the journal away from its steady state (equilibrium) position. By this means the oil-film forces can be expressed in terms of linearised displacement and velocity coefficients, that is, stiffness and damping coefficients respectively (see Chapter 2). Lund (69) states that linear theory can be used to represent bearing reaction forces with satisfactory accuracy for amplitudes as large as 40% of the clearance. This should cover the operating range in most practical applications.

Linear treatment of the equations of motion representing rotor-bearing systems is only feasible for a limited number of degrees of freedom. For more complex systems the equations of motion tend to be intractable, and solving for stability thresholds using standard techniques such as the Routh-Hurwitz criteria can be a tedious time consuming exercise.

Both McCallion (70) and Thomson (71) deal with several well known methods for predicting stability characteristics from a knowledge of the linear system equations. However, these techniques involve locating the eigen-values from the matrix or characteristic equation of the system. This can entail certain computational difficulties in achieving numerical stability and speed of convergence.

A frequently used method for solving the system matrix in stability analysis is the Q-R algorithm (see Wilkinson (72)). It is quite general in application, converges quickly and is numerically very stable. Computational run time is proportional to:

$$8N^3$$

where N is the order of the system equations to be reduced.

Another technique, somewhat less popular as it entails solving for the eigen-values from the characteristic polynomial equation in its explicit form, is that of Muller detailed by Bishop et al (73). This involves searching for the eigen-values and extracting them in ascending order of modulus. In the present circumstances this is fortuitous as the stability of the rotor-bearing system is assessed by the eigen-value with smallest modulus.

As both the above methods are iterative in nature, their application to stability analysis of complex rotor-bearing systems can lead to excessive use of computer time and result in costly analysis, cf Lund (41), Ruhl and Booker (74).

6.2 STABILITY ANALYSIS USING THE TRANSFER MATRIX TECHNIQUE

In the present work a combination of numerical and graphical methods are used to assess the stability of the test rotor-bearing system for various operating conditions. The Transfer Matrix Method of Chapter 3 is used to generate the frequency determinant of the system, equation (3.51):

$$D \left| \bar{T}_{TB} \right| = 0$$

This determinant is a function of the imaginary exponent $i\Omega$ of equations (3.1) and (3.2), for synchronous vibration of shaft. The motion of the shaft can be generalised to include non-synchronous vibration by replacing $i\Omega$ with the complex variable exponent λ, where

$$\lambda = \sigma + i\Omega \qquad 6.1$$

and σ represents an exponential growth or decay, that is, a damping factor of the system. A positive value of σ corresponds to an unstable system, and a negative value to a stable system.

The state variables given in equations (3.1) and (3.2) can be expressed in a simplified form by using state vector notation, that is:

$$[\bar{z}] = [\bar{z}_A]\, e^{\lambda t} \qquad 6.2$$

where $[\bar{z}_A]$ is an amplitude vector. Equation (3.50) which represents the overall transfer system matrix, relating state variables at either ends of the rotor is still valid for the more general type of motion. But now $[\bar{T}_{TB}]$ is a function of the complex variable λ, instead of the real variable Ω. For a non-trivial solution, the determinant of $[\bar{T}_{TB}]$ must be zero.

Thus:

$$D|\lambda| = [\bar{T}_{TB}] \qquad 6.3$$

$$D|\lambda| = 0 \qquad 6.4$$

Equation (6.4) can be regarded as the frequency equation of the system, and $D|\lambda|$ as the frequency determinant.

If the motion of the shaft is proportional to $e^{\lambda t}$, then λ must be an eigen-valvue of equation (6.4). Thus, for a given set of operating conditions, the system will be stable if all the values of λ which satisfy equation (6.4) are such that their real parts are negative. If only one eigen-value has a positive real part, this is a sufficient indication that the system is unstable. The eigen-values, in general, will occur in complex conjugate pairs.

As equation (6.4) is a function of the complex variable λ, it is clear that a numerical search for the eigen-values using one of the techniques mentioned in Section 6.1 is likely to be time consuming.

6.3 LEONHARD LOCUS PLOT

Considering the complex λ-plane and complex D-plane and plotting the locus of the determinant, each point or eigen-value in the λ-plane will be mapped to a corresponding point in the D-plane.

If σ is set to zero, than a point in the λ-plane travelling along the imaginary axis from $\Omega=0$ to $\Omega=\infty$, will map to a curved locus in the D-plane called the Leonhard Locus (75). This locus enables the stability of the system to be ascertained. For a stable system all the eigen-values will occur to the left hand side of the origin in the λ-plane, and in the D-plane the Leonhard locus will encircle the origin, moving clockwise or anticlockwise as Ω increases from zero. At the threshold of stability the locus will pass exactly through the origin of the D-plane. Several researchers have applied this technique successfully to complex rotor-bearing systems, eg: Morrison (28), (40), (46) and (60).

A typical Leonhard plot of the test rotor-bearing system stability is shown in Figure 6.1, for c=0.003in, $\alpha=30^{\circ}$, $\gamma=0$ and $\delta/c=1.7$. Three loci are shown representing the system

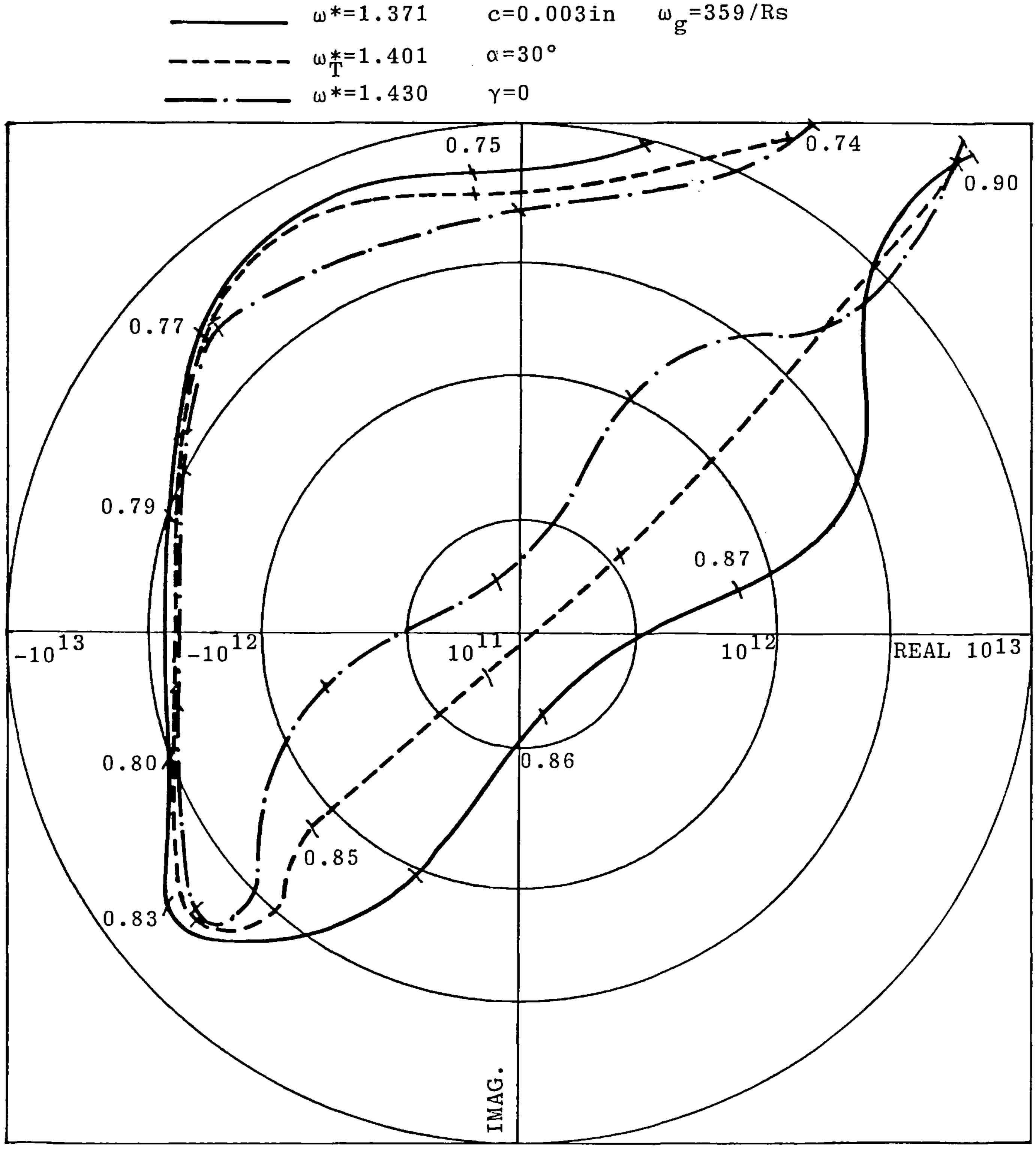

Figure 6.1 Leonhard Locus Plot

when it is stable, at the stability threshold and running in the unstable region.

Marked on the loci are values of non-dimensional frequency $\Omega^*(=\Omega/\omega_g)$ for three values of non-dimensional shaft speed $\omega^*(=\omega/\omega_g)$. It can be seen that in the stable region for $\omega^*=1.371$, the locus rotates successively through each quadrant, encircling the origin. At $\omega^*=1.430$, it is observed that the locus does not encompass the origin and the sytem is unstable. For an intermediate value of $\omega^*_T=1.401$, the Leonhard locus indicates that the speed is very close to the threshold of stability, with an instability frequency of $\Omega^*_T=0.859$ and a ratio of $\Omega^*_T/\omega^*_T=0.614$.

To check the accuracy of the Transfer Matrix Method in conjunction with the Leonard Locus Plot, a comparison is made with published data. Lund (76) computed the stability threshold of a symmetric rotor mounted in two Ocvirk short bearings of L/D=0, with a disc positioned midway between the bearings. The stiffness and damping coefficients of the bearing are given in (76). Lund assessed the stability of the system from an eigen-value analysis, neglecting gyroscopic effects.

To compare the present method of analysis with that of Lund, it is necessary to non-dimensionalise the transfer matrices representing the bearing element, massless elastic beam element and point mass element (neglecting gyroscopic terms) as detailed in (59). For the simple symmetric bearing-rotor system modelled by Lund, non-dimensionalising the transfer matrices is a relatively easy exercise.

Figure 6.2 is a plot of non-dimensional threshold speed ω^*_T against eccentricity ε for five values of flexibility parameter δ/c. Generally, the agreement between Lund's results and the present work is very good. It is observed that decreasing the flexibility parameter raises the threshold of stability, with $\delta/c=0$ representing the case of a stiff rotor. Above $\varepsilon=0.79$ the rotor becomes infinitely stable for all values of δ/c.

6.4 CHARACTERISTIC PATTERNS OF WHIRL AND WHIP

This section describes the general patterns of oil-whip (resonant whip) and oil-whirl as exhibited in the series of experiments performed in this investigation. The phenomena of whipping and whirling that were qualitatively common to all cases regardless of bearing parameters or operating conditions will be classified as inherent characteristics of whip and whirl.

In the test runs, during which the shaft speed was gradually increased, the commencement of self-excited vibration was usually characterised by small vibrations

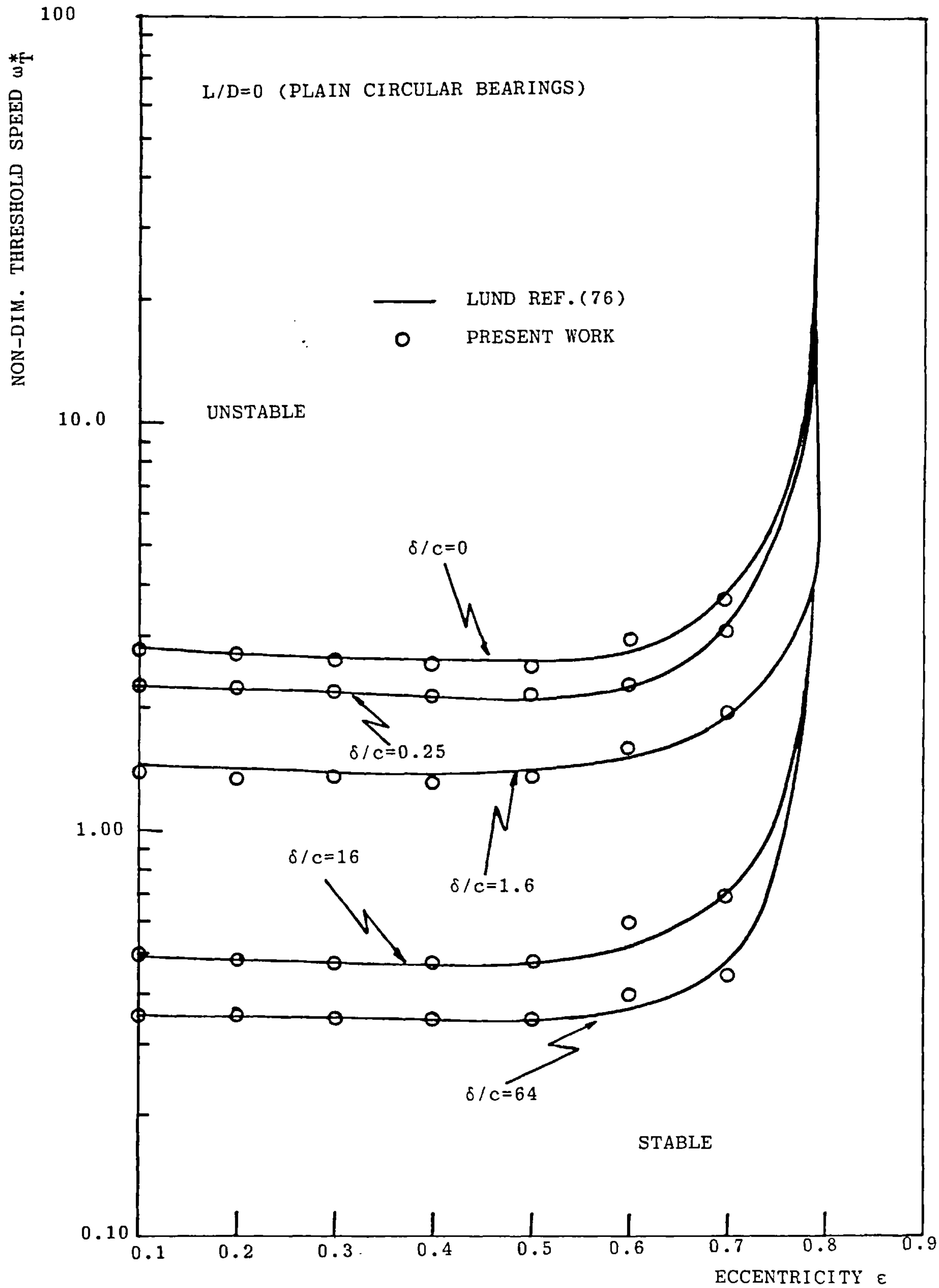

Figure 6.2 Stability Threshold for Several Shaft Flexibilities

whose frequency was approximately half the running speed. This occured over a speed range of several hundred R.P.M before large amplitude vibration set-in, that is, the threshold of stability. In some cases small vibrations were observed on the frequency spectrum corresponding to the critical speed of the rotor.

For small clearances it was found that as the speed was increased, the frequency corresponding to the critical speed of the rotor became the predominant frequency of the system and the rotor could be said to be in a state of whip. The transition usually occurred at speeds just above twice the value of the first critical. As the speed was increased further the vibration persisted with only a small change in frequency. The whip frequency was found to approach an asymptotic value.

For larger clearances, the predominant frequency at a particular shaft speed, was found to be slightly less than half the running speed, and below the frequency corresponding to the critical speed. As the shaft speed was increased beyond the threshold a corresponding increase in the non-synchronous frequency was observed. This indicated that the rotor was subjected to whirl. For safety reasons the shaft speed was increased further by only a few hundred R.P.M. to verify that whirl was the predominant phenomenon. It was expected that with further increase in shaft speed the whirl frequency would eventually reach the critical frequency, and the rotor would then be in a state of whip. This would result in the characteristics described earlier in this section.

When a whirl or whip frequency predominated in the system, an increase in amplitude was observed. In most cases the change in magnitude was extremely pronounced, particularly at large clearances. With increase in speed, whip amplitude tended to rise initially and then level off. Whereas, when whirl occurred the amplitude was found to increase steadily with speed. Tondl (53) has observed similar effects. With the onset of large amplitude vibration associated with non-synchronous motion, the running frequency was usually reduced.

Earlier in this section, it was noted that initally small amplitude non-synchronous vibration were observed before the actual onset of whirl and whip at the stability threshold. This was observed on the oscilliscope screen as a transient motion in which the rotor would alternatively be stable and unstable, and the mainly synchronous orbit would grow and decay by small amounts in a cyclic manner.

With further increase in shaft speed, a small cusp would, in certain cases, form within the orbit. The cusp would grow rapidly into a large non-synchronous orbit at the threshold. With the shaft speed held steady, the orbit would rotate slowly round on the oscilliscope screen, growing and decaying by small amounts. The rotation of the orbit was probably due to the ratio of synchronous and non-synchronous motions being less than one-half.

Sub-harmonic frequencies equal to 1/2 and 1/3 of the running speed were also observed in the frequency spectrum. The associated amplitude was very small. Tondl (53) observed this phenomenon and attributed it to non-linear stiffness effects of the oil-film, excited by synchronous vibration of the rotor. It is possible to eliminate these effects by improving the balancing of the rotor.

6.5 SOME FACTORS AFFECTING STABILITY

This section deals with experimental and theoretical investigations of certain variables and their affect on the stability of the test rotor-bearing system. These variables and the order in which they are discussed are:

(1) bearing oil supply feed pressure
(2) position of oil feed groove
(3) oil feed groove angle extent
(4) journal bearing pedestal flexibility

For each variable, changes in the bearing clearance are also investigated.

6.5.1 Oil Supply Feed Pressure

As described in Section 4.3.3 oil was supplied to the test bearing through two axial feed ports, positioned at 90^o with respect to the vertical plane. Figures 6.3, 6.4 and 6.5 depict the measured variation in non-dimensional stability threshold speed $\omega^*_T(=\omega_T/\omega_g)$ versus non-dimensional feed pressure ratio $\gamma(P_f/P_b)$. P_f is the oil supply pressure and P_b is the specific bearing load W/LD. The experiments were conducted with a groove angle of 30^o and for three values of bearing radial clearance c, that is, 0.003in, 0.004in and 0.005in respectively.

Figure 6.3 also shows the computed variation of ω^*_T with γ for c=0.003in, for the test rotor-bearing system. Also shown for reference is the computed stability threshold point mass rigid rotor mounted in two identical journal bearings of L/D=1/2 and $\alpha=30^o$. The stability of this rotor was obtained using the Routh-Hurwitz criteria, Den Hartog (77).

Rigid rotor predictions of ω^*_T are considerably higher than those of the flexible rotor with gyroscopic effects included. The agreement between the trends of the computed results for the flexible rotor and measured values is good, but the experimental values are higher by as much as 31% when compared with theory. Several possible explanations will be discussed later in this section.

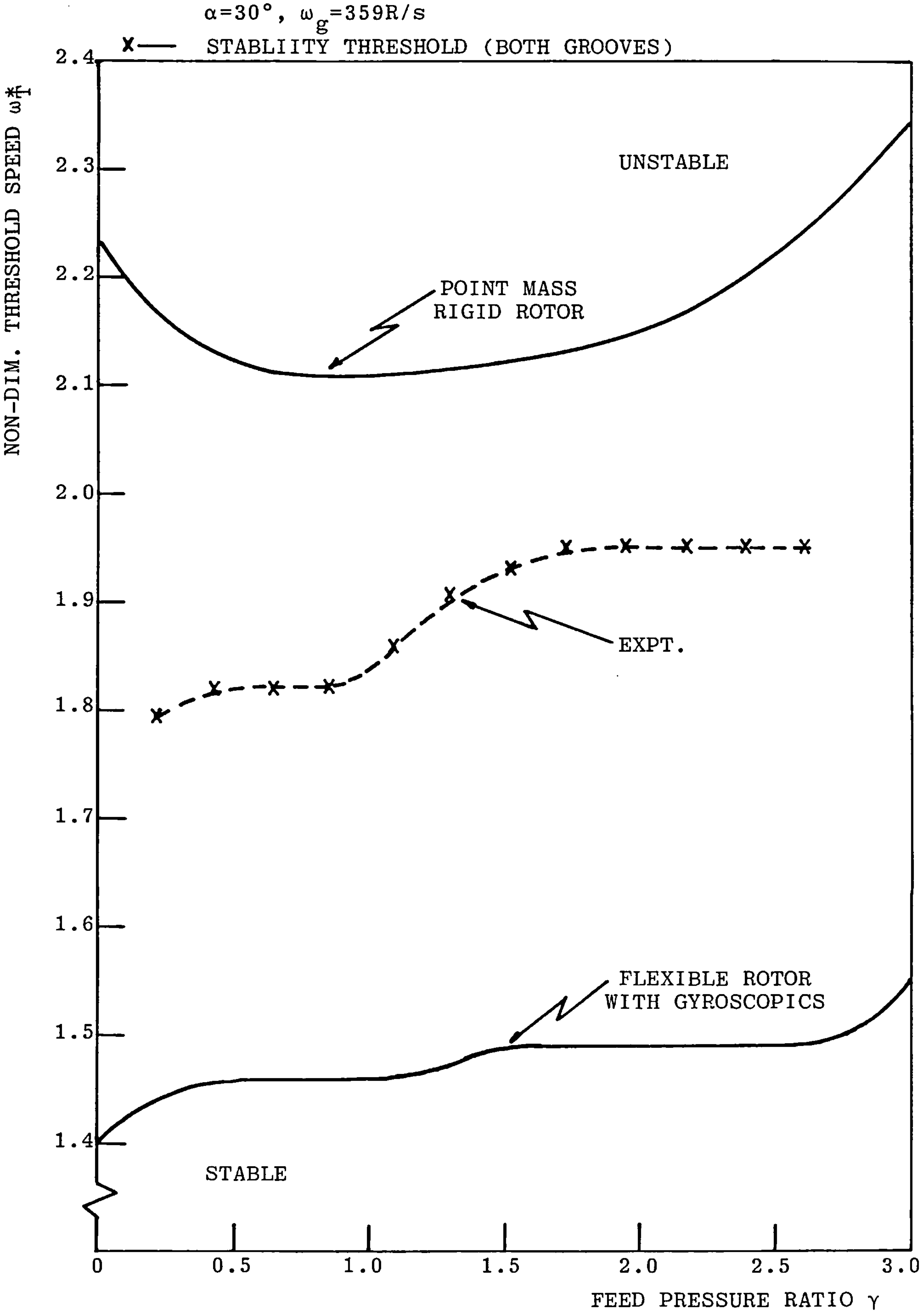

Figure 6.3 Stability Threshold Versus Feed Pressure Ratio for c=0.003in

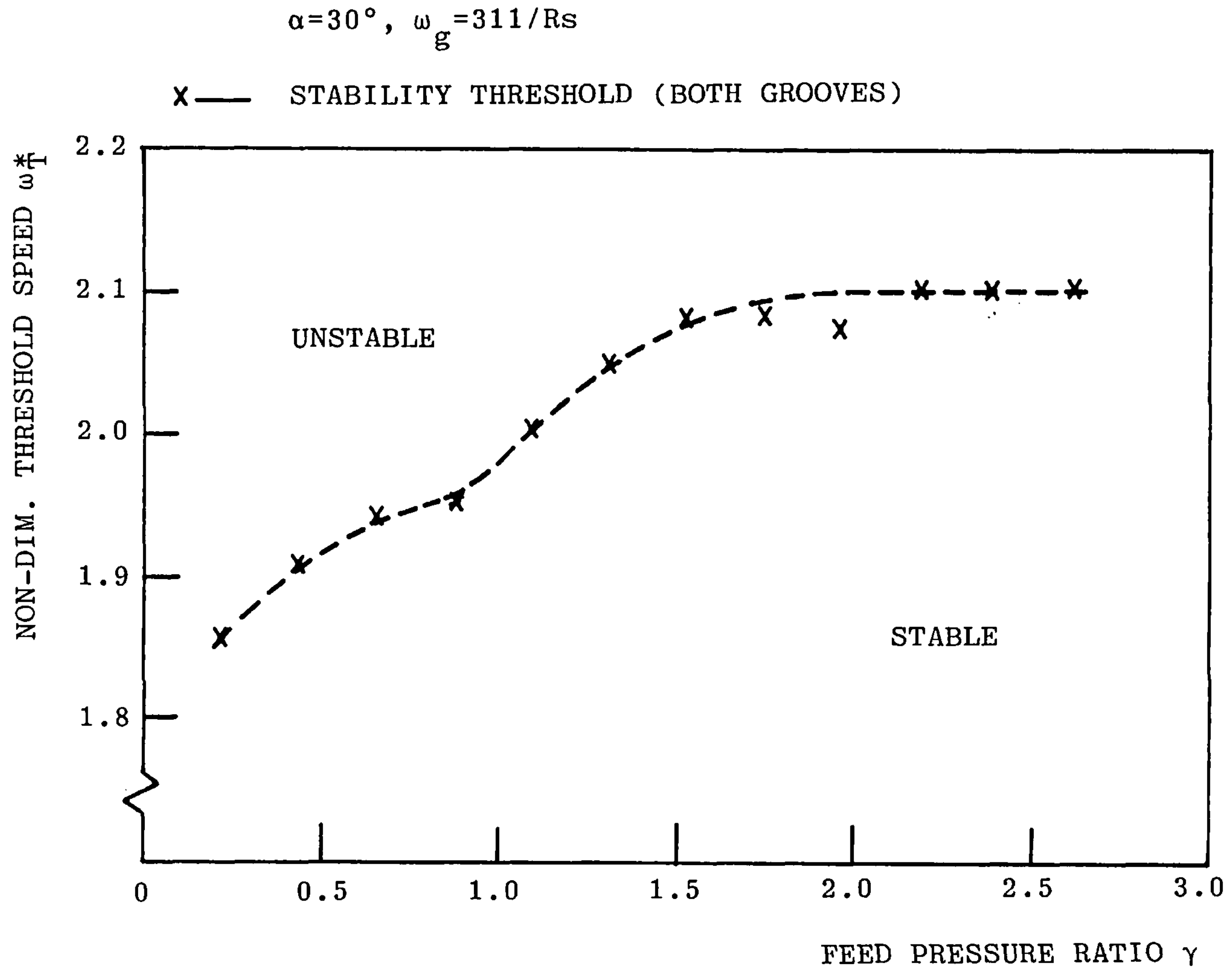

Figure 6.4 Stability Threshold Versus Feed Pressure Ratio for c=0.004in

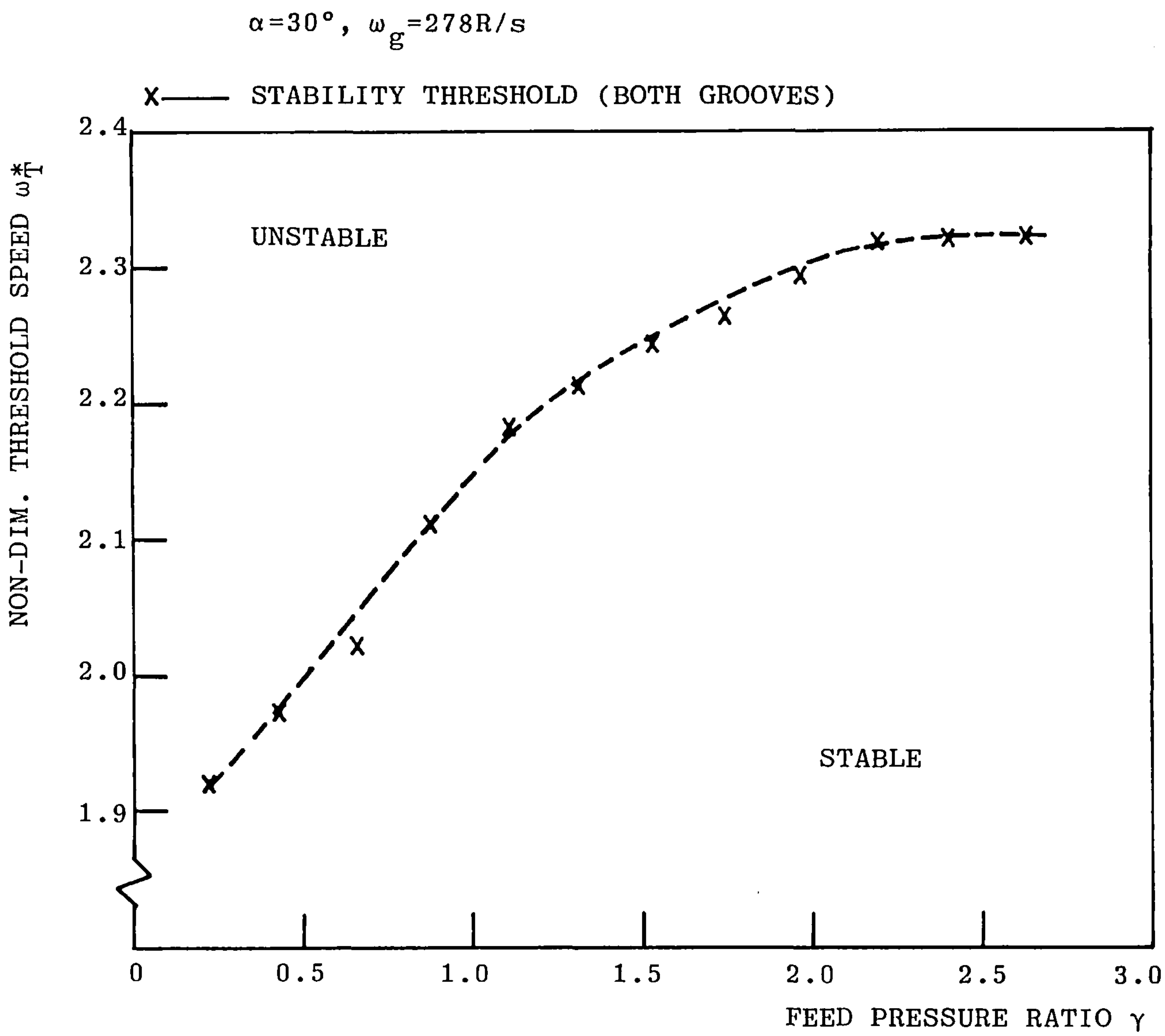

Figure 6.5 Stability Threshold Versus Feed Pressure Ratio for c=0.005in

Increasing the feed pressure has a stabilising effect, which becomes more pronounced as the clearance is increased, (see Figures 6.3, 6.4 and 6.5). It is also observed that at a particular value of γ, additional increase in feed pressure has no effect on stability. The stabilising effect of feed pressure occurs at lower values as the clearance is increased. It was not practical to increase γ beyond about 2.6, because of excessive side leakage from the bearing.

It is thought likely that the stabilising effect is due to preloading of the bearing as the feed pressure is increased. Cole (48) and Newkirk and Lewis (19) have observed similar effects. Whereas, Akkok and Ettles (47), Pinkus (16) and Pope (49) have reported that increased feed pressure has a destabilising effect. Tondl (53) and Lund (52) observed that increased oil pressure did not effect stability.

As the test bearing was lightly loaded (9.2p.s.i. or 0.63bar), a low specific bearing load would only generate small hydrodynamic pressures, and hence an increase in supply pressure would tend to be more effective in preloading of the bearing. The increase in threshold speed with increasing clearance noted earlier can be explained by assuming that an increase in clearance, results in greater amounts of oil passing through the bearing. This oil would be pumped to considerable pressure within the bearing, producing a greater preloading effect.

The destabilising effect of increased feed pressure as reported by the authors in (16), (47) and (49) can be explained by noting that generally, their test rotors ran with higher bearing loads. This implies that the cavitation boundary region is sharply defined, and hydrodynamic pressures are larger than those for light loads. Increase in feed pressure tends to suppress cavitation with a consequent generation of full,360^{o} film conditions which promotes instability.

Figures 6.6. and 6.7 respectively, show plots of measured non-dimensional threshold frequency $\Omega^*_T (=\Omega_T/\omega_g)$ and the threshold ratio of Ω^*_T/ω^*_T against γ , for c=0.005in, 0.004in and 0.003in. Computed values are also shown for the case of c=0.003in.

From Figure 6.6 it is seen that the value of Ω^*_T increases with γ, a more noticeable increase occurring with larger clearances. Above certain values of γ , Ω^*_T remains constant. For c=0.003in, a small increase in Ω^*_T is observed. Comparing these results with Figure 5.11, it can be seen that for c=0.004in and 0.005in, the limit of the instability frequency at higher γ values corresponds approximately to the critical speed for each clearance. Hence, constant values of Ω^*_T indicate that the rotor is subjected to oil-whip. However, below these same values of γ, the rotor is whirling. This was verified by holding the supply pressure constant and increasing shaft speed to obtain the expected increase in whirl frequency.

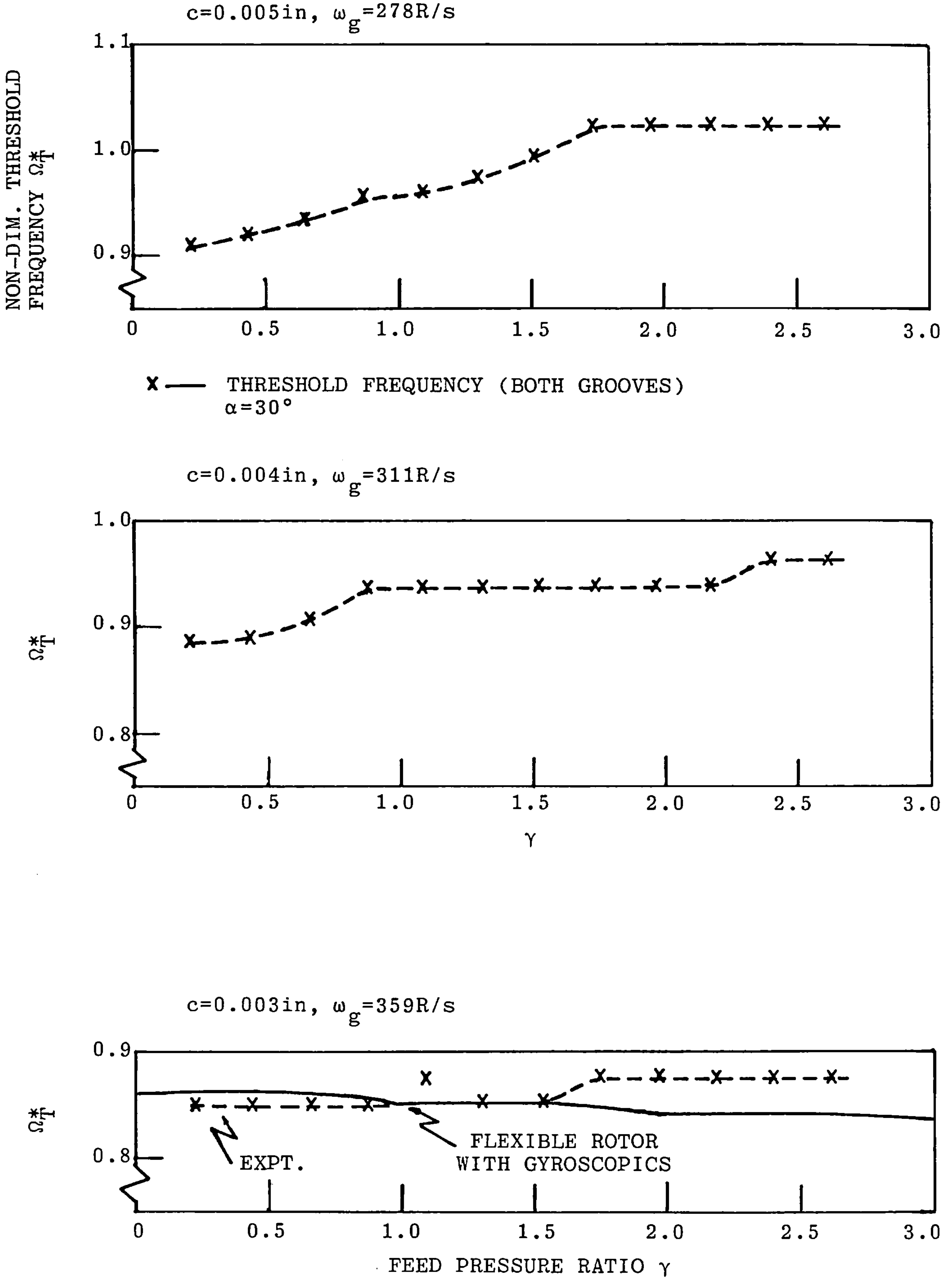

Figure 6.6 Threshold Frequency Versus Feed Pressure Ratio

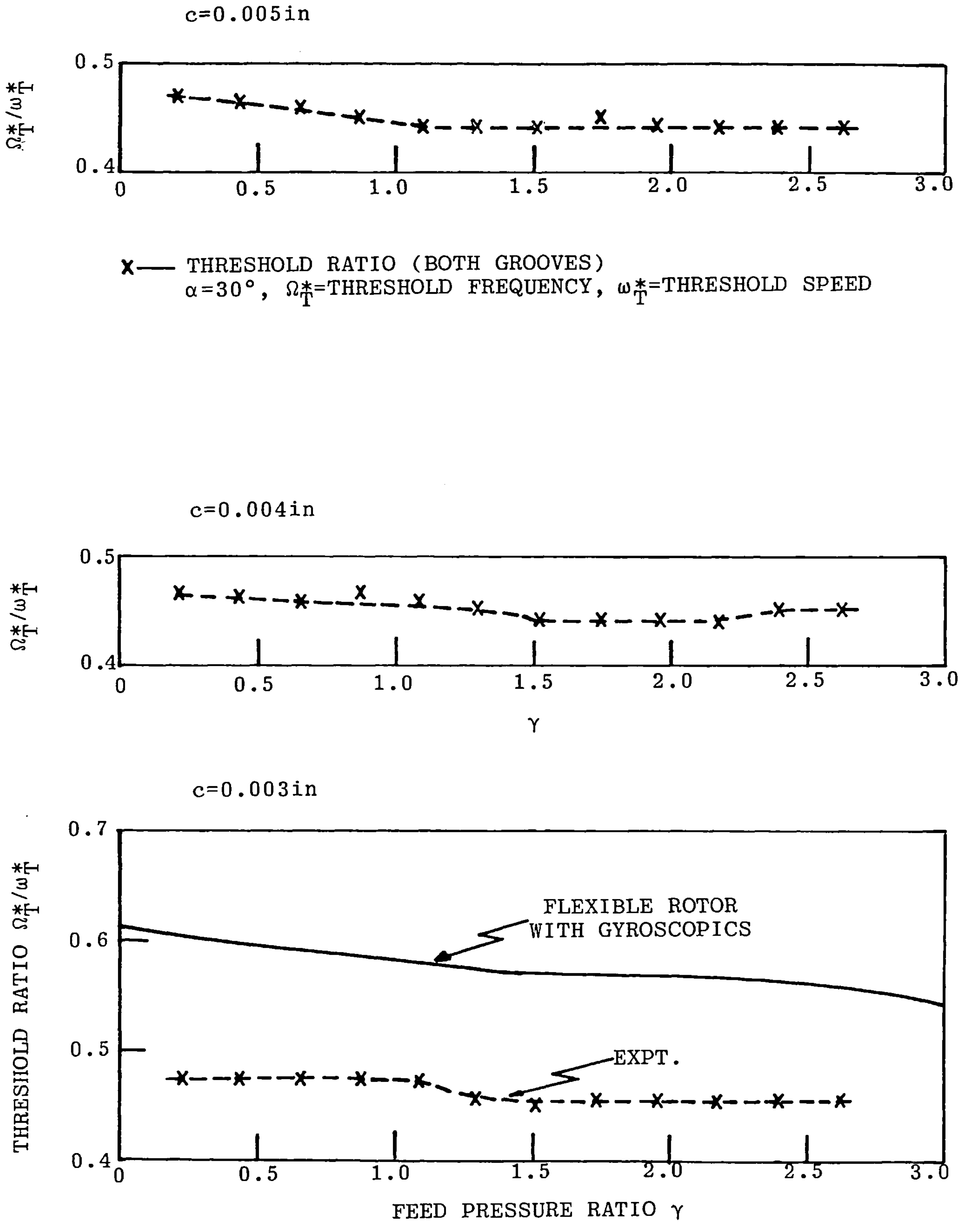

Figure 6.7 Threshold Ratio Versus Feed Pressure Ratio

It is seen in Figure 6.6 that little increase of Ω^*_T occurs for c=0.003in. The value of Ω^*_T corresponds closely to the critical speed of the rotor over the measured range of γ values and thus, indicates that the rotor is subjected to whip. Agreement between predicted and measured values of Ω^*_T is good.

The occurrence of whip at different values of supply pressure explains why no increase in the instability speed ω^*_T is observed in Figures 6.3, 6.4 and 6.5, beyond a particular value of γ. Hence, as the shaft speed is increased beyond the onset of whip, the whip frequency persists and, therefore, represents the maximum attainable stability limit of the system.

Figure 6.7 shows that the threshold ratio decreases gradually, and becomes constant when Ω^*_T and ω^*_T reach their respective maximum values. The predicted values of Ω^*_T/ω^*_T for c=0.003in are higher than the corresponding measured values. The computed values decrease from 0.615 at $\gamma=0$ to 0.540 at $\gamma=3$. Measured values did not exceed 0.475 and decreased to 0.455. The computed values of the ratio are higher because, although, the predicted values of Ω^*_T are accurate, the corresponding values of ω^*_T are considerably on the conservative side, (see Figures 6.3 and 6.6).

The differences between the theoretical and experimental thresholds of Figure 6.3 are attributed to a combination of four possible factors. These are listed and discussed below:

(i) inaccurate specification of boundary conditions (that is, cavitation occurring at ambient or sub-ambient pressures) in the bearing calculations

(ii) inaccurate estimates of an effective oil viscosity

(iii) misalignment of the journal within the bush

(iv) reduced gyroscopic effects

(i) As the test bearing was lightly loaded (9.2p.s.i. or 0.63 bar) it is plausible that the assumed Reynolds boundary conditions for the bearing calculation were incorrect. This is because of the possibility of sub-ambient pressures developing within the bearing oil-film.

Akkok and Ettles (47) examined theoretically and experimentally the effect of small bearing loads P_b, on the stability threshold. On their test apparatus it was possible to vary P_b up to a maximum value of 50p.s.i. (3.45bar). They observed experimentally that changing p_b had no signficant effect on stability.

In their calculations they allowed for sub-ambient cavitation and cavitation at ambient pressure (Reynolds condition). It was observed that good agreement between theory and experiment was obtained using the Reynolds boundary condition for a range of bearing loads. When sub-ambient pressures were allowed, reduction in P_b resulted in a lower stability threshold. This was in disagreement with observation.

It would, thus, appear that sub-ambient pressures were not present, and the cavitated area vented at atmospheric pressure as assumed in Reynolds boundary condition.

This evidence is supported by the successful running of flexible test rotors with light bearing loads. In references (16), (49), (53), Woodcock and Holmes (78), and Mayes and Davies (79), bearing loads varied between 7.2 and 24.6p.s.i. (0.5 to 1.7bar) without any effect on stability. In three of the references, that is, (16), (78) and (79), the loading was of the order of 8.7p.s.i. (0.6bar) or less. Under such light loads, almost pure Sommerfeld conditions would be expected producing instability over a wide speed range.

(ii) Experiments showed no increase in bearing temperatures as the shaft speed was increased with increase in feed pressure to determine the change in stability threshold. Thus, the effective viscosity could be considered constant. This simplified the theoretical analysis, and subsequently only occasional checks of the temperature were carried out.

To examine the effects of inaccurate temperature measurements and consequently inaccurate effective viscosity determinations, several values of viscosity were used in the computations of ω^*_T. The values of η used correspond to a range of values of Sommerfeld Number or eccentricity centred around the original value. The computed results of ω^*_T against γ are shown in Figure 6.8, for c=0.003in. For comparison the experimental results of Figure 6.3 are also shown.

The trend of the results corresponding to an effective viscosity of 57cP agrees quite well with the measured values. The value 57cP represents an increase of 68% on the original value of 34cP, and corresponds to a drop in mean temperature of 18.6%. However, it is thought unlikely that temperature measurements could be in error to such an amount. The maximum increase in ω^*_T for η=57cP, when compared with the value corresponding to η=34cP is only 6.4%.

Figure 6.9 shows the computed variation of ω^*_T with eccentricity ε, for four values of γ. This confirms that, in general, increasing γ results in a gradual increase in ω^*_T over most of the eccentricity range.

(iii) As stated in Section 5.4, misalignment of the journal within the bearing bush introduces moments in the oil-film. The additional forces within the bearing can be represented

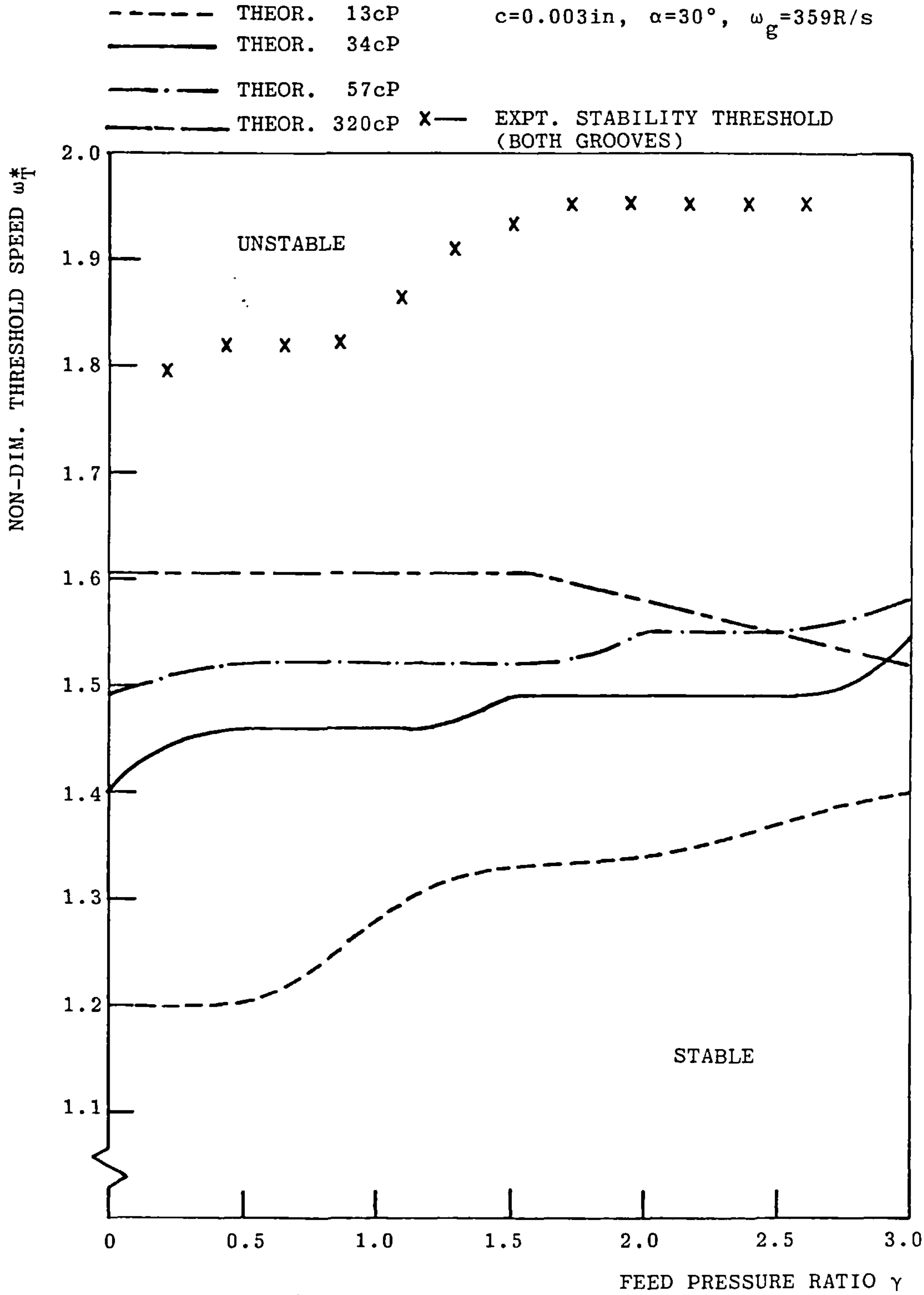

Figure 6.8 Stability Threshold Versus Feed Pressure Ratio for Several Values of Effective Viscosity

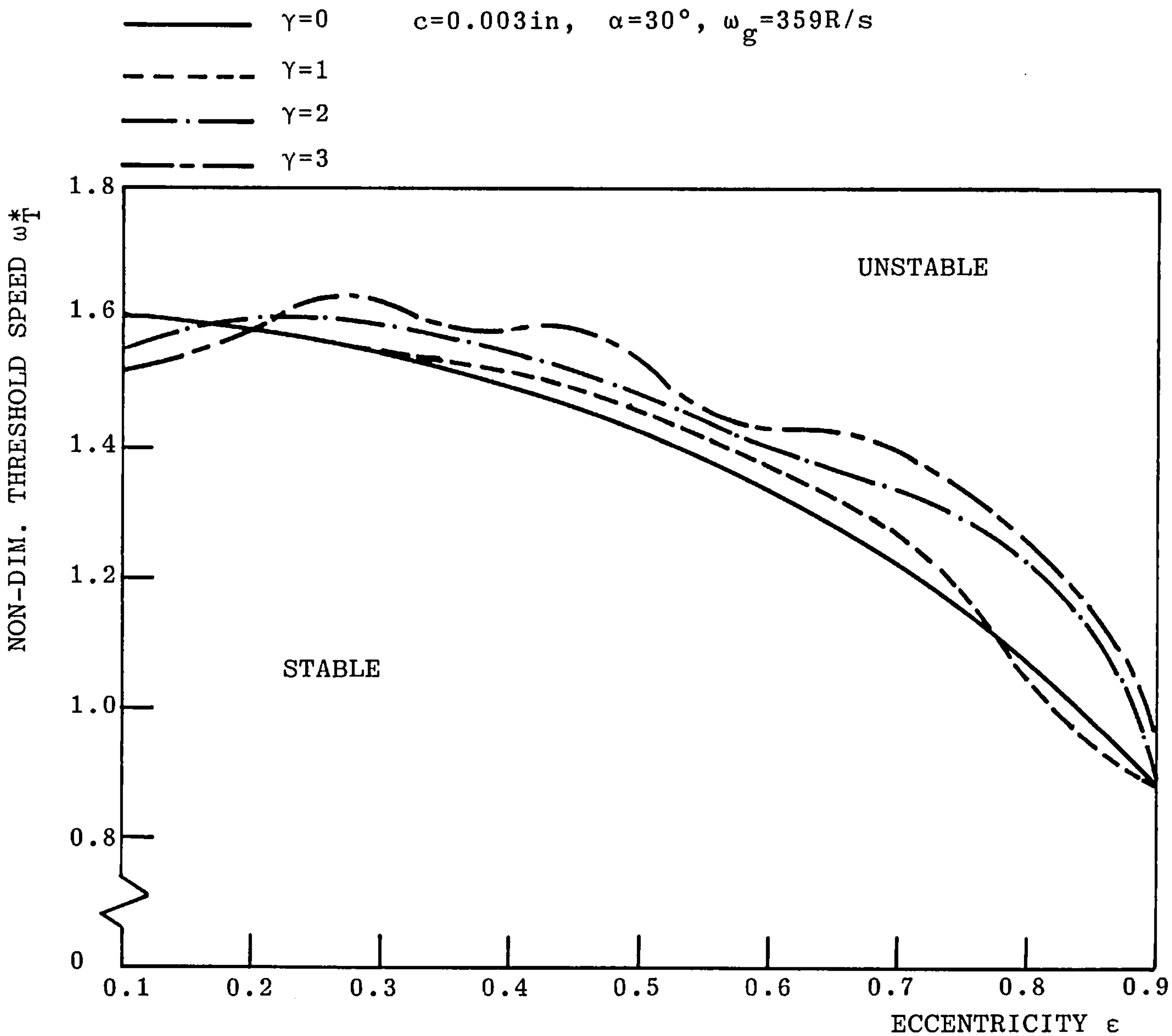

Figure 6.9 Stability Threshold Versus Eccentricity for Several Values of Feed Pressure Ratio

by four rotational stiffness coefficients and four rotational damping coefficients. This is in addition to the eight linear or direct coefficients which are usually applied.

Static misalignment was present in the test rotor-bearing, due to the deflection of the rotor under gravity. Some misalignment was also present in the system due to its design. That is, one end of the rotor was free (test bearing) and the other end pinned or simply supported. It was estimated from the design of the rotor, and for typical operating conditions that static misalignment was approximately thirty times greater than the misalignment due to the pinned support. Thus, static deflection of the shaft was considered the most important factor contributing towards shaft and bearing misalignment.

However, Kikuchi (46) states that although oil-film moment tends to raise the stability threshold, its effect is insignificant in ordinary shaft systems. In the present work it was found that the introduction of a flexible pedestal (Section 6.5.4) resulted in better agreement between theory and experiment. For low flexibility, agreement is typically 7%. This was attributed to the achievement of better alignment between the bearing and shaft, permitted by support flexibility. This leads the present researcher to the conclusion that misalignment can be an important factor.

Another possible influence on the computed values of ω^*_T arises from the occurrence of small orbital motions of the journal within the bearing bush. This could result in transient variations of the stiffness and damping characteristics of the oil-film.

(iv) Owing to the rotor design gyroscopic moments must have been present, and their effect on the stability of the system could be important (46). In general, reducing the gyroscopic moment raises the threshold of stability. For a typical set of operating conditions it was calculated that with zero gyroscopic moment the threshold of stability, ω^*_T, is raised by 8.6% above the non-zero case. The effect of zero gyroscopic moment is more pronounced with increase in eccentricity, (see Section 6.5.3.3).

The flywheel was attached securely to the shaft as discussed in Section 4.3.2. Reduced gyroscopic effects may have occurred, however, if the flywheel axis could skew relative to that of the shaft by a small amount during running.

Another possible explanation for the discrepancy between theory and experiment could have arisen if damping were present in the Ringfeder locking device. This was considered possible since the Ringfeder was assembled with thin layers of oil on the tapered rings.

This damping would manifest its presence as a reduction of inertia. However, from Chapter 5 agreement between computed and measured critical speeds were good. Thus, reduced inertia effects were discounted, as they would have resulted in lower measured critical speeds.

6.5.2 Position of Feed Grooves

This section is concerned with the effect on stability, of supplying oil to the bearing through either the upstream or downstream groove. Figures 6.10, 6.11 and 6.12 depict the variation in measured non-dimensional threshold speed ω^*_T with non-dimensional feed pressure γ . Tests were conducted for three values of bearing radial clearance c; 0.003in, 0.004in and 0.005in. The groove angle α was 30^o in all cases.

In these experiments oil was supplied separately to each groove and a series of tests were conducted to ascertain the effect of increased feed pressure upon stability speed.

The major conclusion of these particular experiments is that supplying oil to the downstream groove alone, has a marked destabilising effect compared with supplying oil to both grooves, Figures 6.10, 6.11 and 6.12. For reference the upper graph represents the case of oil supply to both grooves, that is, Figures 6.3, 6.4 and 6.5 respectively. Cole (48) has observed a similar effect, although he made no further attempt to investigate in any detail.

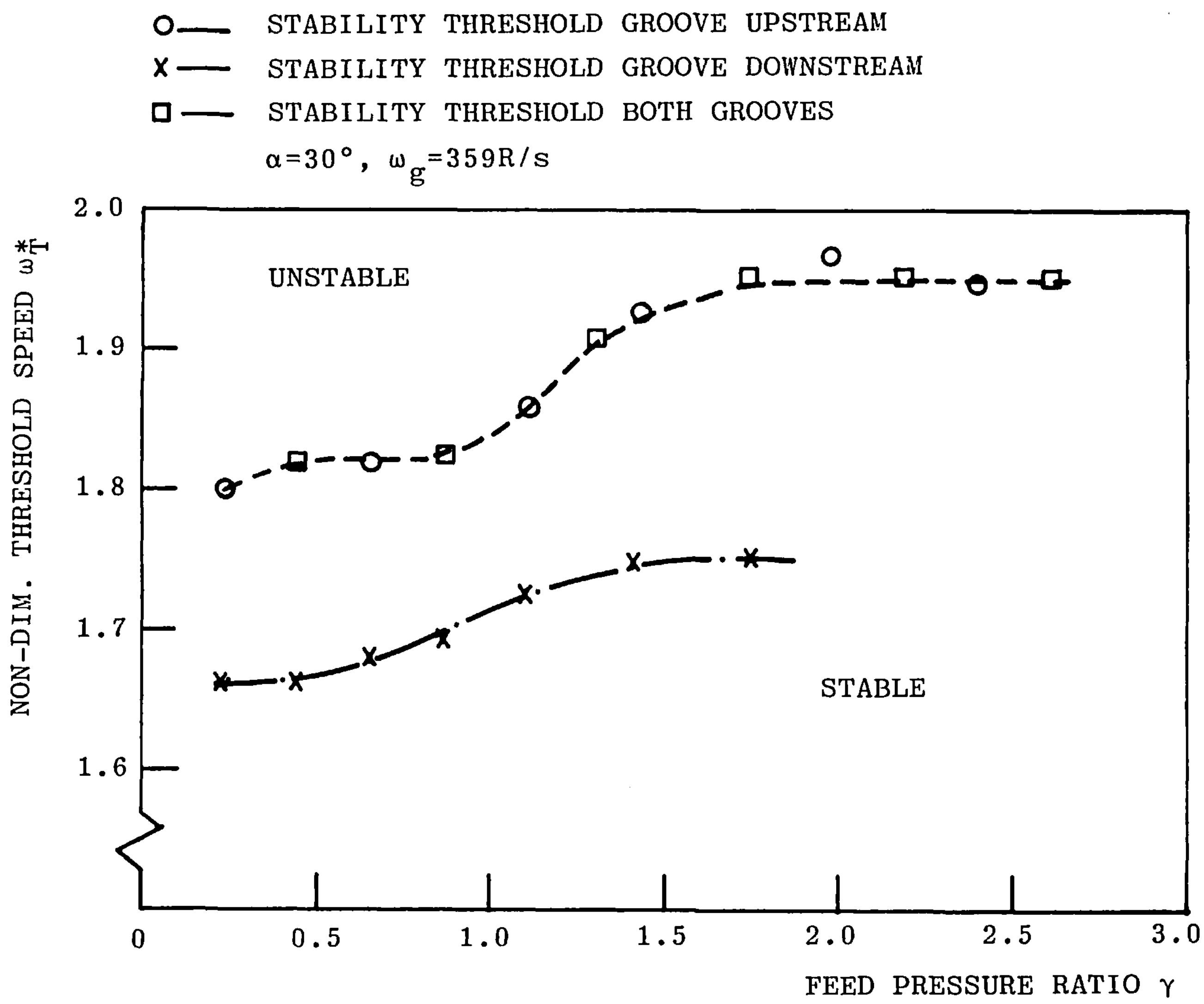

Figure 6.10 Threshold Speed Versus Feed Pressure Ratio for Different Groove Positions and c=0.003in

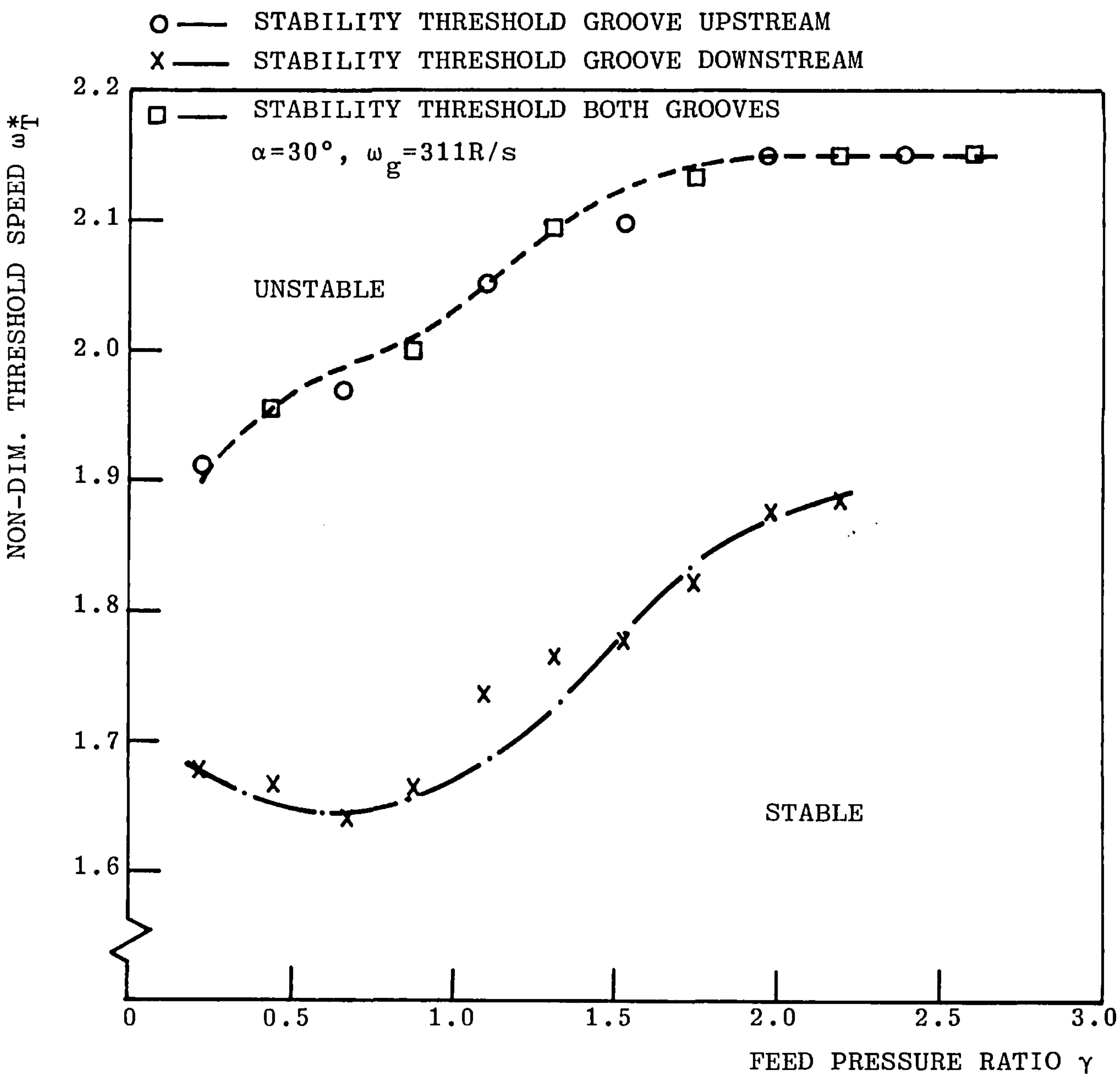

Figure 6.11 Threshold Speed Versus Feed Pressure Ratio for Different Groove Positions and c=0.004in

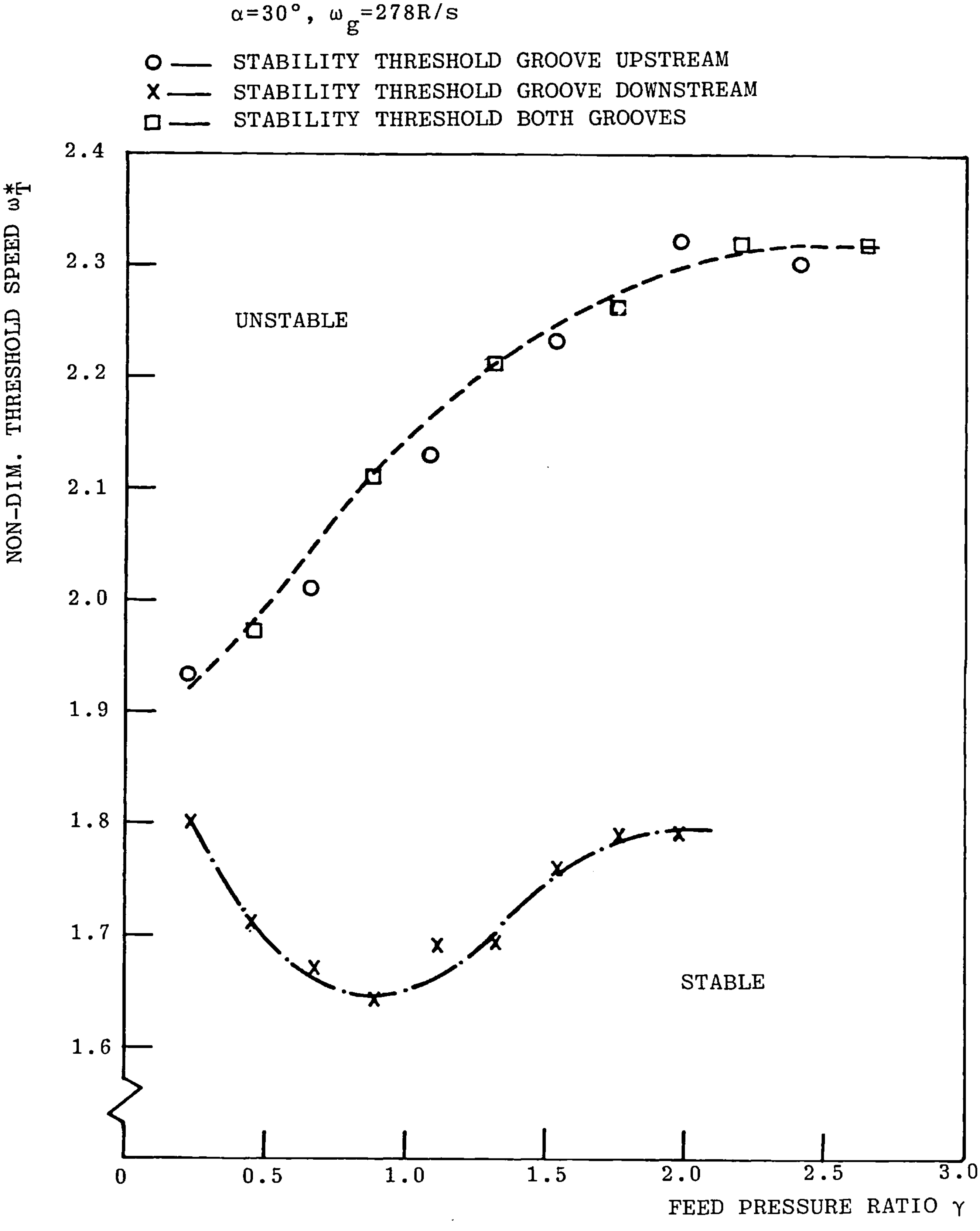

Figure 6.12 Threshold Speed Versus Feed Pressure Ratio for Different Groove Positions and c=0.005in

Plotted alternatively on the upper graphs of Figures 6.10, 6.11 and 6.12 are points representing oil supply to both grooves and the upstream groove alone. Close agreement is obtained between the graph representing both grooves and the alternative points representing the upstream groove. It is deduced that the upstream groove alone produces the same change in stability threshold with increase in feed pressure as that obtained by using both grooves.

It is thought that supplying oil to the groove in the diverging film region, that is, 90° after the load, would tend to promote film continuity. Suppressing cavitation in this manner will promote instability. Conversely, supplying oil to the groove position 90° before the load, that is, in the converging film region will tend to reduce film continuity. A reduction in film continuity will promote cavitation and increase the stability of the rotor.

Another interesting observation can be made from Figures 6.10, 6.11 and 6.12, by comparing the separate factors influencing speed with the upstream and downstream grooves. For a given value of γ , the destabilising effect is, generally, greater for an increase in clearance. This is probably due to the increase in clearance generating a greater film extent and, hence, moving the cavitation boundary downstream closer to the downstream groove. In this case it is expected that feed pressure will be more effective in destabilising the rotor.

6.5.3 Feed Groove Width

This section deals with the effect on stability of an increase in the width or angular extent of both feed ports. Three values of groove angle α are compared, and they are 30^o, 60^o and 90^o. Several other effects were investigated in combination with groove angle, and so it is convenient to subdivide this section under the headings of these effects.

In this section oil feed pressure to the bearing p_f, was fixed at 2p.s.i. (13.8KPa).

6.5.3.1 Hysteresis effect

The hysteresis effect is characterised by a reluctance of the rotor to enter into a state of whirl or whip. However, once this state has been entered and shaft speed is reduced, the whirl or whip will persist to a speed lower than the one at which it commenced. Tondl (53) and Pinkus (16) have observed this phenomenon.

Figure 6.13, 6.14 and 6.15 depict the change in measured threshold speed N_T(R.P.M.) with bearing radial clearance c(in), for $\alpha=30^o$, 60^o and 90^o respectively. These figures also show the end of instability on rundown (hysteresis effect). It is generally observed that increasing bearing clearance reduces the stability threshold, and produces a more pronounced hysteresis effect.

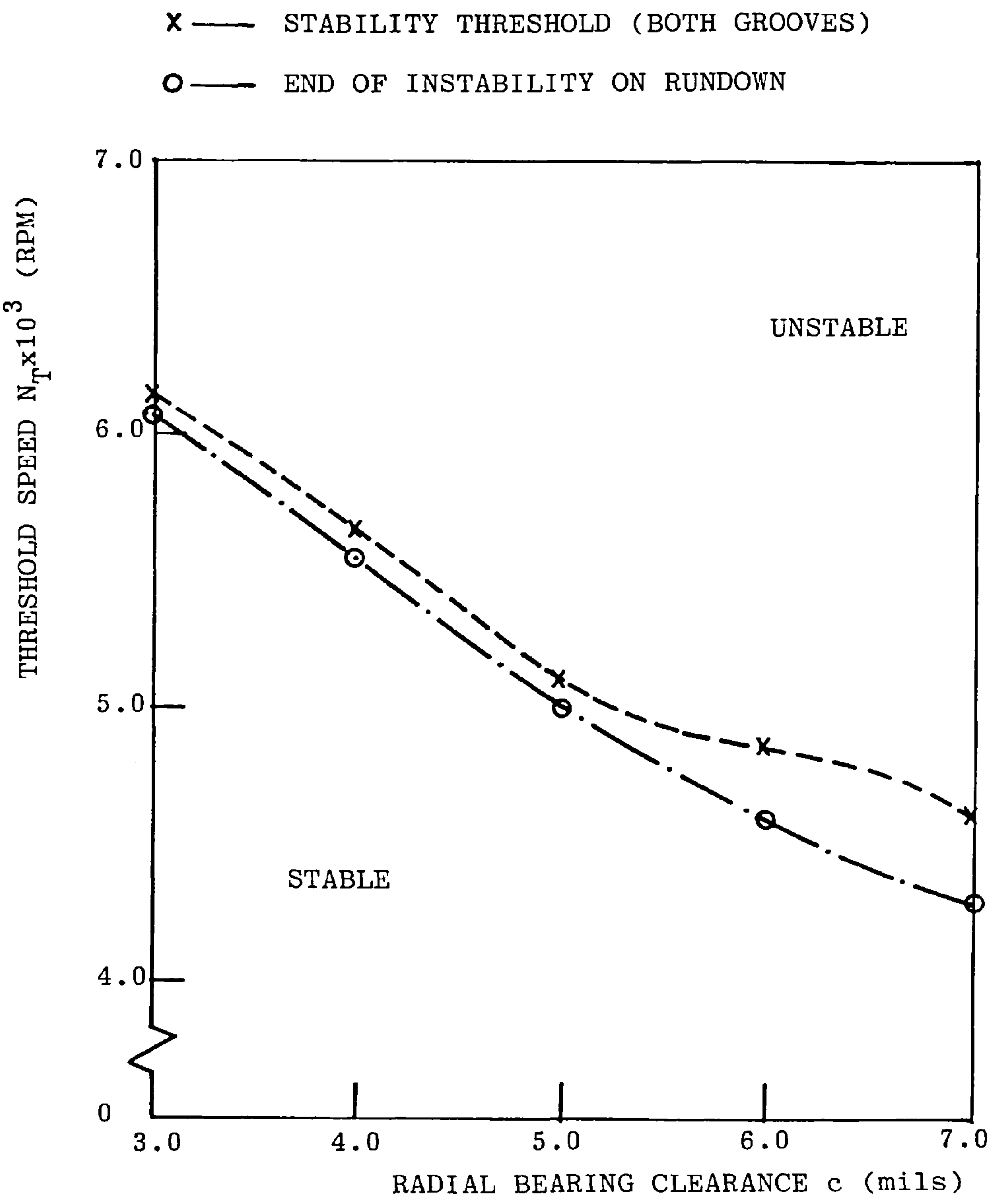

Figure 6.13 Threshold Speed Versus Bearing Clearance for α=30°

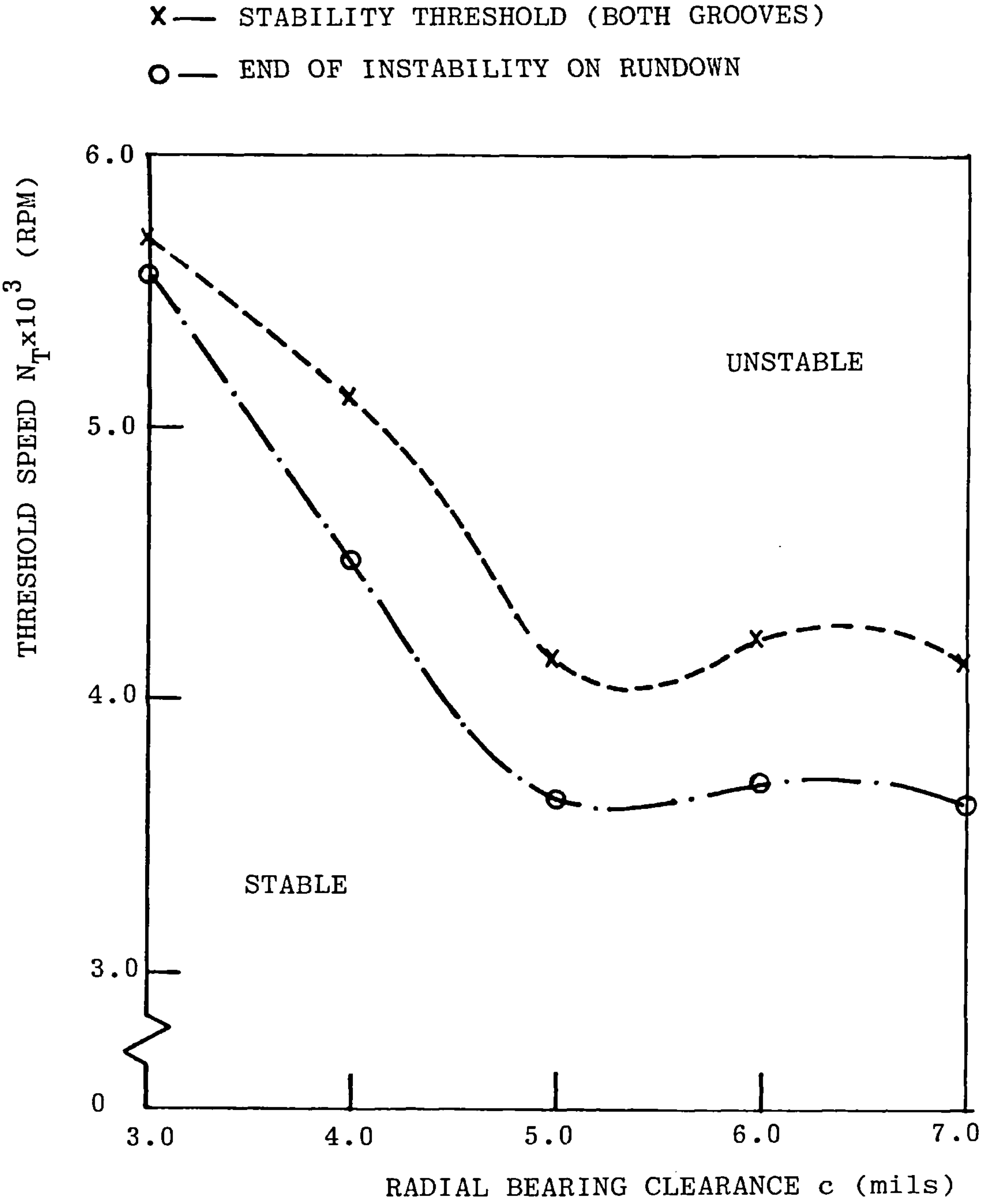

Figure 6.14 Threshold Speed Versus Bearing Clearance for α=60°

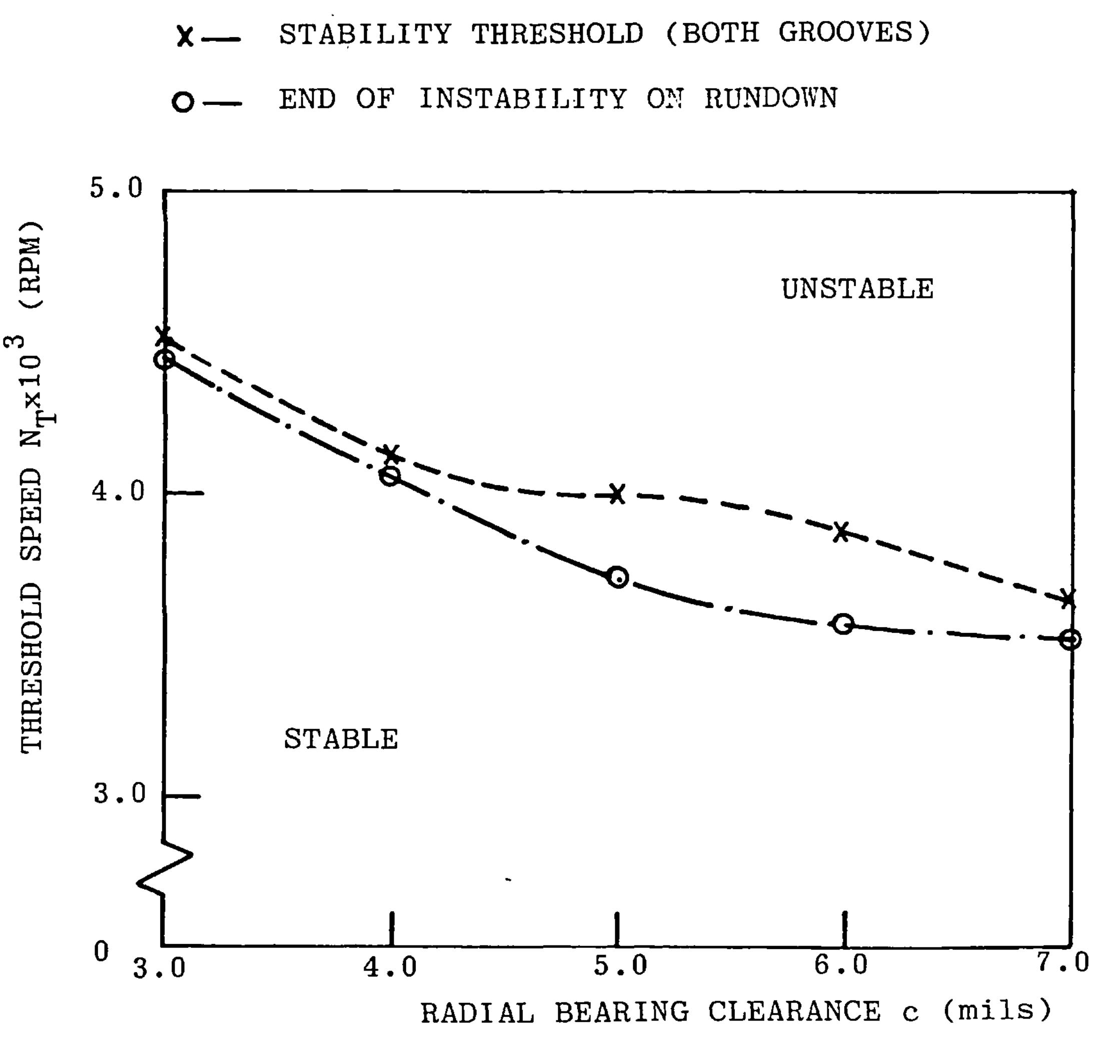

Figure 6.15 Threshold Speed Versus Bearing Clearance for $\alpha=90°$

Figure 6.16 shows the variation in measured N_T against c, for $\alpha=30^o$, 60^o and 90^o. This enables a direct comparison of groove angle effect to be made. It is observed that increase in groove angle reduces the stability threshold. Akkok (51) and Akkok and Ettles (50) have observed the same trends from rigid rotor investigations.

In Figure 6.17 the change in measured threshold frequency f_T(CPM) against radial clearance c(in) is shown for $\alpha=30^o$, 60^o and 90^o. Increase in groove angle lowers threshold frequency, and is particularly noticeable for $\alpha=90^o$. f_T also reduces in value as c is increased. From comparing these results with those of Figure 5.11 it is observed that the rotor is in a state of oil-whip for c=0.003in and $\alpha=30^o$ and 60^o. Only at these particular values does the threshold frequency correspond to the critical speed of the rotor. At all other values of c and α a state of oil-whirl would arise in which the instability frequency is less than the critical speed.

<u>6.5.3.2 Feed groove position</u>

The tests detailed in this section are similar to those described in Section 6.5.2. The effect of supplying oil to the downstream groove alone was investigated for three groove angles. Figures 6.18, 6.19 and 6.20 depict the variation in measured threshold speed N_T with clearance c for groove angles $\alpha=30^o$, 60^o and 90^o. Also shown for reference are the stability thresholds obtained using both

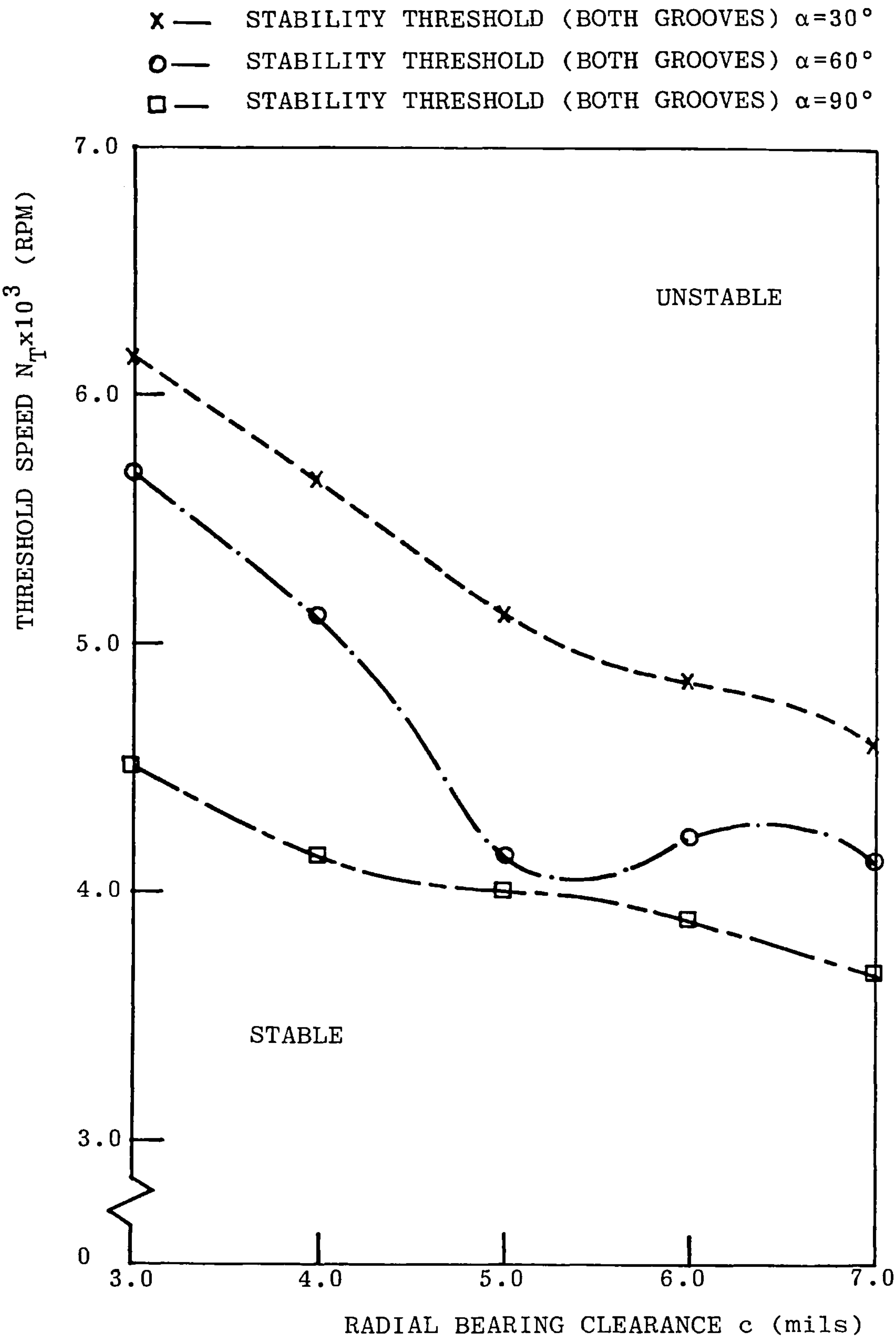

Figure 6.16 Comparison of Stability Threshold for Three Groove Angle

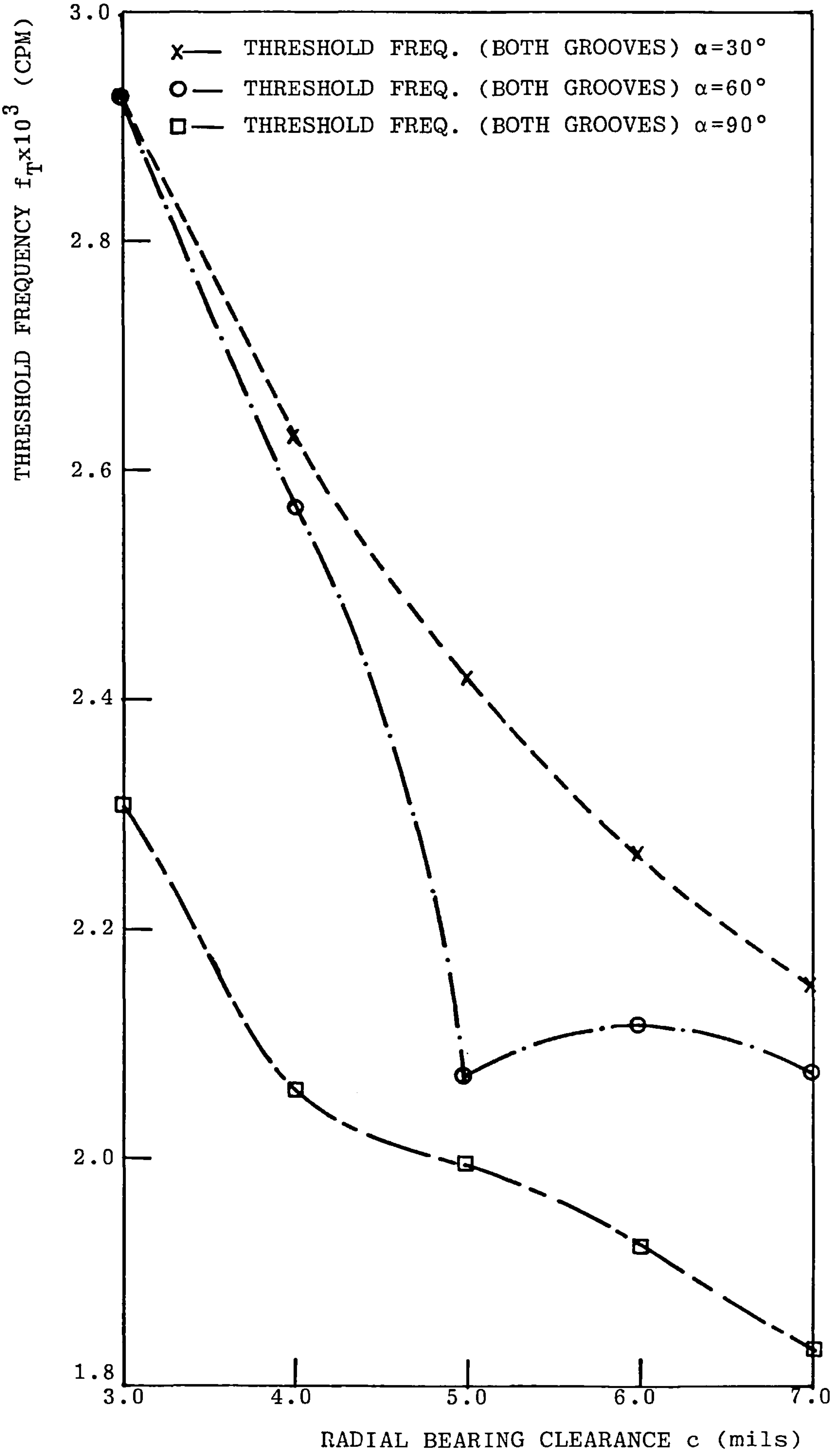

Figure 6.17 Comparison of Threshold Frequency for Three Groove Angle

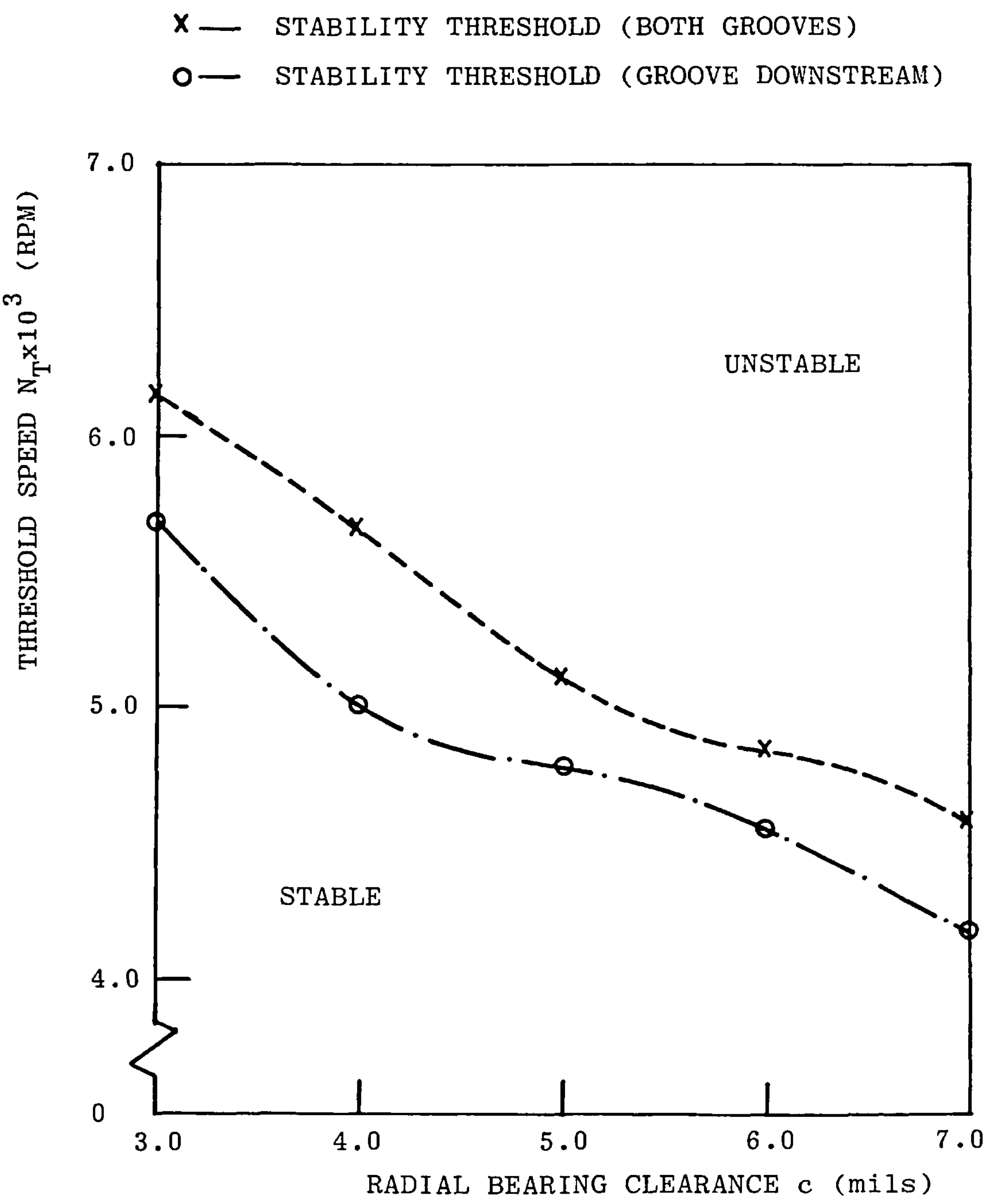

Figure 6.18 Comparison of Stability Threshold for α=30°

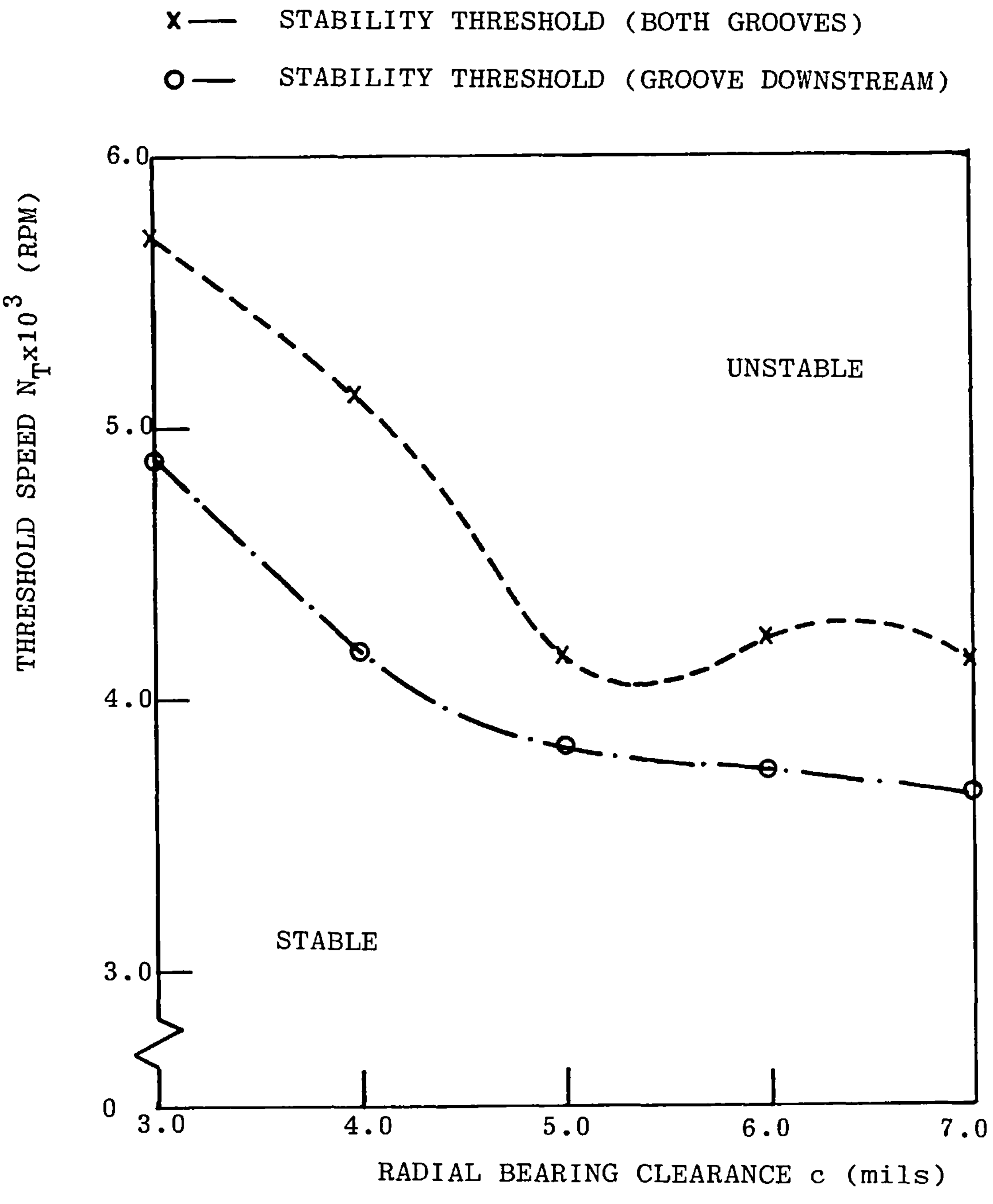

Figure 6.19 Comparison of Stability Threshold for α=60°

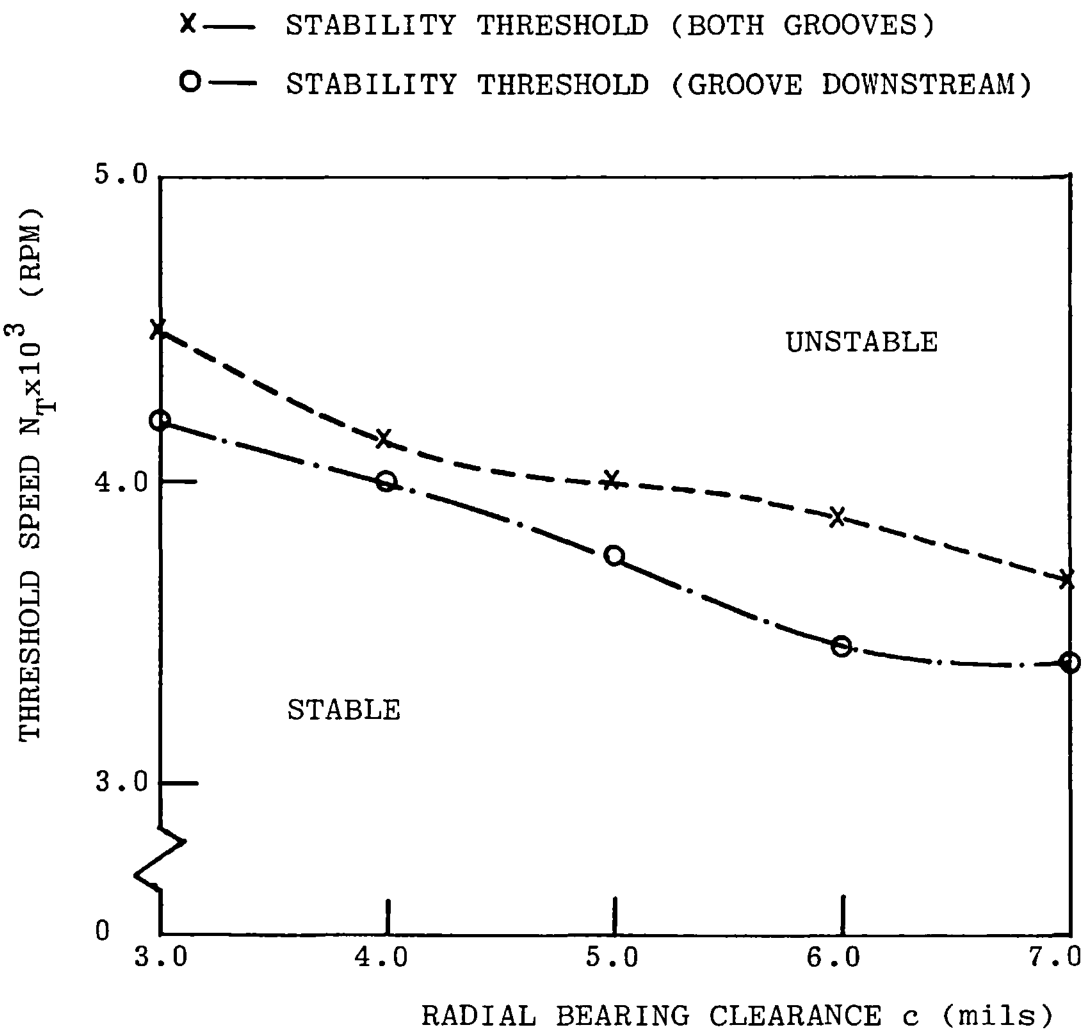

Figure 6.20 Comparison of Stability Threshold for α=90°

grooves. For all values of α, use of the downstream groove alone yeilds a lower threshold than that obtained using both grooves.

In Figure 6.21 the effect of downstrem groove threshold against clearance for the same three groove angles are shown for comparison. Thresholds for $\alpha=60^{\circ}$ and 90° are close together and an appreciable amount lower than the threshold for $\alpha=30^{\circ}$. This would seem to indicate that an increase in the downstream groove angle tends to suppress cavitation and helps promote instability.

6.5.3.3 Theoretical predictions

Figures 6.22, 6.23 and 6.24 depict the computed non-dimensional threshold speed ω^*_T versus eccentricity ε, for the test rotor-bearing system when employing groove angles $\alpha=30^{\circ}$, 60° and 90° respectively. The bearing radial clearance c=0.003in and the non-dimensional feed pressure $\gamma=0$. The values of ω^*_T corresponding to the case where the model of the system has zero gyroscopic moment are also plotted. Included in the figures for reference are values of ω^*_T for a point mass rigid rotor mounted in two identical bearings having the same dimensions as the test bearing. The threshold of this latter sytem was determined using the method described in Section 6.5.1.

Several conclusions can be drawn from Figures 6.22, 6.23 and 6.24. The stability threshold of the rigid rotor is

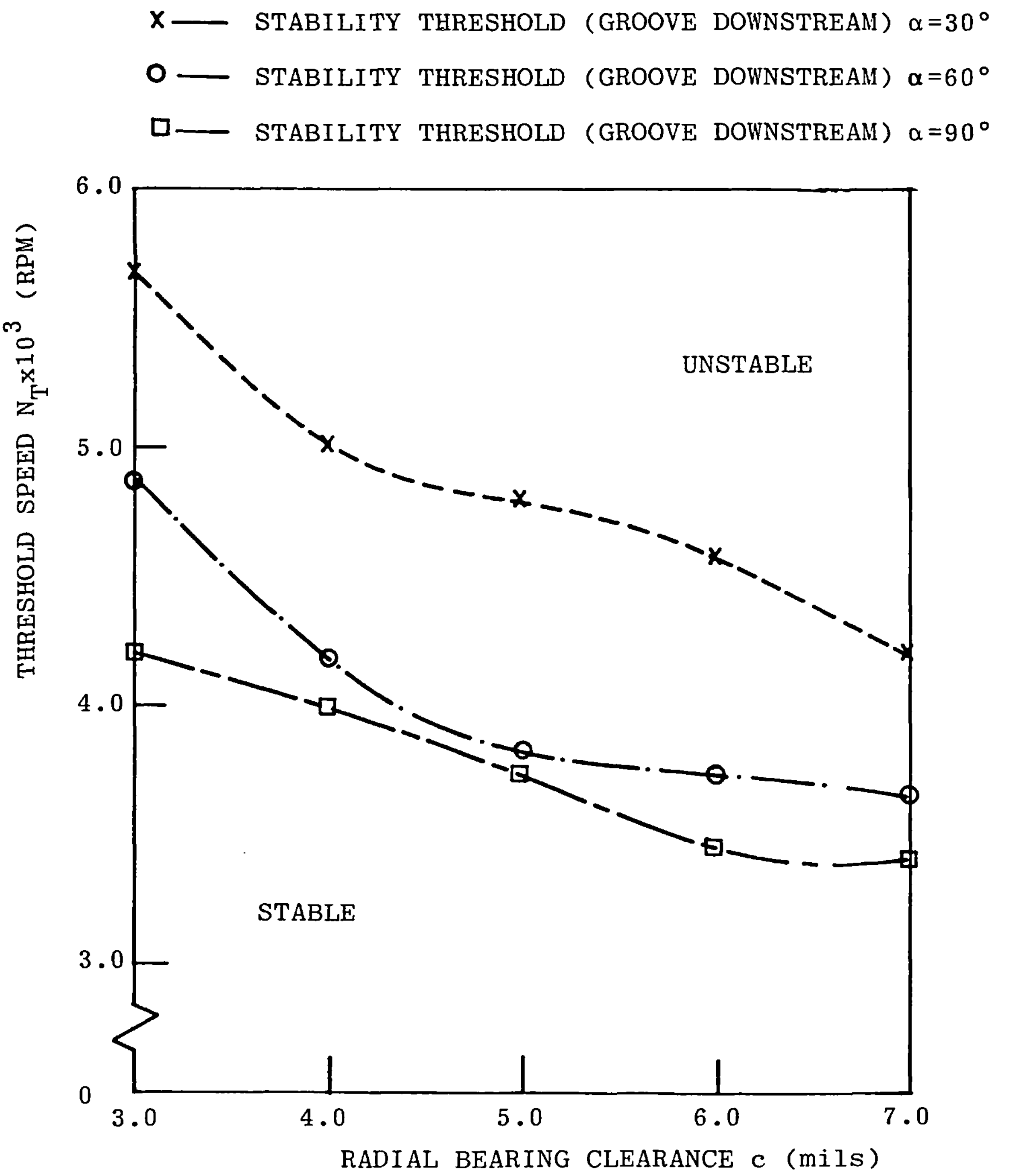

Figure 6.21 Comparison of Stability Threshold for Three Groove Angle

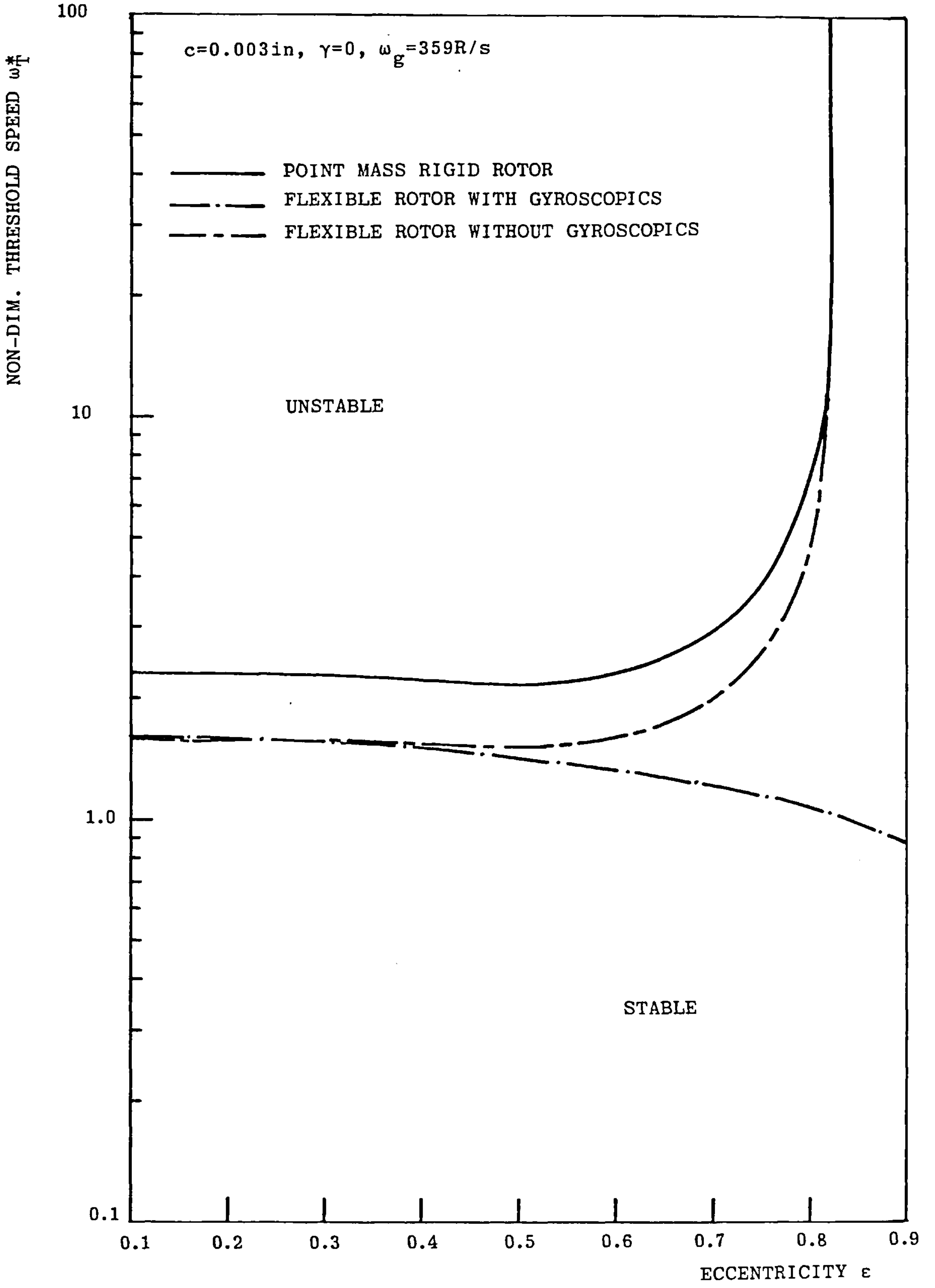

Figure 6.22 Stability Threshold Versus Eccentricity for $\alpha = 30°$

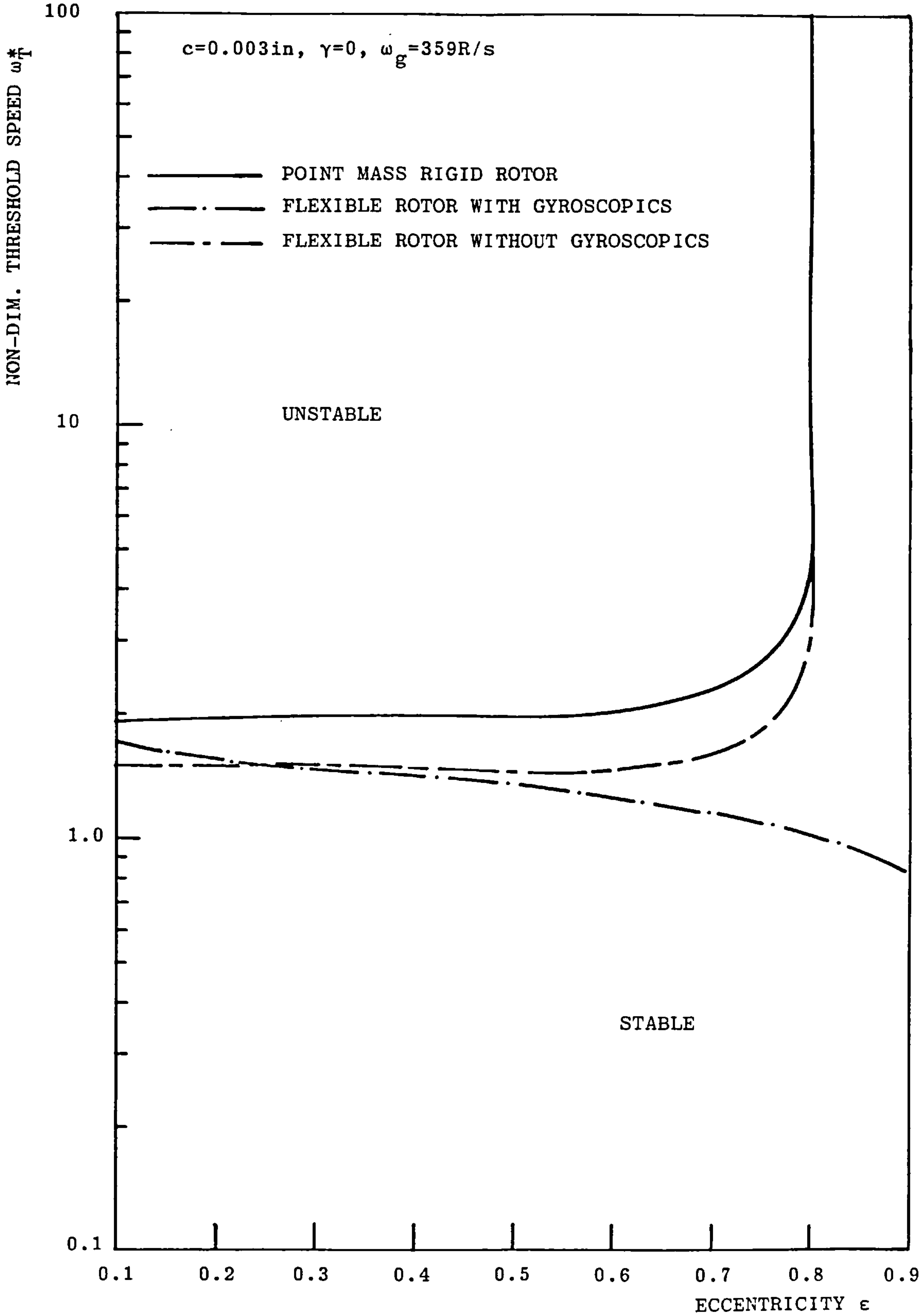

Figure 6.23 Stability Threshold Versus Eccentricity for $\alpha = 60°$

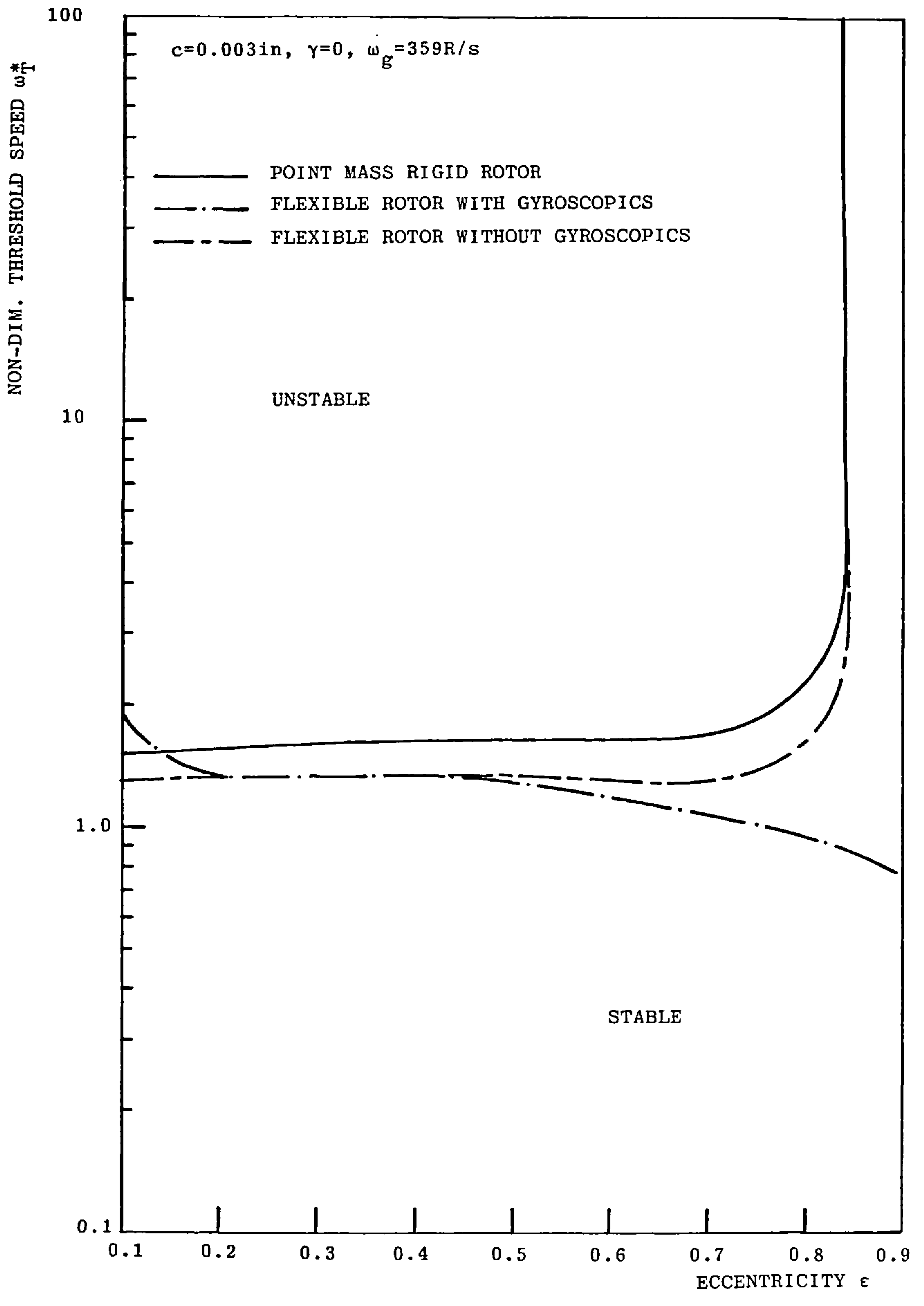

Figure 6.24 Stability Threshold Versus Eccentricity for $\alpha = 90°$

higher than that of the flexible rotor, with and without gyroscopic effects. At high eccentricity ($\varepsilon \geqslant 0.8$) both the rigid rotor and flexible rotor without gyroscopic effects have a infinite stability threshold at infinite speed. At low values of ε, the thresholds for the flexible rotor with and without gyroscopic effects are very similar and, thus, gyroscopic effects are not important. However, for higher values of ε, Figures 6.22, 6.23 and 6.24 indicate that gyroscopic effects can have an influence on the stability of the system. For the rigid rotor and flexible rotor without gyroscopic effects, the change in threshold speed over a large range of eccentricity is quite small. As the groove angle increases the stability threshold for the rigid rotor approaches that of the flexible rotor.

Figure 6.25 is plotted to provide a direct comparison of the effect of groove angle on the threshold speed of the flexible rotor with gyroscopic effects. Reference to this figure indicates that over almost the entire eccentricity range, increasing groove angle produces a destabilising effect. This is in agreement with the experimental findings discussed in Section 6.5.3.1.

Table 6.1 lists the theoretical and experimental results along with their percentage difference for c=0.003in and groove angles of 30^{o}, 60^{o} and 90^{o}. The experimental values were obtained for a γ value of 0.22 which corresponds to P_f=2psi (13.8KPa). Theoretical threshold speeds are given

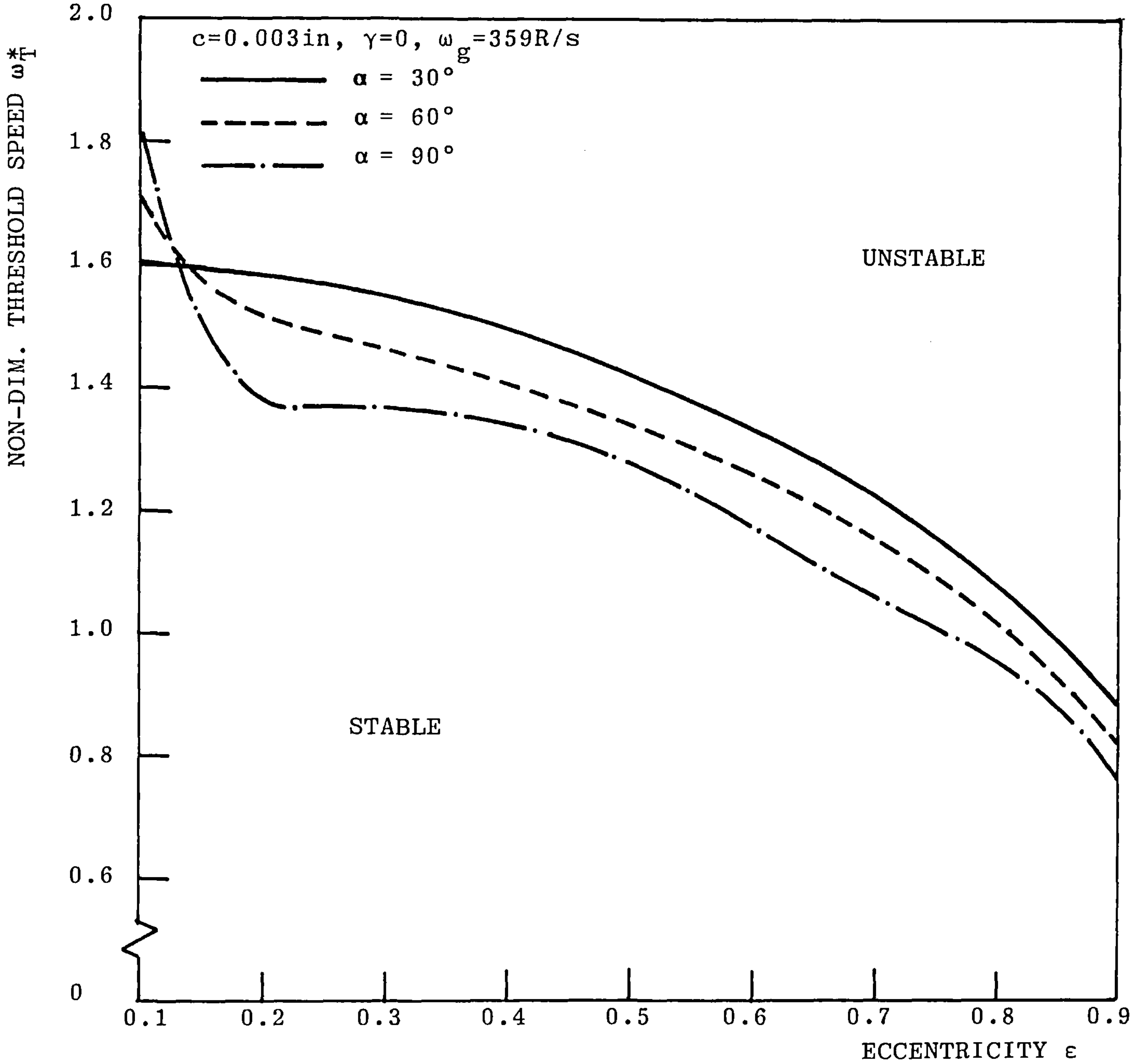

Figure 6.25 Comparison of Stability Threshold for Three Groove Angles

GROOVE ANGLE α°	EXPT. $\omega^{*}T$	THEOR. $\omega^{*}T$ g.e.$\neq$0	% DIFF. EXPT-THEOR/ THEOR	THEOR. $\omega^{*}T$ g.e.=0	% DIFF. EXPT-THEOR/ THEOR
30	1.79	1.40	27.8	1.52	17.8
60	1.66	1.28	29.7	1.48	12.2
90	1.32	1.22	8.2	1.33	0.7

Table 6.1 Gyroscopic Effect on Instability Threshold for Three Groove Angles

both for cases which include gyroscopic effects (g.e.) and those which do not.

The theoretical cases with zero gyroscopic effects show better agreement with the experimental results. In Section 6.5.1 the possibility of reduced experimental gyroscopic effects were discussed. Allowing for the possibility that the flywheel could have skewed by a small amount, it is thought likely from the test rotor design that some gyroscopic effect was present.

Figure 6.26 depicts the computed mode shape at the instability threshold for $\alpha=30^{\circ}$, $\gamma=0$ and c=0.003in. It shows the peak to peak amplitude in inches in the x-direction plotted against distance along the shaft in inches.

The mode shape was calculated using the method described in Section 3.4.4, in which one of the non-zero state variables at the left hand end of the rotor was assigned an arbitrary value. It is then possible to solve for the remaining state variables. Intermediate state vector variables along the length of the rotor-bearing system were then obtained by matrix multiplication. By measuring the non-synchronous amplitdue at the threshold, and at a particular axial position on the rotor it is possible to assign values to all other stations along the computed mode shape.

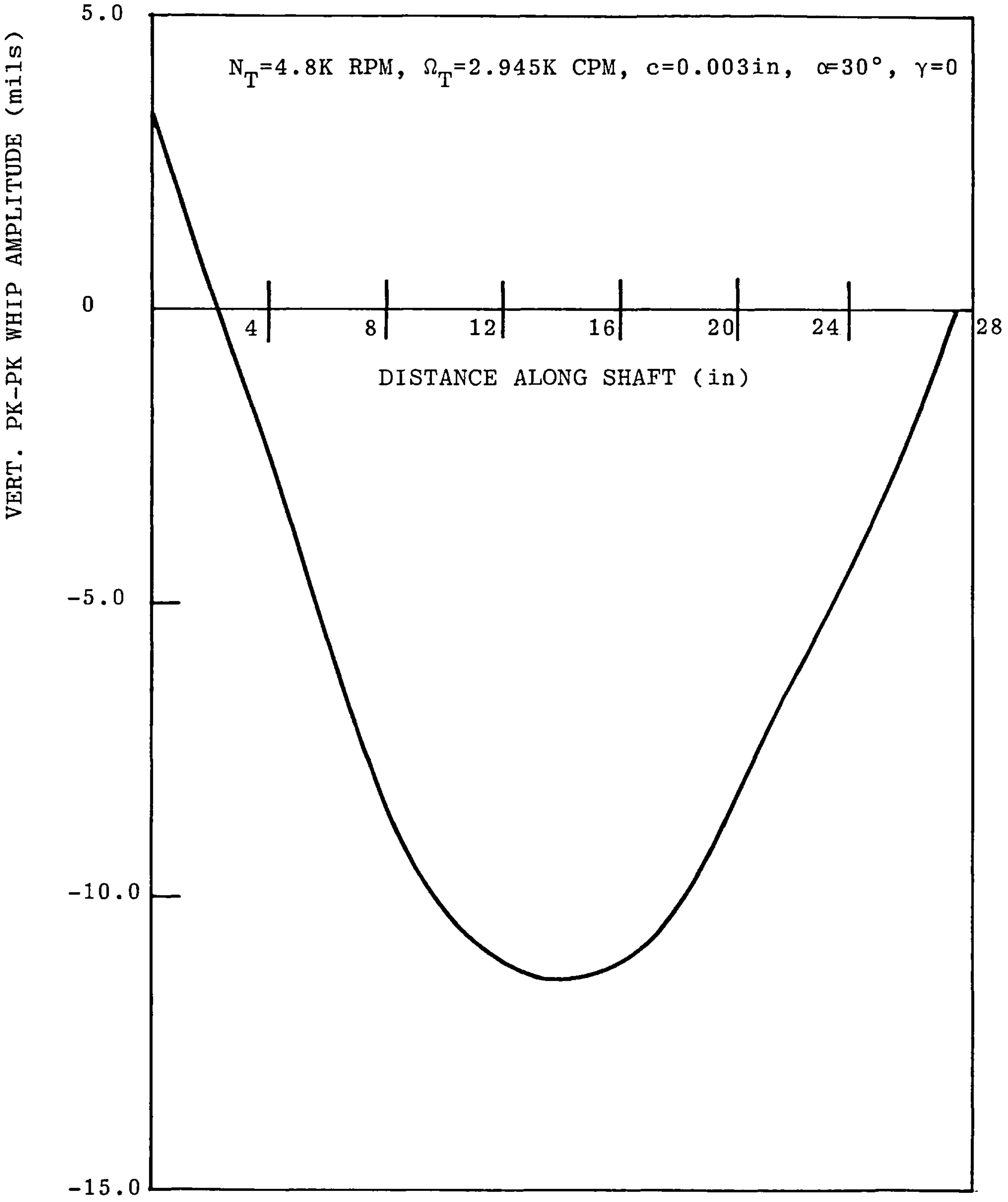

Figure 6.26 Mode Shape at Stability Threshold

The mode shape is similar to the critical speed mode shape of Figure 5.14. This is because the frequency of Figure 5.26 is almost identical to the critical speed of Figure 5.14. Figure 6.26 thus represents the whip mode shape in which the critical speed resonance of the rotor is excited.

<u>6.5.4 Pedestal Flexibility</u>

This section deals with experimental and theoretical investigations of the effects of mounting the test bearing on a flexible pedestal without damping, on stability of the test rotor-bearing system. The method of obtaining support flexibility is described in Section 4.3.4. In all the tests conducted, the feed pressure P_f was set at 2psi (13.8KPa) and the oil feed groove angle was 30^o.

Figures 2.27, 2.28 and 2.29 depict the change in measured non-dimensional threshold speed ω^*_T with non-dimensional pedestal stiffness $k_{p,x}/k_R$. $k_{p,x}$ is the stiffness of the support of the x-direction and k_R is the stiffness of the rotor which remains constant. The method of non-dimensionalising the support stiffness is given in Appendix H. Figures 2.27, 2.28 and 2.29 correspond to radial clearances c of 0.003in, 0.004in and 0.005in respectively, and they show the end of instability on rundown.

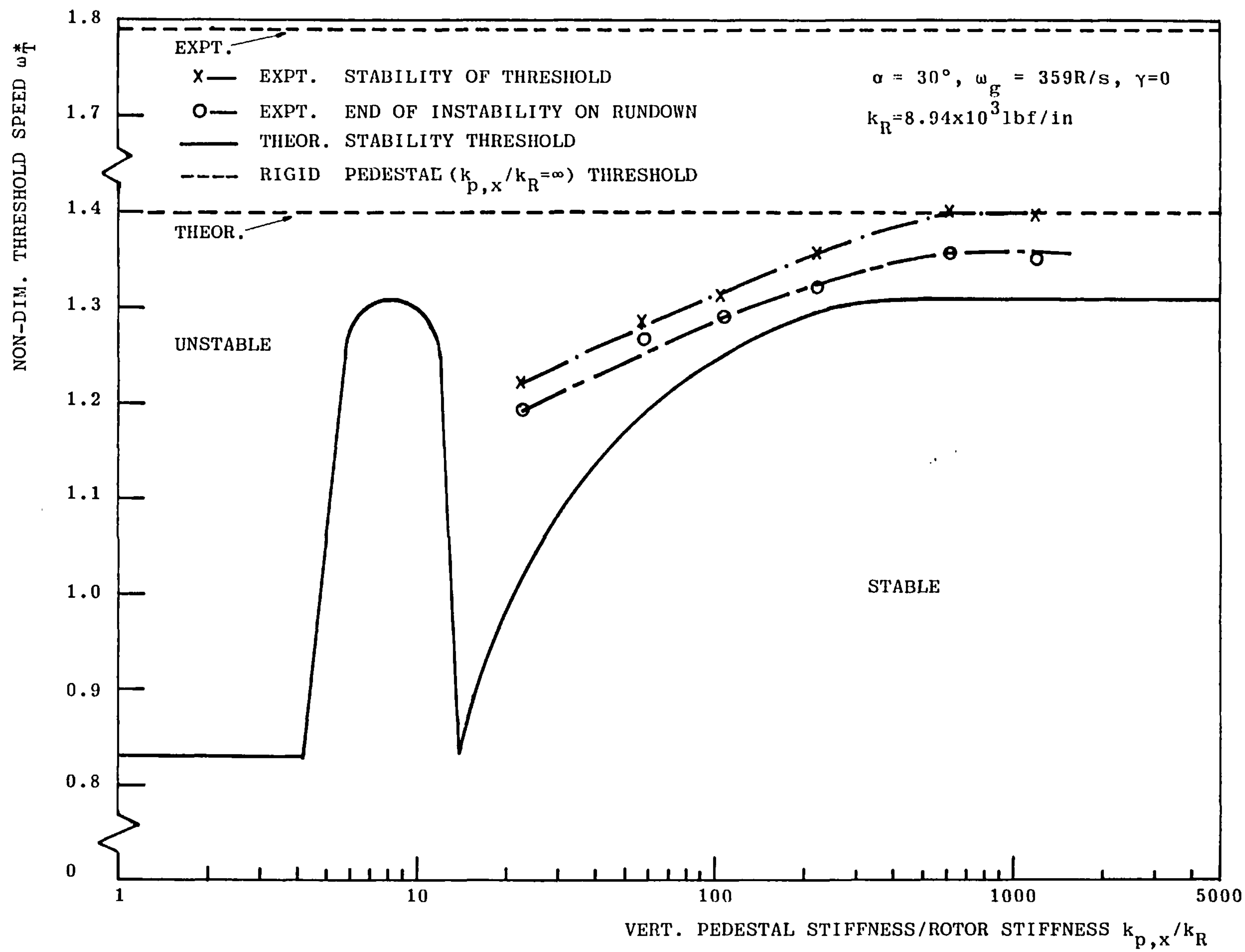

Figure 6.27 Stability Threshold Versus Vertical Pedestal Stiffness Ratio for c=0.003in

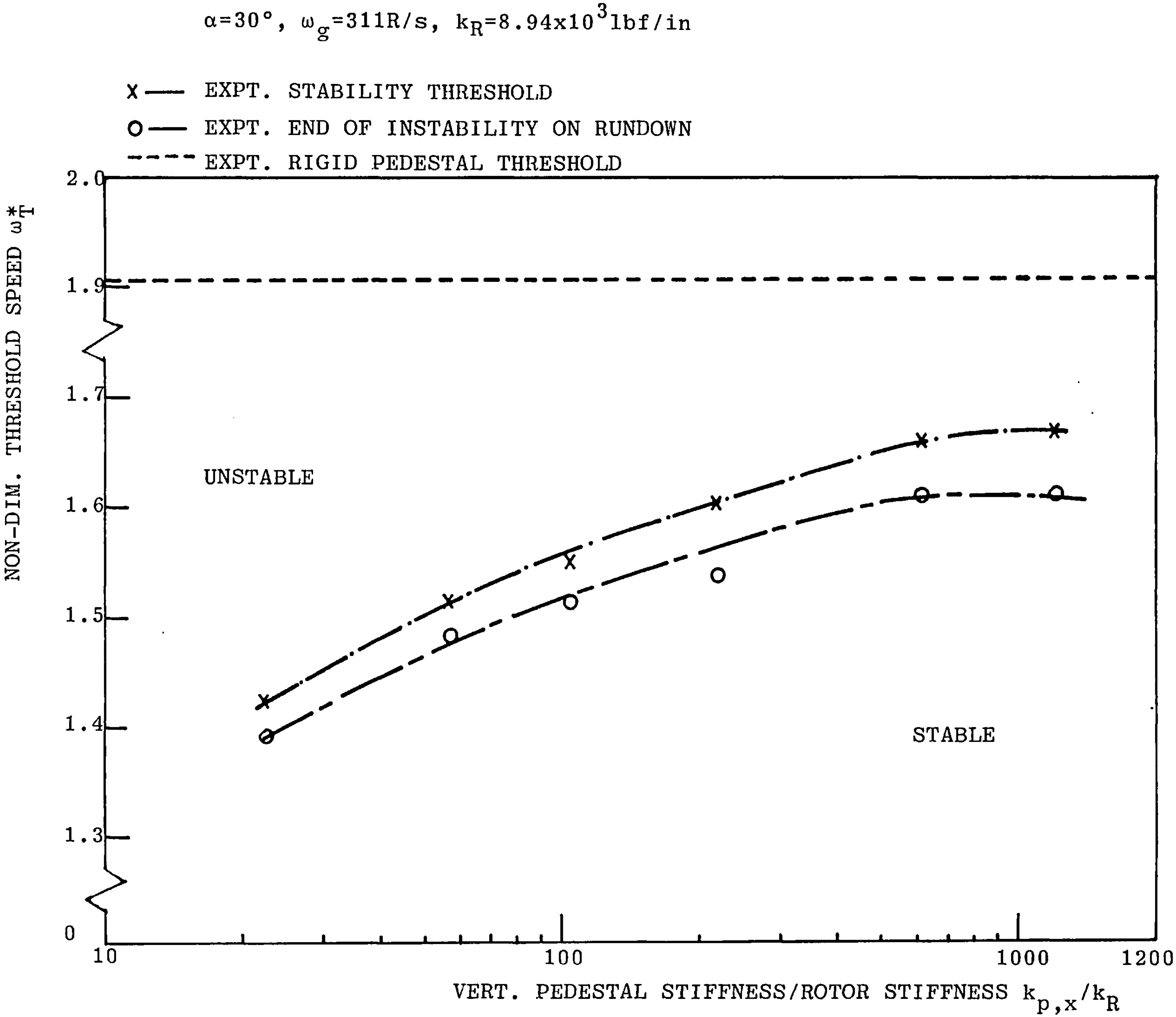

Figure 6.28 Stability Threshold Versus Vertical Pedestal Stiffness Ratio for c=0.004in

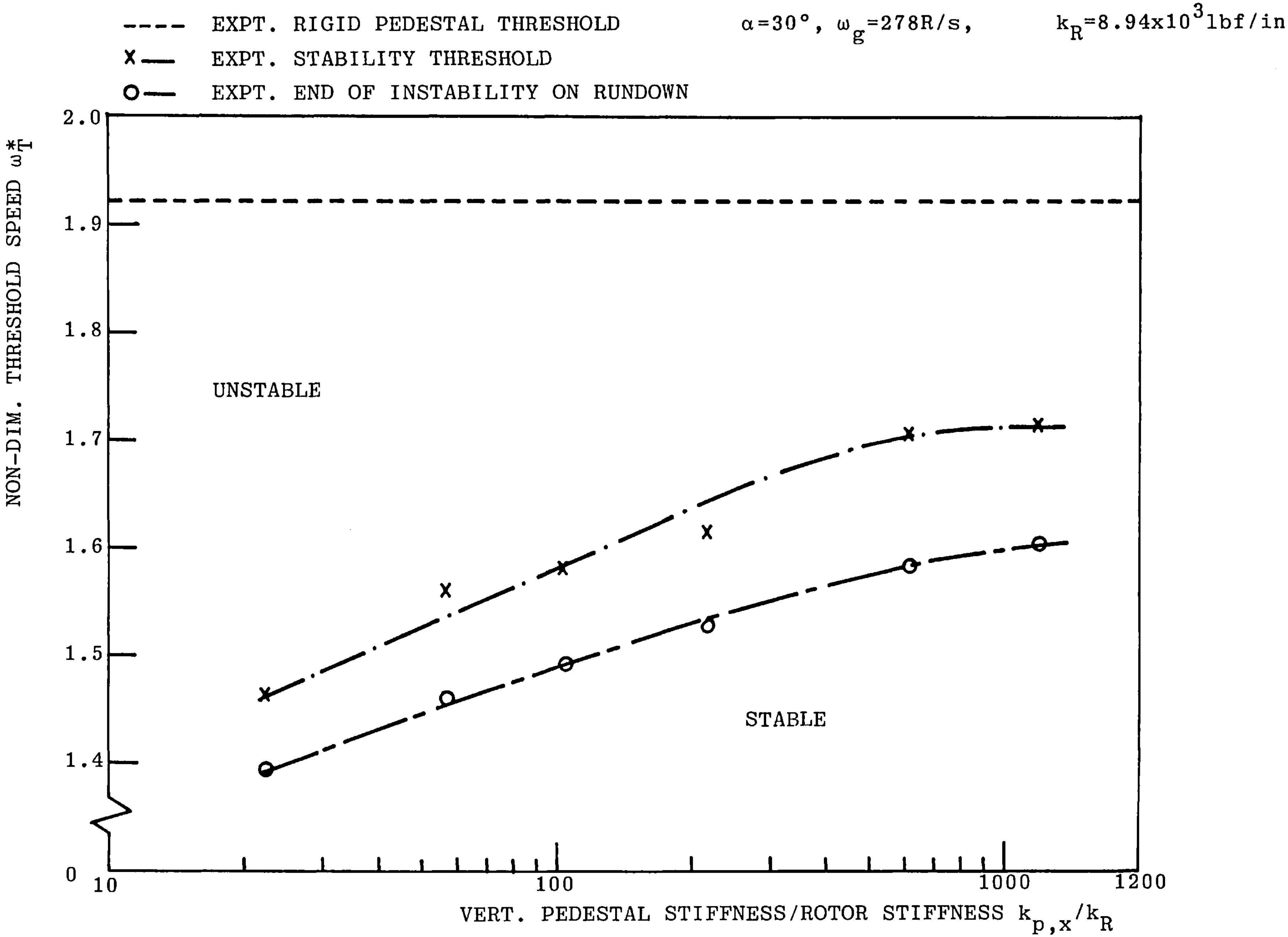

Figure 6.29 Stability Threshold Versus Vertical Pedestal Stiffness Ratio for c=0.005in

In Figure 6.27 the computed values of ω^*_T are plotted against $k_{p,x}/k_R$ are shown for c=0.003in, $\alpha=30^o$ and $\gamma=0$. Also shown for reference are the theoretical and experimental thresholds on rigid supports.

For all three values of clearance it is seen that the introduction of support flexibility lowers the stability threshold. Newkirk (5) in his pioneering experimental investigations of 1925 observed similar effects for fluid-film bearings on flexible supports. To limit the bearing housing vibration to an acceptable level, particularly when running through the critical speed, pedestal flexibility was not reduced below $k_{p,x}/k_R=22.5$.

From the theoretical results of Figure 6.27 it is interesting to note that at $k_{p,x}/k_R=14$, the stability threholds obtains a minimum. Subsequent reduction in $k_{p,x}/k_R$ below this value results in a sudden increase in ω^*_T to the maximum value obtained over the range $k_{p,x}/k_R=1$ to 5000. AT $k_{p,x}/k_R=4.2$, ω^*_T again obtains a minimum, with an increase of $k_{p,x}/k_R$ above this value again resulting in a sudden increase in ω^*_T. From $k_{p,x}/k_R=4.2$ to 1, the value of ω^*_T remains constant.

This minimum threshold value corresponds to the system critical speed of the rotor. That is, the critical speed of the rotor mounted in its journal bearing and supported on the flexible pedestal. The corresponding theoretical threshold ratio is $\Omega^*_T/\omega^*_T=1$.

Thus, in general, the rotor stability threshold is always equal to or greater than the system critical speed, and is a function of $k_{p,x}/k_R$. The introduction of support flexibility without damping will therefore reduce the system critical speed (Section 5.5) and the instability threshold. Lund (32) reached similar conclusions from a theoretical analysis of a flexible rotor mounted in gas bearings on flexible undamped supports. Gunter (31) studying theoretically the Jeffcott rotor with rigid bearings on undamped flexible supports also observed comparable trends. His rotor model was subjected to whirl instability arising from internal friction.

It can be observed from Figure 6.27 that good agreement is obtained between theory and experiment. The agreement in most cases is better than that obtained between similar experiment and theory for a rigid pedestal. A possible explanation is that with a flexible pedestal the bearing was allowed to align with the shaft, thus, reducing the misalignment present in the system.

Figure 6.30 is a plot of measured threshold speed N_T(RPM) against bearing radial clearance c(in) for the six values of support flexibility considered. Also shown is the threshold speed for rigid support case. It is seen that for a flexible support, an increase in clearance results in a gradual reduction in stability threshold. An increase in support flexibility also produces gradual lowering of the

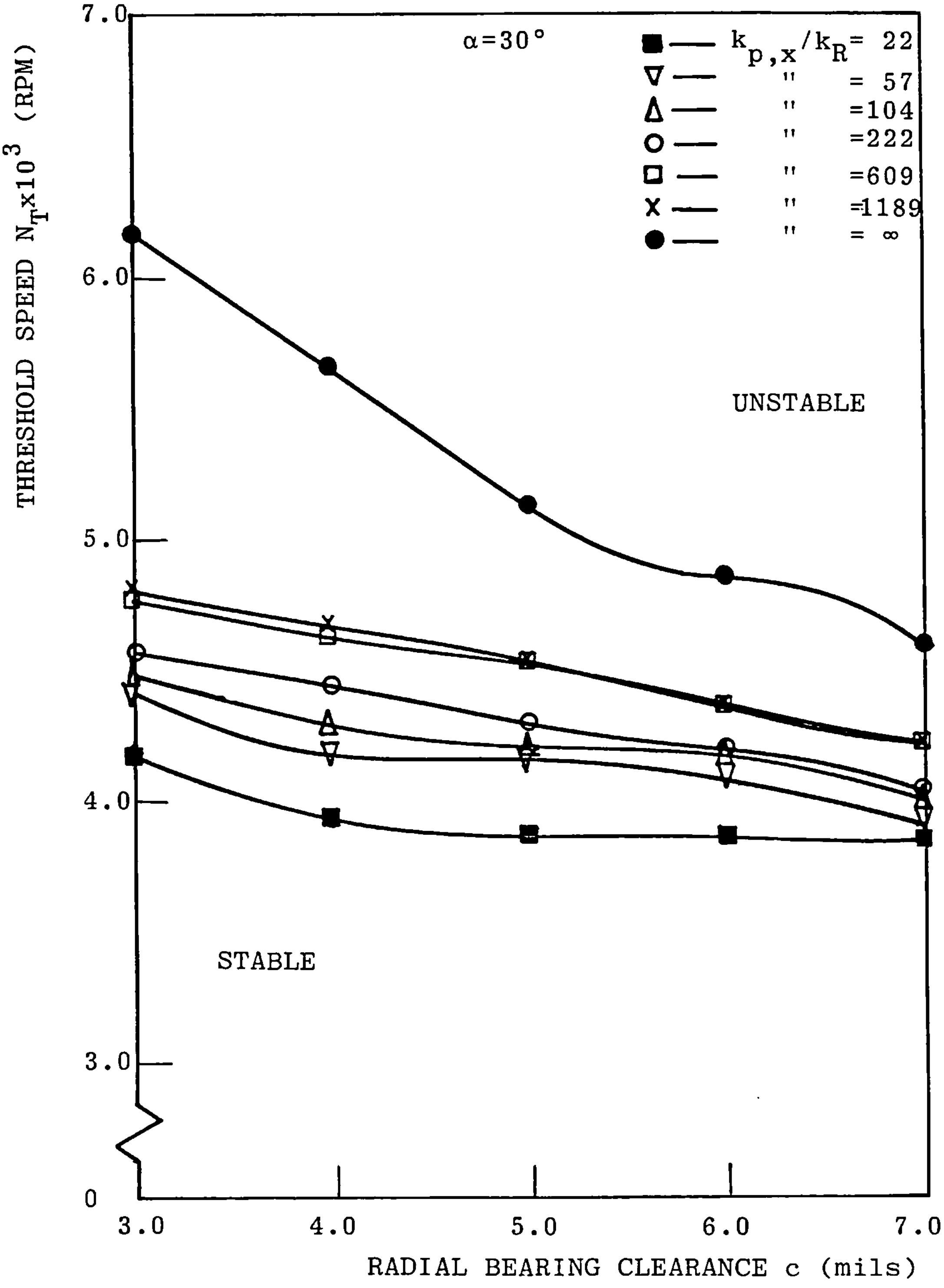

Figure 6.30 Comparison of Threshold Speeds for Different Pedestal Flexibilities

threshold. For the rigid support case ($k_{p,x}/k_R=\infty$) a more pronounced reduction in threshold speed occurs as the clearance is increased. There is also marked decrease in N_T from the rigid support to the first flexible support, that is, $k_{p,x}/k_R=1189$. This would appear to substantiate the idea that misalignment was reduced for the flexible support case, particularly as misalignment would be more pronounced at smaller clearances.

Figure 6.31 shows computed values of non-dimensional threshold speed ω^*_T plotted against non-dimensional support mass ratio M_B/M_R, where M_B is the support mass and M_R is the mass of the rotor which is constant. The clearance c is 0.003in, the groove angle $\alpha=30^o$ and the non-dimensional feed pressure γ is 0. The stability threshold for a rigid support is also shown for reference. Three values of $k_{p,x}/k_R$ are considered and for the test rotor M_B/M_R was fixed at 0.63.

From Figure 6.31, it can be seen that an increase in support mass results in a reduction of the stability threshold. At particular values of M_B/M_R, the threshold reaches a minimum value. Subsequent increase in M_B has no effect on the threshold. This minimum threshold value corresponds to the critical speed of the system including support mass and stiffness. Over the range in which computations were performed, varying the support mass produced no signficant effect on critical speed.

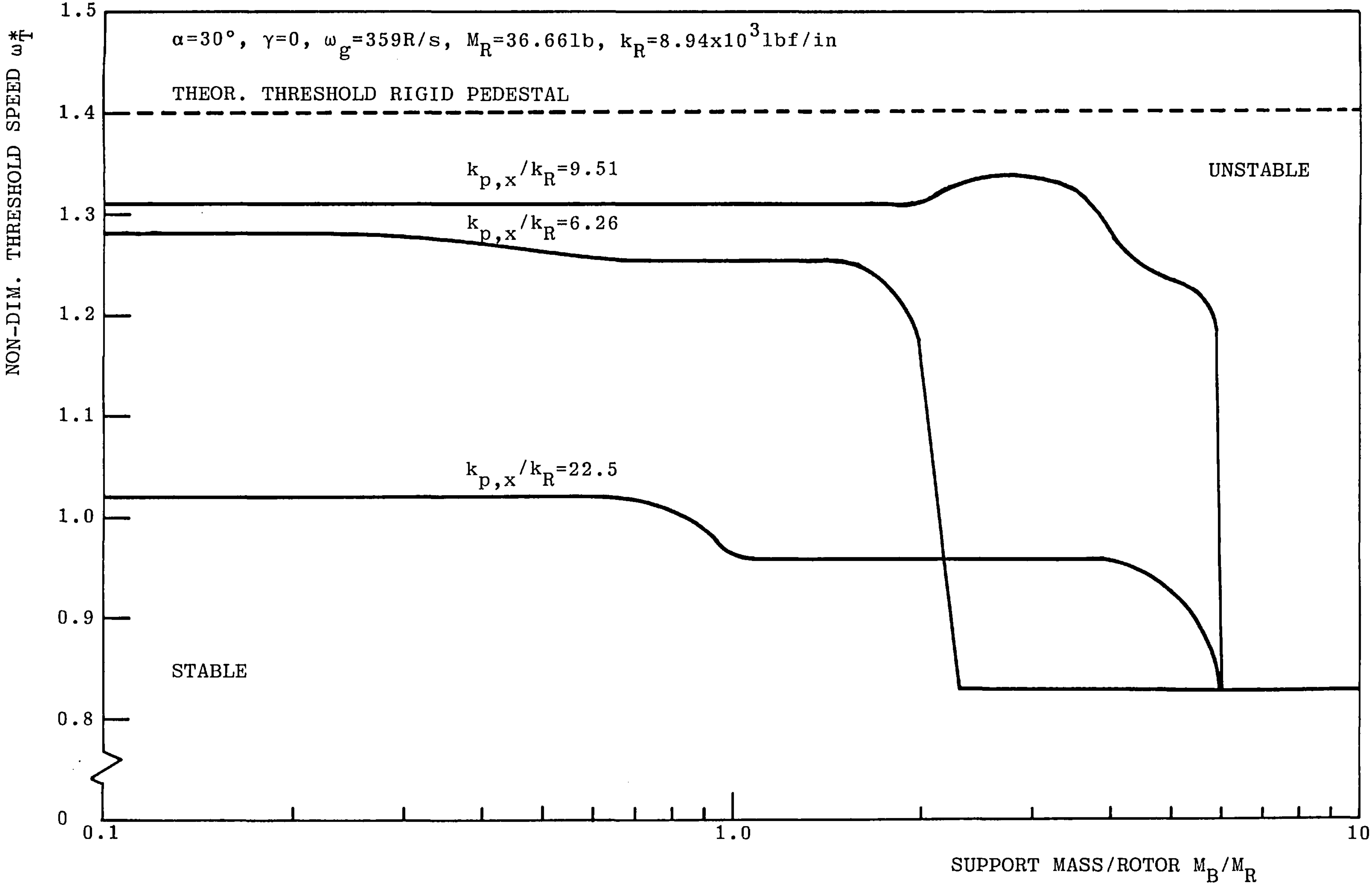

Figure 6.31 Effect of Support Mass Ratio on Threshold Speed for c=0.003in

Thus, an increase in support mass lowers the stability threshold, and the threshold is always equal to or greater than the system critical speed. Gunter (31) made similar deductions from his model of the Jeffcott rotor supported on rigid bearings with flexible supports.

6.6 SOME FURTHER THEORETICAL PREDICTIONS

This section describes a number of additional theoretical investigations on the test rotor-bearing system for which no comparison was made experimentally.

6.6.1 Elliptical Bearing

Figure 6.32 shows the non-dimensional threshold speed ω^*_T plotted against eccentricity ε for an elliptical or two-lobe bearing. The bearing had an L/D=1/2, groove angle $\alpha=30^o$, a clearance c=0.003in and a non-dimensional feed pressure $\gamma=0$. The preload $\Delta=0.6$, where $\Delta=d/c$ and d is the offset between bearing centres. The threshold for the model of the flexible rotor without gyroscopic effects, and the threshold of a point mass rigid rotor are also depicted in the figure for comparison.

Figure 6.32 resembles that of Figure 6.22, for a circular bearing with the same bearing parameter values. However, for the two-lobe bearing, the difference between threshold values for the flexible rotor with and without

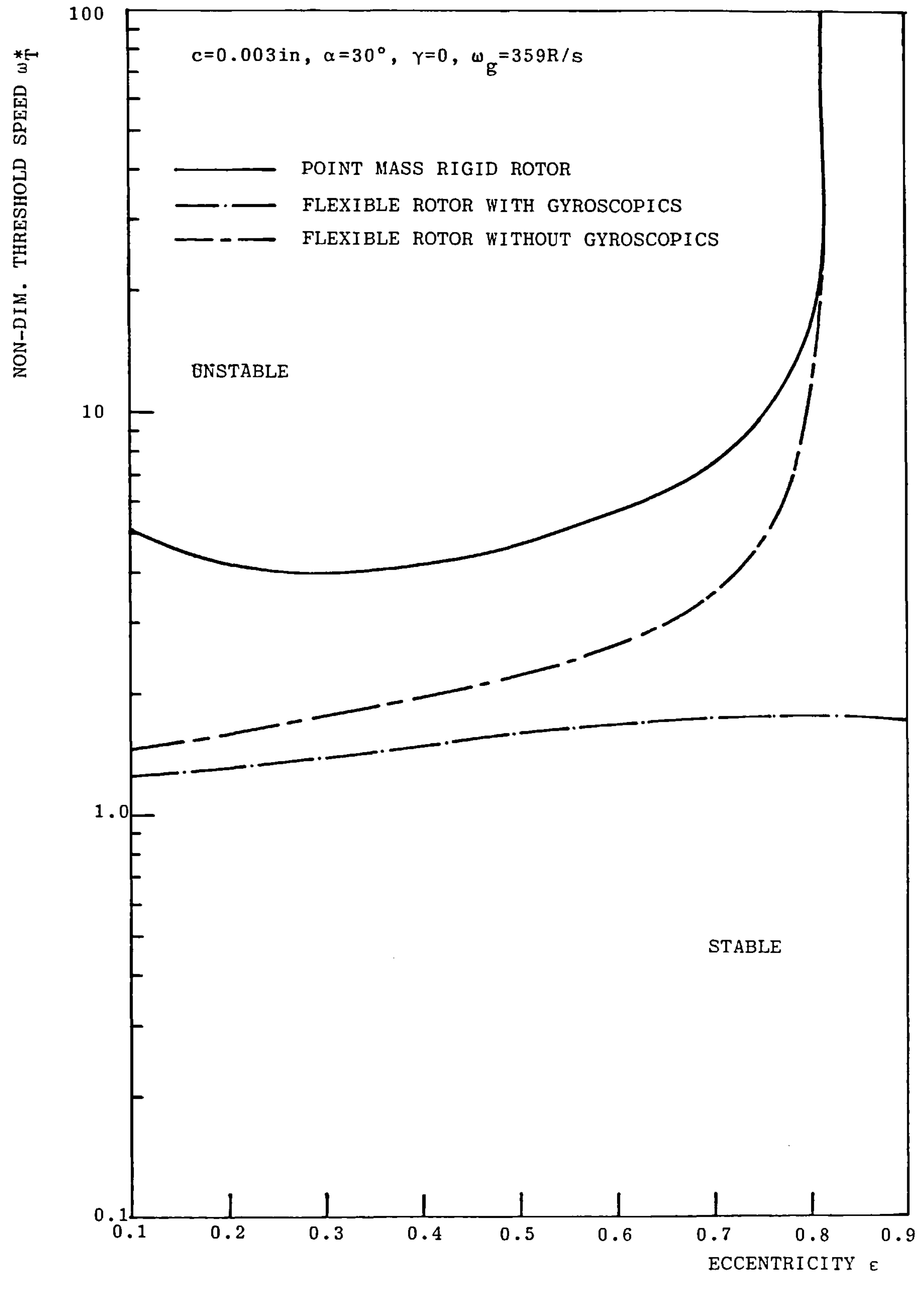

Figure 6.32 Stability Threshold for Elliptical Bearing Δ=0.6

gyroscopic effects and the rigid rotor are considerably more pronounced.

For the case of the flexible rotor with gyroscopic effects, Figure 6.33 compares the stability threshold for the two-lobe and circular bearings, each shown individually in Figures 6.32 and 6.22 respectively. The circular bearing has better stability properties for values of eccentricity up to 0.4. However, beyond $\varepsilon \approx 0.4$, the two-lobe bearing is considerably more stable.

6.2.2 Flexibility of the Rotor

For the test rotor the maximum static deflection δ was fixed at 0.005in. It is possible to define a flexibility parameter for the rotor-bearing system in terms of the ratio of δ/c, where c is the radial clearance of the bearing and is constant.

Figure 6.34 depicts the stability threshold plotted against eccentricity for four values of the flexibility parameter. $\delta/c=1.7$ corresponds to the case of the test rotor-bearing system for c=0.003in, $\alpha=30^{\circ}$ and $\gamma=0$.

It can be observed that an increase in flexibility parameter results in a reduction in the stability threshold over the entire range of eccentricity. This arises because an increase in rotor flexibility lowers its critical speed and, hence, the speed at which instability is encountered.

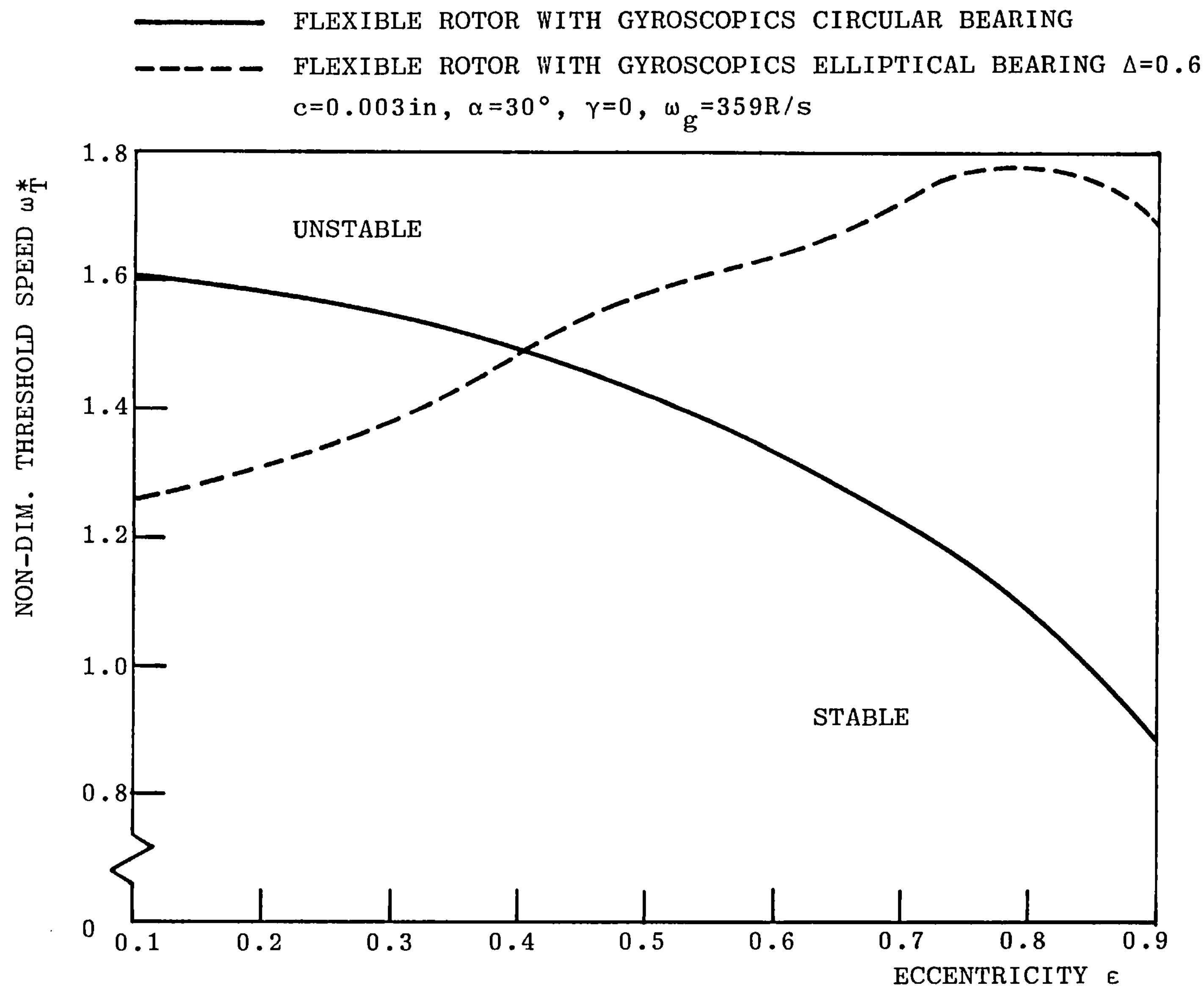

Figure 6.33 Comparison of Threshold Speed for Circular and Elliptical Bearings

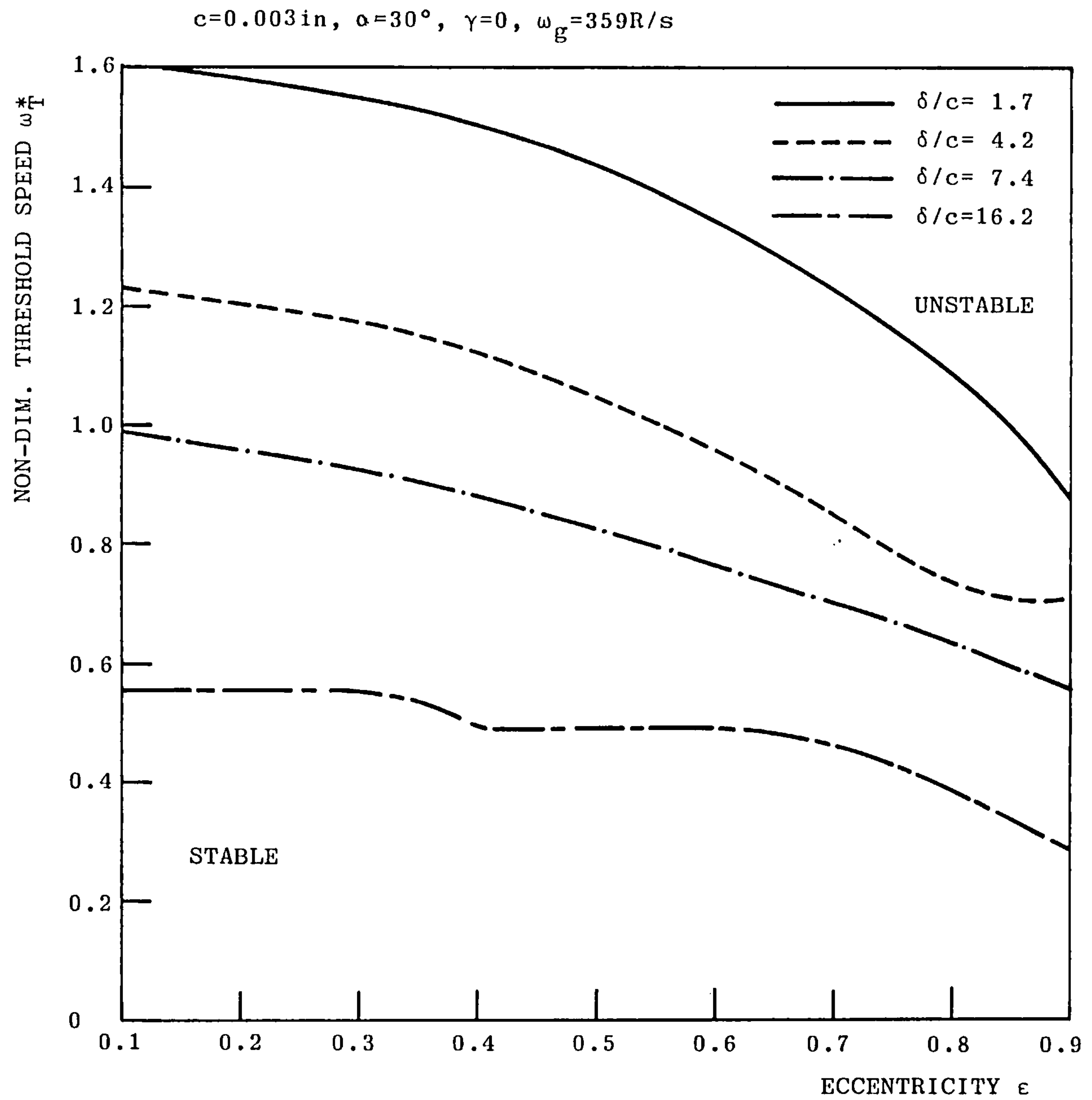

Figure 6.34 Effect of Shaft Flexibility on Threshold Speed

CHAPTER 7

CONCLUSIONS

7.1 MAJOR CONCLUSIONS

The main conclusions of the experimental and theoretical results are now summarised.

(1) The experimental work has confirmed the overall validity of the linear analytical model of the rotor-bearing system. The model predicts damped critical speeds, amplitude responses and instability thresholds. The stability of the system is assessed using a graphical method based on the Leonhard Locus.

(2) Reducing the bearing clearance increases the first critical speed of the rotor. For small clearances (e.g. 0.003in), agreement between theory and experiment is within 3%.

(3) Introducing an undamped flexible support reduces the rotor critical speed. Experimentally determined critical speeds are somewhat lower than those predicted theoretically. With high support stiffness the difference was 11%. The discrepancy rose to 26% with low support stiffness.

(4) Theoretical predictions of amplitude response are considerably lower than the measured values. Several possible explanations are given of which the most likely are; flywheel skew, shaft bending and journal misalignment.

(5) A decrease in bearing clearance has a pronounced stabilising effect. This is partly attributed to an enhancement of misalignment with reduction in clearance. In general, the rotor-bearing system exhibits whirl for large clearances, whereas, the system tends to whip for small clearances.

(6) A hysteresis effect on the instability threshold was observed for rigid as well as flexible supports. This phenomenon becomes more pronounced as the bearing clearance increases.

(7) The groove angle has a strong influence on stability. Improvement in the stability performance can be obtained by decreasing the groove angle. Differences of up to 30% between theoretical and experimental values of threshold speed are found. Some possible reasons are given for this.

(8) It is demonstrated that oil feed from two pressurised axial grooves influences stability, probably causing a preloading effect. Higher feed pressure enhances stability. Discrepancies of up to 31% between theory and measured values are observed, the theoretical results being the lower ones. Some possible reasons are investigated.

(9) It is observed that supply of oil to the downstream groove alone has a destabilising effect. For larger clearances (e.g. 0.005in), increasing the feed pressure lowers the stability threshold, probably by control over film extent.

(10) Supplying oil to the upstream groove alone produces no significant observable changes to the system stability, compared with supplying oil to both grooves.

(11) The use of an undamped flexible pedestal affects the system stability. An increase in the threshold boundary is achieved by increasing the pedestal stiffness. Experimental values are higher than those predicted; a discrepancy of 6% obtained with high support stiffness, increasing to 20% with low support stiffness.

(12) Experimental work appears to justify the use of Reynolds boundary condition, implying that cavitation occurs at ambient pressure for a lightly loaded bearing, even for conditions close to the threshold of instability.

7.2 SUGGESTIONS FOR FURTHER WORK

In Section 6.6.2 some theoretical predictions are presented, indicating the effect of an elliptical bearing and an increase in shaft flexibility on the stability of the rotor-bearing system.

It is recommended that experimental and theoretical work be undertaken to ascertain the effect of different bearing designs (e.g. variation in preload of elliptical bearings, off-set halves etc.) and shaft flexibility on the dynamic behaviour of the rotor-bearing system. Introducing extra discs on the shaft and changing oil viscosity together with the existing variables could also be examined. Pedestal damping could also be investigated together with the existing flexible pedestal facility.

BIBLIOGRAPHY

(1) RANKINE, A.W.
On the Centrifugal Force of Rotating Shafts.
Engineer, London, 1869, Vol. 27, p249.

(2) DUNKERLEY, S.
On the Whirling and Vibration of Shafts.
Phil. Trans. A, 1894, Vol. 185, p279.

(3) JEFFCOTT, H.H.
The Lateral Vibration of Loaded Shafts in the Neighbourhood of a Whirling Speed - The Effect of Want of Balance.
Phil. Mag., 1919, Vol. 37, Ser. 6, p304.

(4) NEWKIRK, B.L.
Shaft Whipping.
Gen. Elec. Rev., 1924, Vol. 27, p169.

(5) NEWKIRK, B.L., & TAYLOR, H.D.
Shaft Whipping Due to Oil Action in Journal Bearing.
Gen. Elec. Rev., 1925, Vol. 28, pp559-568.

(6) STODOLA, A.
Kritische Wellenstorung infolge der Nachgiebigkeit des Olpolsters im Lager.
Schweiz Bauzeitung, 1925, Vol 85, p265.

(7) HUMMEL, C.H.
Kritsche Drehzahlen als Folge der Nachgiebigkeit des Schmiermittels im Lager.
Forschungsarbeiten, 1926, V.D.I., No. 287.

(8) ROBERTSON, D.
Whirling of a Journal in a Sleeve Bearing.
Phil. Mag., 1933, Vol 15, Ser. 7, pp113-130.

(9) HARRISON, W.J.
The Hydrodynamic Theory of Lubrication With Special Reference to Air as Lubricant.
Trans. Camb. Phil. Soc., 1913, Vol. 22, p39.

(10) SMITH, D.M.
The Motion of a Rotor Carried by a Flexible Shaft in Flexible Bearings.
Proc. Roy. Soc. (A), 1933, Vol. 142, pp92-118.

(11) NEWKIRK, B.L., & GROBEL, L.P.
Oil-Film Whirl - A Non-Whirling Bearing.
Trans. ASME, 1934, Vol. 56, pp607-615.

(12) HAGG, A.C.
The Influence of Oil-Film Journal Bearings on the Stability of Rotating Machines.
Trans. ASME, 1946, Vol 68, J. Appl. Mech., Vol. 13, No. 13, ppA211-A220.

(13) HAGG, A.C., & WARNER, P.C.
Oil-Whip of Flexible Rotors.
Trans. ASME, 1953, Vol. 75, pp1339-1344.

(14) PORITSKY, H.
Contribution to the Theory of Oil-Whip.
Trans. ASME, 1953, Vol. 75, pp1153-1161.

(15) CAMERON, A., & WOOD, L.W.
The Full Journal Bearing.
Proc. I.M.E., 1949, War Emergency Proc., pp59-72.

(16) PINKUS, O.
Experimental Investigation of Resonant Whip.
Trans. ASME, 1956, Vol. 78, pp975-983.

(17) TONDL, A.
Experimental Investigation of Self-Excited Vibrations of Rotors Due to the Action of Lubrication Oil-Film in Journal Bearings.
Wear, 1962, Vol. 5, pp136-137.

(18) HORI, Y.
A Theory of Oil-Whip.
Trans. ASME, 1959, Vol. 81, J. Appl. Mech., Vol. 26, pp189-198.

(19) NEWKIRK, B.L., & LEWIS, J.F.
Oil-Film Whirl - An Investigation of Disturbances Due to Oil-Films in Journal Bearings.
Trans. ASME, 1956, Vol. 78, pp21-27.

(20) NEWKIRK, B.L.
Varieties of Shaft Disturbances Due to Fluid-Films in Journal Bearings.
Trans. ASME, 1956, Vol. 78, pp985-988.

(21) BISHOP, R.E.D.
The Vibration of Rotating Shafts.
J. Mech. Eng. Sci., 1959, Vol. 1, No. 1, p50.

(22) BISHOP, R.E.D., & GLADWELL, G.M.L.
The Vibration and Balancing of an Unbalanced Flexible Rotor.
J. Mech. Eng. Sci., 1959, Vol. 1, No. 1 p66.

(23) GLADWELL, G.M.L., & BISHOP, R.E.D.
The Vibration of Rotating Shafts Supported in Flexible Bearings.
J. Mech. Eng. Sci., 1959, Vol. 1, No. 3, p195.

(24) GLADWELL, G.M.L., & BISHOP, R.E.D.
The Receptance of Uniform and Non-Uniform Rotating Shafts.
J. Mech. Eng. Sci., 1959, Vol. 1, No. 1, p78.

(25) STERNLICHT, B.
Elastic and Damping Properties of Cylindrical Journal Bearings.
Trans. ASME, 1959, Vol. 81, J. Basic Eng., pp101-108.

(26) HAGG, A.C., & SANKEY, G.O.
Elastic and Damping Properties of Oil-Film Journal Bearings for Application to Unbalanced Vibration Calculations.
Trans. ASME, 1958, Vol. 80, J. Appl. Mech., p1419.

(27) HOLMES, R.
The Vibration of a Rigid Shaft in Short Sleeve Bearings.
J. Mech. Eng. Sci., 1960, Vol. 2, No. 4, pp337-341.

(28) MORRISON, D.
Influence of Plain Journal Bearings on the Whirling Action of an Elastic Rotor.
Proc. I.M.E., 1962, Lub. and Wear Group, Vol. 176, No. 22, pp542-553.

(29) LUND, J.W., & STERNLICHT, B.
Rotor-Bearing Dynamics With Emphasis on Attenuation.
Trans. ASME, 1962, Vol. 84, No. 4, J. Basic Eng., pp491-502.

(30) MORTON, P.G.
On the Dynamics of Large Turbo-Generator Rotors.
Proc. I.M.E., 1965, Appl. Mech. Group, Vol. 181, Pt. 1, No. 12, pp295-329.

(31) GUNTER, E.J.
Dynamic Stability of Rotor-Bearing Systems.
NASA, 1966, SP-113.

(32) LUND, J.W.
The Stability of an Elastic Rotor in Journal Bearings With Flexible Damped Supports.
Trans. ASME, 1965, Vol. 87, J. Appl. Mech., Vol. 32, pp911-920.

(33) LUND, J.W., & SAIBEL, E.
Oil-Whip Whirl Orbits of a Rotor in Sleeve Bearings.
Trans. ASME, 1967, Vol. 89, J. Eng. Ind., pp813-823.

(34) LUND, J.W., & ORCUTT, F.K.
Calculations and Experiments on the Unbalance Response of a Flexible Rotor.
Trans. ASME, 1967, Vol. 89, J. Eng. Ind., pp785-796.

(35) PHROL, M.A.
A General Method for Calculating Critical Speeds of Flexible Rotors.
Trans. ASME, 1945, Vol. 67, J. Appl. Mech., Vol. 12, ppA142-A148.

(36) MORTON, P.G.
Influence of Coupled Asymmetric Bearings on the Motion of a Massive Flexible Rotor.
Proc. I.M.E., 1967, Appl. Mech. Group, Vol. 182, Pt. 1, No. 13, pp255-275.

(37) HOLMES, R., & PARKINS, D.W.
Assessing Unbalance Effects in a Small Turborotor.
ASME Paper No. 69-DE-9, 1969.

(38) KIKUCHI, K.
Analysis of Unbalance Vibration of Rotating Shaft System With Many Bearings and Discs.
Bulletin JSME, 1970, Vol. 13, No. 61, pp861-872.

(39) KIRK, R.G., & GUNTER, E.J.
The Effect of Support Flexibility and Damping on the Synchronous Response of a Single-Mass Flexible Rotor.
Trans. ASME, 1972, Vol. 94, J. Eng. Ind., pp221-232.

(40) DOSTAL, M., ROBERTS, J.B., & HOLMES, R.
Stability Control of Flexible Shafts Supported on Oil-Film Bearings.
J. Sound & Vibration, 1974, Vol. 35, No. 3, pp361-377.

(41) LUND, J.W.
Stability and Damped Critical Speeds of a Flexible Rotor in Fluid Film Bearings.
Trans. ASME, 1974, Vol. 96, J. Eng. Ind., pp509-517.

(42) MYKLESTAD, N.O.
A New Method of Calculating Natural Modes of Uncoupled Bending Vibration of Airplane Wings and Other Types of Beams.
J. Aeronaut. Sci., 1944, Vol. 11, No. 2, pp153-162.

(43) BANSAL, P.N., & KIRK, R.G.
Stability and Damped Critical Speeds of Rotor-Bearing Systems.
Trans. ASME, 1975, Vol. 97, J. Eng. Ind., pp1325-1332.

(44) HAHN, E.J.
The Excitability of Flexible Rotors in Short Sleeve Bearings.
Trans. ASME, 1975, Vol. 97, J. Lub. Tech., pp105-115.

(45) POLLMANN, E., & SCHWERDTFEGER, H.
Characteristic Vibration of Flexural Rotors in Journal Bearings.
I.M.E., 1976, Conf. on Vibrations in Rotating Machinery, pp21-26.

(46) KIKUCHI, K., & KOBAYASHI, S.
Stability Analysis of a Rotating Shaft System with Many Bearings and Discs.
Bulletin JSME, 1977, Vol. 20, No. 150, pp1592-1600.

(47) AKKOK, M., & ETTLES, C.M.Mc.
The Effect of Load and Feed Pressure on Whirl in a Grooved Journal Bearing.
Trans. ASLE, 1980, Vol. 23, No. 2, pp175-184.

(48) COLE, J.A.
Film Extent and Whirl in Couple Journal Bearing.
Proc. I.M.E., 1957, Conference on Lubrication and Wear.

(49) POPE, A.W., & HEALY, S.P.
Anti-Vibration Journal Bearings.
Proc. I.M.E., 1966, Vol. 181, Part 3B, pp94-111.

(50) AKKOK, M., & ETTLES, C.M.Mc.
The Effect of Grooving and Bore Shape on the Stability of Journal Bearings.
ASLE Preprint No. 79-AM-6D, 1979.

(51) AKKOK, M.
Dynamic Characteristics of Turbine Journal Bearings.
Ph.D. Thesis, 1980, Applied Mechs., Imperial College.

(52) TONNESEN, J., & LUND, J.W.
Some Experiments on Instability of Rotors Supported in Fluid-Film Bearings.
Trans. ASME, 1978, Vol. 100, J. Mech. Design, pp147-155.

(53) TONDL, A.
Some Problems of Rotor Dynamics.
Chapman & Hall, 1965, London.

(54) LANES, R.F., FLACK, R.D., & LEWIS, D.W.
Experiment on the Stability and Response of a Flexible Rotor in Three Types of Journal Bearings.
Trans. ASLE, 1981, Vol. 25, No. 3, pp289-298.

(55) CAMERON, A.
The Principles of Lubrication.
Longmans, 1966, London.

(56) PINKUS, O., & STERNLICHT, B.
Theory of Hydrodynamic Lubrication.
McGraw-Hill, 1961, New York.

(57) THOMSON, W.T.
Matrix Solution for the Vibration of Non-Uniform Beams.
Trans. ASME, 1950, Vol. 72, J. Appl. Mech., Vol. 17, pp337-339.

(58) PESTEL, E.C., & LECKIE, F.A.
Matrix Methods in Elastomechanics.
McGraw-Hill, 1963, New York.

(59) RUHL, R.L.
Dynamics of Distributed Parameter Rotor Systems: Transfer Matrix and Finite Element Techniques.
Ph.D. Thesis, 1970, Mech. Eng., Cornell University.

(60) DOSTAL, M.
Vibration Control of Rotor-Bearing System.
Ph.D. Thesis, 1974, Mech. Eng., Sussex University.

(61) RUDDY, A.V.
Dynamics of Rotor-Bearing Systems With Particular Reference to the Influence of Fluid-Film Journal Bearings and the Modelling of Flexible Rotors.
Ph.D. Thesis, 1979, Mech. Eng., Leeds University.

(62) ROARK, R.J., & YOUNG, W.C.
Formulas for Stress and Strain - Fifth Edition.
McGraw-Hill, 1975, New York.

(63) KIMBALL, A.L., & LOVELL, D.E.
Internal Friction in Solids.
Trans. ASME, 1926, Vol. 48, p479.

(64) LUND, J.W., & THOMSEN, K.K.
A Calculation Method and Data for Dynamic Coefficients of Oil-Lubricated Journal Bearings.
ASME Design Eng. Conf., 1978, Topics in Fluid-Film Bearing and Rotor Bearing System Design and Optimisation, ASME Pub. No. 100118.

(65) DE CHOUDHURY, P., ZSOLCSAK, S.J., & BARTH, E.W.
Effect of Damping on the Lateral Critical Speeds of Rotor-Bearing Systems.
Trans. ASME, 1976, Vol. 98, J. Eng. Ind., pp506-513.

(66) RUDDY, A.V., & SUMMERS-SMITH, D.
An Introduction to the Influence of the Bearings on the Dynamics of Rotatating Machinery.
Tribology International, 1980, pp199-203.

(67) BISHOP, R.E.D., & MAHALINGHAM, S.
Some Experiments on the Vibration of a Rotating Shaft.
Proc. Roy. Soc. (A), 1966, Vol. 292, p537.

(68) BARRETT, L.E., GUNTER, E.J., & ALLAIRE, P.E.
Optimum Bearing and Support Damping for Unbalance Response and Stability of Rotating Machinery.
Trans. ASME, 1978, Vol. 100, J. Eng. Power, pp89-94.

(69) LUND, J.W.
Review of Analytical Methods in Rotor-Bearing Dynamics.
Tribology International, 1980, pp233-236.

(70) McCALLION, H.
Vibration of Linear Mechanical Systems.
Longmans, 1973, London.

(71) THOMSON, W.T.
Theory of Vibration with Applications.
George, Allen and Unwin, 1981, London.

(72) WILKINSON, J.H.
The Algebraic Eigenvalue Problem.
Clarendon Press, 1965, Oxford.

(73) BISHOP, R.E.D., GLADWELL, G.M.L., & MICHAELSON, S.
The Matrix Analysis of Vibration.
Cambridge University Press, 1965.

(74) RUHL, R.L., & BOOKER, J.F.
A Finite Element Model for Distributed Parameter Turborotor Systems.
Trans. ASME, 1972, Vol. 94, J. Eng. Ind., pp126-132.

(75) LEONHARD, A.
Die Selbsttatige Regelung.
Springer-Verlag, 1949, Berlin.

(76) LUND, J.W.
Self Excited Stationary Whirl Orbits of a Journal in a Sleeve Bearing.
Ph.D. Thesis, 1966, Mech. Eng., Rensselaer Polytechnic.

(77) DEN HARTOG, J.P.
Mechanical Vibrations - 4th Edition.
McGraw-Hill, 1968, New York.

(78) WOODCOCK, J.S., & HOLMES, R.
Determination and Application of the Dynamic Properties of a Turbo-Rotor Bearing Oil-Film.
Proc. I.M.E., 1970, Vol. 184, Pt. 3L, pp111-119.

(79) MAYES, I.W., & DAVIES, W.G.R.
The Vibration Behaviour of a Rotating Shaft System Containing a Transverse Crack.
Proc. I.M.E., 1976, Conf. on Vibrations in Rotating Machinery, p53.

APPENDIX A

FEED PRESSURE RATIO

Define non-dimensional feed pressure ratio γ, with respect to projected or specific bearing load F/LD:

i.e. $$\gamma = P_f/(F/LD) \tag{A.1}$$

where P_f = feed pressure

Non-dimensional bearing pressure is:

$$P = P^* \, 6\omega\eta \frac{R^2}{c^2} \tag{A.2}$$

Define non-dimensional feed pressure P_f^* using equation (A.2)

i.e. $$P_f = P_f^* \, 6\omega\eta \frac{R^2}{c^2} \tag{A.3}$$

Non-dimensional bearing load is:

$$F = F^* \, 6\omega\eta \, L \frac{R^3}{c^2} \tag{A.4}$$

Substituting P_f and F from equations (A.3) and (A.4) respectively, into equation (A.1) gives:

$$\gamma = P_f^*/(F^*R/D) \tag{A.5}$$

Substituting D=2R into equation (A.5) gives:

$$P_f^* = 0.5\gamma F^* \tag{A.6}$$

APPENDIX B

FINITE DIFFERENCE SOLUTION OF REYNOLDS EQUATION

The non-dimensional form of Reynolds equation (2.10) is (dropping *):

$$h^3 \frac{\partial^2 P}{\partial \theta^2} + 3h^2 \frac{\partial h}{\partial \theta} \frac{\partial P}{\partial \theta} + \left(\frac{D}{L}\right)^2 h^3 \frac{\partial^2 P}{\partial z^2} = -\varepsilon(0.5-\dot{\phi})\sin\theta + \dot{\varepsilon}\cos\theta \quad \text{(B.1)}$$

Introducing the finite difference representation of the first and second order partial derivatives for pressure P:

$$\frac{\partial^2 P}{\partial \theta^2} = (P_{j+1,k} + P_{j-1,k} - 2P_{j,k})/(\Delta\theta)^2 \qquad \text{(B.2)}$$

$$\frac{\partial P}{\partial \theta} = (P_{j+1,k} - P_{j-1,k})/2\Delta\theta \qquad \text{(B.3)}$$

$$\frac{\partial^2 P}{\partial z^2} = (P_{j,k+1} + P_{j,k-1} - 2P_{j,k})/(\Delta z)^2 \qquad \text{(B.4)}$$

Figure B.1 shows the "computing molecule" for the θ -z co-ordinate system. Points P_N, P_E, P_S and P_W refer to the pressure at compass points North, East, South and West respectively, on the molecule.

Substituting equations (B.2) to (B.4) into equation (B.1) and rearranging gives:

$$2(1/(\Delta\theta)^2 + \sigma/(\Delta z)^2)P_{j,k} = (1/(\Delta\theta)^2 + a(\theta)/2\Delta\theta)P_{j+1,k} + (1/(\Delta\theta)^2$$
$$-a(\theta)/2\Delta\theta)P_{j-1,k} + (\sigma/(\Delta z)^2)P_{j,k+1} + (\sigma/(\Delta z)^2)P_{j,k-1} - b(\theta) \quad \text{(B.5)}$$

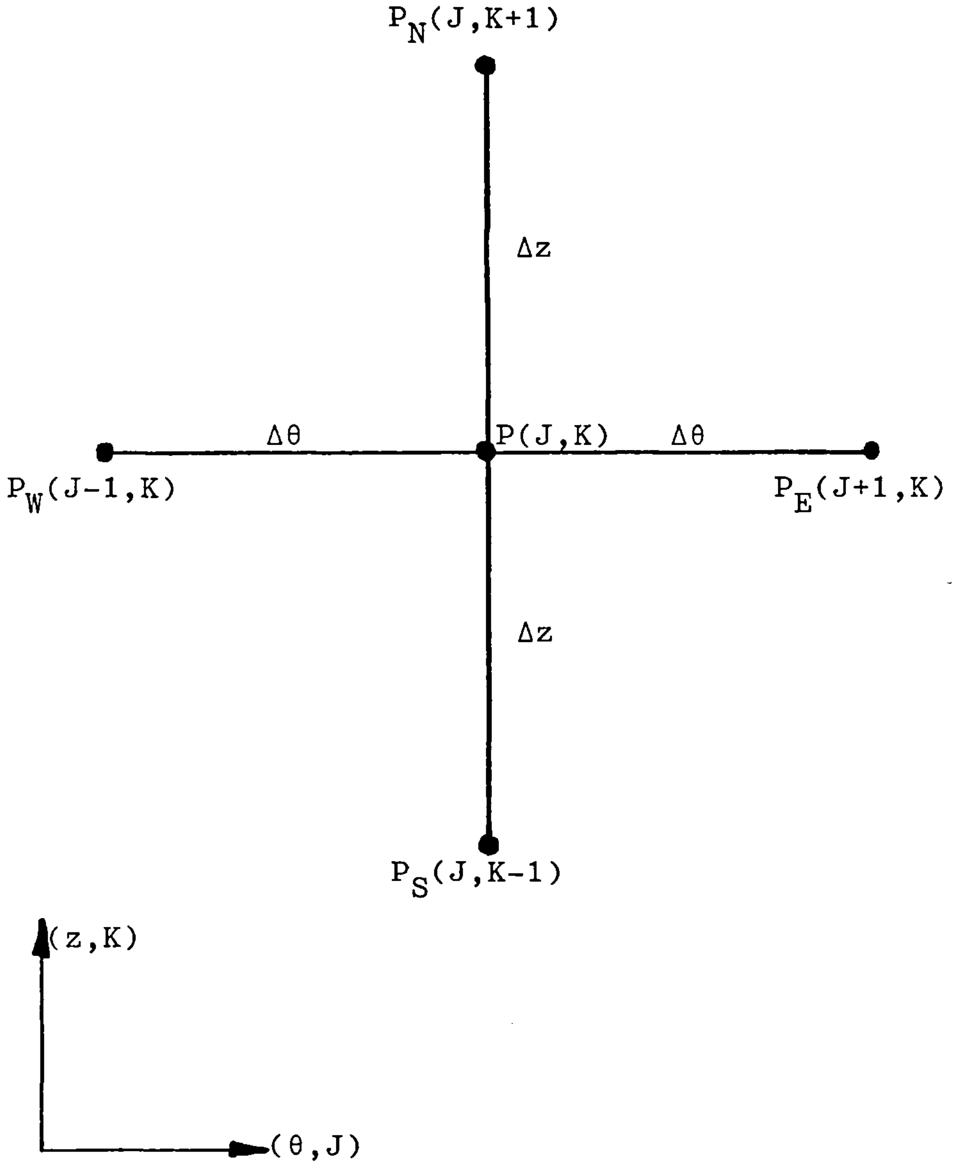

Figure B.1 Finite Difference Computing Molecule where $a(\theta) = \frac{3}{h}\frac{\partial h}{\partial \theta}$, $b(\theta) = \frac{1}{h^3}$ [RHS of (B.1)] and $\sigma = \left(\frac{D}{L}\right)^2$

Writting equation (B.5) in algorithm form gives:

$$P(J,K) = \frac{CE}{C} P(J+1,K) + \frac{CW}{C} P(J-1,K) + \frac{CN}{C} P(J,K+1) + \frac{CS}{C} P(J,K-1) - \frac{b(\theta)}{C} \quad (B.6)$$

where
$$C = 2(1/(\Delta\theta)^2 + \sigma/(\Delta z)^2)$$
$$CE = 1/(\Delta\theta)^2 + a(\theta)/2\Delta\theta$$
$$CW = 1/(\Delta\theta)^2 - a(\theta)/2\Delta\theta$$
$$CN = CS = \sigma/(\Delta z)^2$$

APPENDIX C

COMPUTER LISTING FOR JOURNAL BEARING SOLUTION

```
      PROGRAM ROUTH(INPUT,OUTPUT,TAPE5=INPUT,TAPE6=OUTPUT)
      COMMON P(100,20),TH(100),THB(100),CE(100),CW(100),G(100),H(100)
      COMMON H3(100),IP(100,20),EC(10),AT(10),ATD(10),CN,CS,DT,DTS,DZ
      COMMON DZS,DLS,JT,JTN,JR,JS,JSN,KT,KTN,KT1,PIE,ATT,PSI,PSID,ECC
      COMMON DELTA,WT,W,SMF,WX1,WY1,X1,Y1,NITER,WRES,AXX,AXY,AYX,AYY
      COMMON BXX,BXY,BYX,BYY,WX,WY,NMAX,CC2,RELAX2
      COMMON/DATA/ XD,YD,DELX,DELY,IBT
C
C*****MAIN PROGRAM FOR A LEMON BEARING WITH PRELOAD OR CIRCULAR
C*****BEARING*****
C     SET BEARING TYPE IBT
C     1 FOR CIRCULAR BEARING
C     2 FOR LEMON BEARING
      IBT=1
C
      WRITE(6,102)
      WRITE(6,106)
      WRITE(6,103)
C
C     DERIVE CONSTANTS FOR FINITE DIFFERENCE PROCEDURE
      PIE=4.*ATAN(1.)
C
C     SET NO. OF NODES IN CIRCUMFERENTIAL DIRECTION
      JT=73
      JTN=JT-1
      JR=(JT+1)/2
      JSN=JR+1
      JS=JR-1
      DT=2.*PIE/FLOAT(JTN)
      DTS=DT**2
C
C     SET GROOVE ANGLE IN DEGREES
      IBETA=30
C
C     CONVERT GROOVE ANGLE TO HALF NODAL WIDTH
      JP=IBETA*JTN/(360*2)
      JP1=JP+1
      J1=JR-JP
      J2=JR+JP
      J3=JT-JP
C
C     SET NO. OF NODES IN AXIAL DIRECTION
      KT=11
      KTN=KT-1
      KT1=KT+1
      DZ=1./FLOAT(KTN)
      DZS=DZ**2
C
C     SET AXIAL LENGTH TO DIAMETER RATIO
C     L/D=1/2
      DL=2.
      DLS=DL**2
C
C     SET VELOCITY XDOT YDOT
      XD=0.001
      YD=XD
C
C     SET DISPLACEMENT DELTA X DELTA Y
      DELX=0.001
      DELY=DELX
C
C     READ NON-DIMENSIONAL FEED PRESSURE RATIO
      READ(5,150)GAMMA
      WRITE(6,107)GAMMA
C
C     INITIALISE PRESSURE FIELD TO ZERO
      DO 11 J=1,JT
      DO 12 K=1,KT1
      P(J,K)=0.
   12 CONTINUE
   11 CONTINUE
C
C     INITALISE INTEGER PRESSURE FIELD TO ZERO
      DO 22 J=1,JT
      DO 23 K=1,KT1
      IP(J,K)=0
   23 CONTINUE
   22 CONTINUE
C
C     INITALISE INTEGER PRESSURE FIELD TO 1 AT GROOVES
      DO 19 K=3,KT1
      DO 18 J=1,JP1
      IP(J,K)=1
   18 CONTINUE
      DO 17 J=J1,J2
```

```
      IP(J,K)=1
   17 CONTINUE
      DO 16 J=J3,JT
      IP(J,K)=1
   16 CONTINUE
   19 CONTINUE
C
C     SET PRELOAD FACTOR DELTA
      DELTA=0.5
      IF(IBT.EQ.1)DELTA=0.0
C
C     SET LOOP COUNTER LIMIT FOR ATTITUDE ANGLE
      LIMIT=5*JT
C
C     SET LOOP COUNTER LIMIT FOR LOAD
      LIMIT1=5*JT
C
C     SET LOOP COUNTER LIMIT FOR PRESSURE
      NMAX=5*JT
C
C     SET RELAXATION FOR ATTITUDE ANGLE
      RELAX=0.5
C
C     SET RELAXATION FOR LOAD
      RELAX1=0.5
C
C     SET RELAXATION FOR PRESSURE
      RELAX2=1.8
C
C     SET LIMIT FOR CONVERGENCE OF ATTITUDE ANGLE IN RADIANS
      CC=1.75E-05
C
C     SET LIMIT FOR CONVERGENCE OF LOAD
      CC1=1.0E-07
C
C     SET LIMIT FOR CONVERGENCE OF PRESSURE
      CC2=1.0E-07
C
C     SET ATTITUDE ANGLE IN DEGREES
      ATTD=80.0
      ATT=ATTD*PIE/180.
C
C     SET NON-DIM. LOAD
      W=0.01
      DO 30 I=1,9
C
C     SET VALUE OF ECCENTRICITY
      ECM=FLOAT(I)/10.
      ECC=ECM*(1.-DELTA)
C
      WRITE(6,100)ECM,ECC
C
C     SET LOOP COUNTER FOR LOAD TO ZERO
      NITER1=0
   21 NITER1=NITER1+1
C
C     DERIVE NON-DIM. FEED PRESSURE
      PF=0.5*GAMMA*W
C
C     SET GROOVE PRESSURE EQUAL TO FEED PRESSURE
C
      DO 25 K=3,KT1
      DO 26 J=1,JP1
      P(J,K)=PF
   26 CONTINUE
      DO 27 J=J1,J2
      P(J,K)=PF
   27 CONTINUE
      DO 28 J=J3,JT
      P(J,K)=PF
   28 CONTINUE
   25 CONTINUE
C     SET LOOP COUNTER FOR ATTITUDE ANGLE TO ZERO
      NITERS=0
   14 NITERS=NITERS+1
      IF(IBT.EQ.1)GO TO 10
C
C     CALLS SUBROUTINES TO EVALUATE COEFFICIENTS AND FILM THICKNESS
      CALL LOBE
   10 CALL FILM(IBT)
      CALL FINITE(0.,0.,IBT)
      CALL ITERATE
      CALL LOAD
      ANG=PSI-ATT
      IF(ABS(ANG).LT.CC)GO TO 15
```

```
      IF(NITERS.GT.LIMIT)GO TO 15
      ATT=ATT+RELAX*ANG
      GO TO 14
   15 DW=WT-W
      IF(ABS(DW).LT.CC1)GO TO 24
      IF(NITER1.GT.LIMIT1)GO TO 24
      W=W+RELAX1*DW
      GO TO 21
   24 SMF=6.*W
      ATTD=ATT*180./PIE
      ANGLE=ANG*180./PIE
      IF(IBT.EQ.1)GO TO 20
      DO 13 NN=1,2
      ATD(NN)=AT(NN)*180./PIE
      WRITE(6,130)EC(NN),ATD(NN)
   13 CONTINUE
   20 WRITE(6,113)PF
      WRITE(6,112)NITER1,DW
      WRITE(6,104)NITEPS,ANGLE
C
C     PRINT OUT RESIDUAL AND P(J,K) FOR VALUE OF NRES
      WRITE(6,105)NITER,WRES
      WRITE(6,110)((P(J,K),K=1,KT,2),J=1,JT)
      WRITE(6,111)
C
C     PRINT TOTAL LOAD SOMMERFELD NO. AND ATTITUDE ANGLE
      WRITE(6,101)WX,WY,W,SMF,ATTD
      WX1=W
      WY1=0.
      X1=ECC*COS(ATT)
      Y1=ECC*SIN(ATT)
      CALL DAMP
      CALL STIFF
C
C     CALL SUBR STABLE TO DETERMINE STABILITY OF DYNAMIC SYSTEM
      CALL STABLE
   30 CONTINUE
  100 FORMAT(5X,*LOBE ECCENTRICITY=*,F4.3,5X,*BEARING ECCENTRICITY=*,
     +F4.3/)
  113 FORMAT(5X,*NON.-DIM.FEED PRESSURE=*,1PE13.6/)
  101 FORMAT(5X,*WX=*,1PE13.6,2X,*WY=*,1PE13.6,2X,*W=*,1PE13.6,2X,
     +*SOMMERFELD NO.=*,1PE13.6,2X,*ATTITUDE ANGLE=*,1PE13.6,1X,
     +*DEGREES*,/)
  102 FORMAT(5X,*CIRCULAR BEARING WITH THIRTY DEGREE AXIAL GROOVES*/)
  106 FORMAT(5X,*GROOVE COMMENCING THREE NODES IN FROM BEARING EDGE*/)
  103 FORMAT(5X,*L OVER D HALF*/)
  107 FORMAT(5X,*FEED PRESSURE RATIO GAMMA=*,F3.1///)
  104 FORMAT(5X,*ATTITUDE ANGLE CONVERSION NO.=*,I3,2X,
     +*CONVERSION VALUE=*,1PE13.6,1X,*DEGREES*/)
  112 FORMAT(5X,*LOAD CONVERSION NO.=*,I3,2X,
     +*CONVERSION VALUE=*,1PE13.6/)
  105 FORMAT(5X,*PRESSURE CONVERSION NO.=*,I3,2X,*CONVERSION VALUE=*,
     +1PE13.6/)
  110 FORMAT(6(2X,1PE13.6))
  111 FORMAT(/)
  130 FORMAT(5X,*EC=*,1PE13.6,2X,*ATD=*,1PE13.6/)
  150 FORMAT(F3.1)
      STOP
      END
      SUBROUTINE LOBE
      COMMON P(100,20),TH(100),THB(100),CE(100),CW(100),G(100),H(100)
      COMMON H3(100),IP(100,20),EC(10),AT(10),ATD(10),CN,CS,DT,DTS,DZ
      COMMON DZS,DLS,JT,JTN,JR,JS,JSN,KT,KTN,KT1,PIE,ATT,PSI,PSID,ECC
      COMMON DELTA,WT,W,SMF,WX1,WY1,X1,Y1,NITEP,WRES,AXX,AXY,AYX,AYY
      COMMON BXX,BXY,BYX,BYY,WX,WY,NMAX,CC2,RELAX2
C
C*****PROGRAM TO CALCULATE LOBE ATTITUDE ANGLES AND ECCENTRICIES*****
C
      DO 16 NN=1,2
      IF(NN.EQ.2)GO TO 17
      EC(NN)=SQRT(ECC**2+DELTA**2+2*ECC*DELTA*COS(ATT))
      GO TO 18
   17 EC(NN)=SQRT(ECC**2+DELTA**2-2*ECC*DELTA*COS(ATT))
   18 AT(NN)=ASIN(ECC*SIN(ATT)/EC(NN))
   16 CONTINUE
      RETURN
      END
      SUBROUTINE FILM(IBT)
      COMMON P(100,20),TH(100),THB(100),CE(100),CW(100),G(100),H(100)
      COMMON H3(100),IP(100,20),EC(10),AT(10),ATD(10),CN,CS,DT,DTS,DZ
      COMMON DZS,DLS,JT,JTN,JR,JS,JSN,KT,KTN,KT1,PIE,ATT,PSI,PSID,ECC
      COMMON DELTA,WT,W,SMF,WX1,WY1,X1,Y1,NITER,WRES,AXX,AXY,AYX,AYY
      COMMON BXX,BXY,BYX,BYY,WX,WY,NMAX,CC2,RELAX2
C
C*****PROGRAM TO CALCULATE OIL FILM THICKNESS FOR LEMON AND CIRCULAR
```

```
C      BEARING*****
C
C
C      DEFINE CONSTANTS FOR FILM THICKNESS
C
C      GENERATE THETA INCREMENTS FOR CENTRE OF BEARING W.R.T.
C      THE LINE OF CENTRES
       THB(1)=PIE/2.-ATT
       IF(ATT.GT.PIE/2.)THB(1)=ATT-PIE/2.
       H(1)=1.+ECC*COS(THB(1))
       H3(1)=H(1)**3
       DO 12 J=2,JT
       THB(J)=THB(J-1)+DT
       H(J)=1.+ECC*COS(THB(J))
       H3(J)=H(J)**3
    12 CONTINUE
       IF(IBT.EQ.1)GO TO 13
C
C      BOTTOM LOBE FILM THICKNESS
       TH(1)=PIE/2.-AT(1)
       H(1)=1.+EC(1)*COS(TH(1))
       H3(1)=H(1)**3
       DO 10 J=2,JS
       TH(J)=TH(J-1)+DT
       H(J)=1.+EC(1)*COS(TH(J))
       H3(J)=H(J)**3
    10 CONTINUE
C
C      TOP LOBE FILM THICKNESS
       TH(JR)=PIE/2.+AT(2)
       H(JR)=1.+EC(2)*COS(TH(JR))
       H3(JR)=H(JR)**3
       DO 11 J=JSN,JT
       TH(J)=TH(J-1)+DT
       H(J)=1.+EC(2)*COS(TH(J))
       H3(J)=H(J)**3
    11 CONTINUE
    13 RETURN
       END
       SUBROUTINE FINITE(XD,YD,IBT)
       COMMON P(100,20),TH(100),THB(100),CE(100),CW(100),G(100),H(100)
       COMMON H3(100),IP(100,20),EC(10),AT(10),ATD(10),CN,CS,DT,DTS,DZ
       COMMON DZS,DLS,JT,JTN,JR,JS,JSN,KT,KTN,KT1,PIE,ATT,PSI,PSID,ECC
       COMMON DELTA,WT,W,SMF,WX1,WY1,X1,Y1,NITER,WRES,AXX,AXY,AYX,AYY
       COMMON BXX,BXY,BYX,BYY,WX,WY,NMAX,CC2,RELAX2
C
C*****PROGRAM TO CALCULATE COEFFICIENTS AT NODAL POINTS WITH SQUEEZE
C*****VELOCITY TERM*****
C
       C=2./DTS+2.*DLS/DZS
       DO 10 J=1,JT
       IF(IBT.NE.1)GO TO 13
       FC=-3.*ECC*SIN(THB(J))/H(J)
       F1=-ECC*SIN(THB(J))/(H3(J)*C)
       F2=2./(H3(J)*C)*(YD*COS(ATT)-XD*SIN(ATT))*SIN(THB(J))
       F3=2./(H3(J)*C)*(XD*COS(ATT)+YD*SIN(ATT))*COS(THB(J))
       GO TO 12
    13 IF(J.LE.JS)NN=1
       IF(J.GE.JR)NN=2
       FC=-3.*EC(NN)*SIN(TH(J))/H(J)
       F1=-EC(NN)*SIN(TH(J))/(H3(J)*C)
       IF(NN.EQ.2)GO TO 11
       F2=2./(H3(J)*C)*(YD*COS(AT(NN))-XD*SIN(AT(NN)))*SIN(TH(J))
       F3=2./(H3(J)*C)*(XD*COS(AT(NN))+YD*SIN(AT(NN)))*COS(TH(J))
       GO TO 12
    11 F2=2./(H3(J)*C)*(-YD*COS(AT(NN))-XD*SIN(AT(NN)))*SIN(TH(J))
       F3=2./(H3(J)*C)*(-XD*COS(AT(NN))+YD*SIN(AT(NN)))*COS(TH(J))
    12 G(J)=F1+F2+F3
       CE(J)=(1./DTS+FC/(2.*DT))/C
       CW(J)=(1./DTS-FC/(2.*DT))/C
    10 CONTINUE
       CN=DLS/(DZS*C)
       CS=CN
       RETURN
       END
       SUBROUTINE ITERATE
       COMMON P(100,20),TH(100),THB(100),CE(100),CW(100),G(100),H(100)
       COMMON H3(100),IP(100,20),EC(10),AT(10),ATD(10),CN,CS,DT,DTS,DZ
       COMMON DZS,DLS,JT,JTN,JR,JS,JSN,KT,KTN,KT1,PIE,ATT,PSI,PSID,ECC
       COMMON DELTA,WT,W,SMF,WX1,WY1,X1,Y1,NITER,WRES,AXX,AXY,AYX,AYY
       COMMON BXX,BXY,BYX,BYY,WX,WY,NMAX,CC2,RELAX2
C
C*****PROGRAM TO CAL. PRESSURE USING ITERATION TECHNIQUE*****
C
C
```

```
C     ITERATION CONTROLS VARIABLES
      NRES=1
C
C     SET LOOP COUNTER FOR PRESSURE TO ZERO
      NITER=0
C
C     MAIN LOOP
   14 NITER=NITER+1
      RESUM=0.
      XSUM=0.
C
C     CARRY OUT ONE SWEEP
      DO 15 J=2,JTN
      DO 16 K=2,KT
C
C     BOUNDARY CONDITION TO SET GROOVE PRESSURE EQUAL TO FEED PRESSURE
      IF(IP(J,K).NE.1)GO TO 23
      GO TO 16
   23 CONTINUE
      Z=P(J,K)
      ZN=CE(J)*P(J+1,K)+CW(J)*P(J-1,K)+CN*P(J,K+1)+CS*P(J,K-1)-G(J)
      P(J,K)=Z+RELAX2*(ZN-Z)
C
C     REYNOLDS BOUNDARY CONDITION
      IF(P(J,K).GE.0.)GO TO 13
      P(J,K)=0.
      GO TO 16
C
C     FIND WEIGHTED RESIDUAL
   13 RABS=ABS(1.-Z/P(J,K))
      XSUM=XSUM+ABS(P(J,K))
      RESUM=RESUM+RABS*ABS(P(J,K))
   16 CONTINUE
   15 CONTINUE
      WRES=RESUM/ XSUM
C
C     END OF SINGLE SWEEP
C
C     PRESSURES EITHER SIDE OF CENTRE LINE SET EQUAL
      DO 17 J=2,JTN
      P(J,KT1)=P(J,KTN)
   17 CONTINUE
      IF((NITER+NRES-1)/NRES-NITER/NRES)19,18,19
   18 CONTINUE
C
C     TEST FOR EXCESSIVE ITERATION
   19 IF(NITER-NMAX)21,21,22
C
C     TEST FOR CONVERGENCE
   21 IF(WRES-CC2)22,22,14
   22 CONTINUE
      RETURN
      END
      SUBROUTINE LOAD
      COMMON P(100,20),TH(100),THB(100),CE(100),CW(100),G(100),H(100)
      COMMON H3(100),IP(100,20),EC(10),AT(10),ATD(10),CN,CS,DT,DTS,DZ
      COMMON DZS,DLS,JT,JTN,JR,JS,JSN,KT,KTN,KT1,PIE,ATT,PSI,PSID,ECC
      COMMON DELTA,WT,W,SMF,WX1,WY1,X1,Y1,NITER,WRES,AXX,AXY,AYX,AYY
      COMMON BXX,BXY,BYX,BYY,WX,WY,NMAX,CC2,RELAX2
      DIMENSION FNC(100),FNS(100),FX(100),FY(100)
C
C*****PROGRAM TO CAL. LOAD SOMMERFELD NO. AND ATTITUDE ANGLE*****
C     FOR CENTRE OF LEMON AND CIRCULAR BEARING*****
C
      DO 15 J=1,JT
      DO 14 K=1,KT
C
C     FORM ARRAY OF P(J,K)COS(J) P(J,K)SIN(J)
      FNC(K)=P(J,K)*COS(THB(J))
      FNS(K)=P(J,K)*SIN(THB(J))
   14 CONTINUE
C
C     CALL SUBR SIMP IN Z DIRN *KT
      CALL SIMP(FNC,1,KT,DZ,FNNC)
      CALL SIMP(FNS,1,KT,DZ,FNNS)
      FX(J)=FNNC
      FY(J)=FNNS
   15 CONTINUE
C
C     CALL SUBR SIMP IN THETA DIRN
      CALL SIMP(FX,1,JT,DT,WX)
      CALL SIMP(FY,1,JT,DT,WY)
C
C     EQUATIONS FOR ATTITUDE ANGLE TOTAL LOAD AND SOMMERFELD NUMBER
      PSI=ATAN(-WY/WX)
```

```
      IF(PSI.LT.0.0)PSI=PIE-ABS(PSI)
      PSID=PSI*180./PIE
      WT=SQRT(WX**2+WY**2)
      SMF=6.*WT
      RETURN
      END
      SUBROUTINE DAMP
      COMMON P(100,20),TH(100),THB(100),CE(100),CW(100),G(100),H(100)
      COMMON H3(100),IP(100,20),EC(10),AT(10),ATD(10),CN,CS,DT,DTS,DZ
      COMMON DZS,DLS,JT,JTN,JR,JS,JSN,KT,KTN,KT1,PIE,ATT,PSI,PSID,ECC
      COMMON DELTA,WT,W,SMF,WX1,WY1,X1,Y1,NITER,WRES,AXX,AXY,AYX,AYY
      COMMON BXX,BXY,BYX,BYY,WX,WY,NMAX,CC2,RELAX2
      COMMON/DATA/ XD,YD,DELX,DELY,IBT
C
C*****PROGRAM TO CAL. DAMPING COEFFICIENTS*****
C
C
C     FOR VELOCITY XD
      CALL FINITE(XD,0.,IBT)
      CALL ITERATE
      CALL LOAD
C
C     OBTAIN CHANGE IN FORCES IN X AND Y
      ALPHA=ATT-PSI
      WX2=WT*COS(ALPHA)
      WY2=WT*SIN(ALPHA)
      WRITE(6,101)WX,WY,WT,PSID
C
C     OBTAIN COEFFICIENTS BXX BYX
      BXX=(WX2-WX1)/(XD*W)
      BYX=(WY2-WY1)/(XD*W)
C
C     FOR VELOCITY YD
      CALL FINITE(0.,YD,IBT)
      CALL ITERATE
      CALL LOAD
C
C     OBTAIN CHANGE IN FORCES IN X AND Y
      ALPHA=ATT-PSI
      WX2=WT*COS(ALPHA)
      WY2=WT*SIN(ALPHA)
      WRITE(6,101)WX,WY,WT,PSID
C
C     OBTAIN COEFFICIENTS BXY BYY
      BXY=(WX2-WX1)/(YD*W)
      BYY=(WY2-WY1)/(YD*W)
C
C     PRINT DAMPING COEFFICIENTS
      WRITE(6,100)BXX,BXY,BYX,BYY
  100 FORMAT(5X,*BXX=*,1PE13.6,2X,*BXY=*,1PE13.6,2X,*BYX=*,1PE13.6,2X,
     +*BYY=*,1PE13.6/)
  101 FORMAT(5X,*WX=*,1PE13.6,2X,*WY=*,1PE13.6,2X,*WT=*,1PE13.6,2X,
     +*PSID=*,1PE13.6/)
      RETURN
      END
      SUBROUTINE STIFF
      COMMON P(100,20),TH(100),THB(100),CE(100),CW(100),G(100),H(100)
      COMMON H3(100),IP(100,20),EC(10),AT(10),ATD(10),CN,CS,DT,DTS,DZ
      COMMON DZS,DLS,JT,JTN,JR,JS,JSN,KT,KTN,KT1,PIE,ATT,PSI,PSID,ECC
      COMMON DELTA,WT,W,SMF,WX1,WY1,X1,Y1,NITER,WRES,AXX,AXY,AYX,AYY
      COMMON BXX,BXY,BYX,BYY,WX,WY,NMAX,CC2,RELAX2
      COMMON/DATA/ XD,YD,DELX,DELY,IBT
C
C*****PROGRAM TO CAL. STIFFNESS COEFFICIENTS*****
C
C
C     DISPLACEMENT IN X DIR.
      X2=X1+DELX
      Y2=Y1
C
C     OBTAIN NEW VALUE OF ECCENTRICITY AND ATTITUDE ANGLE
      ATT=ATAN(Y2/X2)
      ATTD=ATT*180./ PIE
      ECC=SQRT((X2)**2+(Y2)**2)
      IF(IBT.EQ.1)GO TO 10
      CALL LOBE
   10 CALL FILM(IBT)
      CALL FINITE(0.,0.,IBT)
      CALL ITERATE
      CALL LOAD
C
C     OBTAIN CHANGE IN FORCES IN X AND Y
      ALPHA=ATT-PSI
      WX2=WT*COS(ALPHA)
      WY2=WT*SIN(ALPHA)
```

```
      WRITE(6,101)WX,WY,WT,ATTD,PSID
C
C     OBTAIN COEFFICIENTS AXX AYX
      AXX=(WX2-WX1)/(DELX*W)
      AYX=(WY2-WY1)/(DELX*W)
C
C     DISPLACEMENT IN Y DIR.
      X2=X1
      Y2=Y1+DELY
C
C     OBTAIN NEW VALUE OF ECCENTRICITY AND ATTITUDE ANGLE
      ATT=ATAN(Y2/X2)
      ATTD=ATT*180./ PIE
      ECC=SQRT((X2)**2+(Y2)**2)
      IF(IBT.EQ.1)GO TO 11
      CALL LOBE
   11 CALL FILM(IBT)
      CALL FINITE(0.,0.,IBT)
      CALL ITERATE
      CALL LOAD
C
C     OBTAIN CHANGE IN FORCES IN X AND Y
      ALPHA=ATT-PSI
      WX2=WT*COS(ALPHA)
      WY2=WT*SIN(ALPHA)
      WRITE(6,101)WX,WY,WT,ATTD,PSID
C
C     OBTAIN COEFFICIENTS AXY AYY
      AXY=(WX2-WX1)/(DELY*W)
      AYY=(WY2-WY1)/(DELY*W)
C
C     PRINT STIFFNESS COEFFICIENTS
      WRITE(6,100)AXX,AXY,AYX,AYY
  100 FORMAT(5X,*AXX=*,1PE13.6,2X,*AXY=*,1PE13.6,2X,*AYX=*,1PE13.6,2X,
     +*AYY=*,1PE13.6/)
  101 FORMAT(5X,*WX=*,1PE13.6,2X,*WY=*,1PE13.6,2X,*WT=*,1PE13.6,2X,
     +*ATTD=*,1PE13.6,2X,*PSID=*,1PE13.6/)
      RETURN
      END
      SUBROUTINE STABLE
      COMMON P(100,20),TH(100),THB(100),CE(100),CW(100),G(100),H(100)
      COMMON H3(100),IP(100,20),EC(10),AT(10),ATD(10),CN,CS,DT,DTS,DZ
      COMMON DZS,DLS,JT,JTN,JR,JS,JSN,KT,KTN,KT1,PIE,ATT,PSI,PSID,ECC
      COMMON DELTA,WT,W,SMF,WX1,WY1,X1,Y1,NITER,WRES,AXX,AXY,AYX,AYY
      COMMON BXX,BXY,BYX,BYY,WX,WY,NMAX,CC2,RELAX2
C
C*****PROGRAM TO CAL. ROUTHS STABILITY CRITERION*****
C
C
C
C     ROUTHS STABILITY CRITERION IN TERMS  OF STIFFNESS AND DAMPING
C     COEFFICIENTS
      U1=BXX+BYY
      U2=AXX+AYY
      U3=BXX*BYY-BXY*BYX
      U4=AXX*BYY+AYY*BXX-AXY*BYX-AYX*BXY
      U5=AXX*AYY-AXY*AYX
      ST=(U5*U1**2+U4**2-U1*U2*U4)/(U1*U3*U4)
C
C     PRINT VALUE OF STABILITY PARAMETER FOR BOUNDARY BETWEEN STABLE
C     AND UNSTABLE CONDITION
      WRITE(6,175)ST
  175 FORMAT(5X,*STABILITY PARAMETER=*,1PE13.6//)
      RETURN
      END
      SUBROUTINE SIMP(F,NA,NZ,DH,ANSWER)
      DIMENSION F(NZ)
C
C*****SIMPSONS NUMERICAL INTEGRATION METHOD*****
C
C
C     SIMPSONS RULE OF INTEGRATION
C
C     ADD TERMS WITH COEFFICIENTS 4
      SUM4=0.
      NN=NZ-1
      NB=NA+1
      DO 10 K=NB,NN,2
      SUM4=SUM4+F(K)
   10 CONTINUE
C
C     ADD TERMS WITH COEFFICIENTS 2
      SUM2=0.
      NM=NZ-2
      NC=NA+2
      DO 11 K=NC,NM,2
```

```
      SUM2=SUM2+F(K)
   11 CONTINUE
C
C     SIMPSONS FORMULA
      ANSWER=(DH/3.)*(F(NA)+F(NZ)+4.*SUM4+2.*SUM2)
      RETURN
      END
```

APPENDIX D

WHIRL ORBIT REPRESENTATION

The semiaxes and orientation of the elliptical whirl orbit Figure D.1, are calculated from (reference (34)):

$$a = \left[\frac{1}{2}(x_R{}^2+x_I{}^2+y_R{}^2+y_I{}^2) + \sqrt{\frac{1}{4}(x_R{}^2+x_I{}^2-y_R{}^2-y_I{}^2)^2 + (x_R y_R+x_I y_I)^2}\right]^{1/2} \tag{D.1}$$

$$b = \frac{x_I y_R - x_R y_I}{a} \tag{D.2}$$

$$\gamma = \frac{1}{2}\tan^{-1}\left[\frac{2(x_R y_R+x_I y_I)}{x_R{}^2+x_I{}^2-y_R{}^2-y_I{}^2}\right] \tag{D.3}$$

$$\psi = \frac{1}{2}\tan^{-1}\left[\frac{2(x_R x_I+y_R y_I)}{x_R{}^2-x_I{}^2+y_R{}^2-y_I{}^2}\right] \tag{D.4}$$

where a is the major semiaxis, b is the minor semiaxis, γ the angle from the x-axis to the major semiaxis in the direction of shaft rotation, and ψ is the phase angle. The directions of the axes are as adopted in Chapters 2 and 3, that is, the x-axis is vertically downwards and the y-axis is horizontal. The z-axis is in the direction of the rotor axis.

The definition of the phase angle ψ is such that, if the x-y coordinate system is rotated through the angle γ into an x'-y' system (that is, x' long the major semiaxis), then the

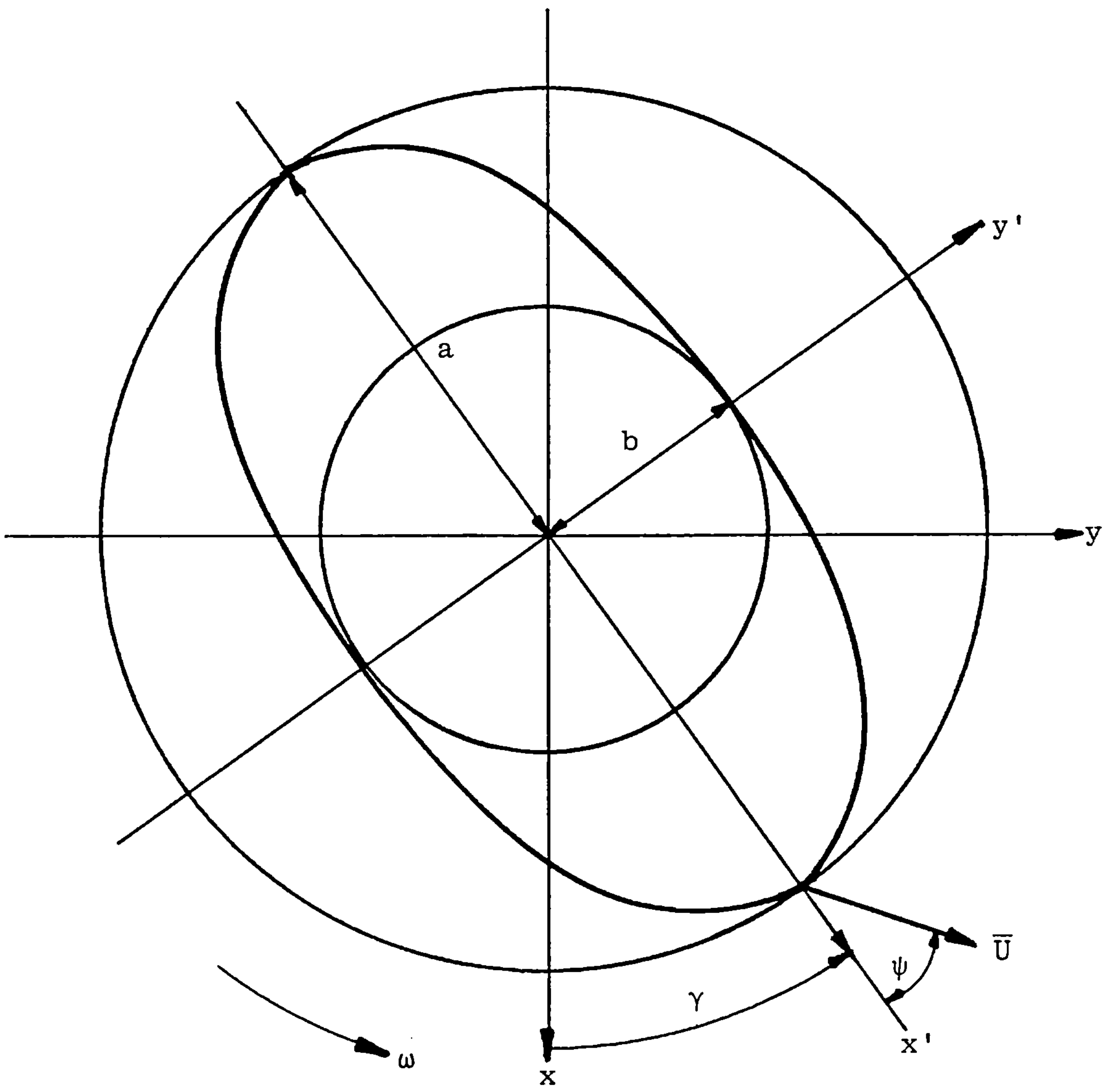

Figure D.1 Whirl Orbit Representation

rotation motion can be expressed as:

$$x' = a \cos(\omega t + \psi) \tag{D.5a}$$

$$y' = b \sin(\omega t + \psi) \tag{D.5b}$$

If the value for the minor semiaxis b is negative, then the rotor is precessing or whirling backwards.

Equations (D.1) to (D.4) can be used to compute the elliptical whirl orbit of the rotor-bearing system at any position where a station is located.

APPENDIX E

COMPUTER LISTING FOR ROTOR-BEARING SYSTEM DYNAMICS

```
      PROGRAM STABLE(INPUT,OUTPUT,TAPE5=INPUT,TAPE6=OUTPUT)
      COMPLEX F,FB,AA,A,Z,ZXX,ZXY,ZYX,ZYY,ZXXF,ZXYF,ZYXF,ZYYF,ZXXP,ZXYP
      COMPLEX ZYXP,ZYYP,CPSI,SUM,ALAMBDA,ALAMS,C1,C2,C3,C4,C5,C6,C7,C8
      COMPLEX C9,C10,C11,AC,BC,CC,BHFX,BHFY,BFFX,BFFY,XP,YP
      COMPLEX ZTT,ZTP,ZPT,ZPP
      REAL KXX,KXY,KYX,KYY,KXP,KYP,MXP,MYP,LOAD,MEER,KTT,KPP
      COMMON ECC(10),AXX(10),AXY(10),AYX(10),AYY(10),BXX(10),BXY(10)
      COMMON BYX(10),BYY(10),WSS(10),AXX1(10),AXY1(10),AYX1(10)
      COMMON AYY1(10),BXX1(10),BXY1(10),BYY1(10),BYY1(10),ECC1(10)
      COMMON WSS1(10),DIA(25),BEAM(25),SI(25),AMASS(25),PI(25),TI(25)
      COMMON PIE,C,FORCE,E,KI,KN,KS,KB,KF,RPM,OMEGA,RPMBETA,BETA,MXP,MYP
      COMMON KXP,KYP,CXP,CYP,PSI,ALIMIT,ALIMIT1,TINC,TINC1,ECCX,ZXXP
      COMMON WSSY,IPZ,KXX,KXY,KYX,KYY,ALAMBDA,ALAMS,CXX,CXY,CYX,CYY,ZYYP
      COMMON F(25,9,9),FB(9,9),AA(9,9),A(9,9),Z(25,9),AC(17,17),BC(17,1)
      COMMON CC(17,1),XR(25),XI(25),XM(25),YR(25),YI(25),YM(25),RMXP
      COMMON THR(25),THI(25),THM(25),PHR(25),PHI(25),PHM(25),BMXR(25)
      COMMON BMXI(25),BMXM(25),BMYR(25),BMYI(25),BMYM(25),SFXR(25)
      COMMON SFXI(25),SFXM(25),SFYR(25),SFYI(25),SFYM(25),AMAJOR(25)
      COMMON BMINOR(25),PHASED(25),ATTD(25),XD(25),YD(25),THD(25)
      COMMON AREA(25),UNBL(10),LOAD(10),CR(10),GM,ALP,ALPHA,KF1,KF2,KF3
      COMMON ISP,IBN,KB1,IF1,IF2,IF3,G,TINC2,RPM1,RPMBT1,PHD(25),RMYP
      COMMON PSID(10),PSIR(10),OMEGAG,OMEGA1,RPMBET1(200),ALIMIT2,ILP
      COMMON BETA1(200),OMEGAT(200),OMEGAC(200),OMEGAW(200),RMOD(200)
      COMMON RMOD1(200),THETAD(200),DETR(200),DETI(200),RNORM(200)
      COMMON XRP(25),XIP(25),YRP(25),YIP(25),GAM,ALIMIT3,V1,V2,KTT,KPP
      COMMON FLEX1
C*****MAIN PROGRAM*****
C     ALL UNITS IMPERIAL
C     SET INTEGER WRITE PARAMETER IWR FOR MAIN PROGRAM
C     1 FOR WRITTING
C     2 FOR NOT WRITTING
C     SET LHS AND RHS SUPPORT PARAMETER ISP
C     1 FOR FREE-PINNED CONDITION
C     2 FOR FREE-FREE CONDITION
      ISP=1
C     SET TYPE OF ANALYSIS PARAMETER IBN
C     1 FOR FORCED RESPONCE ANALYSIS
C     2 FOR STABILITY ANALYSIS(SELF EXCITED RESPONCE AND
C     LEONARD LOCUS)
C     3 FOR MODE SHAPE AT STABILITY THRESHOLD
C     SET IMPEDANCE PARAMETER IPZ
C     1 FOR OIL-FILM
C     2 FOR OIL-FILM+PEDESTAL
C     SET INTEGER GYROSCOPIC PARAMETER IGP
C     1 FOR NON-ZERO GYROSCOPIC TERMS
C     2 FOR ZERO GYROSCOPIC TERMS
C     SET INTEGER PARAMETTER FOR LEONARD LOCUS PLOT ILP
C     1 FOR PLOT NOT REQUIRED
C     2 FOR PLOT REQUIRED
C     SET UNBALANCE PARAMETER IF
C     1 FOR 1ST. UNBALANCE
C     1 FOR 2ND. UNBALANCE
C     1 FOR 3RD. UNBALANCE
      IF1=1
      IF2=1
      IF3=2
C     SET UNBALANCE STATION NUMBERS FROM LEFT TO RIGHT
      KF1=6
      KF2=KF1+1
      KF3=30
C     SET PIE
      PIE=4.*ATAN(1.)
C     SET BEARING LOADS(LBF)
      LOAD(1)=0.
      LOAD(2)=0.
C     SET BEARING CLEARANCES(IN)
      CR(1)=0.
      CR(2)=0.
C     SET BEARING STATION POSITIONS
      KB=3
      KB1=70
C     SET GRAVITY CONSTANT
      G=386.4
C     SET DENSITY OF SHAFT MATERIAL
      POE=0.283
C     SET YOUNGS MODULUS FOR SHAFT
      E=2.98E+07
C     SET SHEAR MODULUS FOR SHAFT
      GM=1.18E+07
C     SET CROSS-SECTION SHAPE FACTOR FOR SHEAR DEFORMATION OF SHAFT
      ALP=0.75
C     READ WRITE,ANALYSIS AND PEDESTAL IMPEDANCE PARAMETERS
C     AND NON-DIM.LOAD AND FEED PRESSURE,CLEARANCE AND PEDESTAL
C     MASS, LINEAR AND ROTARY STIFFNESS IN X-Y DIRS.
      READ(5,*)IWP,IBN,IPZ,WSSY,GAM,C,RMXP,RMYP,KXP,KYP,KTT,KPP
```

```
C     READ INITIAL SPEED,SPEED INCREMENTS,SPEED LIMIT FOR IBN=1,2
C     IN RPM FOR RESPONCE AND STABILITY THRESHOLD
C     AND INITIAL FREQUENCY INCREMENTS AND FREQUENCY INCREMENTS NEAR
C     CRITICAL FREQUENCY FOR IBN=2,IN CPM, FOR STABILITY THRESHOLD
C     AND SHAFT SPEED(RPM) AND WHIP FREQUENCY(CPM) FOR IBN=3,FOR
C     MODE SHAPE AT STABILITY THRESHOLD
      READ(5,*)RPM,TINC,ALIMIT,TINC1,TINC2,RPM1,RPMBT1
C     READ INITIAL NO. OF STATIONS, FLEXIBILITY PARAMETER,
C     INTEGER PARAMETER FOR GYROSCOPIC MOMENTS & LEONARD LOCUS,
C     AND CONSTANTS FOR INITIAL AND FINIAL VALUES OF FREQUENCY FOR
C     IBN=2, AND LOWER AND UPPER VALUES OF CRITICAL SPEED(RPM)
      READ(5,*)KI,FLEX1,IGP,ILP,V1,V2,ALIMIT2,ALIMIT3
C     READ MASS UNBALANCE(LB-IN) & ANGULAR POSITION(DEGREES) AT
C     THE CORRESPONDING STATIONS SET ABOVE
      DO 17 I=1,3
   17 READ(5,*)UNBL(I),PSID(I)
C     CONVERT UNBALANCE ANGLE TO RADIANS
      DO 15 N=1,3
   15 PSIR(N)=PSID(N)*PIE/180.0
C     READ IN NON-DIM. ECCENTRICITY DYNAMIC COEFFICIENTS AND BEARING
C    +LOAD
      DO 1 I=1,9
      READ(5,*)ECC(I),AXX(I),AXY(I),AYX(I),AYY(I),BXX(I),BXY(I),
     +BYX(I),BYY(I),WSS(I)
      IF(IWR.EQ.1)WRITE(6,101)ECC(I),AXX(I),AXY(I),AYX(I),AYY(I),
     +BXX(I),BXY(I),BYX(I),BYY(I),WSS(I)
      ECC1(I)=ECC(I)
      AXX1(I)=AXX(I)
      AXY1(I)=AXY(I)
      AYX1(I)=AYX(I)
      AYY1(I)=AYY(I)
      BXX1(I)=BXX(I)
      BXY1(I)=BXY(I)
      BYX1(I)=BYX(I)
      BYY1(I)=BYY(I)
    1 WSS1(I)=WSS(I)
  101 FORMAT(5X,F2.1,2X,9(F8.4,2X)/)
C     SET FINIAL NO. OF STATTIONS
      KN=KI+1
C     SET NON-DIM. SPEED PARAMETER (RPM)
      OMEGAG=SQRT(G/C)*60./(2.*PIE)
C     SET 1ST. LATERAL BENDING FREQUENCY (CPM)
      OMEGA1=2950.
C     READ IN SHAFT BEND AND SLOPE IN X AND Y DIRS.
C     AND BEAM LENGTH AND DIAMETER AT EACH STATION
      DO 16 I=1,KI
   16 READ(5,107)XD(I),YD(I),THD(I),PHD(I),BEAM(I),DIA(I)
  107 FORMAT(4(E10.4,2X),2(F5.3,2X))
C     SET BEARING DIAMETER
      BDIA=2.5
C     SET BEARING LENGTH
      BLEN=1.25
C     SET DISTANCE OF DISC FROM LHS AND RHS SUPPORTS RESP.
      A1=5.
      B1=22.50
C     SET SHAFT LENGTH BETWEEN SUPPORTS
      SL=27.50
C     SET DIAMETER OF SHAFT
      DI=0.984
C     SET DISC DIAMETER AND LENGTH RESPECTIVELY
      DDIA=6.765
      DLEN=2.950
C     DERIVE DISC MASS(LB)
      WT=PIE*(DDIA**2-DI**2)*DLEN*ROE/4.-0.781
C     DERIVE SHAFT MASS(LB)
      SM=PIE*DI**2*SL*ROE/4.
C     DERIVE BEARING FORCE(LBF)INCLUDING REACTION OF SHAFT AND JOURNAL
      FORCE=WT*B1/SL+(SM-0.343)/2.+2.499
C     DERIVE BEARING SPECIFIC LOAD(PSI)
      BLOAD=FORCE/(BDIA*BLEN)
C     DERIVE STATIC DEFLEECTION AT LOAD
      DELTA=64.*WT*A1**2*B1**2/(3.*E*PIE*DI**4*SL)
C     DERIVE MAX. STATIC DEFLECTION
      DELTMAX=64.*WT*A1*SQRT((SL**2-A1**2)**3)/(15.5884*E*PIE*DI**4*
     +SL)
C     DERIVE POSITION OF MAX. DEFLECTION
      XMAX=SL-SQRT((SL**2-A1**2)/3.)
C     DERIVE POSITION OF MAX. DEFLECTION FROM CENTRE OF SHAFT
      X1=SL/2.-XMAX
C     DERIVE FLEXIBILITY PARAMETER
      FLEX=DELTMAX/C
C     DERIVE ROTOR PINNED-PINNED NATURAL FREQUEENCY(CPM)
      PN=SQRT(G/DELTA)*30./PIE
      IF(IWR.EQ.1)WRITE(6,105)A1,B1,SL,DI,WT,SM
  105 FORMAT(5X,4(F6.3,2X),2(F5.2,2X)/)
```

```
      IF(IWP.EQ.1)WRITE(6,106)DELTA,DELTMAX,XMAX,X1,FLEX,PN
  106 FORMAT(5X,2(F5.4,2X),F5.2,2X,2(F4.2,2X),F7.2/)
      IF(IWP.EQ.1)WRITE(6,102)FORCE,BLOAD,C,UNBL(1),UNBL(2)
  102 FORMAT(5X,2(F5.2,2X),3(F5.4,2X)/)
      DO 12 KP=1,KI
C     DERIVE AREA OF SHAFT AT EACH STATION
      AREA(KP)=PIE*DIA(KP)**2/4.
C     DERIVE MASS AT EACH STATION
      AMASS(KP)=AREA(KP)*BEAM(KP)*ROE
C     DERIVE CROSS-SECTIONAL M. I. AT EACH STATION
   12 SI(KP)=PIE*DIA(KP)**4/64.
C     SET POLAR AND TRANSVERSE INERTIA AT STATION 1 TO ZERO
      PI(1)=0.
      TI(1)=0.
      DO 13 KP=2,KI
C     DERIVE MASS AT LAST STATION
      IF(KP.EQ.KI)AMASS(KP)=AMASS(KP)/2.
      IF(KP.EQ.KI)GO TO 14
C     LUMP MASS TO LEFT AND RIGHT AT EACH STATION
      AMASS(KP)=(AMASS(KP)+AMASS(KP+1))/2.
C     DERIVE POLAR AND TRANSVERSE INERTIA AT EACH STATION
   14 PI(KP)=AMASS(KP)*DIA(KP)**2/8.
      TI(KP)=AMASS(KP)*(DIA(KP)**2/16.+BEAM(KP)**2/12.)
      IF(IGP.NE.1)PI(KP)=0.0
   13 IF(IGP.NE.1)TI(KP)=0.0
      NCOUNT=0
      DO 11 KP=1,KI
      NCOUNT=NCOUNT+1
      IF(IWP.EQ.1)WRITE(6,110)NCOUNT,BEAM(KP),DIA(KP),AMASS(KP),
     +SI(KP),PI(KP),TI(KP),XD(KP),YD(KP),THD(KP),PHD(KP)
   11 CONTINUE
  110 FORMAT(5X,I2,2(2X,F5.3),8(2X,1PE12.4)/)
C     DIVIDE STATION MASS(LB) POLAR & TRANSVERSE INERTIAS(LB-IN2)
C     BY GRAVITY
      DO 18 KP=1,KI
      AMASS(KP)=AMASS(KP)/G
      PI(KP)=PI(KP)/G
   18 TI(KP)=TI(KP)/G
C     DIVIDE PEDESTAL MASS(LB) IN X AND Y DIRECTIONS BY GRAVITY
      MXP=RMXP/G
      MYP=RMYP/G
C     SET PEDESTAL DAMPING IN X AND Y DIRECTIONS
      CXP=0.
      CYP=0.
C     CALL INTERPOLATION ROUTINE
      CALL INTERP
      CALL SPEED
      STOP
      END
      SUBROUTINE INTERP
      COMPLEX F,FB,AA,A,Z,ZXX,ZXY,ZYX,ZYY,ZXXF,ZXYF,ZYXF,ZYYF,ZXXP,ZXYP
      COMPLEX ZYXP,ZYYP,CPSI,SUM,ALAMBDA,ALAMS,C1,C2,C3,C4,C5,C6,C7,C8
      COMPLEX C9,C10,C11,AC,BC,CC,BHFX,BHFY,BFFY,BFFY,XP,YP
      COMPLEX ZTT,ZTP,ZPT,ZPP
      REAL KXX,KXY,KYX,KYY,KXP,KYP,MXP,MYP,LOAD,MEER,KTT,KPP
      COMMON ECC(10),AXX(10),AXY(10),AYX(10),AYY(10),BXX(10),BXY(10)
      COMMON BYX(10),BYY(10),WSS(10),AXX1(10),AXY1(10),AYX1(10)
      COMMON AYY1(10),BXX1(10),BXY1(10),BYX1(10),BYY1(10),ECC1(10)
      COMMON WSS1(10),DIA(25),BEAM(25),SI(25),AMASS(25),PI(25),TI(25)
      COMMON PIE,C,FORCE,E,KI,KN,KS,KB,KF,RPM,OMEGA,RPMBETA,BETA,MXP,MYP
      COMMON KXP,KYP,CXP,CYP,PSI,ALIMIT,ALIMIT1,TINC,TINC1,ECCX,ZXXP
      COMMON WSSY,IPZ,KXX,KXY,KYX,KYY,ALAMBDA,ALAMS,CXX,CXY,CYX,CYY,ZYYP
      COMMON F(25,9,9),FB(9,9),AA(9,9),A(9,9),Z(25,9),AC(17,17),BC(17,1)
      COMMON CC(17,1),XR(25),XI(25),XM(25),YR(25),YI(25),YM(25),RMXP
      COMMON THR(25),THI(25),THM(25),PHR(25),PHI(25),PHM(25),BMXR(25)
      COMMON BMXI(25),BMXM(25),BMYR(25),BMYI(25),BMYM(25),SFXR(25)
      COMMON SFXI(25),SFXM(25),SFYR(25),SFYI(25),SFYM(25),AMAJOR(25)
      COMMON BMINOR(25),PHASED(25),ATTD(25),XD(25),YD(25),THD(25)
      COMMON AREA(25),UNBL(10),LOAD(10),CR(10),GM,ALP,ALPHA,KF1,KF2,KF3
      COMMON ISP,IBN,KB1,IF1,IF2,IF3,G,TINC2,RPM1,RPMBT1,PHD(25),RMYP
      COMMON PSID(10),PSIR(10),OMEGAG,OMEGA1,RPMBET1(200),ALIMIT2,ILP
      COMMON BETA1(200),OMEGAT(200),OMEGAC(200),OMEGAW(200),RMOD(200)
      COMMON RMOD1(200),THETAD(200),DETR(200),DETI(200),RNORM(200)
      COMMON XRP(25),XIP(25),YRP(25),YIP(25),GAM,ALIMIT3,V1,V2,KTT,KPP
      COMMON FLEX1
      DIMENSION RC(40)
C*****PROGRAM TO INTERPOLATE STIFFNESS AND DAMPING COEFFICIENTS*****
      I1=9
      NB=8
      N1=NB+1
      N2=NB*(NB+1)/2
C     CALL ROUTINE E01AAF TO INTERPOLATE ECCENTRICITY FROM LOAD
      CALL E01AAF(WSS,ECC,RC,N1,N2,NB,WSSY)
      ECCX=RC(N2)
      DO 14 I=1,I1
```

```
      WSS(I)=WSS1(I)                                                    INTERP
   14 ECC(I)=ECC1(I)                                                    INTERP
C     CALL ROUTINE E01AAF TO INTERPOLATE DYNAMIC COEFFICIENTS           INTERP
C     FROM ECCENTRICITY                                                 INTERP
      CALL E01AAF(ECC,AXX,RC,N1,N2,NB,ECCX)                             INTERP
      KXX=RC(N2)                                                        INTERP
      DO 15 I=1,I1                                                      INTERP
      ECC(I)=ECC1(I)                                                    INTERP
   15 AXX(I)=AXX1(I)                                                    INTERP
      CALL E01AAF(ECC,AXY,RC,N1,N2,NB,ECCX)                             INTERP
      KXY=RC(N2)                                                        INTERP
      DO 16 I=1,I1                                                      INTERP
      ECC(I)=ECC1(I)                                                    INTERP
   16 AXY(I)=AXY1(I)                                                    INTERP
      CALL E01AAF(ECC,AYX,RC,N1,N2,NB,ECCX)                             INTERP
      KYX=RC(N2)                                                        INTERP
      DO 17 I=1,I1                                                      INTERP
      ECC(I)=ECC1(I)                                                    INTERP
   17 AYX(I)=AYX1(I)                                                    INTERP
      CALL FO1AAF(ECC,AYY,RC,N1,N2,NB,ECCX)                             INTERP
      KYY=RC(N2)                                                        INTERP
      DO 18 I=1,I1                                                      INTERP
      ECC(I)=ECC1(I)                                                    INTERP
   18 AYY(I)=AYY1(I)                                                    INTERP
      CALL E01AAF(ECC,BXX,RC,N1,N2,NB,ECCX)                             INTERP
      CXX=RC(N2)                                                        INTERP
      DO 19 I=1,I1                                                      INTERP
      ECC(I)=ECC1(I)                                                    INTERP
   19 BXX(I)=BXX1(I)                                                    INTERP
      CALL E01AAF(ECC,BXY,RC,N1,N2,NB,ECCX)                             INTERP
      CXY=RC(N2)                                                        INTERP
      DO 20 I=1,I1                                                      INTERP
      ECC(I)=ECC1(I)                                                    INTERP
   20 BXY(I)=BXY1(I)                                                    INTERP
      CALL E01AAF(ECC,BYX,PC,N1,N2,NB,ECCX)                             INTERP
      CYX=RC(N2)                                                        INTERP
      DO 21 I=1,I1                                                      INTERP
      ECC(I)=ECC1(I)                                                    INTERP
   21 BYX(I)=BYX1(I)                                                    INTERP
      CALL E01AAF(ECC,BYY,RC,N1,N2,NB,ECCX)                             INTERP
      CYY=RC(N2)                                                        INTERP
      DO 22 I=1,I1                                                      INTERP
      ECC(I)=ECC1(I)                                                    INTERP
   22 BYY(I)=BYY1(I)                                                    INTERP
      WRITE(6,100)GAM,C,ECCX,KXX,KXY,KYX,KYY,CXX,CXY,CYX,CYY,WSSY       INTERP
  100 FORMAT(5X,F3.1,2X,F5.4,10(2X,F8.4)/)                              INTERP
      WRITE(6,101)FLEX1,RMXP,RMYP,KXP,KYP,KTT,KPP                       INTERP
  101 FORMAT(5X,F5.2,2X,2(F6.3,2X),4(1PE10.3,2X)/)                      INTERP
      RETURN                                                            INTERP
      END                                                               INTERP
      SUBROUTINE SPEED                                                  SPEED
      COMPLEX F,FB,AA,A,Z,ZXX,ZXY,ZYX,ZYY,ZXXF,ZXYF,ZYXF,ZYYF,ZXXP,ZXYP COM1
      COMPLEX ZYXP,ZYYP,CPSI,SUM,ALAMBDA,ALAMS,C1,C2,C3,C4,C5,C6,C7,C8  COM1
      COMPLEX C9,C10,C11,AC,BC,CC,BHFX,BHFY,BFFX,BFFY,XP,YP             COM1
      COMPLEX ZTT,ZTP,ZPT,ZPP                                           COM1
      REAL KXX,KXY,KYX,KYY,KXP,KYP,MXP,MYP,LOAD,MEER,KTT,KPP            COM1
      COMMON ECC(10),AXX(10),AXY(10),AYX(10),AYY(10),BXX(10),BXY(10)    COM1
      COMMON BYX(10),BYY(10),WSS(10),AXX1(10),AXY1(10),AYX1(10)         COM1
      COMMON AYY1(10),BXX1(10),BXY1(10),BYX1(10),BYY1(10),ECC1(10)      COM1
      COMMON WSS1(10),DIA(25),BEAM(25),SI(25),AMASS(25),PI(25),TI(25)   COM1
      COMMON PIE,C,FORCE,E,KI,KN,KS,KB,KF,RPM,OMEGA,RPMBETA,BETA,MXP,MYP COM1
      COMMON KXP,KYP,CXP,CYP,PSI,ALIMIT,ALIMIT1,TINC,TINC1,ECCX,ZXXP    COM1
      COMMON WSSY,IPZ,KXX,KXY,KYX,KYY,ALAMBDA,ALAMS,CXX,CXY,CYX,CYY,ZYYP COM1
      COMMON F(25,9,9),FB(9,9),AA(9,9),A(9,9),Z(25,9),AC(17,17),BC(17,1) COM1
      COMMON CC(17,1),XR(25),XI(25),XM(25),YR(25),YI(25),YM(25),RMXP    COM1
      COMMON THR(25),THI(25),THM(25),PHR(25),PHI(25),PHM(25),BMXR(25)   COM1
      COMMON BMXI(25),BMXM(25),BMYR(25),BMYI(25),BMYM(25),SFXR(25)      COM1
      COMMON SFXI(25),SFXM(25),SFYR(25),SFYI(25),SFYM(25),AMAJOR(25)    COM1
      COMMON BMINOR(25),PHASED(25),ATTD(25),XD(25),YD(25),THD(25)       COM1
      COMMON AREA(25),UNBL(10),LOAD(10),CR(10),GM,ALP,ALPHA,KF1,KF2,KF3 COM1
      COMMON ISP,IBN,KB1,IF1,IF2,IF3,G,TINC2,RPM1,RPMBT1,PHD(25),RMYP   COM1
      COMMON PSID(10),PSIR(10),OMEGAG,OMEGA1,RPMBET1(200),ALIMIT2,ILP   COM1
      COMMON BETA1(200),OMEGAT(200),OMEGAC(200),OMEGAW(200),RMOD(200)   COM1
      COMMON RMOD1(200),THETAD(200),DETR(200),DETI(200),RNORM(200)      COM1
      COMMON XRP(25),XIP(25),YRP(25),YIP(25),GAM,ALIMIT3,V1,V2,KTT,KPP  COM1
      COMMON FLEX1                                                      COM1
C*****PROGRAM TO SET SHAFT SPEED AND FREQUENCY*****                     SPEED
C     SET ARRAYS TO ZERO                                                SPEED
      DO 13 KS=1,KN                                                     SPEED
      DO 13 J=1,9                                                       SPEED
      Z(KS,J)=(0.,0.)                                                   SPEED
      DO 13 K=1,9                                                       SPEED
   13 F(KS,J,K)=(0.,0.)                                                 SPEED
C     VARY NUMBER OF STATIONS                                           SPEED
      DO 99 KS=KI,KN                                                    SPEED
```

```
      IF(KS.GT.KI)GO TO 98
C     SET INITIAL COMPLEX VARIABLE LAMBDA EIGENVALUES TO ZERO
C     REAL PART(1/SEC)
      ALPHA=0.
C     IMAGINARY PART(RADS/SEC)
      BETA=0.
C     SET LOOP COUNTER FOR NO. OF STABILITY RUNS TO ZERO
      NSTOP=0
C     SET NO. OF CHECKS FOR INSTABILITY FROM THRESHOLD BOUNDARY
      NCHECK=2
   11 RPM=RPM+TINC
      IF(IBN.EQ.2.AND.NSTOP.GE.NCHECK)GO TO 99
      IF(RPM.GT.ALIMIT)GO TO 99
C     SHAFT SPEED IN RADIANS/SEC.
      OMEGA=2.*PIE*RPM/60.
      IF(IBN.EQ.3)OMEGA=2.*PIE*RPM1/60.
      IF(IBN.EQ.3)BETA=2.*PIE*RPMBT1/60.
      IF(IBN.EQ.3)WRITE(6,101)RPM1,RPMBT1
  101 FORMAT(5X,2(F7.2,2X)/)
      IF(IBN.EQ.3)GO TO 10
C     DERIVE NON-DIM. SPEED RATIOS
      RPMT=RPM/OMEGAG
      RPMC=RPM/OMEGA1
      WRITE(6,100)RPM,OMEGA,RPMT,RPMC
      IF(IBN.EQ.1)BETA=OMEGA
      IF(IBN.EQ.1)GO TO 10
C     SET FREQUENCY LIMIT
      ALIMIT1=V2*OMEGA
C     SET INITIAL FREQUENCY RPM
      RPMBETA=V1*RPM
C     SET FREQUENCY COUNTER
      NW=0
C     SET FREQUENCY INCREMENTS RPM
   28 TINC3=TINC1
      NW=NW+1
      IF(RPMBETA.GE.ALIMIT2.AND.RPMBETA.LE.ALIMIT3)TINC3=TINC2
      RPMBETA=RPMBETA+TINC3
      RPMBET1(NW)=RPMBETA
      BETA=2.*PIE*RPMBETA/60.
      BETA1(NW)=BETA
      IF(BETA.GT.ALIMIT1)NW=NW-1
      IF(BETA.GT.ALIMIT1)CALL LEONARD(NW,NSTOP)
      IF(BETA.GT.ALIMIT1)GO TO 11
C     DERIVE COMPLEX LAMBDA EIGENVALUES
   10 ALAMBDA=CMPLX(ALPHA,BETA)
      ALAMS=ALAMBDA**2
      CALL MATRIX
      IF(IBN.EQ.1)I1=9
      IF(IBN.EQ.2.OR.IBN.EQ.3)I1=8
      CALL MULT(I1)
      IF(IBN.EQ.3)CALL MODES
      IF(IBN.EQ.3)GO TO 99
      IF(IBN.EQ.2)CALL DETERM(NW)
      IF(IBN.EQ.2)GO TO 28
      IF(IBN.EQ.1)CALL RESP
      IF(IPZ.EQ.1)GO TO 11
      CALL SUPPORT
      GO TO 11
   99 CONTINUE
  100 FORMAT(5X,F8.2,2X,F7.2,2(2X,F5.3)/)
   98 RETURN
      END
      SUBROUTINE MATRIX
      COMPLEX F,FB,AA,A,Z,ZXX,ZXY,ZYX,ZYY,ZXXF,ZXYF,ZYXF,ZYYF,ZXXP,ZXYP
      COMPLEX ZYXP,ZYYP,CPSI,SUM,ALAMBDA,ALAMS,C1,C2,C3,C4,C5,C6,C7,C8
      COMPLEX C9,C10,C11,AC,BC,CC,BHFX,BHFY,BFFX,BFFY,XP,YP
      COMPLEX ZTT,ZTP,ZPT,ZPP
      REAL KXX,KXY,KYX,KYY,KXP,KYP,MXP,MYP,LOAD,MEER,KTT,KPP
      COMMON ECC(10),AXX(10),AXY(10),AYX(10),AYY(10),BXX(10),BXY(10)
      COMMON BYX(10),BYY(10),WSS(10),AXX1(10),AXY1(10),AYX1(10)
      COMMON AYY1(10),BXX1(10),BXY1(10),BYX1(10),BYY1(10),ECC1(10)
      COMMON WSS1(10),DIA(25),BEAM(25),SI(25),AMASS(25),PI(25),TI(25)
      COMMON PIE,C,FORCE,E,KI,KN,KS,KB,KF,RPM,OMEGA,RPMBETA,BETA,MXP,MYP
      COMMON KXP,KYP,CXP,CYP,PSI,ALIMIT,ALIMIT1,TINC,TINC1,ECCX,ZXXP
      COMMON WSSY,IPZ,KXX,KXY,KYX,KYY,ALAMBDA,ALAMS,CXX,CXY,CYX,CYY,ZYYP
      COMMON F(25,9,9),FB(9,9),AA(9,9),A(9,9),Z(25,9),AC(17,17),BC(17,1)
      COMMON CC(17,1),XR(25),XI(25),XM(25),YR(25),YI(25),YM(25),RMXP
      COMMON THR(25),THI(25),THM(25),PHR(25),PHI(25),PHM(25),BMXR(25)
      COMMON BMXI(25),BMXM(25),BMYR(25),BMYI(25),BMYM(25),SFXR(25)
      COMMON SFXI(25),SFXM(25),SFYR(25),SFYI(25),SFYM(25),AMAJOR(25)
      COMMON BMINOR(25),PHASED(25),ATTD(25),XD(25),YD(25),THD(25)
      COMMON AREA(25),UNBL(10),LOAD(10),CR(10),GM,ALP,ALPHA,KF1,KF2,KF3
      COMMON ISP,IBN,KB1,IF1,IF2,IF3,G,TINC2,RPM1,RPMBT1,PHD(25),RMYP
      COMMON PSID(10),PSIR(10),OMEGAG,OMEGA1,RPMBET1(200),ALIMIT2,ILP
      COMMON BETA1(200),OMEGAT(200),OMEGAC(200),OMEGAW(200),RMOD(200)
```

```
      COMMON RMOD1(200),THETAD(200),DETR(200),DETI(200),RNORM(200)      COM1
      COMMON XRP(25),XIP(25),YRP(25),YIP(25),GAM,ALIMIT3,V1,V2,KTT,KPP  COM1
      COMMON FLEX1                                                      COM1
C*****PROGRAM TO DERIVE TRANSFER MATRIX AT EACH SHAFT STATION******     MATRIX
C     SET UP STANDARD TRANSFER MATRICES AT STATIONS 2 TO KS             MATRIX
      DO 12 K=2,KS                                                      MATRIX
C     SET BEARING LINEAR AND ROTORY IMPEDANCE TO ZERO                   MATRIX
      ZXX=(0.,0.)                                                       MATRIX
      ZXY=(0.,0.)                                                       MATRIX
      ZYX=(0.,0.)                                                       MATRIX
      ZYY=(0.,0.)                                                       MATRIX
      ZTT=(0.,0.)                                                       MATRIX
      ZTP=(0.,0.)                                                       MATRIX
      ZPT=(0.,0.)                                                       MATRIX
      ZPP=(0.,0.)                                                       MATRIX
      IF(ISP.EQ.1)GO TO 14                                              MATRIX
      IF(K.NE.KB)GO TO 19                                               MATRIX
      KXX=AXX(1)                                                        MATRIX
      KXY=AXY(1)                                                        MATRIX
      KYX=AYX(1)                                                        MATRIX
      KYY=AYY(1)                                                        MATRIX
      CXX=BXX(1)                                                        MATRIX
      CXY=BXY(1)                                                        MATRIX
      CYX=BYX(1)                                                        MATRIX
      CYY=BYY(1)                                                        MATRIX
      C=CR(1)                                                           MATRIX
      FORCE=LOAD(1)                                                     MATRIX
      GO TO 15                                                          MATRIX
   19 IF(K.NE.KB1)GO TO 16                                              MATRIX
      KXX=AXX(2)                                                        MATRIX
      KXY=AXY(2)                                                        MATRIX
      KYX=AYX(2)                                                        MATRIX
      KYY=AYY(2)                                                        MATRIX
      CXX=BXX(2)                                                        MATRIX
      CXY=BXY(2)                                                        MATRIX
      CYX=BYX(2)                                                        MATRIX
      CYY=BYY(2)                                                        MATRIX
      C=CR(2)                                                           MATRIX
      FORCE=LOAD(2)                                                     MATRIX
      GO TO 15                                                          MATRIX
   14 IF(K.NE.KB)GO TO 16                                               MATRIX
C     DERIVE OIL-FILM BEARING IMPEDANCE                                 MATRIX
   15 ZXXF=FORCE/C*(KXX+ALAMBDA/OMEGA*CXX)                              MATRIX
      ZXYF=FORCE/C*(KXY+ALAMBDA/OMEGA*CXY)                              MATRIX
      ZYXF=FORCE/C*(KYX+ALAMBDA/OMEGA*CYX)                              MATRIX
      ZYYF=FORCE/C*(KYY+ALAMBDA/OMEGA*CYY)                              MATRIX
      IF(IPZ.EQ.1)GO TO 10                                              MATRIX
C     DERIVE PEDESTAL IMPEDANCE                                         MATRIX
      ZXXP=MXP*ALAMS+KXP+ALAMBDA*CXP                                    MATRIX
      ZYYP=MYP*ALAMS+KYP+ALAMBDA*CYP                                    MATRIX
C     DERIVE BEARING AND PEDESTAL IMPEDANCE                             MATRIX
      ZXX=ZXXF*ZXXP/(ZXXF+ZXXP)                                         MATRIX
      ZYY=ZYYF*ZYYP/(ZYYF+ZYYP)                                         MATRIX
      GO TO 13                                                          MATRIX
C     SET IMPEDANCE TO OIL-FILM IMPEDANCE                               MATRIX
   10 ZXX=ZXXF                                                          MATRIX
      ZYY=ZYYF                                                          MATRIX
   13 ZXY=ZXYF                                                          MATRIX
      ZYX=ZYXF                                                          MATRIX
   16 F(K,1,1)=(1.,0.)                                                  MATRIX
      F(K,1,2)=BEAM(K)*F(K,1,1)                                         MATRIX
      F(K,1,3)=BEAM(K)**2/(2.*E*SI(K))*F(K,1,1)                         MATRIX
      F(K,1,4)=(BEAM(K)**3/(6.*E*SI(K))-BEAM(K)/(ALP*AREA(K)*GM))*      MATRIX
     +F(K,1,1)                                                          MATRIX
      F(K,1,9)=XD(K)*F(K,1,1)                                           MATRIX
      F(K,2,2)=F(K,1,1)                                                 MATRIX
      F(K,2,3)=BEAM(K)/(E*SI(K))*F(K,1,1)                               MATRIX
      F(K,2,4)=F(K,1,3)                                                 MATRIX
      F(K,2,9)=THD(K)*F(K,1,1)                                          MATRIX
      C1=TI(K)*ALAMS+ZTT                                                MATRIX
      F(K,3,2)=CMPLX(REAL(C1),AIMAG(C1))                                MATRIX
      C2=1.+C1*F(K,2,3)                                                 MATRIX
      F(K,3,3)=CMPLX(REAL(C2),AIMAG(C2))                                MATRIX
      C2=BEAM(K)*(2.+C1*F(K,2,3))/2.                                    MATRIX
      F(K,3,4)=CMPLX(REAL(C2),AIMAG(C2))                                MATRIX
      C1=-OMEGA*PI(K)*ALAMBDA+ZTP                                       MATRIX
      F(K,3,6)=CMPLX(REAL(C1),AIMAG(C1))                                MATRIX
      C2=C1*F(K,2,3)                                                    MATRIX
      F(K,3,7)=CMPLX(REAL(C2),AIMAG(C2))                                MATRIX
      C2=C1*F(K,1,3)                                                    MATRIX
      F(K,3,8)=CMPLX(REAL(C2),AIMAG(C2))                                MATRIX
      C1=THD(K)*F(K,3,2)+PHD(K)*F(K,3,6)                                MATRIX
      F(K,3,9)=CMPLX(REAL(C1),AIMAG(C1))                                MATRIX
      C1=-(AMASS(K)*ALAMS+ZXX)                                          MATRIX
      F(K,4,1)=CMPLX(REAL(C1),AIMAG(C1))                                MATRIX
```

```
      C2=C1*F(K,1,2)
      F(K,4,2)=CMPLX(REAL(C2),AIMAG(C2))
      C2=C1*F(K,1,3)
      F(K,4,3)=CMPLX(REAL(C2),AIMAG(C2))
      C2=1.+C1*F(K,1,4)
      F(K,4,4)=CMPLX(REAL(C2),AIMAG(C2))
      C1=ZXY
      F(K,4,5)=CMPLX(REAL(C1),AIMAG(C1))
      C2=C1*F(K,1,2)
      F(K,4,6)=CMPLX(REAL(C2),AIMAG(C2))
      C2=C1*F(K,1,3)
      F(K,4,7)=CMPLX(REAL(C2),AIMAG(C2))
      C2=C1*F(K,1,4)
      F(K,4,8)=CMPLX(REAL(C2),AIMAG(C2))
C     SET MASS UNBALANCE  RESPONCE TO ZERO IN X DIR.
      C2=(0.,0.)
      MEER=0.
      PSI=0.
      IF(K.NE.KF1.AND.K.NE.KF2.AND.K.NE.KF3)GO TO 17
      IF(K.EQ.KF1.AND.IF1.EQ.1)MEER=UNBL(1)/G
      IF(K.EQ.KF2.AND.IF2.EQ.1)MEER=UNBL(2)/G
      IF(K.EQ.KF3.AND.IF3.EQ.1)MEER=UNBL(3)/G
      IF(K.EQ.KF1.AND.IF1.EQ.1)PSI=PSIR(1)
      IF(K.EQ.KF2.AND.IF2.EQ.1)PSI=PSIR(2)
      IF(K.EQ.KF3.AND.IF3.EQ.1)PSI=PSIR(3)
      CPSI=CMPLX(COS(PSI),SIN(PSI))
      C1=MEER*OMEGA**2
      C2=-C1*CPSI
   17 C3=C2+XD(K)*F(K,4,1)+YD(K)*F(K,4,5)
      F(K,4,9)=CMPLX(REAL(C3),AIMAG(C3))
      F(K,5,5)=F(K,1,1)
      F(K,5,6)=F(K,1,2)
      F(K,5,7)=F(K,1,3)
      F(K,5,8)=F(K,1,4)
      F(K,5,9)=YD(K)*F(K,1,1)
      F(K,6,6)=F(K,1,1)
      F(K,6,7)=F(K,2,3)
      F(K,6,8)=F(K,1,3)
      F(K,6,9)=PHD(K)*F(K,1,1)
      C1=OMEGA*PI(K)*ALAMBDA+ZPT
      F(K,7,2)=CMPLX(REAL(C1),AIMAG(C1))
      C2=C1*F(K,2,3)
      F(K,7,3)=CMPLX(REAL(C2),AIMAG(C2))
      C2=C1*F(K,1,3)
      F(K,7,4)=CMPLX(REAL(C2),AIMAG(C2))
      C1=TI(K)*ALAMS+ZPP
      F(K,7,6)=CMPLX(REAL(C1),AIMAG(C1))
      C2=1.+C1*F(K,2,3)
      F(K,7,7)=CMPLX(REAL(C2),AIMAG(C2))
      C2=BEAM(K)*(2.+C1*F(K,2,3))/2.
      F(K,7,8)=CMPLX(REAL(C2),AIMAG(C2))
      C1=THD(K)*F(K,7,2)+PHD(K)*F(K,7,6)
      F(K,7,9)=CMPLX(REAL(C1),AIMAG(C1))
      C1=ZYX
      F(K,8,1)=CMPLX(REAL(C1),AIMAG(C1))
      C2=C1*F(K,1,2)
      F(K,8,2)=CMPLX(REAL(C2),AIMAG(C2))
      C2=C1*F(K,1,3)
      F(K,8,3)=CMPLX(REAL(C2),AIMAG(C2))
      C2=C1*F(K,1,4)
      F(K,8,4)=CMPLX(REAL(C2),AIMAG(C2))
      C1=-(AMASS(K)*ALAMS+ZYY)
      F(K,8,5)=CMPLX(REAL(C1),AIMAG(C1))
      C2=C1*F(K,1,2)
      F(K,8,6)=CMPLX(REAL(C2),AIMAG(C2))
      C2=C1*F(K,1,3)
      F(K,8,7)=CMPLX(REAL(C2),AIMAG(C2))
      C2=1.+C1*F(K,1,4)
      F(K,8,8)=CMPLX(REAL(C2),AIMAG(C2))
C     SET MASS UNBALANCE RESPONCE TO ZERO IN Y DIR.
      C2=(0.,0.)
      MEER=0.
      PSI=0.
      IF(K.NE.KF1.AND.K.NE.KF2.AND.K.NE.KF3)GO TO 18
      IF(K.EQ.KF1.AND.IF1.EQ.1)MEER=UNBL(1)/G
      IF(K.EQ.KF2.AND.IF2.EQ.1)MEER=UNBL(2)/G
      IF(K.EQ.KF3.AND.IF3.EQ.1)MEER=UNBL(3)/G
      IF(K.EQ.KF1.AND.IF1.EQ.1)PSI=PSIR(1)
      IF(K.EQ.KF2.AND.IF2.EQ.1)PSI=PSIR(2)
      IF(K.EQ.KF3.AND.IF3.EQ.1)PSI=PSIR(3)
      CPSI=CMPLX(SIN(PSI),-COS(PSI))
      C1=MEER*OMEGA**2
      C2=C1*CPSI
   18 C3=C2+XD(K)*F(K,8,1)+YD(K)*F(K,8,5)
      F(K,8,9)=CMPLX(REAL(C3),AIMAG(C3))
```

```
   12 F(K,9,9)=F(K,1,1)                                                    MATRIX   171
      RETURN                                                               MATRIX   172
      END                                                                  MATRIX   173
      SUBROUTINE MULT(I1)                                                  MULT       2
      COMPLEX F,FB,AA,A,Z,ZXX,ZXY,ZYX,ZYY,ZXXF,ZXYF,ZYXF,ZYYF,ZXXP,ZXYP    COM1       2
      COMPLEX ZYXP,ZYYP,CPSI,SUM,ALAMBDA,ALAMS,C1,C2,C3,C4,C5,C6,C7,C8     COM1       3
      COMPLEX C9,C10,C11,AC,BC,CC,BHFX,BHFY,BFFX,BFFY,XP,YP                COM1       4
      COMPLEX ZTT,ZTP,ZPT,ZPP                                              COM1       5
      REAL KXX,KXY,KYX,KYY,KXP,KYP,MXP,MYP,LOAD,MEER,KTT,KPP               COM1       6
      COMMON ECC(10),AXX(10),AXY(10),AYX(10),AYY(10),BXX(10),BXY(10)       COM1       7
      COMMON BYX(10),BYY(10),WSS(10),AXX1(10),AXY1(10),AYX1(10)            COM1       8
      COMMON AYY1(10),BXX1(10),BXY1(10),BYX1(10),BYY1(10),ECC1(10)         COM1       9
      COMMON WSS1(10),DIA(25),BEAM(25),SI(25),AMASS(25),PI(25),TI(25)      COM1      10
      COMMON PIE,C,FORCE,E,KI,KN,KS,KB,KF,RPM,OMEGA,RPMBETA,BETA,MXP,MYP   COM1      11
      COMMON KXP,KYP,CXP,CYP,PSI,ALIMIT,ALIMIT1,TINC,TINC1,ECCX,ZXXP       COM1      12
      COMMON WSSY,IPZ,KXX,KXY,KYX,KYY,ALAMBDA,ALAMS,CXX,CXY,CYX,CYY,ZYYP   COM1      13
      COMMON F(25,9,9),FB(9,9),AA(9,9),A(9,9),Z(25,9),AC(17,17),BC(17,1)   COM1      14
      COMMON CC(17,1),XR(25),XI(25),XM(25),YR(25),YI(25),YM(25),RMXP       COM1      15
      COMMON THR(25),THI(25),THM(25),PHR(25),PHI(25),PHM(25),BMXR(25)      COM1      16
      COMMON BMXI(25),BMXM(25),BMYR(25),BMYI(25),BMYM(25),SFXR(25)         COM1      17
      COMMON SFXI(25),SFXM(25),SFYP(25),SFYI(25),SFYM(25),AMAJOR(25)       COM1      18
      COMMON BMINOR(25),PHASED(25),ATTD(25),XD(25),YD(25),THD(25)          COM1      19
      COMMON AREA(25),UNBL(10),LOAD(10),CR(10),GM,ALP,ALPHA,KF1,KF2,KF3    COM1      20
      COMMON ISP,IRN,KB1,IF1,IF2,IF3,G,TINC2,RPM1,RPMBT1,PHD(25),RMYP      COM1      21
      COMMON PSID(10),PSIR(10),OMEGAG,OMEGA1,RPMBET1(200),ALIMIT2,ILP      COM1      22
      COMMON BETA1(200),OMEGAT(200),OMEGAC(200),OMEGAW(200),RMOD(200)      COM1      23
      COMMON RMOD1(200),THETAD(200),DETR(200),DETI(200),RNORM(200)         COM1      24
      COMMON XRP(25),XIP(25),YRP(25),YIP(25),GAM,ALIMIT3,V1,V2,KTT,KPP     COM1      25
      COMMON FLEX1                                                         COM1      26
C*****PROGRAM TO MULTIPLY TRANSFER MATRICES*****                           MULT       4
C     CARRYOUT ABRIDGED MATRIX MULT. OMITTING COLUMNS 3,4,7 AND 8          MULT       5
C     TO GIVE FREE BOUNDARY CONDITION AT STATION 1                         MULT       6
C     OBTAIN TRANSFER MATRIX FOR STATIONS 2 AND 3                          MULT       7
      DO 5 J=1,I1                                                          MULT       8
      DO 5 K=1,I1                                                          MULT       9
      IF(K.EQ.3)GO TO 5                                                    MULT      10
      IF(K.EQ.4)GO TO 5                                                    MULT      11
      IF(K.EQ.7)GO TO 5                                                    MULT      12
      IF(K.EQ.8)GO TO 5                                                    MULT      13
      SUM=(0.,0.)                                                          MULT      14
      DO 6 L=1,I1                                                          MULT      15
    6 SUM=SUM+F(3,J,L)*F(2,L,K)                                            MULT      16
      FB(J,K)=SUM                                                          MULT      17
    5 CONTINUE                                                             MULT      18
C     OBTAIN TRANSFER MATRIX FOR COMPLETE SHAFT                            MULT      19
      DO 7 M=4,KS                                                          MULT      20
      DO 8 J=1,I1                                                          MULT      21
      DO 8 K=1,I1                                                          MULT      22
      IF(K.EQ.3)GO TO 8                                                    MULT      23
      IF(K.EQ.4)GO TO 8                                                    MULT      24
      IF(K.EQ.7)GO TO 8                                                    MULT      25
      IF(K.EQ.8)GO TO 8                                                    MULT      26
      SUM=(0.,0.)                                                          MULT      27
      DO 9 L=1,I1                                                          MULT      28
    9 SUM=SUM+F(M,J,L)*FB(L,K)                                             MULT      29
      AA(J,K)=SUM                                                          MULT      30
    8 CONTINUE                                                             MULT      31
      DO 10 J=1,I1                                                         MULT      32
      DO 10 K=1,I1                                                         MULT      33
      IF(K.EQ.3)GO TO 10                                                   MULT      34
      IF(K.EQ.4)GO TO 10                                                   MULT      35
      IF(K.EQ.7)GO TO 10                                                   MULT      36
      IF(K.EQ.8)GO TO 10                                                   MULT      37
      FB(J,K)=AA(J,K)                                                      MULT      38
   10 CONTINUE                                                             MULT      39
    7 CONTINUE                                                             MULT      40
      RETURN                                                               MULT      41
      END                                                                  MULT      42
      SUBROUTINE MULT1(I1)                                                 MULT1      2
      COMPLEX F,FB,AA,A,Z,ZXX,ZXY,ZYX,ZYY,ZXXF,ZXYF,ZYXF,ZYYF,ZXXP,ZXYP    COM1       2
      COMPLEX ZYXP,ZYYP,CPSI,SUM,ALAMBDA,ALAMS,C1,C2,C3,C4,C5,C6,C7,C8     COM1       3
      COMPLEX C9,C10,C11,AC,BC,CC,BHFX,BHFY,BFFX,BFFY,XP,YP                COM1       4
      COMPLEX ZTT,ZTP,ZPT,ZPP                                              COM1       5
      REAL KXX,KXY,KYX,KYY,KXP,KYP,MXP,MYP,LOAD,MEER,KTT,KPP               COM1       6
      COMMON ECC(10),AXX(10),AXY(10),AYX(10),AYY(10),BXX(10),BXY(10)       COM1       7
      COMMON BYX(10),BYY(10),WSS(10),AXX1(10),AXY1(10),AYX1(10)            COM1       8
      COMMON AYY1(10),BXX1(10),BXY1(10),BYX1(10),BYY1(10),ECC1(10)         COM1       9
      COMMON WSS1(10),DIA(25),BEAM(25),SI(25),AMASS(25),PI(25),TI(25)      COM1      10
      COMMON PIE,C,FORCE,E,KI,KN,KS,KB,KF,RPM,OMEGA,RPMBETA,BETA,MXP,MYP   COM1      11
      COMMON KXP,KYP,CXP,CYP,PSI,ALIMIT,ALIMIT1,TINC,TINC1,ECCX,ZXXP       COM1      12
      COMMON WSSY,IPZ,KXX,KXY,KYX,KYY,ALAMBDA,ALAMS,CXX,CXY,CYX,CYY,ZYYP   COM1      13
      COMMON F(25,9,9),FB(9,9),AA(9,9),A(9,9),Z(25,9),AC(17,17),BC(17,1)   COM1      14
      COMMON CC(17,1),XR(25),XI(25),XM(25),YR(25),YI(25),YM(25),RMXP       COM1      15
      COMMON THR(25),THI(25),THM(25),PHR(25),PHI(25),PHM(25),BMXR(25)      COM1      16
      COMMON BMXI(25),BMXM(25),BMYR(25),BMYI(25),BMYM(25),SFXR(25)         COM1      17
```

```
      COMMON SFXI(25),SFXM(25),SFYP(25),SFYI(25),SFYM(25),AMAJOR(25)     COM1        18
      COMMON BMINOR(25),PHASED(25),ATTD(25),XD(25),YD(25),THD(25)        COM1        19
      COMMON AREA(25),UNBL(10),LOAD(10),CR(10),GM,ALP,ALPHA,KF1,KF2,KF3  COM1        20
      COMMON ISP,IBN,KB1,IF1,IF2,IF3,G,TINC2,RPM1,RPMBT1,PHD(25),RMYP    COM1        21
      COMMON PSID(10),PSIR(10),OMEGAG,OMEGA1,RPMBET1(200),ALIMIT2,ILP    COM1        22
      COMMON BETA1(200),OMEGAT(200),OMEGAC(200),OMEGAW(200),RMOD(200)    COM1        23
      COMMON RMOD1(200),THETAD(200),DETR(200),DETI(200),RNORM(200)       COM1        24
      COMMON XRP(25),XIP(25),YRP(25),YIP(25),GAM,ALIMIT3,V1,V2,KTT,KPP   COM1        25
      COMMON FLEX1                                                       COM1        26
C*****PROGRAM TO MULTIPLY FIELD TRANSFER MATRICES AND STATE               MULT1        4
C    +VECTORS*****                                                       MULT1        5
C     DERIVE STATE VECTOR AT STATION 2                                   MULT1        6
      DO 27 K=1,I1                                                       MULT1        7
      SUM=(0.,0.)                                                        MULT1        8
      DO 29 L=1,I1                                                       MULT1        9
   29 SUM=SUM+F(2,K,L)*Z(1,L)                                            MULT1       10
   27 Z(2,K)=SUM                                                         MULT1       11
C     DERIVE STATE VECTORS FOR OTHER STATIONS                            MULT1       12
      DO 30 M=3,KS                                                       MULT1       13
      DO 31 K=1,I1                                                       MULT1       14
      SUM=(0.,0.)                                                        MULT1       15
      DO 32 L=1,I1                                                       MULT1       16
   32 SUM=SUM+F(M,K,L)*Z(M-1,L)                                          MULT1       17
   31 Z(M,K)=SUM                                                         MULT1       18
   30 CONTINUE                                                           MULT1       19
      RETURN                                                             MULT1       20
      END                                                                MULT1       21
      SUBROUTINE DETERM(NW)                                              DETERM       2
      COMPLEX F,FB,AA,A,Z,ZXX,ZXY,ZYX,ZYY,ZXXF,ZXYF,ZYXF,ZYYF,ZXXP,ZXYP  COM1         2
      COMPLEX ZYXP,ZYYP,CPSI,SUM,ALAMBDA,ALAMS,C1,C2,C3,C4,C5,C6,C7,C8   COM1         3
      COMPLEX C9,C10,C11,AC,BC,CC,BHFX,BHFY,BFFX,BFFY,XP,YP              COM1         4
      COMPLEX ZTT,ZTP,ZPT,ZPP                                            COM1         5
      REAL KXX,KXY,KYX,KYY,KXP,KYP,MXP,MYP,LOAD,MEER,KTT,KPP             COM1         6
      COMMON ECC(10),AXX(10),AXY(10),AYX(10),AYY(10),BXX(10),BXY(10)     COM1         7
      COMMON BYX(10),BYY(10),WSS(10),AXX1(10),AXY1(10),AYX1(10)          COM1         8
      COMMON AYY1(10),BXX1(10),BXY1(10),BYX1(10),BYY1(10),ECC1(10)       COM1         9
      COMMON WSS1(10),DIA(25),BEAM(25),SI(25),AMASS(25),PI(25),TI(25)    COM1        10
      COMMON PIE,C,FORCE,E,KI,KN,KS,KB,KF,RPM,OMEGA,RPMBETA,BETA,MXP,MYP COM1        11
      COMMON KXP,KYP,CXP,CYP,PSI,ALIMIT,ALIMIT1,TINC,TINC1,ECCX,ZXXP     COM1        12
      COMMON WSSY,IPZ,KXX,KXY,KYX,KYY,ALAMBDA,ALAMS,CXX,CXY,CYX,CYY,ZYYP COM1        13
      COMMON F(25,9,9),FB(9,9),AA(9,9),A(9,9),Z(25,9),AC(17,17),BC(17,1) COM1        14
      COMMON CC(17,1),XR(25),XI(25),XM(25),YR(25),YI(25),YM(25),RMXP     COM1        15
      COMMON THR(25),THI(25),THM(25),PHR(25),PHI(25),PHM(25),BMXR(25)    COM1        16
      COMMON BMXI(25),BMXM(25),BMYR(25),BMYI(25),BMYM(25),SFXR(25)       COM1        17
      COMMON SFXI(25),SFXM(25),SFYR(25),SFYI(25),SFYM(25),AMAJOR(25)     COM1        18
      COMMON BMINOR(25),PHASED(25),ATTD(25),XD(25),YD(25),THD(25)        COM1        19
      COMMON AREA(25),UNBL(10),LOAD(10),CR(10),GM,ALP,ALPHA,KF1,KF2,KF3  COM1        20
      COMMON ISP,IBN,KB1,IF1,IF2,IF3,G,TINC2,RPM1,RPMBT1,PHD(25),RMYP    COM1        21
      COMMON PSID(10),PSIR(10),OMEGAG,OMEGA1,RPMBET1(200),ALIMIT2,ILP    COM1        22
      COMMON BETA1(200),OMEGAT(200),OMEGAC(200),OMEGAW(200),RMOD(200)    COM1        23
      COMMON RMOD1(200),THETAD(200),DETR(200),DETI(200),RNORM(200)       COM1        24
      COMMON XRP(25),XIP(25),YRP(25),YIP(25),GAM,ALIMIT3,V1,V2,KTT,KPP   COM1        25
      COMMON FLEX1                                                       COM1        26
C*****PROGRAM TO DETERMINE STABILITY THRESHOLD FROM THE LEONARD LOCUS     DETERM       4
C     BY EVALUATING A COMPLEX 4*4 DETERMINANT*****                       DETERM       5
C     SET UP ELEMENTS OF COMPLEX LAMBDA DETERMINANT                      DETERM       6
C     FOR FREE-PINNED AND FREE-FREE BOUNDARY CONDITIONS AT LHS AND       DETERM       7
C     RHS SUPPORTS RESPECTIVELY                                          DETERM       8
      IF(ISP.EQ.1)GO TO 10                                               DETERM       9
      IF(ISP.EQ.2)GO TO 11                                               DETERM      10
   10 A(1,1)=FB(1,1)                                                     DETERM      11
      A(1,2)=FB(1,2)                                                     DETERM      12
      A(1,3)=FB(1,5)                                                     DETERM      13
      A(1,4)=FB(1,6)                                                     DETERM      14
      A(2,1)=FB(3,1)                                                     DETERM      15
      A(2,2)=FB(3,2)                                                     DETERM      16
      A(2,3)=FB(3,5)                                                     DETERM      17
      A(2,4)=FB(3,6)                                                     DETERM      18
      A(3,1)=FB(5,1)                                                     DETERM      19
      A(3,2)=FB(5,2)                                                     DETERM      20
      A(3,3)=FB(5,5)                                                     DETERM      21
      A(3,4)=FB(5,6)                                                     DETERM      22
      A(4,1)=FB(7,1)                                                     DETERM      23
      A(4,2)=FB(7,2)                                                     DETERM      24
      A(4,3)=FB(7,5)                                                     DETERM      25
      A(4,4)=FB(7,6)                                                     DETERM      26
      GO TO 12                                                           DETERM      27
   11 A(1,1)=FB(3,1)                                                     DETERM      28
      A(1,2)=FB(3,2)                                                     DETERM      29
      A(1,3)=FB(3,5)                                                     DETERM      30
      A(1,4)=FB(3,6)                                                     DETERM      31
      A(2,1)=FB(4,1)                                                     DETERM      32
      A(2,2)=FB(4,2)                                                     DETERM      33
      A(2,3)=FB(4,5)                                                     DETERM      34
      A(2,4)=FB(4,6)                                                     DETERM      35
```

```
      A(3,1)=FB(7,1)                                                    DETERM
      A(3,2)=FB(7,2)                                                    DETERM
      A(3,3)=FB(7,5)                                                    DETERM
      A(3,4)=FB(7,6)                                                    DETERM
      A(4,1)=FB(8,1)                                                    DETERM
      A(4,2)=FB(8,2)                                                    DETERM
      A(4,3)=FB(8,5)                                                    DETERM
      A(4,4)=FB(8,6)                                                    DETERM
C     EVALUATE COMPLEX LAMBDA DETERMINANT                               DETERM
   12 C1=A(3,3)*A(4,4)-A(3,4)*A(4,3)                                    DETERM
      C2=A(3,2)*A(4,4)-A(3,4)*A(4,2)                                    DETERM
      C3=A(3,2)*A(4,3)-A(3,3)*A(4,2)                                    DETERM
      C4=A(3,1)*A(4,4)-A(3,4)*A(4,1)                                    DETERM
      C5=A(3,1)*A(4,3)-A(3,3)*A(4,1)                                    DETERM
      C6=A(3,1)*A(4,2)-A(3,2)*A(4,1)                                    DETERM
      C7=A(1,1)*(A(2,2)*C1-A(2,3)*C2+A(2,4)*C3)                         DETERM
      C8=A(1,2)*(A(2,1)*C1-A(2,3)*C4+A(2,4)*C5)                         DETERM
      C9=A(1,3)*(A(2,1)*C2-A(2,2)*C4+A(2,4)*C6)                         DETERM
      C10=A(1,4)*(A(2,1)*C3-A(2,2)*C5+A(2,3)*C6)                        DETERM
      C11=C7-C8+C9-C10                                                  DETERM
      DETR(NW)=REAL(C11)                                                DETERM
      DETI(NW)=AIMAG(C11)                                               DETERM
      RETURN                                                            DETERM
      END                                                               DETERM
      SUBROUTINE LEONARD(NW,NSTOP)                                      LEONARD
      COMPLEX F,FB,AA,A,Z,ZXX,ZXY,ZYX,ZYY,ZXXF,ZXYF,ZYXF,ZYYF,ZXXP,ZXYP COM1
      COMPLEX ZYXP,ZYYP,CPSI,SUM,ALAMBDA,ALAMS,C1,C2,C3,C4,C5,C6,C7,C8  COM1
      COMPLEX C9,C10,C11,AC,BC,CC,BHFX,BHFY,BFFX,BFFY,XP,YP             COM1
      COMPLEX ZTT,ZTP,ZPT,ZPP                                           COM1
      REAL KXX,KXY,KYX,KYY,KXP,KYP,MXP,MYP,LOAD,MEER,KTT,KPP            COM1
      COMMON ECC(10),AXX(10),AXY(10),AYX(10),AYY(10),BXX(10),BXY(10)    COM1
      COMMON BYX(10),BYY(10),WSS(10),AXX1(10),AXY1(10),AYX1(10)         COM1
      COMMON AYY1(10),BXX1(10),BXY1(10),BYX1(10),BYY1(10),ECC1(10)      COM1
      COMMON WSS1(10),DIA(25),BEAM(25),SI(25),AMASS(25),PI(25),TI(25)   COM1
      COMMON PIE,C,FORCE,E,KI,KN,KS,KB,KF,RPM,OMEGA,RPMBETA,BETA,MXP,MYP COM1
      COMMON KXP,KYP,CXP,CYP,PSI,ALIMIT,ALIMIT1,TINC,TINC1,ECCX,ZXXP    COM1
      COMMON WSSY,IPZ,KXX,KXY,KYX,KYY,ALAMBDA,ALAMS,CXX,CXY,CYX,CYY,ZYYP COM1
      COMMON F(25,9,9),FB(9,9),AA(9,9),A(9,9),Z(25,9),AC(17,17),BC(17,1) COM1
      COMMON CC(17,1),XR(25),XI(25),XM(25),YR(25),YI(25),YM(25),RMXP    COM1
      COMMON THR(25),THI(25),THM(25),PHR(25),PHI(25),PHM(25),BMXR(25)   COM1
      COMMON BMXI(25),BMXM(25),BMYR(25),BMYI(25),BMYM(25),SFXR(25)      COM1
      COMMON SFXI(25),SFXM(25),SFYR(25),SFYI(25),SFYM(25),AMAJOR(25)    COM1
      COMMON BMINOR(25),PHASED(25),ATTD(25),XD(25),YD(25),THD(25)       COM1
      COMMON AREA(25),UNBL(10),LOAD(10),CR(10),GM,ALP,ALPHA,KF1,KF2,KF3 COM1
      COMMON ISP,IBN,KB1,IF1,IF2,IF3,G,TINC2,RPM1,RPMBT1,PHD(25),RMYP   COM1
      COMMON PSID(10),PSIR(10),OMEGAG,OMEGA1,RPMBET1(200),ALIMIT2,ILP   COM1
      COMMON BETA1(200),OMEGAT(200),OMEGAC(200),OMEGAW(200),RMOD(200)   COM1
      COMMON RMOD1(200),THETAD(200),DETR(200),DETI(200),RNORM(200)      COM1
      COMMON XRP(25),XIP(25),YRP(25),YIP(25),GAM,ALIMIT3,V1,V2,KTT,KPP  COM1
      COMMON FLEX1                                                      COM1
C*****PROGRAM TO CONVERT REAL AND IMAGINARY PARTS OF EVALUATED COMPLEX   LEONARD
C     DETERMINANT TO POLAR FORM FOR PLOTTING*****                       LEONARD
C     DERIVE NON-DIM. FREQUENCY RATIOS                                  LEONARD
      DO 10 N=1,NW                                                      LEONARD
      OMEGAT(N)=RPMBET1(N)/RPM                                          LEONARD
      OMEGAW(N)=RPMBET1(N)/OMEGAG                                       LEONARD
      OMEGAC(N)=RPMBET1(N)/OMEGA1                                       LEONARD
C     DERIVE MODULUS OF DETERMINANT                                     LEONARD
      RMOD(N)=SQRT(DETR(N)**2+DETI(N)**2)                               LEONARD
C     DERIVE ANGLE BETWEEN MODULUS AND +VE. REAL AXIS                   LEONARD
      ANG=ABS(DETI(N)/DETR(N))                                          LEONARD
      THETA=ATAN(ANG)                                                   LEONARD
      IF(DETR(N).LT.0.0.AND.DETI(N).GT.0.0)THETA=PIE-THETA              LEONARD
      IF(DETR(N).LT.0.0.AND.DETI(N).LT.0.0)THETA=THETA+PIE              LEONARD
      IF(DETR(N).GT.0.0.AND.DETI(N).LT.0.0)THETA=2.*PIE-THETA           LEONARD
   10 THETAD(N)=THETA*180./(10.*PIE)                                    LEONARD
C     DERIVE MIN. VALUE OF MODULUS                                      LEONARD
      RNEW=RMOD(1)                                                      LEONARD
      DO 11 N=2,NW                                                      LEONARD
      XMIN=AMIN1(RNEW,RMOD(N))                                          LEONARD
   11 RNEW=XMIN                                                         LEONARD
C     DERIVE MODULUS LENGTH W.R.T. MIN. VALUE(ORIGIN)                   LEONARD
      DO 12 N=1,NW                                                      LEONARD
   12 RMOD1(N)=RMOD(N)-RNEW                                             LEONARD
C     DERIVE MAX. VALUE OF MODULUS W.R.T. ORIGIN                        LEONARD
      RNEW1=RMOD1(1)                                                    LEONARD
      DO 13 N=2,NW                                                      LEONARD
      XMAX=AMAX1(RNEW1,RMOD1(N))                                        LEONARD
   13 RNEW1=XMAX                                                        LEONARD
      WRITE(6,100)RNEW,RNEW1                                            LEONARD
  100 FORMAT(5X,2(1PE12.4,2X)/)                                         LEONARD
C     NORMALISE MODULUS W.R.T. MAX. VALUE OF MODULUS                    LEONARD
      DO 14 N=1,NW                                                      LEONARD
   14 RNORM(N)=RMOD1(N)/(10.*RNEW1)                                     LEONARD
      IF(ILP.EQ.1)GO TO 98                                              LEONARD
```

```
      DO 32 N=1,NW
      WRITE(6,101)N,RPMBET1(N),BETA1(N),OMEGAC(N),OMEGAW(N),OMEGAT(N),
     +DETR(N),DETI(N),RMOD(N),RMOD1(N),RNORM(N),THETAD(N)
   32 CONTINUE
  101 FORMAT(5X,I3,2X,F7.2,2X,F6.2,3(2X,F5.3),4(2X,1PE12.4),2X,
     +F6.4,2X,F6.1)
      GO TO 99
C     SET LOOP COUNTERS TO ZERO
   98 NC=0
      N1=0
      N4=NW-1
C     CHECK IF LEONARD LOCUS ROTATES ANTI-CLOCKWISE
      DO 15 N=1,N4
      NC=NC+1
      N1=NC+1
      IF(DETR(N).GT.0.0.AND.DETR(N+1).GT.0.0.AND.
     +DETI(N).GT.0.0.AND.DETI(N+1).GT.0.0)GO TO 15
C     CHECK IF LEONARD LOCUS INITIALLY ROTATES CLOCKWISE
      IF(DETR(N).GT.0.0.AND.DETR(N+1).GT.0.0.AND.
     +DETI(N).GT.0.0.AND.DETI(N+1).LT.0.0)GO TO 30
      IF(DETR(N).GT.0.0.AND.DETR(N+1).LT.0.0.AND.
     +DETI(N).GT.0.0.AND.DETI(N+1).GT.0.0)GO TO 16
      GO TO 22
   15 CONTINUE
   16 DO 17 N=N1,N4
      NC=NC+1
      N1=NC+1
      IF(DETR(N).LT.0.0.AND.DETR(N+1).LT.0.0.AND.
     +DETI(N).GT.0.0.AND.DETI(N+1).GT.0.0)GO TO 17
      IF(DETR(N).LT.0.0.AND.DETR(N+1).LT.0.0.AND.
     +DETI(N).GT.0.0.AND.DETI(N+1).LT.0.0)GO TO 18
      GO TO 22
   17 CONTINUE
   18 DO 19 N=N1,N4
      NC=NC+1
      N1=NC+1
      IF(DETR(N).LT.0.0.AND.DETR(N+1).LT.0.0.AND.
     +DETI(N).LT.0.0.AND.DETI(N+1).LT.0.0)GO TO 19
      IF(DETR(N).LT.0.0.AND.DETR(N+1).GT.0.0.AND.
     +DETI(N).LT.0.0.AND.DETI(N+1).LT.0.0)GO TO 20
      GO TO 22
   19 CONTINUE
   20 DO 21 N=N1,N4
      NC=NC+1
      N1=NC+1
      IF(DETR(N).GT.0.0.AND.DETR(N+1).GT.0.0.AND.
     +DETI(N).LT.0.0.AND.DETI(N+1).LT.0.0)GO TO 21
      IF(DETR(N).GT.0.0.AND.DETR(N+1).GT.0.0.AND.
     +DETI(N).LT.0.0.AND.DETI(N+1).GT.0.0)GO TO 99
      GO TO 22
   21 CONTINUE
C     SET LOOP COUNTERS TO ZERO
   30 NC=0
      N1=0
      N4=NW-1
C     CHECK IF LEONARD LOCUS ROTATES CLOCKWISE
      DO 31 N=1,N4
      NC=NC+1
      N1=NC+1
      IF(DETR(N).GT.0.0.AND.DETR(N+1).GT.0.0.AND.
     +DETI(N).GT.0.0.AND.DETI(N+1).GT.0.0)GO TO 31
      IF(DETR(N).GT.0.0.AND.DETR(N+1).GT.0.0.AND.
     +DETI(N).GT.0.0.AND.DETI(N+1).LT.0.0)GO TO 24
      GO TO 22
   31 CONTINUE
   24 DO 25 N=N1,N4
      NC=NC+1
      N1=NC+1
      IF(DETR(N).GT.0.0.AND.DETR(N+1).GT.0.0.AND.
     +DETI(N).LT.0.0.AND.DETI(N+1).LT.0.0)GO TO 25
      IF(DETR(N).GT.0.0.AND.DETR(N+1).LT.0.0.AND.
     +DETI(N).LT.0.0.AND.DETI(N+1).LT.0.0)GO TO 26
      GO TO 22
   25 CONTINUE
   26 DO 27 N=N1,N4
      NC=NC+1
      N1=NC+1
      IF(DETR(N).LT.0.0.AND.DETR(N+1).LT.0.0.AND.
     +DETI(N).LT.0.0.AND.DETI(N+1).LT.0.0)GO TO 27
      IF(DETR(N).LT.0.0.AND.DETR(N+1).LT.0.0.AND.
     +DETI(N).LT.0.0.AND.DETI(N+1).GT.0.0)GO TO 28
      GO TO 22
   27 CONTINUE
   28 DO 29 N=N1,N4
      NC=NC+1
```

```
      N1=NC+1
      IF(DETR(N).LT.0.0.AND.DETR(N+1).LT.0.0.AND.
     +DETI(N).GT.0.0.AND.DETI(N+1).GT.0.0)GO TO 29
      IF(DETR(N).LT.0.0.AND.DETR(N+1).GT.0.0.AND.
     +DETI(N).GT.0.0.AND.DETI(N+1).GT.0.0)GO TO 99
      GO TO 22
   29 CONTINUE
   22 NSTOP=NSTOP+1
      N2=NC-1
      N3=NC+2
      DO 23 N=N2,N3
      WRITE(6,102)N,RPMBET1(N),BETA1(N),OMEGAC(N),OMEGAW(N),OMEGAT(N),
     +DETR(N),DETI(N),RMOD(N),RMOD1(N),RNORM(N),THETAD(N)
   23 CONTINUE
  102 FORMAT(5X,I3,2X,F7.2,2X,F6.2,3(2X,F5.3),4(2X,1PE12.4),2X,
     +F6.4,2X,F6.1/)
   99 RETURN
      END
      SUBROUTINE MODES
      COMPLEX F,FB,AA,A,Z,ZXX,ZXY,ZYX,ZYY,ZXXF,ZXYF,ZYXF,ZYYF,ZXXP,ZXYP
      COMPLEX ZYXP,ZYYP,CPSI,SUM,ALAMBDA,ALAMS,C1,C2,C3,C4,C5,C6,C7,C8
      COMPLEX C9,C10,C11,AC,BC,CC,BHFX,BHFY,BFFX,BFFY,XP,YP
      COMPLEX ZTT,ZTP,ZPT,ZPP
      REAL KXX,KXY,KYX,KYY,KXP,KYP,MXP,MYP,LOAD,MEER,KTT,KPP
      COMMON ECC(10),AXX(10),AXY(10),AYX(10),AYY(10),BXX(10),BXY(10)
      COMMON BYX(10),BYY(10),WSS(10),AXX1(10),AXY1(10),AYX1(10)
      COMMON AYY1(10),BXX1(10),BXY1(10),BYX1(10),BYY1(10),ECC1(10)
      COMMON WSS1(10),DIA(25),BEAM(25),SI(25),AMASS(25),PI(25),TI(25)
      COMMON PIE,C,FORCE,E,KI,KN,KS,KB,KF,RPM,OMEGA,RPMBETA,BETA,MXP,MYP
      COMMON KXP,KYP,CXP,CYP,PSI,ALIMIT,ALIMIT1,TINC,TINC1,ECCX,ZXXP
      COMMON WSSY,IPZ,KXX,KXY,KYX,KYY,ALAMBDA,ALAMS,CXX,CXY,CYX,CYY,ZYYP
      COMMON F(25,9,9),FB(9,9),AA(9,9),A(9,9),Z(25,9),AC(17,17),BC(17,1)
      COMMON CC(17,1),XP(25),XI(25),XM(25),YR(25),YI(25),YM(25),RMXP
      COMMON THR(25),THI(25),THM(25),PHR(25),PHI(25),PHM(25),BMXR(25)
      COMMON BMXI(25),BMXM(25),BMYP(25),BMYI(25),BMYM(25),SFXR(25)
      COMMON SFXI(25),SFXM(25),SFYP(25),SFYI(25),SFYM(25),AMAJOR(25)
      COMMON BMINOR(25),PHASED(25),ATTD(25),XD(25),YD(25),THD(25)
      COMMON AREA(25),UNBL(10),LOAD(10),CR(10),GM,ALP,ALPHA,KF1,KF2,KF3
      COMMON ISP,IBN,KB1,IF1,IF2,IF3,G,TINC2,RPM1,RPMBT1,PHD(25),RMYP
      COMMON PSID(10),PSIR(10),OMEGAG,OMEGA1,RPMBET1(200),ALIMIT2,ILP
      COMMON BETA1(200),OMEGAT(200),OMEGAC(200),OMEGAW(200),RMOD(200)
      COMMON RMOD1(200),THETAD(200),DETR(200),DETI(200),RNORM(200)
      COMMON XRP(25),XIP(25),YRP(25),YIP(25),GAM,ALIMIT3,V1,V2,KTT,KPP
      COMMON FLEX1
      DIMENSION WKSPCE(36)
C*****PROGRAM TO DETERMINE THE MODE SHAPE AT WHIRLING*****
C     EVALUATE STATE VECTOR AT STATION 1, SETTING Y=1
C     SET UP ELEMENTS OF MATRIX FOR FREE-PINNED AND FREE-FREE SUPPORTS
C     AT LHS AND RHS RESPECTIVELY
      IF(ISP.EQ.1)GO TO 11
      IF(ISP.EQ.2)GO TO 12
   11 AC(1,1)=FB(1,1)
      AC(1,2)=FB(1,2)
      AC(1,3)=FB(1,6)
      AC(2,1)=FB(3,1)
      AC(2,2)=FB(3,2)
      AC(2,3)=FB(3,6)
      AC(3,1)=FB(7,1)
      AC(3,2)=FB(7,2)
      AC(3,3)=FB(7,6)
      BC(1,1)=-FB(1,5)
      BC(2,1)=-FB(3,5)
      BC(3,1)=-FB(7,5)
      GO TO 13
   12 AC(1,1)=FB(3,1)
      AC(1,2)=FB(3,2)
      AC(1,3)=FB(3,6)
      AC(2,1)=FB(4,1)
      AC(2,2)=FB(4,2)
      AC(2,3)=FB(4,6)
      AC(3,1)=FB(8,1)
      AC(3,2)=FB(8,2)
      AC(3,3)=FB(8,6)
      BC(1,1)=-FB(3,5)
      BC(2,1)=-FB(4,5)
      BC(3,1)=-FB(8,5)
   13 N=3
      M=1
      IAC=17
      IBC=17
      ICC=17
      IFAIL=1
C     CALL LIBRARY ROUTINE TO INVERT MATRIX AND MULTIPLY BY COLUMN
C     MATRIX
      CALL F04ADF(AC,IAC,BC,IBC,N,M,CC,ICC,WKSPCE,IFAIL)
```

```
      IF(IFAIL.EQ.0)GO TO 98                                              MODES
      WRITE(6,101)IFAIL                                                   MODES
      GO TO 99                                                            MODES
C     MODES OF WHIRLING                                                   MODES
C     ARRANGE ELEMENTS OF STATE VECTOR AT STATION 1                       MODES
   98 Z(1,1)=CC(1,1)                                                      MODES
      Z(1,2)=CC(2,1)                                                      MODES
      Z(1,3)=(0.,0.)                                                      MODES
      Z(1,4)=(0.,0.)                                                      MODES
      Z(1,5)=(1.,0.)                                                      MODES
      Z(1,6)=CC(3,1)                                                      MODES
      Z(1,7)=(0.,0.)                                                      MODES
      Z(1,8)=(0.,0.)                                                      MODES
      CALL MULT1(8)                                                       MODES
C     SET LOOP COUNTER TO ZERO                                            MODES
      NCOUNT=0                                                            MODES
      DO 10 M=1,KS                                                        MODES
      NCOUNT=NCOUNT+1                                                     MODES
C     X-AMPLITUDE                                                         MODES
      XR(M)=REAL(Z(M,1))                                                  MODES
      XI(M)=AIMAG(Z(M,1))                                                 MODES
C     Y-AMPLITUDE                                                         MODES
      YR(M)=REAL(Z(M,5))                                                  MODES
      YI(M)=AIMAG(Z(M,5))                                                 MODES
   10 WRITE(6,100)NCOUNT,XR(M),XI(M),YR(M),YI(M)                          MODES
  100 FORMAT(5X,I2,4(2X,1PE12.4))                                         MODES
  101 FORMAT(5X,*IFAIL=*,I2)                                              MODES
   99 RETURN                                                              MODES
      END                                                                 MODES
      SUBROUTINE SUPPORT                                                  SUPPORT
      COMPLEX F,FB,AA,A,Z,ZXX,ZXY,ZYX,ZYY,ZXXF,ZXYF,ZYXF,ZYYF,ZXXP,ZXYP   COM1
      COMPLEX ZYXP,ZYYP,CPSI,SUM,ALAMBDA,ALAMS,C1,C2,C3,C4,C5,C6,C7,C8    COM1
      COMPLEX C9,C10,C11,AC,BC,CC,BHFX,BHFY,BFFX,BFFY,XP,YP               COM1
      COMPLEX ZTT,ZTP,ZPT,ZPP                                             COM1
      REAL KXX,KXY,KYX,KYY,KXP,KYP,MXP,MYP,LOAD,MEER,KTT,KPP              COM1
      COMMON ECC(10),AXX(10),AXY(10),AYX(10),AYY(10),BXX(10),BXY(10)      COM1
      COMMON BYX(10),BYY(10),WSS(10),AXX1(10),AXY1(10),AYX1(10)           COM1
      COMMON AYY1(10),BXX1(10),BXY1(10),BYX1(10),BYY1(10),ECC1(10)        COM1
      COMMON WSS1(10),DIA(25),BEAM(25),SI(25),AMASS(25),PI(25),TI(25)     COM1
      COMMON PIE,C,FORCE,E,KI,KN,KS,KB,KF,PPM,OMEGA,RPMBETA,BETA,MXP,MYP  COM1
      COMMON KXP,KYP,CXP,CYP,PSI,ALIMIT,ALIMIT1,TINC,TINC1,ECCX,ZXXP      COM1
      COMMON WSSY,IPZ,KXX,KXY,KYX,KYY,ALAMBDA,ALAMS,CXX,CXY,CYX,CYY,ZYYP  COM1
      COMMON F(25,9,9),FB(9,9),AA(9,9),A(9,9),Z(25,9),AC(17,17),BC(17,1)  COM1
      COMMON CC(17,1),XR(25),XI(25),XM(25),YR(25),YI(25),YM(25),RMXP      COM1
      COMMON THR(25),THI(25),THM(25),PHR(25),PHI(25),PHM(25),BMXR(25)     COM1
      COMMON BMXI(25),BMXM(25),BMYR(25),BMYI(25),BMYM(25),SFXR(25)        COM1
      COMMON SFXI(25),SFXM(25),SFYR(25),SFYI(25),SFYM(25),AMAJOR(25)      COM1
      COMMON BMINOR(25),PHASED(25),ATTD(25),XD(25),YD(25),THD(25)         COM1
      COMMON AREA(25),UNBL(10),LOAD(10),CR(10),GM,ALP,ALPHA,KF1,KF2,KF3   COM1
      COMMON ISP,IBN,KB1,IF1,IF2,IF3,G,TINC2,RPM1,RPMBT1,PHD(25),RMYP     COM1
      COMMON PSID(10),PSIR(10),OMEGAG,OMEGA1,RPMBET1(200),ALIMIT2,ILP     COM1
      COMMON BETA1(200),OMEGAT(200),OMEGAC(200),OMEGAW(200),RMOD(200)     COM1
      COMMON RMOD1(200),THETAD(200),DETR(200),DETI(200),RNORM(200)        COM1
      COMMON XRP(25),XIP(25),YRP(25),YIP(25),GAM,ALIMIT3,V1,V2,KTT,KPP    COM1
      COMMON FLEX1                                                        COM1
      DIMENSION WKSPCE(36)                                                SUPPORT
C*****PROGRAM TO DETERMINE RESPONCE OF A FLEXIBLE PEDESTAL *****          SUPPORT
C     DETERMINE FORCE TRANSMITTED TO BEARING HOUSING                      SUPPORT
C     X-DIRECTION                                                         SUPPORT
      BHFX=Z(KB+1,4)-Z(KB-1,4)                                            SUPPORT
      BHFXR=REAL(BHFX)                                                    SUPPORT
      BHFXI=AIMAG(BHFX)                                                   SUPPORT
C     BEARING HOUSING FORCE MODULUS                                       SUPPORT
      BHFXM=SQRT(BHFXR**2+BHFXI**2)                                       SUPPORT
C     Y-DIRECTION                                                         SUPPORT
      BHFY=Z(KB+1,8)-Z(KB-1,8)                                            SUPPORT
      BHFYR=REAL(BHFY)                                                    SUPPORT
      BHFYI=AIMAG(BHFY)                                                   SUPPORT
C     BEARING HOUSING FORCE MODULUS                                       SUPPORT
      BHFYM=SQRT(BHFYR**2+BHFYI**2)                                       SUPPORT
C     DETERMINE PEDESTAL MOTION                                           SUPPORT
C     SET-UP ELEMENTS OF MATRIX AT BEARING STATION                        SUPPORT
      AC(1,1)=ZXXP                                                        SUPPORT
      AC(1,2)=(0.,0.)                                                     SUPPORT
      AC(2,1)=(0.,0.)                                                     SUPPORT
      AC(2,2)=ZYYP                                                        SUPPORT
      BC(1,1)=BHFX                                                        SUPPORT
      BC(2,1)=BHFY                                                        SUPPORT
      N=2                                                                 SUPPORT
      M=1                                                                 SUPPORT
      IAC=17                                                              SUPPORT
      IBC=17                                                              SUPPORT
      ICC=17                                                              SUPPORT
      IFAIL=1                                                             SUPPORT
C     CALL LIBRARY ROUTINE TO INVERT MATRIX AND MULTIPLY BY COLUMN        SUPPORT
```

```
C       MATRIX                                                               SUPPORT
        CALL F04ADF(AC,IAC,BC,IBC,N,M,CC,ICC,WKSPCE,IFAIL)                   SUPPORT
        IF(IFAIL.EQ.0)GO TO 10                                               SUPPORT
        WRITE(6,100)IFAIL                                                    SUPPORT
        GO TO 99                                                             SUPPORT
C       ARRANGE ELEMENTS OF SOLUTION VECTOR                                  SUPPORT
   10   XP=CC(1,1)                                                           SUPPORT
        YP=CC(2,1)                                                           SUPPORT
C       PEDESTAL MOTION IN X-DIRECTION                                       SUPPORT
        XPR=REAL(XP)                                                         SUPPORT
        XPI=AIMAG(XP)                                                        SUPPORT
C       PEDESTAL MOTION MODULUS                                              SUPPORT
        XPM=SQRT(XPR**2+XPI**2)                                              SUPPORT
C       PEDESTAL MOTION IN Y-DIRECTION                                       SUPPORT
        YPR=REAL(YP)                                                         SUPPORT
        YPI=AIMAG(YP)                                                        SUPPORT
C       PEDESTAL MOTION MODULUS                                              SUPPORT
        YPM=SQRT(YPR**2+YPI**2)                                              SUPPORT
C       DETERMINE FORCE TRANSMITTED TO BEARING FOUNDATION                    SUPPORT
C       X-DIRECTION                                                          SUPPORT
        BFFX=BHFX-MXP*ALAMS*XP                                               SUPPORT
        BFFXR=REAL(BFFX)                                                     SUPPORT
        BFFXI=AIMAG(BFFX)                                                    SUPPORT
C       BEARING FOUNDATION FORCE MODULUS                                     SUPPORT
        BFFXM=SQRT(BFFXR**2+BFFXI**2)                                        SUPPORT
C       Y-DIRECTION                                                          SUPPORT
        BFFY=BHFY-MYP*ALAMS*YP                                               SUPPORT
        BFFYR=REAL(BFFY)                                                     SUPPORT
        BFFYI=AIMAG(BFFY)                                                    SUPPORT
C       BEARING FOUNDATION FORCE MODULUS                                     SUPPORT
        BFFYM=SQRT(BFFYR**2+BFFYI**2)                                        SUPPORT
        WRITE(6,101)BHFXR,BHFXI,BHFXM                                        SUPPORT
        WRITE(6,101)BHFYR,BHFYI,BHFYM                                        SUPPORT
        WRITE(6,101)XPR,XPI,XPM                                              SUPPORT
        WRITE(6,101)YPR,YPI,YPM                                              SUPPORT
        WRITE(6,101)BFFXR,BFFXI,BFFXM                                        SUPPORT
        WRITE(6,101)BFFYR,BFFYI,BFFYM                                        SUPPORT
  100   FORMAT(5X,*IFAIL=*,I2)                                               SUPPORT
  101   FORMAT(5X,3(1PE12.4,2X)/)                                            SUPPORT
   99   RETURN                                                               SUPPORT
        END                                                                  SUPPORT
        SUBROUTINE RESP                                                      RESP
        COMPLEX F,FB,AA,A,Z,ZXX,ZXY,ZYX,ZYY,ZXXF,ZXYF,ZYXF,ZYYF,ZXXP,ZXYP    COM1
        COMPLEX ZYXP,ZYYP,CPSI,SUM,ALAMBDA,ALAMS,C1,C2,C3,C4,C5,C6,C7,C8     COM1
        COMPLEX C9,C10,C11,AC,BC,CC,BHFX,BHFY,BFFX,BFFY,XP,YP                COM1
        COMPLEX ZTT,ZTP,ZPT,ZPP                                              COM1
        REAL KXX,KXY,KYX,KYY,KXP,KYP,MXP,MYP,LOAD,MEER,KTT,KPP               COM1
        COMMON ECC(10),AYX(10),AXY(10),AYX(10),AYY(10),BXX(10),BXY(10)       COM1
        COMMON BYX(10),BYY(10),WSS(10),AXX1(10),AXY1(10),AYX1(10)            COM1
        COMMON AYY1(10),BXX1(10),BXY1(10),BYX1(10),BYY1(10),ECC1(10)         COM1
        COMMON WSS1(10),DIA(25),BEAM(25),SI(25),AMASS(25),PI(25),TI(25)      COM1
        COMMON PIE,C,FORCE,E,KI,KN,KS,KB,KF,RPM,OMEGA,RPMBETA,BETA,MXP,MYP   COM1
        COMMON KXP,KYP,CXP,CYP,PSI,ALIMIT,ALIMIT1,TINC,TINC1,ECCX,ZXXP       COM1
        COMMON WSSY,IPZ,KXX,KXY,KYX,KYY,ALAMBDA,ALAMS,CXX,CXY,CYX,CYY,ZYYP   COM1
        COMMON F(25,9,9),FB(9,9),AA(9,9),A(9,9),Z(25,9),AC(17,17),BC(17,1)   COM1
        COMMON CC(17,1),XR(25),XI(25),XM(25),YR(25),YI(25),YM(25),RMXP       COM1
        COMMON THR(25),THI(25),THM(25),PHR(25),PHI(25),PHM(25),BMXR(25)      COM1
        COMMON BMXI(25),BMXM(25),BMYR(25),BMYI(25),BMYM(25),SFXR(25)         COM1
        COMMON SFXI(25),SFXM(25),SFYR(25),SFYI(25),SFYM(25),AMAJOR(25)       COM1
        COMMON BMINOR(25),PHASER(25),ATTD(25),XD(25),YD(25),THD(25)          COM1
        COMMON AREA(25),UNBL(10),LOAD(10),CR(10),GM,ALP,ALPHA,KF1,KF2,KF3    COM1
        COMMON ISP,IBN,KB1,IF1,IF2,IF3,G,TINC2,RPM1,RPMBT1,PHD(25),RMYP      COM1
        COMMON PSID(10),PSIR(10),OMEGAG,OMEGA1,RPMBET1(200),ALIMIT2,ILP      COM1
        COMMON BETA1(200),OMEGAT(200),OMEGAC(200),OMEGAW(200),RMOD(200)      COM1
        COMMON RMOD1(200),THETAD(200),DETR(200),DETI(200),RNORM(200)         COM1
        COMMON XRP(25),XIP(25),YRP(25),YIP(25),GAM,ALIMIT3,V1,V2,KTT,KPP     COM1
        COMMON FLEX1                                                         COM1
        DIMENSION WKSPCE(36)                                                 RESP
C*****PROGRAM TO DETERMINE NATURAL FREQUENCIES AND RESPONCE*****             RESP
C       EVALUATE STATE VECTOR AT STATION 1                                   RESP
C       SET UP ELEMENTS OF MATRIX FOR FREE-PINNED AND FREE-FREE              RESP
C       SUPPORTS AT LHS AND RHS RESPECTIVELY                                 RESP
        IF(ISP.EQ.1)GO TO 20                                                 RESP
        IF(ISP.EQ.2)GO TO 21                                                 RESP
   20   AC(1,1)=FB(1,1)                                                      RESP
        AC(1,2)=FB(1,2)                                                      RESP
        AC(1,3)=FB(1,5)                                                      RESP
        AC(1,4)=FB(1,6)                                                      RESP
        AC(2,1)=FB(3,1)                                                      RESP
        AC(2,2)=FB(3,2)                                                      RESP
        AC(2,3)=FB(3,5)                                                      RESP
        AC(2,4)=FB(3,6)                                                      RESP
        AC(3,1)=FB(5,1)                                                      RESP
        AC(3,2)=FB(5,2)                                                      RESP
        AC(3,3)=FB(5,5)                                                      RESP
```

```
      AC(3,4)=FB(5,6)
      AC(4,1)=FB(7,1)
      AC(4,2)=FB(7,2)
      AC(4,3)=FB(7,5)
      AC(4,4)=FB(7,6)
      BC(1,1)=-FB(1,9)
      BC(2,1)=-FB(3,9)
      BC(3,1)=-FB(5,9)
      BC(4,1)=-FB(7,9)
      GO TO 23
   21 AC(1,1)=FB(3,1)
      AC(1,2)=FB(3,2)
      AC(1,3)=FB(3,5)
      AC(1,4)=FB(3,6)
      AC(2,1)=FB(4,1)
      AC(2,2)=FB(4,2)
      AC(2,3)=FB(4,5)
      AC(2,4)=FB(4,6)
      AC(3,1)=FB(7,1)
      AC(3,2)=FB(7,2)
      AC(3,3)=FB(7,5)
      AC(3,4)=FB(7,6)
      AC(4,1)=FB(8,1)
      AC(4,2)=FB(8,2)
      AC(4,3)=FB(8,5)
      AC(4,4)=FB(8,6)
      BC(1,1)=-FB(3,9)
      BC(2,1)=-FB(4,9)
      BC(3,1)=-FB(7,9)
      BC(4,1)=-FB(8,9)
   23 N=4
      M=1
      IAC=17
      IBC=17
      ICC=17
      IFAIL=1
C     CALL LIBRARY ROUTINE TO INVERT MATRIX AND MULTIPLY BY COLUMN
C     MATRIX
      CALL F04ADF(AC,IAC,BC,IBC,N,M,CC,ICC,WKSPCE,IFAIL)
      IF(IFAIL.EQ.0)GO TO 99
      WRITE(6,100)IFAIL
      GO TO 98
C     ARRANGE ELEMENTS OF STATE VECTOR AT STATION 1
   99 Z(1,1)=CC(1,1)
      Z(1,2)=CC(2,1)
      Z(1,3)=(0.,0.)
      Z(1,4)=(0.,0.)
      Z(1,5)=CC(3,1)
      Z(1,6)=CC(4,1)
      Z(1,7)=(0.,0.)
      Z(1,8)=(0.,0.)
      Z(1,9)=(1.,0.)
      CALL MULT1(9)
C     SET LOOP COUNTER TO ZERO
      NCOUNT=0
      DO 10 M=1,KS
      NCOUNT=NCOUNT+1
C     X-AMPLITUDE
      XR(M)=REAL(Z(M,1))
      XRP(M)=XR(M)*2.
      XI(M)=AIMAG(Z(M,1))
      XIP(M)=XI(M)*2.
C     X-MODULUS
      XM(M)=SQRT(XRP(M)**2+XIP(M)**2)
C     SLOPE IN X-DIR.
      THR(M)=REAL(Z(M,2))
      THI(M)=AIMAG(Z(M,2))
C     SLOPE MODULUS IN X-DIR.
      THM(M)=SQRT(THR(M)**2+THI(M)**2)
C     BENDING MOMENT IN Y-DIR.
      BMYR(M)=REAL(Z(M,3))
      BMYI(M)=AIMAG(Z(M,3))
C     BENDING MOMENT MODULUS IN Y-DIR.
      BMYM(M)=SQRT(BMYR(M)**2+BMYI(M)**2)
C     SHEAR FORCE IN X-DIR.
      SFXR(M)=REAL(Z(M,4))
      SFXI(M)=AIMAG(Z(M,4))
C     SHEAR FORCE MODULUS IN X-DIR.
      SFXM(M)=SQRT(SFXR(M)**2+SFXI(M)**2)
C     Y-AMPLITUDE
      YR(M)=REAL(Z(M,5))
      YRP(M)=YR(M)*2.
      YI(M)=AIMAG(Z(M,5))
      YIP(M)=YI(M)*2.
C     Y-AMPLITUDE MODULUS
```

```
      YM(M)=SQRT(YRP(M)**2+YIP(M)**2)
C     SLOPE IN Y-DIR.
      PHR(M)=REAL(Z(M,6))
      PHI(M)=AIMAG(Z(M,6))
C     SLOPE MODULUS IN Y-DIR.
      PHM(M)=SQRT(PHR(M)**2+PHI(M)**2)
C     BENDING MOMENT IN X-DIR.
      BMXR(M)=REAL(Z(M,7))
      BMXI(M)=AIMAG(Z(M,7))
C     BENDING MOMENT MODULUS IN X-DIR.
      BMXM(M)=SQRT(BMXR(M)**2+BMXI(M)**2)
C     SHEAR FORCE IN Y-DIR.
      SFYR(M)=REAL(Z(M,8))
      SFYI(M)=AIMAG(Z(M,8))
C     SHEAR FORCE MODULUS IN Y-DIR.
      SFYM(M)=SQRT(SFYR(M)**2+SFYI(M)**2)
      F1=XR(M)**2+XI(M)**2+YR(M)**2+YI(M)**2
      F2=XR(M)**2+XI(M)**2-YR(M)**2-YI(M)**2
      F3=XR(M)*YR(M)+XI(M)*YI(M)
      F4=XI(M)*YR(M)-XR(M)*YI(M)
      F5=XR(M)*XI(M)+YR(M)*YI(M)
      F6=XR(M)**2-XI(M)**2+YR(M)**2-YI(M)**2
      F7=0.25*F2**2+F3**2
      IF(F7.GE.0.)GO TO 12
      F7=-F7
      F8=-SQRT(F7)
      GO TO 13
   12 F8=SQRT(F7)
   13 F9=0.5*F1+F8
      IF(F9.GE.0.)GO TO 14
      F9=-F9
C     SEMI-MAJOR AXIS OF ELLIPTICAL ORBIT
      AMAJOR(M)=-SQRT(F9)
      GO TO 15
   14 AMAJOR(M)=SQRT(F9)
C     SEMI-MINOR AXIS OF ELLIPTICAL ORBIT
   15 BMINOR(M)=F4/AMAJOR(M)
C     PHASE ANGLE BETWEEN FORCE AND RESPONCE
      PHASE=0.5*ATAN(2.0*F5/F6)
      PHASED(M)=PHASE*180./PIE
C     PHASE ANGLE BETWEEN SEMI-MAJOR AXIS AND X-AXIS
      ATT=0.5*ATAN(2.0*F3/F2)
      ATTD(M)=ATT*180./PIE
      WRITE(6,101)NCOUNT,XRP(M),XIP(M),XM(M),YRP(M),YIP(M),YM(M)
   10 CONTINUE
      WRITE(6,102)
      GO TO 98
      NCOUNT=0
      DO 19 M=1,KS
      NCOUNT=NCOUNT+1
      WRITE(6,101)NCOUNT,THR(M),THI(M),THM(M),PHR(M),PHI(M),PHM(M)
   19 CONTINUE
      WRITE(6,102)
      NCOUNT=0
      DO 16 M=1,KS
      NCOUNT=NCOUNT+1
      WRITE(6,101)NCOUNT,BMXR(M),BMXI(M),BMXM(M),BMYR(M),BMYI(M),
     +BMYM(M)
   16 CONTINUE
      WRITE(6,102)
      NCOUNT=0
      DO 17 M=1,KS
      NCOUNT=NCOUNT+1
      WRITE(6,101)NCOUNT,SFXR(M),SFXI(M),SFXM(M),SFYR(M),SFYI(M),
     +SFYM(M)
   17 CONTINUE
      WRITE(6,102)
      NCOUNT=0
      DO 11 M=1,KS
      NCOUNT=NCOUNT+1
      WRITE(6,103)NCOUNT,AMAJOR(M),BMINOR(M),ATTD(M),PHASED(M)
   11 CONTINUE
      WRITE(6,102)
  100 FORMAT(5X,*IFAIL=*,I2)
  101 FORMAT(1X,I2,6(2X,1PE12.4))
  102 FORMAT(/)
  103 FORMAT(1X,I2,2(2X,1PE12.4),2(2X,F9.4))
   98 RETURN
      END
```

APPENDIX F

SPECIFICATIONS OF TEST ROTOR AND BEARING

Rotor Mass (total)	36.66lb	16.66Kg
Flywheel Mass	28.59lb	12.99Kg
Shaft Mass	8.07lb	3.67Kg
Bearing Housing Mass	23.19lb	10.54Kg
Length Between Supports	27.5in	698.5mm
Shaft diameter	0.984in	25mm
Flywheel diameter	6.672in	171.8mm
Flywheel Length	3.00in	74.9mm
Bearing Diameter (nominal)	2.50in	63.5mm
Bearing Length (L/D=1/2)	1.25in	31.75mm
Bearing Radial Clearance	0-0.010in	0-0.254mm
Mass Unbalance (plane I)	0.021oz-in	15g-mm
Mass Unbalance (plane II)	0.046oz-in	33g-mm

APPENDIX G

LUMPED MASS MODEL OF THE TEST ROTOR-BEARING SYSTEM

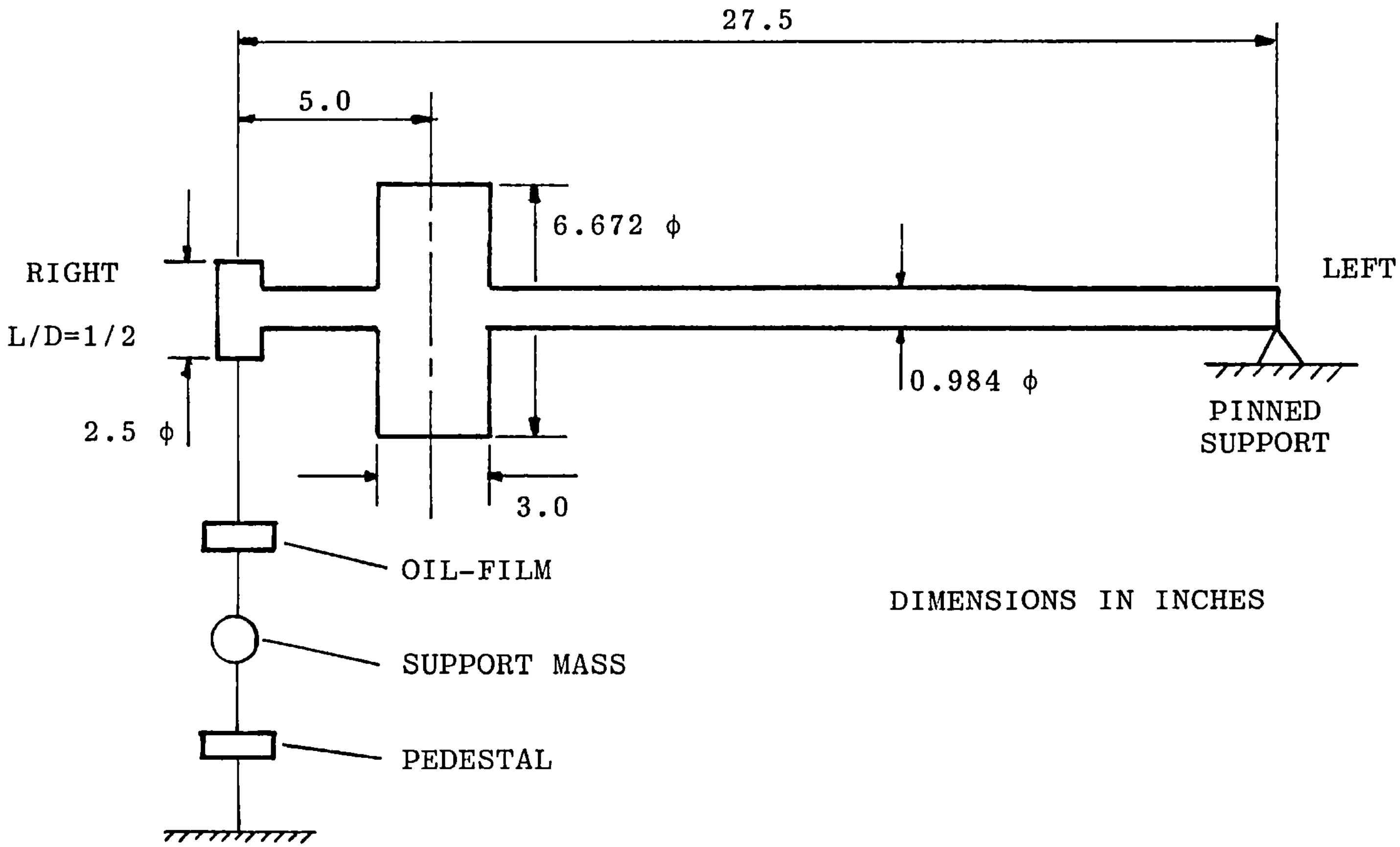

Figure G.1 Principle Dimensions of the Test Rotor-Bearing System

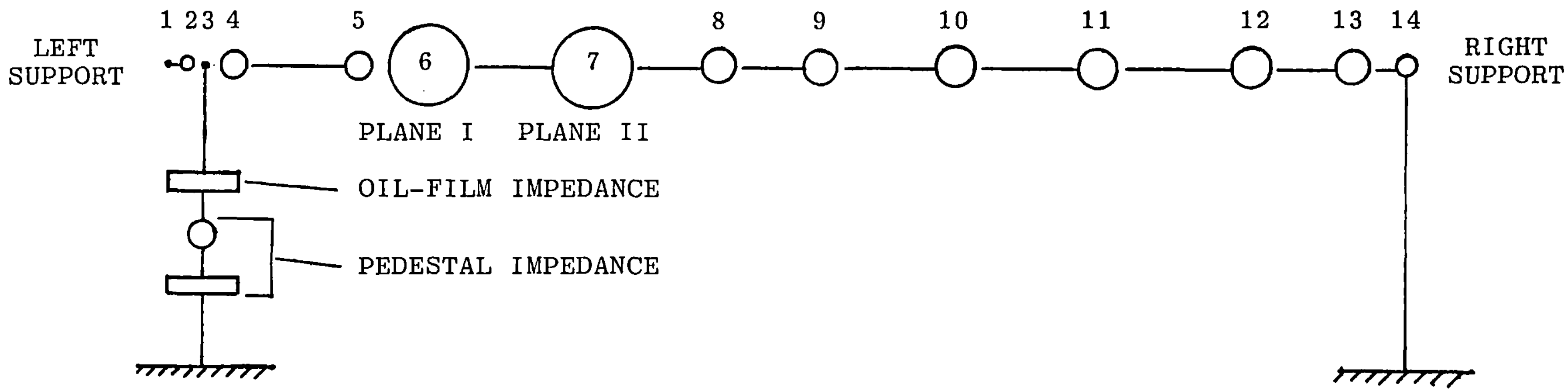

Figure G.2 Lumped Mass Model of Test Rotor-Bearing System

k	l(in)	d(in)	m(lb)	$I(in^4)$	$I_p(lb\text{-}in^2)$	$I_T(lb\text{-}in^2)$	Δx(in)	Δy(in)	$\Delta\theta$(Rad)	$\Delta\phi$(Rad)
1	0.000	2.500	0.	1.9175E+00	0.	0.	0.	0.	0.	0.
2	.001	2.500	6.9459E-04	1.9175E+00	5.4265E-04	2.7132E-04	0.	0.	0.	0.
3	0.000	2.500	0.	1.9175E+00	0.	0.	0.	0.	0.	0.
4	0.000	2.500	3.7662E-01	1.9175E+00	2.9424E-01	1.4712E-01	0.	0.	0.	0.
5	3.500	.984	3.7662E-01	4.6020E-02	4.5583E-02	4.0726E-01	0.	0.	0.	0.
6	0.000	6.672	1.4842E+01	9.7273E+01	8.2585E+01	4.1293E+01	0.	0.	1.5000E-04	5.0000E-05
7	3.000	6.672	1.5057E+01	9.7273E+01	8.3783E+01	5.3184E+01	0.	0.	1.5000E-04	5.0000E-05
8	2.000	.984	4.8423E-01	4.6020E-02	5.8607E-02	1.9071E-01	0.	0.	0.	0.
9	2.500	.984	6.9944E-01	4.6020E-02	8.4655E-02	4.0662E-01	0.	0.	0.	0.
10	4.000	.984	8.6085E-01	4.6020E-02	1.0419E-01	1.1999E+00	0.	0.	0.	0.
11	4.000	.984	8.6085E-01	4.6020E-02	1.0419E-01	1.1999E+00	0.	0.	0.	0.
12	4.000	.984	7.5324E-01	4.6020E-02	9.1166E-02	1.0499E+00	0.	0.	0.	0.
13	3.000	.984	4.8423E-01	4.6020E-02	5.8607E-02	3.9247E-01	0.	0.	0.	0.
14	1.500	.984	1.6141E-01	4.6020E-02	1.9536E-02	4.0032E-02	0.	0.	0.	0.

K = STATION NUMBER

l = STATION LENGTH

d = STATION DIAMETER

m = STATION MASS

I = STATION 2ND MOMENT OF AREA

I_p = STATION POLAR MOMENT OF INERTIA

I_T = STATION TRANSVERSE OF INERTIA

$\Delta x, \Delta y$ = STATION BEND IN x AND y DIRS. RESP.

$\Delta\theta, \Delta\phi$ = STATION SKEW IN x AND y DIRS. RESP.

Table G.1 Physical Properties of Test Rotor-Bearing Model Shown in Figure G.2

APPENDIX H

BEARING PEDESTAL STIFFNESS AND MASS

BEARING SUPPORT STIFFNESS IN THE VERTICAL (x)

Treating the bearing support as a cantilever, its stiffness is given by:

$$k_{p,x} = \frac{3EI_1}{l_1^3} \tag{H.1}$$

where E, I, and l_1 represent Youngs Modulus for the material, second-moment of area and support length, respectively. For a hollow tube:

$$I_1 = \frac{\pi}{64}(D_1^4 - D_2^4) \tag{H.2}$$

where D_1 and D_2 are the external and internal diameters of the support, respectively.

BEARING SUPPORT STIFFNESS IN THE HORIZONTAL (y)

$$k_{p,y} = \frac{3EI_1}{l_1^3} \tag{H.3}$$

For a hollow tube:

$$I_1 = \frac{\pi}{64}(D_1^4 - D_2^4) \tag{H.4}$$

ROTOR STIFFNESS

Treating the rotor as a simply supported beam, with load off-centre, the stiffness at the load is given by:

$$k_R = \frac{3EI_2 l_2}{a^2 b^2} \tag{H.5}$$

where I_2 and l_2 represent the second moment of area and support length, respectively. a and b are the distances between the load and the left and right hand supports, respectively. For a solid circular shaft:

$$I_2 = \frac{\pi d^4}{64} \tag{H.6}$$

where d represents the shaft diameter. When the appropriate values are inserted in equations (H.5), $k_R = 8.94 \times 10^3$ lbf/in (1.56×10^6 N/m).

Dividing equation (H.1) by equation (H.5) gives the non-dimensional ratio of vertical support stiffness to rotor stiffness:

$$\frac{k_{p,x}}{k_R} = \frac{I_1}{I_2}\,\frac{a^2 b^2}{l_1{}^3 l_2} \tag{H.7}$$

The non-dimensional ratio of bearing support mass M_B, to rotor mass is given by:

$$M_B/M_R = 0.63 \tag{H.8}$$

where M_R represents the total rotor mass (flywheel plus shaft),for M_B=23.19lb (10.54Kg) and M_R=36.66lb (16.66Kg).